# Development of a novel *in vitro* system for nasal drug delivery development

Jonathan David Turner

Doctor of Philosophy

ASTON UNIVERSITY

April 2000

Aston University

Development of a novel *in vitro* system for nasal drug delivery development

by

Jonathan David Turner

Submitted for the degree of Doctor of Philosophy, 2000

## Thesis Summary

There is currently, no ideal system for studying nasal drug delivery *in vitro*. The existing techniques such as the Ussing chamber and cell culture all have major disadvantages. Most importantly, none of the existing techniques accurately represent the interior of the nasal cavity, with its airflow and humidity; neither do they allow the investigation of solid dosage forms. The work in this thesis represents the development of such an *in vitro* model system in which the interior characteristics of the nasal cavity are more closely represented, and solid or minimal volume dosage forms can be investigated.

The complete nasal chamber consists of two sections: a lower tissue viability chamber and an upper nasal chamber. The lower tissue viability chamber has been shown, using existing tissue viability monitoring techniques, to maintain the viability of a number of epithelial tissues, including porcine and rabbit nasal tissue, and rat ileal and Payers' patch tissue.

The complete chamber including the upper nasal chamber has been shown to provide tissue viability for porcine and rabbit nasal tissue above that available using the existing Ussing chamber techniques.

Adaptation of the complete system, and the development of the necessary experimental protocols to allow aerosol particle-sizing, together with videography, has shown that the new factors investigated, humidity and airflow, have a measurable effect on the delivered dose from a typical nasal pump.

Similarly, adaptation of the chamber to fit under a confocal microscope, and the development of the necessary protocols has shown the effect of surface and size on the penetration of microparticulate materials into nasal epithelial tissues.

The system developed in this thesis has been shown to be flexible, in allowing the development of the confocal and particle-sizing systems. For future nasal drug delivery studies, the ability to measure such factors as the size of the delivered system in the nasal cavity, the depth of penetration of the formulation into the tissue are essential. Additionally, to have access to other data such as that obtained from drug transport in the same system, and to have the tissue available for histological examination represents a significant advance in the usefulness of such an *in vitro* technique for nasal delivery.

Key Words

Nasal delivery, *In vitro* models, confocal microscopy, tissue viability, particle-sizing

Für Sonja.
Deine Entschlossenheit ist meine Inspiration.
Ich will Dich immer lieben.

## Acknowledgments

I would like to express my sincere thanks to my supervisors, Professor Bill Irwin, and Dr Oya Alpar for their continual supervision, encouragement, and support during this project. Drs Linda Randall, and Gordon Simpkin, my industrial supervisors at Rhone-Poulenc-Rorer, (or Aventis as it is soon to become), deserve special thanks for supporting this project both financially and with their vast breadth of experience.

I also extend special thanks to Dr Erik Bechgaard from the Pharmaceutics section of the Royal Danish School of Pharmacy for allowing my visit to his laboratory, to learn the *ex vivo* techniques developed there, and helpful discussions about tissue viability and using the Ussing chamber. Dr Jim Eyles who dosed and bled the animals used in chapter 6 also deserves special thanks.

I must also acknowledge the technical help I have received from Chris Bache, without whom many of the ideas in this thesis would never have seen the light of day.

During the course of producing this thesis, both here at Aston and also in Denmark, I have met and worked with a remarkable range of people, most of whom I am very fortunate to call my friends now. You are too many to mention, but you know who you are, I would like to acknowledge the help of all my friends for being entertaining, offering companionship, help and advice

My parents deserve a special thank-you for their love, support and continued guidance throughout the trials and tribulations that make everyday life so exciting.

As Lord Rutherford once said "there is physics and stamp collecting"; Sir, I hope there is more to this work than mere stamp collecting; perhaps here is the physics of stamp collecting?

# Contents

## Note on statistics

In all cases unless otherwise explicitly stated, data are all expressed as the mean +/- the standard deviation of the data.

Analysis of the statistical significance of the data has been done using the paired students t-test in all cases, a value of $P<0.05$ has been taken as an indication of a statistical difference existing between two sample populations.

## Note on nomenclature

Throughout this thesis, the terms horizontal and vertical Ussing chamber have been used. To prevent any confusion, this refers to the direction in which the tissue lies. The horizontal Ussing chamber for example has the tissue lying in the horizontal plane.

## List of abbreviations

| | |
|---|---|
| % | per $10^2$ |
| ‰ | per $10^3$ |
| δ | electron density |
| δ | NMR distance (ppm) |
| μ | micro ($x10^{-6}$) |
| [ ] | concentration |
| $[ ]_i$ | initial concentration |
| A | cross-section area of permeability |
| Arg | arginine |
| β-Ala | beta alanine |
| BALT | bronchus-associated lymphoid tissue |
| BSA | bovine serum albumin |
| BCA | bicinchoninic acid |
| Bq | Becquerels |
| BPM | beats per minute |
| C | Centigrade |
| $C_D$ | donor concentration |
| dC/dt | Rate of change of concentration with time (steady state flux) |
| cm | centimetres |
| $cm^2$ | square centimetres |
| $cm^3$ | cubic centimetres (ml) |
| CLSM | confocal laser scanning microscope |
| CM | confocal microscopy |
| CMi | confocal micrograph |
| Cys | cystine |
| 2D | two-dimensional |
| 3D | three-dimensional |
| D | diffusion co-efficient |
| D | deuterium |
| Da | Daltons |
| DAB | 3,3′ diaminobenzidine tetrahydrochloride |
| DT | diphtheria toxoid |
| e | electron |
| ELISA | enzyme linked immunosorbent assay |
| FITC | fluorescein isothiocyanate |
| g | gram |
| GALT | gut-associated lymphoid tissue |
| GIT | gastro-intestinal tract |
| Gly | glycine |
| GR | Krebbs' glucose Ringer solution |
| $^1H$ | proton {in NMR studies} |
| hGH | human growth hormone |
| His | histidine |
| HPLC | high-performance liquid chromatography |
| I | current |
| $I_{sc}$ | short circuit current |
| i.n. | intra nasal |
| IEF | isoelectric focusing |
| IFN | interferon gamma |
| Ig | immunoglobulin |

| | |
|---|---|
| IL | interleukin |
| k | permeability coefficient of a membrane |
| K | partition coefficient |
| k | kilo ($x10^3$) {as a prefix} |
| $k_d$ | rate constant of diffusion |
| $K_m$ | Michaelis (affinity) constant |
| L | litres |
| LP | lamina propria |
| m | milli ($x10^{-3}$) {as a prefix} |
| M | mega ($x10^6$) {as a prefix} |
| M | Molar |
| MALT | mucosal-associated lymphoid tissue |
| MCP-1 | machrophage chemoatractant protein |
| Met | methionine |
| MIP1 | macrophage migration inhibitory protein 1 |
| ml | millilitres |
| mm | millimetres |
| MWt | molecular weight |
| n | nano ($x10^{-9}$) {as a prefix} |
| n | number of repeats performed |
| NALT | nasal-associated Lymphoid tissue |
| NMR | nuclear magnetic resonance |
| OD | optical density |
| p | $-Log_{10}$ |
| P | students t test measure of significance |
| $P_{eff}$ | effective permeability |
| $P_{app}$ | apparent permeability |
| PAGE | polyacrylamide gel electrophoresis |
| PBS | phosphate buffered saline |
| PC | personal computer (IBM compatible) |
| PI, IEP | isoelectric point |
| PLA | poly lactic acid |
| PTFE | teflon |
| Q | total drug transported |
| R | resistance |
| $R^2$ | linear regression coefficient squared |
| RH | percentage relative humidity |
| SDS | sodium dodecyl sulphate |
| t | time |
| TBS | Tris-buffered saline |
| TMS | tetramethyl silane |
| TNF $\alpha$ | tumour necrosis factor alpha |
| Tyr | tyrosine |
| UV | ultra violet |
| UWL | unstirred water layer |
| v | rate of reaction |
| V, PD | voltage |
| $V_r$, $V_R$ | receiver volume |
| $V_{max}$ | maximum rate of enzyme catalysed reaction |
| $V_s$ | sample volume |
| $V_t$ | chamber volume |
| %w/v | percentage composition weight per volume |

$X_R$ receiver concentration
$X_D$ donor concentration

## List of figures

### Chapter 1



### Chapter 2

## Chapter 3



## Chapter 4

## Chapter 6

# List of Tables

# Chapter 1

# Introduction

## 1.1 Introduction to nasal delivery

Proteins and peptides are now of great interest to the pharmaceutical industry and hold significant potential as therapeutic agents. The use of proteins and peptides in therapy is well established, with insulin being an obvious example of this is (Brogden, 1987). A further example of proteins under consideration for nasal delivery are sub unit antigens. These are large proteins, for example F1 and V sub-units of *Yersinia pestis*, the causative agent of the plague, are 48 and 60 kDa respectively, which have been successfully formulated to produce plague vaccines that are efficacious *in vivo* to the plague.

The clinical use of peptides and proteins has been limited by several factors; such as their instability in the gastro-intestinal (G-I) tract, poor transport across mucosal membranes and extensive hepatic first-pass elimination (Humphrey, 1986). This has limited their delivery to the parenteral route; whilst this is acceptable for short-term therapy or life-threatening disorders, it is unsuitable for long-term administration due to patient compliance. For enhanced patient compliance, the preferred route of administration is the oral route; this is also favoured for other reasons such as cost, and its non-invasive nature.

As peptides and proteins are generally unsuitable for this type of delivery, alternative approaches must be considered. Two possible approaches are i) the development of analogues suitable for oral delivery and ii) the development of other delivery routes. Whilst development of analogues is a good method for small peptides, the development of alternative routes of delivery, such as the nasal, ocular, and buccal routes must also be undertaken. Such routes routes need not be limited to the larger peptides and proteins; it could be used for both the small peptides and the larger proteins.

Nasal delivery has been used for many years in traditional medicines such as the Indian Nasaya Karma (nasal therapy), in the Hindu Ayurdeuic medicine system, and by African witch doctors for administration of plant snuffs containing psycho-tropic hallucinogenic compounds (Chien, 1985). It is also currently used "recreationally" for the administration of the powerful narcotic cocaine in its powder form. Untill recently this route has only been used by western medicine for the delivery of locally acting drugs (usually low

molecular mass hydrophobic drugs, such as decongestants, topical steroids and anti-bacterial agents) and for the delivery of a small number of drugs with a systemic action. The drugs that have been delivered nasally for systemic action all have sufficient nasal absorption for this to be a viable route. Recent advances in nasal delivery have resulted in formulations of large proteins specifically for systemic action, such as insulin reaching the market in certain Scandinavian countries based on the work of the Bechgaard research group (Bechgaard *et al.*, 1996).

Initial work on the nasal route in the 1980's indicated that the low bioavailability of peptide and protein drugs after administration vial the nasal route compared to parenteral delivery was still a problem, as shown in Table 1.1 (Wearley, 1991). Research has shown that this poor bioavailability is due to factors differing from those found in oral delivery which will be discussed in more detail later, and as such, nasal delivery is worth considering as an alternative delivery route.

| Compound | Amino acids | Bioavailability (%) |
|---|---|---|
| TRH | 3 | 45 |
| Metkephamid | 5 | 100 |
| Somatostatin | 6 | 75 |
| Oxytocin | 9 | 1 |
| Desmopressin | 9 | 10 |
| Buserelin | 9 | 2.5 |
| LHRH | 10 | 1.5 |
| Nafarelin | 10 | 2 |
| ACTH analogue | 17 | 12 |
| Secretin | 27 | 10 |
| Glucagon | 29 | <1 |
| Calcitonin | 32 | <1 |
| GHRH | 40 | <1 |
| Insulin | 51 | <1 |
| Interferon-γ | 165 | <1 |
| Growth hormone | 191 | <1 |

**Table 1.1** Intranasal bioavailabilities of proteins and peptides as aqueous solutions. Wearley (1991)

## 1.2 The anatomy and function of the nose

### 1.2.1 Function and physiology

The nose is the visible organ of respiration, it has two functions, that of respiration, and of olfaction. The correct functioning of the nose, and in particular the nasal passages, involves the filtration, humidification, and warming of inhaled air. To do this, the nose must control the rate of airflow, remove noxious agents, and introduce large volumes of water into the inhaled air stream.

The nasal passage runs from the nasal vestibule to the nasopharynx. This is typically a distance of 12 to 14 cm (Maron *et al.*, 1984). The nasal passage is split by a vertical cartilaginous and bony nasal septum (Geurkink, 1983). The passage consists of horizontal, epithelium-lined turbinates that mould the air stream to their configuration and changing dimensions (Chien *et al.*, 1989).

The nasal vestibule is the anterior portion of the nose, starting as the double nasal airway at the nostrils, to the beginning of the ciliated epithelium at the anterior end of the septum and turbinates (Geurkink, 1983). The main nasal passage in which most of the physiological functions of the nose are carried out is an area that extends back from the vestibule for approximately 6-8 cm to the turbinate and septum ends. The nasopharynx is where the turbinates and septum end and both airways are joined. Although there is a significant surface area of about 120 $cm^2$ the nasal passage is very narrow, at the top in the olfactory region it is only 2-3 mm wide (Duchene and Ponchel, 1993). The septum and turbinates are lined with a ciliated, highly vascular epithelium that is rich in mucus glands and goblet cells.

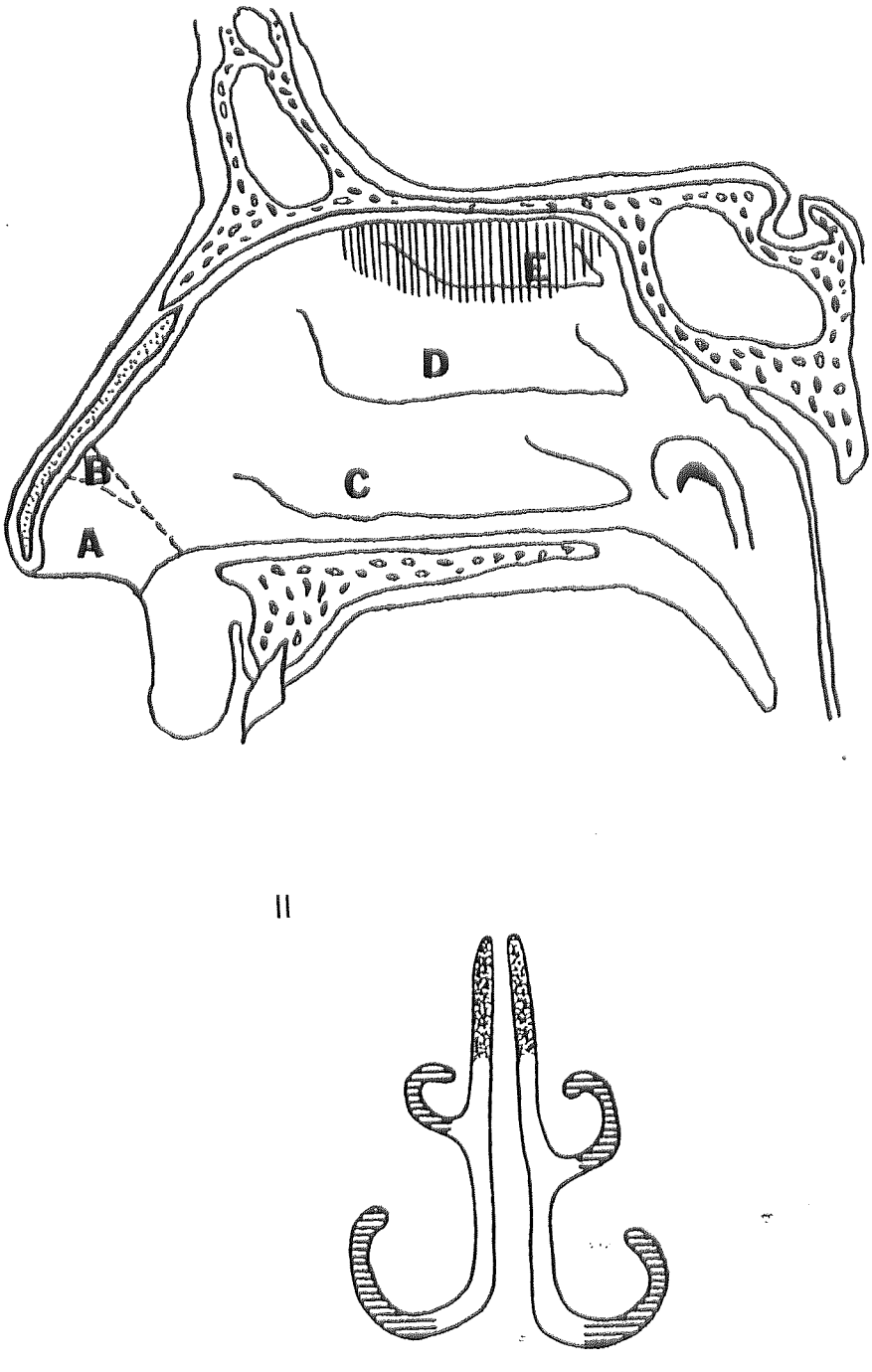


**Figure 1.1** The nasal anatomy. I) Side view and II) cross sectional view. A) nasal vestibule; B) internal ostium; C) inferior turbinate; D) middle turbinate; E) superior turbinate. The shaded area represents the olfactory region. From Proctor and Anderson (1982).

### 1.2.2 The nasal epithelium

The nasal epithelium consists of both olfactory and non-olfactory epithelia (Geurkink, 1983). The olfactory epithelium represents an area of about 2 $cm^2$, which is located above the middle turbinate as shown in Figure 1.1. The non-olfactory epithelium is an area of about 120 $cm^2$ covering the main nasal passage (Duchene and Ponchel, 1993). The epithelial layers consist of pseudo stratified columnar cells. The olfactory area as illustrated in Figure 1.2 consists of bipolar neurones (the actual olfactory cells), supporting cells, and secretary cells. The non-olfactory, respiratory epithelium consisting of ciliated, non-ciliated epithelial cells, basal cells and secretary (goblet) cells as shown in Figure 1.3.

Both the respiratory and olfactory epithelia are covered by mucus. This mucus covering consists of an upper "sticky" layer that adheres to the tips of the cilia and a lower layer round the cilia and over the non-ciliated cells.

The respiratory epithelium is a very thin layer approximately 20-30 µm thick, compared to the olfactory epithelium at 60-70 µm thick. The ciliated cells represent 70-80% of the respiratory epithelium, the rest being goblet and secretary cells. It should be noted that not all intracellular junctions are of the same structure. As a consequence, protection afforded by the epithelial barrier varies according to the region within the nasal cavity (Duchene and Ponchel, 1993). This has led to the nasal epithelium being classed as a "leaky epithelium" (Cremaschi *et al.*, 1991).

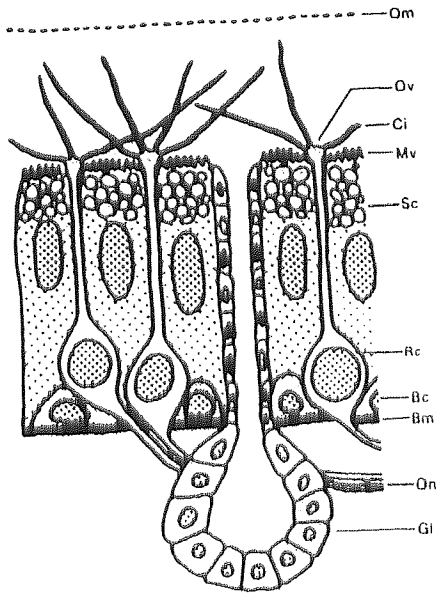


**Figure 1.2** The olfactory epithelium
Om, Surface of the olfactory mucus, Ov olfactory vesicle, Ci olfactory cilia, Mv microvili, Sc supporting cell (secretary granules inside cells shown), Rc olfactory receptor cells, Bc basal cell, Bm basement membrane, On Olfactory nerve, Gl olfactory gland. (Chien *et al.*, 1989)

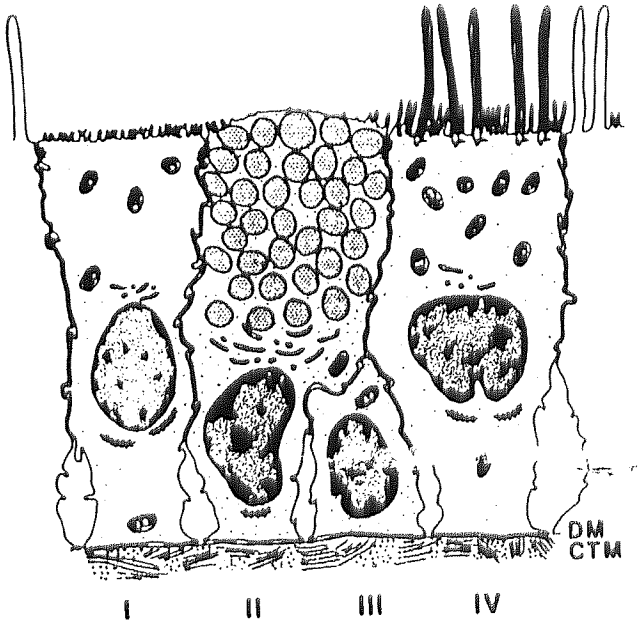


**Figure 1.3** The Respiratory Epithelium.
Representation of transmission electron micrograph of different respiratory nasal cell types. I, nonciliated columnar cell with micovilill, Goblet cell with mucus granules and Golgi apparatus. III, basal cell. IV, ciliated columnar cell with mitochondria in the apical part. DM double membrane. CTM connective tissue membrane. (Chien *et al.*, 1989)

The nasal openings and the initial part of the nasal cavity are covered in a squamous epithelium that plays no part in the uptake of nasally administered drugs. There are also small areas of immunogenic tissue, the nasal-associated lymphoid tissue (NALT), that is composed of areas of M-cells; whilst this is not of prime concern for the delivery of peptide drugs, it is thought to play a significant role in the uptake of particulate matter and antigens (Section 1.4.3.1) and, due to their immunological properties, are very much targeted for vaccine delivery (Chapter 6) (Almeida and Alpar, 1996).

### 1.2.3 Nasal blood flow

It has been shown that the nasal epithelium and its underlying tissues are highly vascular (Cuana, 1982). Since the respiratory epithelium lies over a layer of erectile cavernous tissue this provides a rich surface for drug absorption. The structure of this highly vascular bed is such that rapid exchange of fluids and dissolved substances between the blood vessels and the other nasal tissues is possible. This is a significant advantage when it comes to consideration of the nasal route as a means of systemic drug delivery. Another advantage due to the anatomy of the nose is that, once the drug has passed into the blood stream, the venous flow is into the portal system, thus ensuring delivery to the various tissues and organs of the body before the liver, and thus avoiding the hepatic first pass effect.

### 1.2.4 Nasal secretions

As previously mentioned, a mucus layer covers the respiratory and olfactory epithelia. In a healthy subject this is clear in appearance and consists of 90-95% water, 1-2% salt, 2-3% mucin (a mucus-specific glycoprotein), and <1% other proteins.

There are several functions associated with the mucus layer, as shown in Figure 1.4. These functions can best be described as the first line of defence within the respiratory tract against xenobiotics and the debris of everyday life introduced in the inhaled air. (Taylor, 1974; Sarkar, 1992).

The mucus layer consists of two layers; the lower watery (perciliary layer) layer is adjacent to the cell surface, and the more viscous mucous (gel) layer at the top. The perciliary layer is watery and of low viscosity. This layer is slightly less than the height of an extended cillium and is "probably formed of cell exudates" (Widdicombe, 1984; Martiin *et al.*, 1998). The gel layer lies above the perciliary layer and varies between 0.5 and 5μm thick. The gel layer consists of mucins that are between 700 and 1 x $10^7$ Daltons. The mucins are glycoproteins and are about 80% carbohydrate (Verdugo, 1990). Mucins are produced in the goblet cells of the nasal epithelium and are exuded as highly condensed granules by exocytosis (Verdugo, 1990). These granules, on leaving the goblet cells swell, as they absorb water. As they swell, the mucins are mixed and annealed to form a gel that is suitable for transportation by the cilia. As the mucins are mixed and absorb water, they form an entangled network that is stabilised by non-covalent bonds, mostly disulphide bridges, between the mucin strands. The gel loses its viscosity if these disulphide bridges are reduced (Verdugo, 1990).

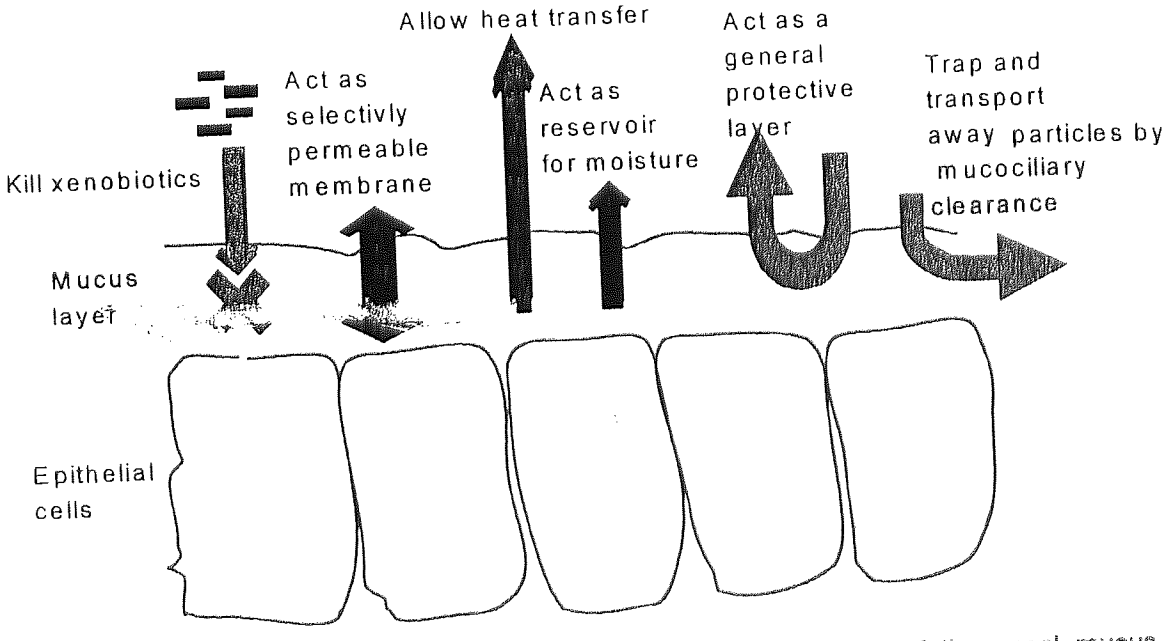


**Figure 1.4** A schematic representation illustrating the function of the nasal mucus layer.

The non-mucin proteins present in the nasal secretions includes lysosymes (Ogawa *et al.*, 1979, Rossen *et al.*, 1966a), enzymes (Schorn 1979), immunoglobulins such as IgA, IgE, IgG, and some serum proteins such as albumin and siderophilin (Rossen *et al.*, 1966b).

The majority of the secreted proteins have a specific purpose, for example proteases to digest inhaled biological agents, and antibodies as a means of biological defence.

### 1.2.5 Mucociliary clearance

The upper mucus layer is continually being moved in the posterior direction, this process is mucociliary clearance. This is the mechanism whereby the thin mucus layer is continually moved towards the nasopharynx by the beating cilia. This ensures that any trapped material is removed from the nasal cavity quickly and efficiently.

Clearance of substances from the nasal cavity is a biphasic process; the first phase is the active transport of foreign matter by mucociliary clearance, and the slower second phase is the removal of an applied substance from the non-ciliated areas. Since, for nasal drug delivery interest is in the respiratory epithelium, not the squamous epithelium found in areas of no mucociliary clearance, the second phase of clearance is of little consequence (Martiin *et al.*, 1998).

The epithelial cilia beat at about 1000 strokes *per* min (Laurenzi *et al.*, 1973), on the forward stroke the cilia are extended into the upper viscous layer moving it along, on the return stroke the cilia are not extended, moving in the lower watery layer. Studies in humans have shown that the rate of mucociliary clearance is in the range 0-24 mm *per* min, giving a total time of 20 mins for the complete removal of an applied substance with times of more than 30 mins being considered as indicative of impaired mucociliary clearance (Andersen and Proctor, 1983). Mucociliary clearance is vital to the continued functioning of the nasal mucosa. A reduction in mucociliary clearance will increase the time that invasive agents such as bacteria and viruses have to reach the epithelium, and will increase the exposure of the mucosa to any irritating or carcinogenic substances in the inhaled air. The result of this would be infection or damage to the mucosa.

Efficiency of mucociliary clearance is dependent upon four factors, i) the mechanical properties of the mucus, ii) volume of mucus, iii) the depth of the lower perciliary layer, and iv) the condition of the cilia (Martiin *et al.*, 1998). Loss or impairment of mucociliary

clearance is due to either external factors, for example contact with toxic agents, or by pathological conditions. Examples of pathological conditions affecting mucociliary clearance are primary ciliary diskinesia, cystic fibrosis, the common cold, and diabetes mellitus. In all of these cases, with the exception of the common cold, the reduction in mucociliary clearance is also associated with an increased susceptibility to respiratory diseases, although whether the loss of mucociliary clearance is the cause, or a result of the increase in respiratory disease is not clear (Camner *et al.*, 1988).

Mucociliary clearance plays a major part in the protection of the respiratory tract, however, should this fail there are other mechanisms to protect the lower areas such as the lungs, for example coughing. Studies on the life expectancy of patients with primary ciliary diskinesia, a condition where there are no cilia, or those present are diskinetic, show that there is no change in life expectancy, provided that respiratory infections are adequately treated (Newhouse *et al.*, 1983), providing evidence that mucociliary clearance is an important, integrated part of the respiratory tracts defence, although not vital (Afzelius, 1997). The speed with which the mucociliary clearance process removes applied substances is highlighted in Figure 1.5 where the removal of radiolabelled drugs was investigated after delivery from two different types of device. In all of the cases below after 30 mins a significant amount of the drug has been removed to the nasopharynx and further down the respitatory tract.

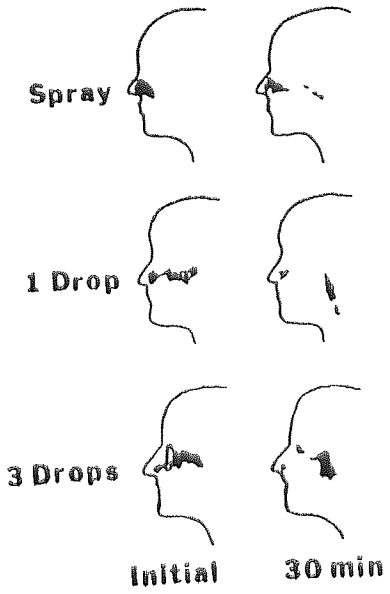


**Figure 1.5** Diagram showing the sites of deposition and the mucocilliary clearance patterns after intranasal administration by spray and nose drops. (Hardy *et al.*, 1985)

### 1.2.6 Recovery of the nasal epithelium

Several pathological conditions cause the loss of mucociliary clearance, either over the short term (for example the common cold), or the long term (for example primary ciliary diskinesia). In cases such as the common cold, the mucociliary clearance is lost primarily due to a loss of cilia, although partly due to the change in mucus rheology. Studies have revealed loss of cilia within the first weak of the common cold, recovering to full activity within the following three weeks (Rutiainen *et al.*, 1992).

*In vivo* studies on the regeneration of the nasal mucosa from both chemical and mechanical challenge in both rats and rabbits show that the respiratory epithelium regenerates within 5-10 days if the basal cells and membrane are intact, and within 6 weeks if the entire epithelium is removed (Ohashi *et al.*, 1991; Zhou and Donovan, 1996).

More recently, a study was performed in an attempt to correlate epithelial damage caused by an applied substance to the clinical situation. Ephedrine nasal drops 1%, a well-known decongestant preparation containing the local irritant benzalkonium chloride and EDTA, was administered to rabbits and the effect on the mucosa observed. Within 4 h there was pronounced atrophy and disorganisation within the epithelium, which was devoid of goblet cells and cilia. However, 24 h after administration these changes were only observed

to "a minor extent", the loss of cilia and goblet cells was reversible, and within 24 h the epithelium had only minor defects visible (Bechgaard *et al.*, 1997).

## 1.3 Biological barriers to nasal delivery

### 1.3.1 Biological barriers and their contribution to the overall barrier

Nasally administered peptide and protein drugs will encounter significant barriers to absorption. These barriers are depicted in Figure 1.6. The overall barrier consists of those from the mucus layer, the nasal epithelium, and the basal membrane. It has been shown that the two most important biological barriers are the enzymatic, and cell membrane barriers.

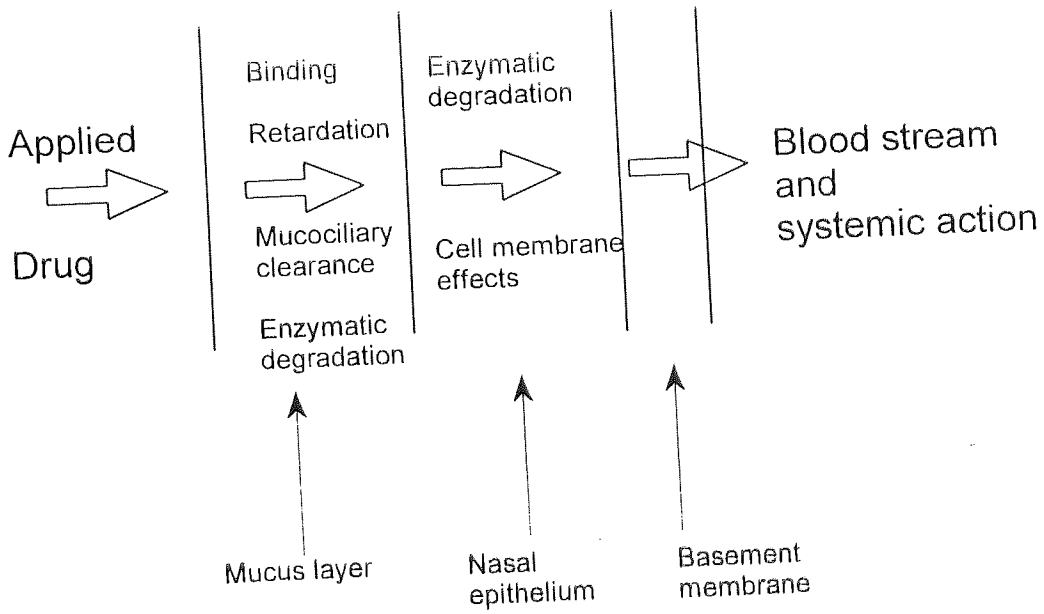


**Figure 1.6** A schematic representation of the biological barriers to nasal drug absorption

### 1.3.2 Mucus layer barrier

The mucus layer represents a significant barrier to nasal drug delivery (Schipper *et al.*, 1991). This barrier is significant because the nasal mucosa is continuously being moved by mucociliary clearance and replaced with freshly secreted mucus. The mucus layer

covering the nasal epithelium is changed every 20 mins or so (Section 1.2.5): since, for any drug to reach the epithelium and hence reach the systemic circulation it must first pass this moving mucus layer this represents a time-limit for any uptake or transport of the applied drug. As well as acting as a gel through which the drug must diffuse, applied drug may bind to the mucus or be degraded by the proteases present in the mucus, which is discussed in detail in section 1.3.3.4.

The mucus layer itself as a barrier to nasal delivery of proteins/peptides was studied extensively by Holbrook (Holbrook, 1991). The mucus was found to be a minor mechanical barrier to the diffusion of drugs where molecular mass was inversely proportional to the rate of diffusion, although no definitive structure - activity relationship could be generated since other interactions such as mucus glcoprotein – drug interactions were evident.

### 1.3.3 The epithelial barrier

The epithelium is a single layer of cells with a selectively, semi-permeable, and hydrophobic membrane. The barrier that drugs experience is not just the cell layer, but degradation from both membrane - bound and cellular proteases. The cell membranes permit the entry of required material, removal of waste products, and, in the goblet cells, the secretion of the mucus layer proteins. The cell membrane represents the most significant barrier in the epithelium itself. There are two ways in which any applied drug molecules can cross the nasal epithelium, either transcellularly (intracellular) or paracellularly (intercellular).

Transcellular transport is the transportation of drug molecules into and subsequently through the epithelial cells as a direct result of either passive or active transport. Paracellular transport is the transport of the drug molecules directly into the lower tissue layer *via* the inter-cellular junctions (Wilson and Washington, 1990).

Typically a peptide drug has a high molecular mass, is hydrophilic, and is charged. Hydrophilicity and charge make the transcellular transport mechanisms unfavourable, while the high molecular mass makes the paracellular route unfavourable (Lee, 1988b).

The active transport mechanisms in the nasal epithelium have not been significantly studied, however, amino acid and dipeptide transporters have been found (Huang *et al.*, 1985a; Huang *et al.*, 1985b). To study the transport of drugs across epithelial membranes, knowledge of the kinetics of active, passive, and mixed transport systems, especially in model systems, requires knowledge of transport kinetics.

### 1.3.3.1 Kinetics of trans- and para-cellular passive diffusion

Passive diffusion through the membranes of an epithelial cell by a small molecule in aqueous solution involves the transfer of the molecule from the aqueous solution, which in this case is the mucus layer (90-95% water) into the cell membrane. The cell membrane is a phospholipid bilayer. The transfer is then followed by transport into the aqueous solution inside the cell. Since this process is driven by the concentration gradient across the membrane, and the transferring of the drug molecule from an aqueous phase to an essentially organic phase, and then to a further aqueous phase, it is dependent upon both the concentration of the drug and its hydrophobicity. Provided that the rate limiting step is in the diffusion across the membrane this will be dependant upon the hydrophobicity or hydrophilicityof the drug.

Hydrophobicity and hydrophilicity are quantified by the partition coefficient, K, of the drug. The partition coefficient is an equilibrium constant for the two-phase system.

$$\text{Drug (Aqueous phase)} \underset{}{\overset{K}{\rightleftharpoons}} \text{Drug (Organic phase)}$$

This can be considered mathematically,

$$K = \frac{[\text{Drug (Organic phase)}]}{[\text{Drug (Aqueous phase)}]}$$

The higher the value of K the more drug is present in the organic phase and the higher the hydrophobicity of the drug.

The most simple way of modelling the diffusion process is the application of Fick's first law. Fick's first law states that the rate of permeation is directly proportional to the thickness of the membrane, the partition coefficient of the permeant between both the membrane and solvent, and the ability of the permeant to diffuse through the membrane material. Fick's first law states mathematically that:

$$k = \frac{KD}{x}$$

k = permeability coefficient of membrane,
K= partition coefficient,
D = diffusion coefficient of molecule (cm $min^{-1}$)
x = membrane thickness. (cm)

This is described as zero order kinetics since it is a simple linear relationship. Since this is zero order, for a specific drug passing through a cell or complete tissue layer a more general equation can be produced, since the values for k and K can be considered as one constant when considering biological barriers such as a complete epithelial layer. This equation is much simpler:

$$\text{rate of transport} = k_d [S]_i$$

Here, $k_d$ is the rate constant of passive diffusion, and $[S]_i$ is the initial drug concentration.

Any passive diffusional mechanism results in zero order kinetics.

### 1.3.3.2 Kinetics of transcellular active transport

Active transport of drug molecules relies on a membrane bound transporter protein that will accept the drug molecule as a substrate in a similar manner to enzyme substrate binding, and as such follows standard Michaelis Menten kinetics with the relationship

$$v = \frac{V_{max}[S]_i}{K_m + [S]_i}$$

Where $K_m$ is the standard Michaelis constant, $V_{max}$ is the maximum transport rate, v is the rate of transport, and $[S]_i$ is the initial drug concentration.

As with enzyme activity, transporter activity is subject to competitive, non-competitive, reversible and irreversible inhibition, and the kinetics are the some for these as they are for the inhibition of enzymatic activity.

### 1.3.3.3 Kinetics of mixed transport systems

Since the uptake and transport of a drug across the nasal epithelium is most likely to be a mixture of both passive and active mechanisms, the overall instantaneous rate v is given by the sum of the two different rates.

$$v = \frac{V_{max}[S]_i}{K_m + [S]_i} + kd[S]_i$$

### 1.3.3.4 The enzymatic barrier

It was originally thought (Harris, 1986) that the nasal mucosa was deficient in proteolytic activity; however, it has been shown that nasally delivered peptide and protein drugs are susceptable to enzymatic degradation both by luminal and membrane-bound proteases as well as intra cellular degradation (Hussain *et al.*, 1990; Stratford and Lee, 1986)

Proteolytic enzymes cleave peptide bonds either in the middle of the amino-acid sequence (endopeptidase) or remove a terminal amino acid (exopeptidase). Exopeptidases are then divided into two categories depending on their site of action, with carboxy- and amino- peptidases cleaving at the C and N terminal ends of the protein respectively. Both carboxy- and amino- exopeptidases together with endopeptidases are present in the human

nasal tissue. Work performed by Lee and co-workers (Stratford and Lee, 1986; Kashi and Lee, 1986) analysing the breakdown products suggests that the principal cellular enzymes involved in the degradation of proteins and peptides in the nasal cavity are aminopeptidases, with dipeptidyl peptidase, and dipeptidyl-carboxypeptidase playing a more minor role. The level of enzyme activity in tissue homogenates was found to be similar to that in the gut.

Since the level of peptidase activity can directly affect the breakdown of the applied protein/peptide, to overcome this barrier, peptides and proteins have been formulated with enzyme inhibitors to improve bioavailability. Inclusion of the powerful aminopeptidase inhibitor boroleucin with the pentapeptide thymopentin increased the unformulated elimination half-life from 12 to 37 mins during *in vivo* perfusion experiments. Concurrently, the levels of breakdown products found in the perfusion fluid was reduced. These increases in the elimination half-life suggests that cellular (and extra cellular) proteolytic enzymes play an important role in the degradation of the peptides and proteins within the nasal cavity.

## 1.4 Enhancement of nasal drug absorption

Peptide and protein drugs have many potential beneficial uses, however, almost without exception they have poor bioavailabilities when administered intranasally unformulated (Table 1.1). There is significant interest in formulation and development to improve the bioavailability of such compounds so that it reaches a level acceptable for therapeutic use. To increase the amount of drug absorbed, there are several strategies, as well as those already discussed to overcome specific barriers. Whatever strategy is employed the morphology of the nasal cavity must remain unaltered, together with the mucociliary transport rate and ciliary beat frequency since the nasal epithelium represents the first line of defence against inhaled xenobiotics.

### 1.4.1 Synthesis of stabilised and more lypophilic analogues

The synthesis of drug analogues to increase potency, stability, and bioavailability is a long established technique. For small peptide drugs this can be achieved by several

methods, blocking N- and C- termini by derivitisation or cyclisation, by the use of amino acids that are of the D- conformation (as opposed to the usual L-enantiomer) or other non-natural amino acids, or by the replacement of the hydrolysable peptide bond by a non hydrolysable analogue. This technique has been put to good use, for example, in the development of the anti-diuretic drug desmopressin (Christolini *et al.*, 1991), although for LHRH agonists such as buserelin, analogues can be produced with potencies of up to 200 times that of the parent compound; however, the bioavailabilities remain unchanged (Smitz *et al.*, 1988)

Since degradation by proteolysis seems to be the major breakdown route for administered protein and peptide drugs, the development of prodrugs using this enzymatic susceptibility to release the drug molecule is possible. The most abundant enzyme seems to be aminopeptidase, so, any pro-drug developed will probably take advantage of the proteolytic activity available. To take advantage of this, the N- terminus of the peptide should be derivitised either with an amino acid or a derivitised amino-acid analogue, with the derivitising group being chosen to give controlled release of the parent peptide or protein (Banerjee and Amidon, 1985; Bundgaard, 1992).

### 1.4.2 Formulation with protease inhibitors

As proteolytic processing represents one of the major routes of breakdown, especially at the delivery site, the inclusion of protease inhibitors in the formulation is an obvious strategy in dealing with the poor nasal bioavailabilities of peptide and protein drugs (Sarkar 1992). Very little work has been reported on this method of absorption enhancement although the work that has been reported has shown enhancement of drug absorption. The delivery of aminopeptidase inhibitors bactiricin, bestatin and amastatin together with LHRH peptides (Raehs *et al.*, 1988) increased the levels of the LHRH peptides absorbed. However, the work of Gizurarson and Bechgaard (1991) suggests that for insulin at least this is not a necessary process as it was estimated that only 0.6% of the insulin administered was destroyed by proteolytic enzymes in the nasal cavity.

### 1.4.3 Formulation with absorption enhancers

Absorption enhancers traditionally are surfactants, bile salts, chelating agents, cyclodextrins, fatty acids and phospholipids. With the exception of the chelating agents, these are all compounds that act as phase-transfer (soluablising) agents by having one part of the molecule that is hydrophobic, and another that is hydrophilic (Figure 1.7). Usually they form micelles or vesicles, and drug molecules can then be trapped inside them, however cyclodextrins work by having a hydrophilic interior and a hydrophobic exterior (Figure 1.8). Recently solid particles have been used as absorption enhancers, rather than having drug molecules trapped inside a vesicle or formulated with an enhancer, particles such as micro- and nano- spheres are a polymer matrix in which drug can be trapped. The drug is then released as these particles degrade in the body. All of these compounds are known to improve the amount of drug that crosses the epithelial layer, however relatively little work has been done on their mechanism of action. Drug delivery systems to enhance absorption can be split into particulate and non-particulate carrier systems.

#### 1.4.3.1 Particulate carrier systems

Particulate systems have been well studied, and they are known to increase drug absorption in a number of ways depending on the system used (Oechslein *et al.*, 1996).

Bioadhesive microspheres such as degradable starch microspheres (DSM) increase the bioavailability of drugs due to their enhanced residence time in the nasal cavity, with their bioadhesive properties being quoted as the reason for their enhancement of drug absorption (Illum *et al.*, 1987) whilst their ability to "induce a transient opening of the cellular tight junctions" is also quoted as their mechanism of action (Edman *et al.*, 1991). This transient opening of cellular tight junctions was investigated in Caco-2 cells (Björk *et al.*, 1995). The opening of the tight junctions was visible under transmision electron microscopy (TEM) after only 3 mins, the opening of the tight junctions had then been reversed after 3 h. It is thought that hyperosmotic enhancement is responcible for these observed changes. Microspheres absorb water, in doing so they swell, and the epithelial cells are dehydrated causing the tight junctions to separate (Björk and Edman, 1988; Björk and Edman, 1990; Björk, 1993). In

contrast to this Oeschslein (Oeschslein *et al.*, 1996) studied dry powders including dextran microspheres, which like the starch microspheres swell when in contact with water. The degree of pre-soaking, and the degree to which the dextran microspheres were pre-swollen affects their $Ca^{2+}$ binding capacity, however, for effective $Ca^{2+}$, binding it was estimated that significant pre-swelling of the microspheres (>30 mins) was required. In this study there was the suggestion that the $Ca^{2+}$ binding capacity of the microspheres affected the bioavailability of the administered drug and the time to maximum plasma levels. However, when similar work using non-pre-swollen dextran microspheres was performed (Pereswetoff-Morath and Edman 1995) using insulin rather than octreotide results similar to those obtained with starch microspheres were obtained. In both cases, the plasma glucose minima at 30-40 mins, together with the peak insulin level at 10 mins using the starch microspheres, would suggest that the involvement of any swelling process and $Ca^{2+}$ binding process is unlikely.

Although the mechanism of absorption enhancement is not fully known, microspheres with a mean volume size of approximately 1 μm have been shown to cross the nasal epithelium and enter the systemic circulation (Alpar *et al.*, 1994). It was suggested that the NALT tissue played some role in their uptake. In the case of vaccine delivery, particle translocation across the epithelium is not necessarily required, however for a systemic as well as local response translocation is considered necessary. The nasal epithelium contains mucosal immune induction sites (M-cells) that sample viruses and bacteria in the nasal cavity performing a vital immune surveillance role. In vaccine delivery, the delivery of the antigen to these sites for presentation to the immune system *via* the macrophages present in the pocket at the bottom of the M cell. Although for vaccine delivery it is important for the antigen to reach this point, the M-cells are also capable of transporting microparticles across the epithelium. In the immunocompetent individual these M-cells bind and subsequently take up viruses, bacteria and protozoa with the express intent of presenting them to the underlying macrophage and lymphocytes. There has been a significant amount of work performed on the targeting of microspheres to these M-cells

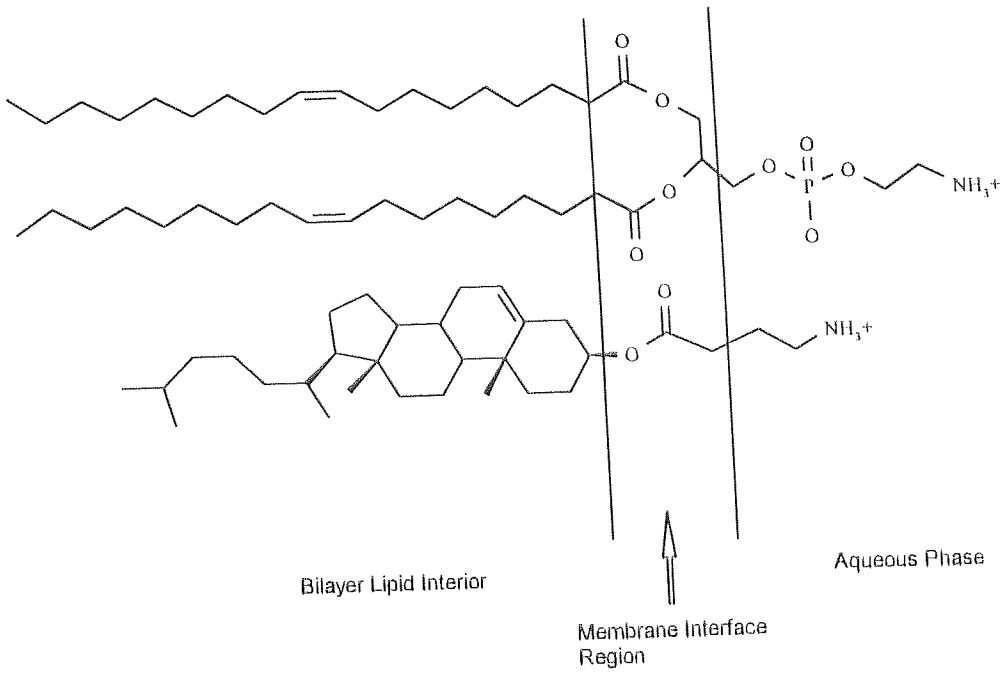


**Figure 1.7** Hypothetical alignment of DOPE (dioleoylphosphatidylathanolamine) and DC-Chol (3β[(N,N'-dimethylaminoethyl)carbamoyl] cholesterol) in DOPE/DC-Chol vesicle membranes.

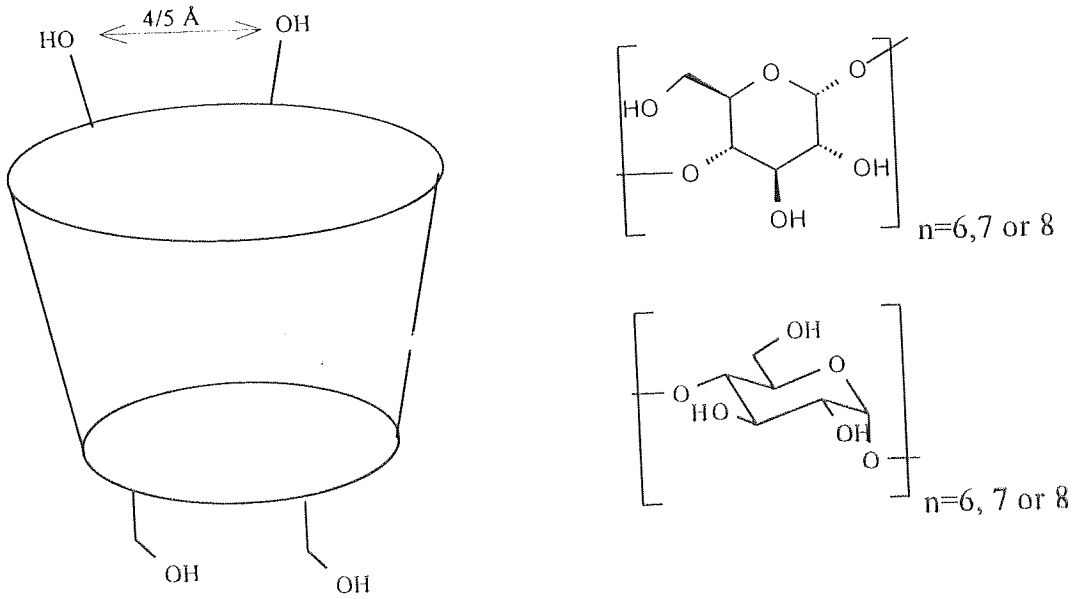


**Figure 1.8** Cyclodextrins, a graphical representation, and α-D-Glucose the base unit of cyclodextrins. This illustration is of underivatised cyclodextrins.

either for conventional drug delivery, or for delivery of antigens to the mucosal immune system. Systems used for the targeting of particles to M-cells include monoclonal antibody (mAb 5B11), IgA conjugation, and lectin targeting. All three of these systems rely on selective binding by the targeting molecule to the apical surface of the M cell.

Monoclonal antibodies such as mAb 5B11, which have a specificity for the apical cell surface of M-cells, have been investigate as a targeting system both *in vitro* and *in vivo*. Antibodies were conjugated to fluorescent latex microspheres (Pappo *et al.*, 1991) and co-incubated in isolated intestinal loops with non-conjugated microspheres containing a different fluorescent label. The increase in the uptake of the latex particles was monitored after tissue sectioning. However, the antibodies used in this system have not been optimised and it was thought that, as more specific antibodies became available, the increase in particle uptake could be significantly improved (Kabok *et al.*, 1994). However, this work to date has only been a "proof of principle" (Ermack and Giannasca, 1998).

It is well known that secretory IgA (sIgA) has a significant function in protecting epithelial surfaces of mucosal tissues by a number of methods. IgA is also known to bind selectively to M cell surfaces (Roy & Varvayanis 1987; Kato 1990) and delivered IgA is known to be transported by the M-cells. In murine experiments, liposomes conjugated with sIgA gave a 4-fold increase in the uptake of the liposomes in comparison to liposomes conjugated with a control protein (BSA).

M cell surface oligosaccharides, as with other oligosaccharides can be targetted using lectins. The nasal lectin histochemistry in many species has been known for several years. Experiments performed in ligated murine intestinal loops not only showed surface conjugation of the lectins to oligosaccharides, but also showed clear endocytosis of the lectin (Clark *et al.*, 1995). In this study, after a 30-min incubation the lectin was clearly visible bound to the surface of the M-cells, and after 1 h the lectins were visible on the basolateral membrane and in the intracellular vesicles of M-cells. *In vivo*, 500 nm tomato lectin-conjugated latex microspheres showed a 50-fold increase in the translocation of latex microspheres into the systemic circulation following oral delivery, in comparison with unconjugated microspheres (Hussain *et al.*, 1997)

Of all the targeting techniques that have been investigated, only lectin conjugation has been tested as a delivery system *in vivo* using either a suitable antigen or drug and monitoring the physiological effects. Antigen delivery as antigen-lectin conjugates to hamster nasal tissue showed increased serum antibody responses in comparison to unconjugated antigen alone (Giannasca *et al.*, 1997).

Targeting particles with large macromolecules such as specific antibodies, IgA, and lectins has been shown to increase the presence of particulates within M-cells. The vast majority of the work would appear to have been done *in vitro*, with very little work having been reported *in vivo*, although available reports indicate that targeting to M-cells is a viable method of increasing the efficacy of drug or antigen delivery.

With particulate systems such as those designed specifically to be taken up by M-cells, or pass paracellularly there is a size dependence, with the size of the particle also playing a role in determining which route is taken. Sub micron particles are though to be able to pass paracellularly, whilst particles above 10 μm were not taken up, similarly the effect of the particle surface charge has a significant effect on their uptake (Eldrich *et al.*, 1990).

### 1.4.3.2 Non-particulate carrier systems

The mechanisms of enhancement by non-particulate carrier systems are better understood. Chelating agents, usually chelators of calcium ions such as sodium EDTA (ethylenediaminetetraacetic acid) and citric acid are known to act by complexing the $Ca^{+}$ ions that are functionally important in, maintaining the integrity of intercellular tight junctions (Artursson & Magnusson, 1989). Chelating agents do have the disadvantage that if they do get into a cell they can chelate the intracellular $Ca^{2+}$ ions possibly causing cell death. Surfactants such as bile salts and Laureth-9 have been shown to enhance drug absorption by forming reverse micelles in the cell membranes making an aqueous channel in the cell membrane through which hydrophilic drugs and other molecules present can diffuse (Chien

*et al.*, 1989). Bile salts have been studied extensively; however, their toxicity has been established using the frog palette model as being above that acceptable. Most bile salts caused irreversible ciliostasis in the test animal at concentrations that would be used therapeutically (Gizurarson *et al.*, 1990). Traditional surfactants such as Laureth-9 have also been shown to disrupt membrane integrity at therapeutically useful concentrations (Hirai *et al.*, 1981a). However, recent work with compounds such as glycofurol 75, a compound regularly used in co-solvent systems, have shown vast improvements in both reducing toxicity and enhancing systemic drug levels. Glycofurol 75 has shown good absorption enhancing effects and in the frog palette model shows only a slight reduction in mucociliary clearance Bechgaard *et al.*, (1996). Absorption enhancement by modifying the apparent surface of the molecule by means such as inclusion complexes, for example cyclodextrins, where a hydrophilic molecule nestles into the centre of the cup, with the hydrophobic outside of the cyclodextrin being presented to the body, have been proved to be efficient absorption enhancers and tolerable to the body to a lesser extent than the Glycofurol 75, but much better tolerated than the bile salts (Merkus *et al.*, 1993)

### 1.4.4 Formulation effects

The final form of a nasally administered dosage form has a significant effect on the effectiveness of the formulation. The most obvious example is the removal of particulate matter, by the hairs in the squamous epithelium before they reach the respiratory epithelium. There are several possible ways of delivering nasal doses: as nose drops, as a spray, an aerosol spray, and an insufflator. They each have different characteristics as to the pattern of drug deposition on administration (Chien *et al.*, 1989), however there is very little information available as to these characteristics.

The use of spray and nose-drop systems has been studied; $^{99}$Tc labelled human serum albumin was administered as either nose drops or as a spray and the biodistribution and progress of the label monitored. After an initial rapid clearance phase, the spray formulation proved to have a longer retention time in the nasal cavity than the nose drop formulation. Similarly, studying systems such as dimethyl cyclodextrin administered with

insulin as either a solution or a powder (Schipper *et al.*, 1993) reveals that the powder formulation is significantly more efficacious, although no reason for the difference seen in this study have yet been proposed.

## 1.5 Models for nasal delivery

Models are available for many of the potential routes of administration, both *in vivo*, and *in vitro*. These systems aim to represent the conditions experienced when the drug is presented to the human system.

For nasal delivery, the results that have been reported are, with a small number of exceptions based on animal experiments, or those using *ex vivo* techniques such as isolated rabbit mucosa in an Ussing chamber. There have been many different animal models used and also a variety of techniques. In some instances, such as vaccine delivery there is no alternative to *in vivo* experiments as there is no way at present to model an immune response.

During development, *in vitro* techniques hold the advantages over *in vivo* techniques in a number of ways, firstly the experimental control of the conditions encountered; secondly, the separation of the initial permeation or uptake from subsequent *in vivo* effects such as body distribution and [illegible] thereby limiting the number of animal experiments performed.

### 1.5.1 *In vivo* models for nasal delivery

For *in vivo* work there are three main techniques that are or have been used, these are i) *in vivo* perfusion, ii) *in vivo* surgical delivery and iii) *in vivo* non surgical-delivery. There are disadvantages associated with each technique, and more importantly, because of the differences in experimental methods results can not be compared between techniques.

### 1.5.1.1 The *in vivo* perfusion technique.

This is the earliest reported technique (Hirai *et al.*, 1981b), and can be considered as an isolated organ perfusion model. The nasal cavity is isolated by the sealing of the nasopalatine passage, cannulation of the trachea, and the cannulation of the oesophagus with the cannula extending in the direction of the nasal cavity and entering the posterior part of the cavity. A drug solution is then perfused into and through the nasal cavity, entering *via* the oesophageal canula, and draining from the nostril into a reservoir to be re-cycled back to the nasal cavity. This technique is performed under terminal anaesthesia with the animal on its back in a head slightly down position as shown in Figure 1.9.

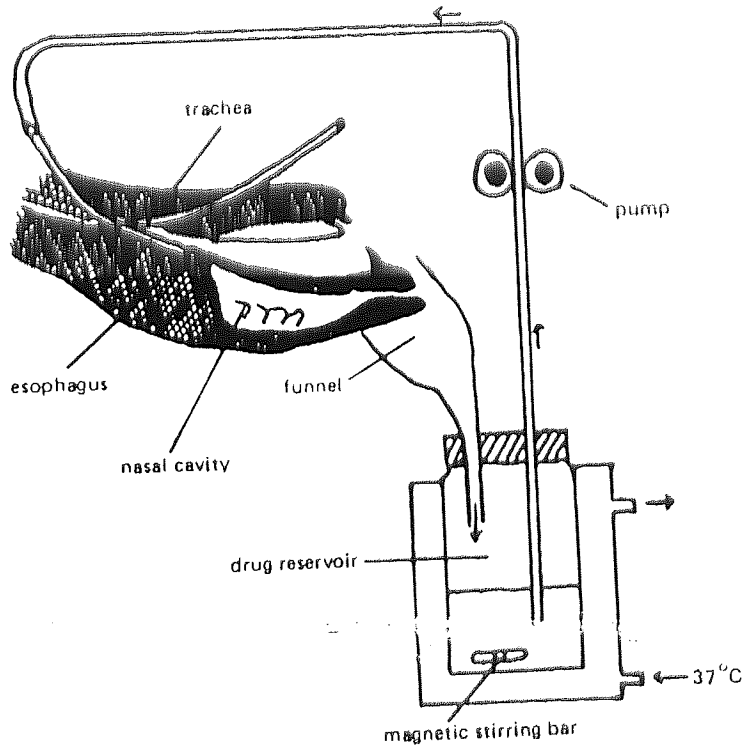


**Figure 1.9** The experimental set-up for *ex vivo* nasal perfusion studies. (Chien *et al.*, 1989)

This technique has been used extensively to study drug absorption and permeability (Chien *et al.*, 1989) and also enzymatic stability studies. Using this technique, sampling is easily performed as the disappearance of the drug, or the appearance of metabolites in the perfusate, can be monitored. However, there are two disadvantages of this technique, they are: the sorption of the drug onto the plastic or glass used in the apparatus and the evaporation of the solvent used, especially in long experiments (Illum, 1996). This

technique also introduces a variable that no other techniques use, that of perfusate volume. The volume of the perfusate has been shown to affect the levels of drug absorption (Hirai, 1981b).

### 1.5.1.2 *In vivo* surgical delivery

The *in vivo* surgical technique (Hirai *et al.*, 1981a) is a whole animal model that is mostly used in rats. Like the *in vivo* perfusion technique the trachea is cannulated, however, the oesophagus is cannulated with a blocked cannula, having the effect of blocking the oesophagus (Figure 1.10). The nasopalatine passage is sealed, the drug (generally a liquid) is administered to the nasal passage *via* the nostrils, and then the nostrils are sealed to prevent any drug loss. The absorption of the drug can then be monitored by its appearance in the blood stream. As with the perfusion technique this is done under terminal anaesthesia with the animal on its back.

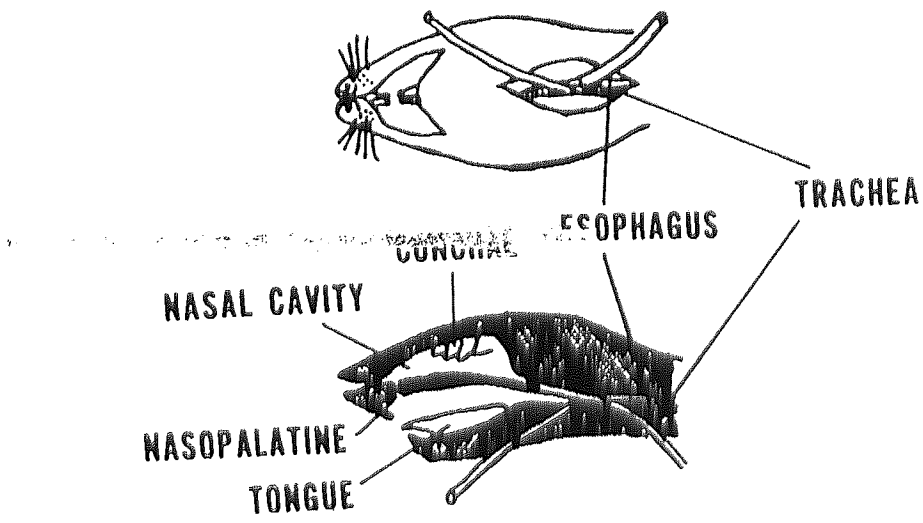


**Figure 1.10** *In vivo* surgical delivery, top and side view showing cannula arrangement for studies performed in rats. (Chien *et al.*, 1989)

Unlike the perfusion technique (1.5.1.1) this is a whole animal model rather than an isolated organ system. A small volume of a more pharmaceutically relevant solution can be administered and, rather than monitoring the drug disappearance from the donor solution,

either the pharmacological effect (for example, blood glucose levels after insulin delivery) or plasma concentration can be monitored.

### 1.5.1.3 *In vivo* non-surgical technique

This is a development from the surgical delivery technique, that has the advantage that there is no surgical modification. The animal is sedated but usually still conscious to allow delivery of the drug *via* the nostrils without loss from reflexes such as sneezing. Since this technique has the closest resemblance to the delivery that a drug would experience in humans this is the most currently used system.

All animal techniques use sedation of the animal to some degree. However, work (Mayor and Illum, 1994) has shown that the degree of sedation, from mild sedation to deep surgical anaesthesia, has a significant effect on the amount of drug absorbed, which increases as the depth of sedation through to anaesthesia increases. Long-acting injected anaesthetics such as pentobarbitone have a greater effect than short-acting inhalation anaesthetics such as halothane (or fluothane) which have a greater effect than a sedative. It is suggested that the mechanism of this absorption enhancement is the inhibition of mucociliary clearance accompanied by the lack of drainage of the nasal mucosa during anaesthesia, increasing the length of time the drug is in contact with the nasal mucosa. The inhibition of mucociliary clearance by anaesthesia has been shown in the rat trachea (Patrick and Sterling, 1977). This increase in absorption across models is well illustrated by a study on the absorption enhancing properties of dimethyl-β-cyclodextrin (Merkus *et al.*, 1991), the absorption of insulin from a cyclodextrin formulation was reported as 108% in the anaesthetised rat, however, in the sedated rabbit and unsedated human, the absorption was practically zero. Although this is a comparison across 3 different species it is unlikely that the difference is due entirely to interspecies difference.

### 1.5.2 Animals used for *in vivo* studies

There are several animal models used for *in vivo* work, each model has its advantages and disadvantages. When considering animal models on the anatomical scale, there are major differences between humans and the commonly available laboratory animals. The most fundamental difference is that human noses are microsomatic and the majority of animals used have macrosomatic noses. Human (microsomatic) noses are relatively simple organs and primarily concerned with the modification of inhaled air, however macrosomatic noses are much more complicated, significantly they have a much larger (*per* kg body mass) epithelial surface area, with a larger proportion of this dedicated to olfaction which is of great importance to the typical laboratory animals in their natural environment. Table 1.2 shows the nasal cavity characteristics of laboratory animals compared with humans. Although on the anatomical scale there are significant differences, morphologically they are similar to the human nose (Phallen *et al.*, 1984).

#### 1.5.2.1 The rat model

The rat is the most commonly used laboratory animal for nasal delivery studies (Illum 1996; Chien *et al.*, 1989). The rat holds many advantages over other species of laboratory animal, i) cost, ii) easy to maintain iii) breeds and matures readily, iv) easy to handle and v) only small drug quantities are needed (Illum, 1996). Typically, rats are used in the mass range 250 to 300g. Although there are many strains of laboratory rats, the Sprague-Dawley and Wistar rats are the most commonly used.

| Species | Surface Area ($cm^2$) | Surface Area/kg bodymass | Volume ($cm^3$) | Length (cm) | Complexity |
|---|---|---|---|---|---|
| Man | 181.0 | 2.5 | 19.0 | 6.0 | Simple scroll |
| Monkey | 61.6 | 7.7 | 8.0 | 5.3 | Simple scroll |
| Sheep | 327.0 | 8.2 | 114.0 | 18.0 | Double scroll |
| Rabbit | 61.0 | 20.3 | 6.0 | 5.2 | Complex scroll |
| Guinea Pig | 27.0 | 45.0 | 0.9 | 3.4 | Complex scroll |
| Rat | 10.4 | 41.6 | 0.4 | 2.3 | Complex scroll. |

**Table 1.2** Nasal characteristics of different species. (Illum L. 1996)

As with all of these laboratory animals, rats have a larger proportion of their nasal epithelium as olfactory in nature, around 50% (Popp and Monteiro-Riviere, 1985). The nasal mucosa has a much larger surface area *per* kg body mass than humans due to the more complicated nature of the turbinates, there are also other anatomical differences such as the presence of the nasopalatine duct and the septum being incomplete allowing air to pass from one side of the nasal cavity to the other. The nostrils of the rat are small, making it difficult to get drugs especially those in powder form, into the nasal cavity.

### 1.5.2.2 The guinea pig model

The guinea pig, (from the number of papers published) is a much less frequently used animal. Compared to the rat, the guinea pig is more expensive to keep, takes longer to mature, breeds less readily and is less easy to handle. Within the UK, there are also significant problems using the guinea pig, under the Animals (Scientific Procedures) Act (1986) for example, removal of blood is difficult. Volumes of up to 0.2 ml can be removed from the leg vein with some difficulty, however larger volumes have to be removed *via* cardiac puncture under sedation. This is only allowed twice, once in surviving animals, then the second blood removal immediately prior to sacrifice. Since the guinea pig is a larger animal, larger amounts of drug are required, this might not be a problem for development work using an existing drug, for example insulin, however, for novel compounds, this can quite easily become an important factor. The strains that are used are the Dunkin-Hartley and Sewel-Wright, experimented on at about 2-3 months old, weighing about 250 to 300g.

### 1.5.2.3 The rabbit model

Rabbits, although a lot more expensive than rats, are commonly used as an experimental model, both *in vivo* and also *ex vivo* (Bechgaard *et al.*,. 1992). Since rabbits are friendly, calm and easy to handle there are no difficulties associated with their dosing and they can be dosed without anaesthetic, although a mild sedative would help prevent drug loss by sneezing. Studies on both the delivery of vaccines (Gizurarson *et al.*, 1991) and drugs have been reported. Typically New Zealand white rabbits are used within the mass range 2.5 to 3 kg.

The nasal anatomy of the rabbit is significantly different from both humans and the other commonly used laboratory animals. The nasal cavity consists of two parts, the anterior respiratory epithelium, and the posterior olfactory and sensory epithelium. These can be considered as separate units as the mucus from the anterior region does not come into contact with the posterior region and, instead, drains into the pharynx before contact with the latter region. The septum runs the entire length of the region and has turbinates over both the anterior and posterior regions.

### 1.5.2.4 The sheep model

The sheep has had very little use as a model, being only used by two research groups, those of Longenecker and of Illum. This lack of use is possibly due to some of the disadvantages of the sheep, it is a large outdoor animal, hence requires significantly more space than other species, and it is difficult to keep under controlled conditions. The animals size is probably the major problem, as animals are usually 30-60 kg at the start of an experiment, large quantities of drug are required. The only reported studies have been on existing drugs that have poor bioavailabilities by other routes such as insulin (Longenecker *et al.*, 1987), and human growth hormone (hGH) (Baldwin *et al.*, 1990).

Of all the animals being considered, we can see from Table 1.3 that the sheep has the closest nasal cavity characteristics to that of the human, the obvious exception being the primates which are not under consideration as a model due to the controversy which surrounds their use (Baldwin *et al.*, 1990).

Previously the absorption enhancing properties of dimethyl-β-cyclodextrin (Merkus *et al.*, 1991) was considered, this was a comparison across 3 different techniques, different levels of anaesthesia, and different species. The large differences reported between the species are a result of both the method, anaesthesia and species. This highlights the pitfalls that are introduced when results obtained from several species (needing different techniques) are compared.

### 1.5.3 *In vitro* models of the nasal epithelium

The *in vitro* models of the human nasal epithelium can be divided into two types, cell or tissue culture, and *ex vivo* techniques such as the isolated rabbit mucosa used in an Ussing chamber. The advantage of *in vitro* models is that they represent a way of producing reproducible results and that they permit the mass screening of both drugs and formulations. Transport and uptake of either drugs, or complete formulations can be studied.

#### 1.5.3.1 Cell and tissue culture epithelial models

Traditionally, cell and tissue culture models have been used to study both drug transport and uptake for oral delivery, cell lines such as Caco-2 and HT-29 are well established for this purpose (Bailey *et al.*, 1996), and are developed to such a level that they can be used to screen drugs produced in drug discovery programmes for potential absorption problems, and for selection of drugs with "optimal passive transport kinetics" (Artursson *et al.*, 1996). Cell culture can be split into two kinds, primary and secondary culture. Primary cell culture is the growth *in vitro* of freshly obtained mammalian cells, whereas secondary culture is the growth and maintenance of an immortalised cell line. In primary culture, the cells have a very limited time-span as they can only survive in culture for a limited time. However, in secondary cell culture, the cells are usually from a cancerous source and can multiply indefinitely. So with periodic reduction in numbers of cells present (splitting, or passaging) and judicious management of cell stocks, the cell line remains indefinitely, however the characteristics of the cells do change over time with the formulation of sub-cultures. Both Caco-2 and HT-29 intestinal cell lines are secondary cultures. However, for nasal delivery there is at the moment no secondary cell culture model. For nasal cell culture and also respiratory cell culture in general (Mathias *et al.*, 1996), models are limited to primary cell culture for a variety of reasons, but mainly the loss of ultrastructural characteristics such as the ability to form tight junctions.

Primary culture of nasal epithelial cells as a model for delivery studies has been reported by only one group, that of Kissel (Werner and Kissel, 1995). This method relies on

the enzymatic separation of the epithelial cells from the underlying tissue (*in vitro*) after surgical removal of nasal turbinates during operations such as turbinatectomies. Before this work, the nearest model was explanted tracheal tissue from the hamster (Newton *et al.*, 1980). Previous attempts at culturing nasal and tracheal tissue resulted in poor morphological characteristics (Audus *et al.*, 1990). However, human nasal and tracheal cells have been maintained in culture to allow analysis of their basic functional and biochemical characteristics. The lectin biochemistry (Mariassy *et al.*, 1988), electrical resistance (Widdicombe *et al.*, 1981), of nasal tissue has been investigated.

Secondary cell culture of cell lines based on the nasal epithelium is possible with two well-established cell lines, BT (bovine in origin), and RPMI 2650 (from cancerous human septum). Comparison of the lectin biochemistry and other characteristics of these cell lines with the primary cultures of human nasal epithelium however, proves their unsuitability for transport studies as they have been proved to have lost the ability to form tight inter-cellular junctions and are undifferentiated in nature (Werner and Kissel, 1996).

The conclusions that can be drawn from the data available in the literature is that at the moment, with the exception of primary culture of human nasal epithelium acquired from turbinates removed during surgery there is no cell culture model available.

If a cell culture model, especially a secondary cell culture model can be developed there are several advantages that it will offer, i) rapid assessment of potential permeability and potential drug metabolism, ii) elucidation of molecular mechanism of drug transport and pathways of drug degradation, iii) rapid evaluation of methods of drug targeting, enhancement of transport and minimising metabolism, iv) use of human rather than animal tissues, and v) minimise expensive and controversial animal experiments (Audus *et al.*, 1990).

### 1.5.3.2 The vertical Ussing chamber

The vertical Ussing chamber has been used as a model system for nasal delivery studies (Bechgaard *et al.*, 1992; Wheatley *et al.*, 1988). The Ussing chamber was developed in the 1950's by Professor Ussing at Copenhagen University; it consists of two independent half-cells with excised tissue clamped between them as illustrated in Figure 1.11. Since the tissue is mounted vertically this chamber system is called the vertical Ussing chamber. The tissue is bathed in an oxygenated buffer solution such as glucose ringer solution (Bechgaard *et al.*, 1992), bicarbonate ringer solution (Wheatley *et al.*, 1988), or Krebbs ringer solution (Östh & Björk, 1997a)

However, the disadvantage of the Ussing chamber, or any other chamber, is that a membrane is needed to separate the two chambers. This membrane is nasal epithelial tissue excised after sacrifice of a suitable donor, for nasal epithelium to be used the smallest animal that can be used is a rabbit, and each animal sacrificed only provides tissue samples for two experimental runs. The use of isolated rabbit mucosa has been reported by a number of people, (Cremaschi *et al.*, 1990; Bechgaard *et al.*, 1992). The viability of the excised tissue in this system has been thoroughly tested, the electrophysiological data suggests that the isolated membrane is viable for well in excess of the time that any experiment of stability or transport would require at over 12 h.

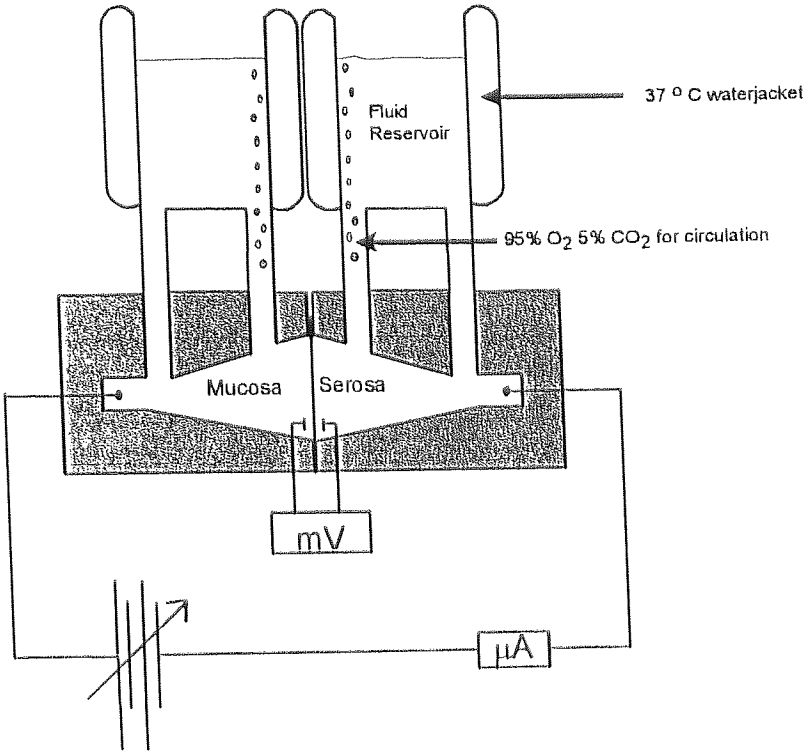


**Figure 1.11** Arrangement of the traditional vertical Ussing chamber

### 1.5.3.3 The horizontal Ussing chamber

The vertical Ussing chamber is a well-established technique; recently a horizontal version has been marketed by Corning Costar. This chamber system (Figure 1.12) is similar to that of the vertical chamber with electrodes for viability measurement, and is marketed for use with the Costar Snapwell cell culture insert system. The major difference is that the tissue is mounted horizontally. Recently, Östh *et al.* have tried to use this system with pig nasal tissue. They used this system in very much the same way as the vertical system, however they achieved poor reproducibility with regards to the operation of the chamber (Östh and Björk, 1997a) and non optimal conditions such as poor oxygenation method, large liquid volumes (>100ml), and other unspecified problems (Östh and Björk 1997b).

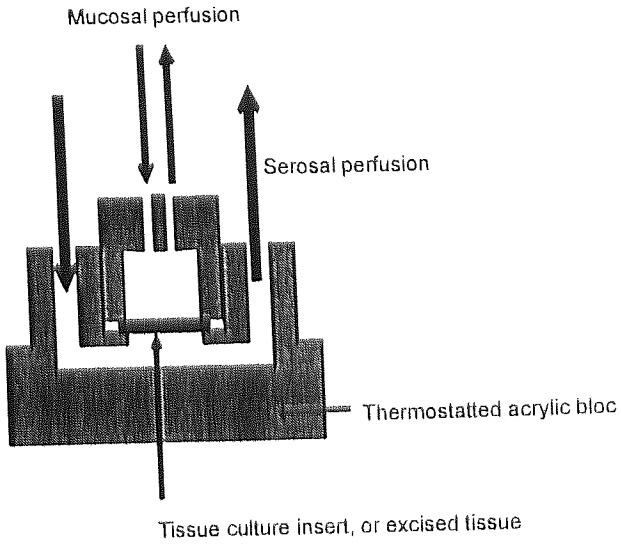


**Figure 1.12** Arrangement of Costar horizontal Ussing chamber

As experimental techniques the vertical and horizontal Ussing chambers are not without their disadvantages, from experience the excision and mounting of the tissue in the chamber is a very difficult and exceptionally delicate procedure, which is not helped by the necessity of excising the tissue as quickly as possible to avoid any unnecessary loss of viability. However, work such as this is done using animals such as the rabbit (Bechgaard *et al.*, 1992) and the sheep (Wheatley *et al.*, 1988), there is unfortunately no information concerning the correlation between Ussing chamber data and those obtained from both *in vivo* studies and from clinical trials. For drug transport or permeation studies, there could be several factors affecting the results obtained, most obviously the thickness of the mucosa. The technique used for the removal of the mucosa is described in detail in chapter 3, but the technique used does result in variations in the thickness of the tissue obtained. From simple observation, rabbit mucosa is very thin at less than 1 mm, sheep mucosa is much thicker at 2-3 mm whilst that of the pig is about 1mm thick. As well as these inter-species differences, there are also the expected inter-animal variations and the differences within each tissue sample if different areas of the tissue are considered. These techniques were not developed specifically for nasal tissue, they are both techniques more commonly applied to tissues from within the GIT. From the dearth of literature available on the use of either the vertical or horizontal Ussing chamber as a viability system for nasal tissue, it could be concluded that there is either a lack of interest in this area, or there are unreported problems

with these systems that have resulted in such low levels of *in vitro* / *ex vivo* work being performed.

## 1.6 Aims and objectives of this study

Nasal delivery is a subject in which there is significant current interest, there are however, only two *in vitro* models currently available for nasal delivery studies, the horizontal, and vertical Ussing chambers. Both of these systems provide an artificial environment for excised nasal tissues. The broad aim of this thesis is to devise and develop a novel system for the *in vitro* or *ex vivo* investigation of nasal delivery. The resulting system should encompass the following key objectives.

- The chamber system produced should be equally suitable for the nasal tissue it is designed for, and for potential use with cultured cells.
- Viability should be comparable, or superior to those obtainable using existing techniques.
- Tissue should be maintained in such a way that pharmaceutically realistic formulations, such as powders or aerosols, can be applied.
- The chamber should, as a function of its design, be simple, readily produced, easily used, and reliable in all of its workings.
- The chamber should be able to provide mechanistic insight into the processes following administration of powder (especially microparticulate) delivery systems as well providing kinetic data similar to those available currently from the Ussing chamber.
- The resulting system should be as flexible as possible in allowing further development for both other epithelial tissues such those from the GIT, and for adaptation to other pieces of scientific apparatus for general development of delivery devices and systems.

It should be borne in mind that the viability of the system will be dependent on the ability of the eventual user to produce reliable, relevant data from this system.

# Chapter 2

## Tetrapeptide stability
## – development of an NMR Technique for stability investigations

## Overview

In this chapter a real-time, *in vitro* model for assaying the enzymatic stability of drugs is developed. In this model small peptide drugs (tetrapeptides) that are difficult to quantify by either HPLC or gel electrophoresis are studied by NMR spectroscopy. The advantage of using this technique is that not only is the quantification of the degradation possible, but that the result of the degradation can be seen.

## 2.1 Introduction. The stability of peptide and protein drugs

Peptide and protein therapeutics are prone to degradation once they enter the body. There are several ways that they can be broken down, the most important of which is the enzymatic hydrolysis of the peptide bond resulting in its cleavage. There are also many other reactions that occur which have a negative effect on proteins and peptides, these include deamination of asparagine residues, oxidation of residues such as methionine, and cysteine, rearrangement of aspartic acid residues, and the reduction of disulphide bridges. With larger peptides and proteins, instability does not have to result in their breakdown to smaller units, aggregation to form for example dimers can destroy the action of a protein.

The model peptides that are being used in this study should in theory be susceptible to proteolysis (2.1.1), rearrangement (2.1.2, the aspartate rearrangement) and oxidation (2.1.3). These mechanisms are considered below.

### 2.1.1 Proteolysis

Proteolysis is the hydrolysis of a peptide bond catalysed by a proteolytic enzyme. The mechanism of peptide bond hydrolysis is shown in Figure 2.1.

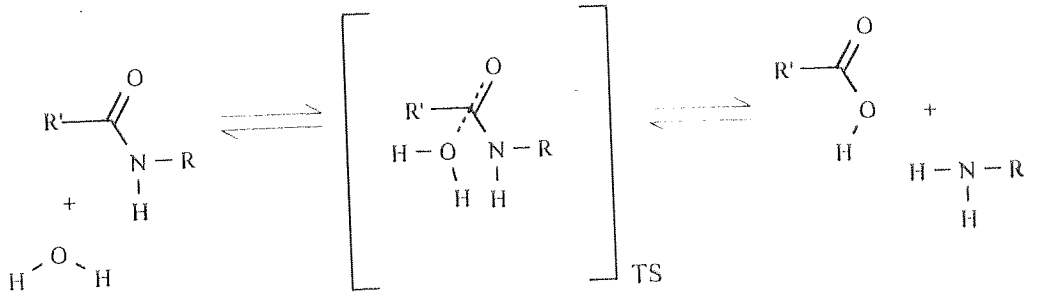


**Figure 2.1** Uncatalysed peptide bond hydrolysis
TS is the Transition State.

This uncatalysed reation is very slow, water is a poor nucleophile (electron-donating agent), and the carbonyl group in that state is a poor electrophile (electron-receiving group),

so the formation of the transition state is very slow and difficult. As previously discussed (section 1.3.3.4) proteolytic enzymes come in many categories depending upon their site of action, however they all act by one of a number of mechanisms, of which three are shown in Figure 2.2. All of these mechanisms increase the rate of hydrolysis by facilitating the formation of the transition state, and susequent the stabilisation of the transition state either by removing the charge from it, or by binding the transition state to the enzyme itself.

In general acid catalysis a weak acid donates a proton ($H^+$ ion) which attacks the carboxyl oxygen. The carboxyl oxygen is electron rich (δ-) and so this is an electrophilic attack, causing the movement of $e^-$ density from the carbon of the carboxyl group to the oxygen atom. This increases the net positive charge at the carboxyl carbon (ie more δ+). This net positive charge makes the carboxyl carbon more susceptable to nucleophilic attack, in this case it is then susceptible enough for water, which is a relatively poor nucleophile to attack, with the water losing a proton in the process.

1. General acid catalysis

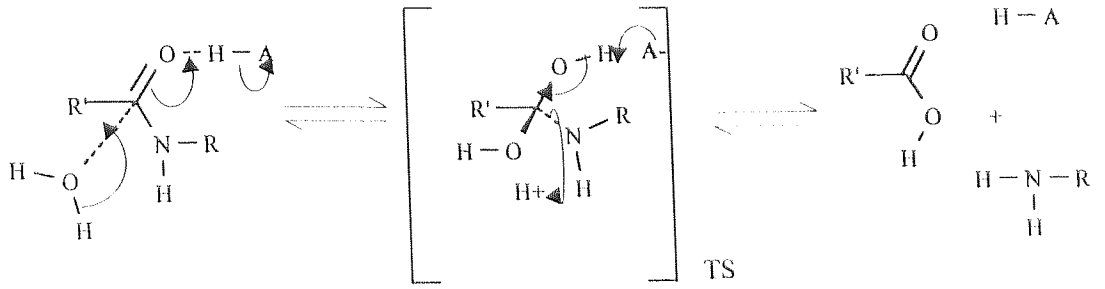


2. General base catalysis

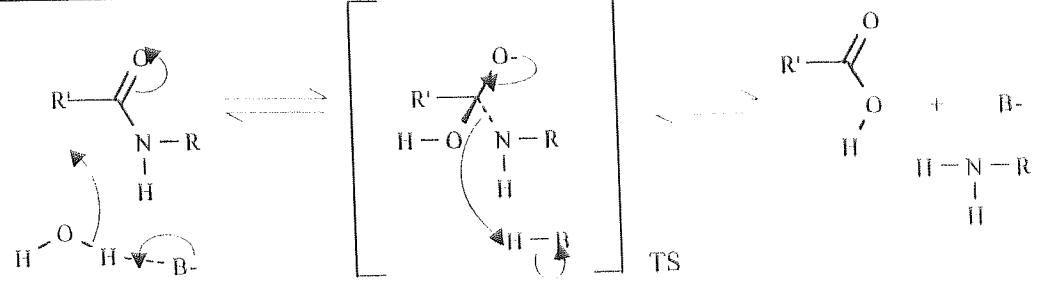


3. Metal ion catalysis

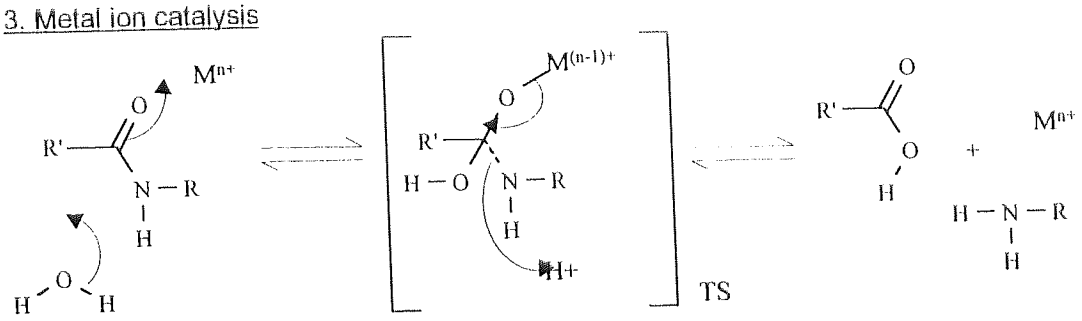


**Figure 2.2** General mechanisms for proteolysis.

In general base catalysis, rather than increasing the susceptability of the carboxyl carbon to nucleophilic attack, the nucleophile is made stronger, and hence the nucleophile is a strong enough agent to attack the relativley unsusceptable carboxyl group. The nucleophile in the uncatalysed reaction is water. In general base catalysis this is deprotonated in situ by a strong base, to form a hydroxide ion.

Metal ion catalysis involves the presence of a positivley charged ion in the active site of the enzyme. The positive charge of the ion initially interacts with the carboxyl oxygen changing the $e^-$ density distribution, increasing the net positive charge on the carboxyl

carbon. As with the general acid catalysis this causes sufficient change in the susceptability of the carboxyl group to nucleophilic attack that the water can then react to form the tetrahedral transition state.

### 2.1.2 The aspartate rearrangement

Aspartic-acid residues, under the correct conditions, undergo a rearrangement leading to the formation of a cyclic imide. This ring can then open in one of two ways, one reforming the aspartic acid, and the other forming the β form of aspartic acid. The mechanism is shown in Figure 2.3 (adapted from Wright *et al.*, 1991). This mechanism and that of the deamination of asparagine and glutamine to aspartic acid and glutamic acid respectivley are identical in all respects other than starting material.

Stage One:- formation of cyclic imide

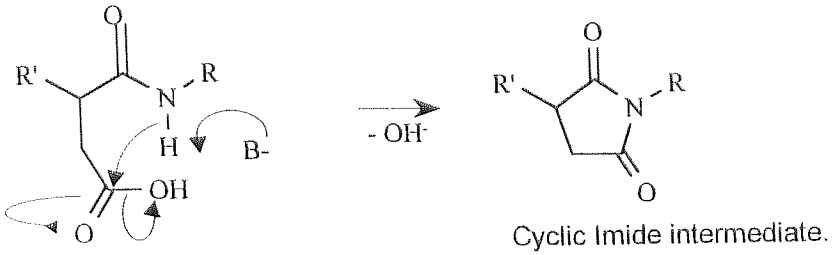


Cyclic Imide intermediate.

Stage Two:- Ring opening

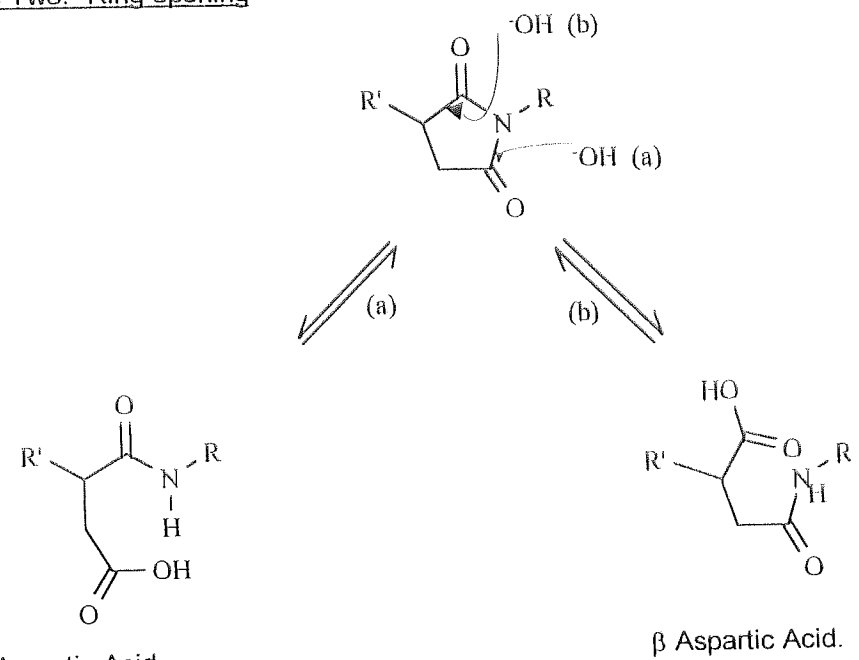


Aspartic Acid

β Aspartic Acid.

**Figure 2.3** Mechanism of the aspartate rearrangement.

## 2.1.3 Oxidation

Several amino acids are susceptable to oxidation including methionine and cysteine. From studies done on human growth hormone (hGH) oxidation has been seen as a degradation pathway in solution (Becker *et al.*, 1988) and when stored as a lyophilised powder (Pikal *et al.*, 1991). The rate of degradation by oxidation was increased when the lyophylised powder was stored under 90% $O_2$, suggesting that atmospheric oxygen plays a significant role in this degradation pathway. In the case of hGH the residue that was most susceptable to degradation was methionine, however, with larger peptides and proteins such as hGH (191 residues) that have a well defined tertiary structure, there exist the possibility that susceptible residues can be in such a place that oxidation does not occur

possibly due to their inaccessibility to oxidising agents. An example of this resistance to oxidation occurs at Met-170 of hGH, under conditions that the other two methionine residues in the protein are oxidised.

Oxidation of specific residues does not necessarily remove the activity of the peptide or protein. Again, using hGH as an example, the partial oxidation of the two oxidisable residues had no effect on its activity, whereas in the fully oxidised state the activity was reduced to a quarter of what it was (Teh *et al.*, 1987).

The oxidation of one amino acid, cysteine, is very common. Cysteine residues form di-sulphide bridges on oxidation. These are links between two cysteines that are some distance apart. These bridges are a fundamental part of the 3-dimensional (3D) structure of a protein or peptides. However, their oxidation can lead to bonding that distorts the 3D structure of the protein or peptide.

These residues that are susceptable to oxidation, and their oxidation products are illustrated in Figure 2.4

### 2.1.4 Detection of tetrapeptides, and rationale for NMR study

The tetrapeptides used in this study (Figure 2.5) are analogues of a peptide under investigation by Rhône-Poulenc Rorer. Detection of the tetrapeptides by gel electrophoresis is not possible since the minimum molecular weight that can be retained on an SDS-PAGE gel is 6kDa. However, techniques such as HPLC can be used for peptides that have significant UV absorption, electrochemical potential, or fluorescence. Inspection of the structures would suggest that there is no potential for the use of any of these techniques. Using either of these two techniques would result in data describing the remaining complete peptide but not its degradation products.

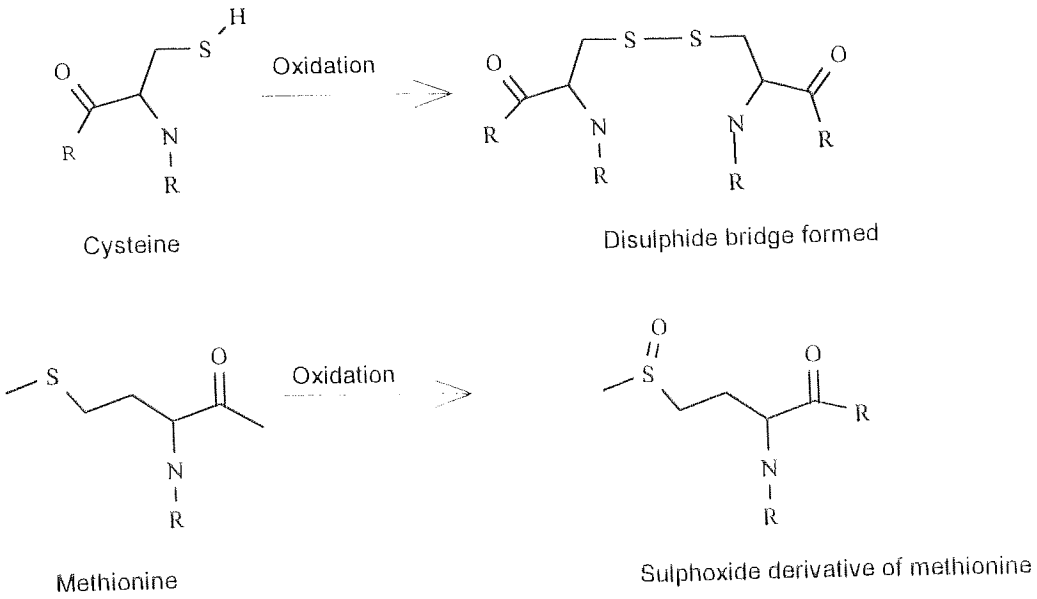


**Figure 2.4** Common oxidation products of amino acids.

$^1$H-NMR, on the other hand, relies on the presence of hydrogen nuclei which are present in all of the compounds of interest here, and since the degradation of the tetrapeptides is happening *in situ*, the technique should also pick up the appearance of the degradation products. The changes in the NMR spectrum should enable the rate of decomposition to be determined, and the structure of any degradation product also to be determined.

## 2.2 Materials

### 2.2.1 Peptides

Stability studies were carried out on the five tetrapeptides shown in Figure 2.5 (CBI, Richmond, Vancouver, Canada).

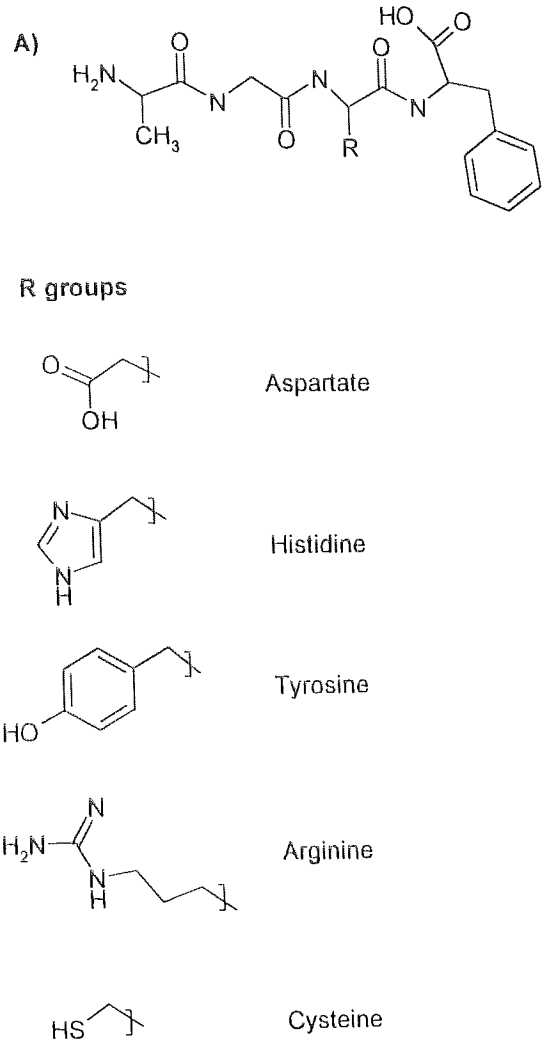


**Figure 2.5** Tetrapeptides used in NMR study. A) peptide backbone, R represents the amino acid changed during the study.

### 2.2.2 General reagents

Sodium dodecylsulphate polyacrylamide gel electrophoresis (SDS-PAGE) reagents were obtained from Bio-Rad (Hemel Hempsted, UK). All other chemicals, unless otherwise stated were purchased from Sigma (Poole, Dorset, UK).

### 2.2.3 NMR Reagents

For NMR experiments the solvents used were all obtained from Sigma, without TMS, greater than 99.9 atom %D, and designed specifically for NMR use. NMR Tubes used were Norell 506P acquired from Sigma.

## 2.3 Methods

### 2.3.1 SDS-Page Electrophoresis.

Electrophoretic separation of proteolytically active proteins collected from human nasal wash was carried out by SDS-PAGE using a BioRad Miniprotean vertical gel apparatus. SDS-PAGE gels were made according to the protocols set out in Maniatis *et al.*, (1989). In all gels a molecular weight marker was used (SDS-7, Sigma). Gels were stained using Coomassie Blue stain, destained and photographed using a UVP transilluminator and camera attached to an IBM-compatible computer (PC) running the Grab-It software package.

### 2.3.2 NMR sample preparation, and NMR operation

For all NMR stability studies NMR spectra were collected on a Bruker AC250 spectrometer. All spectra obtained were of $^1H$ and each one was 64 scans. Unless otherwise stated the machine was equilibrated to $37^0C$ before each run. Samples were referenced to the DOH peak.

For identification and peak analysis $^1H$ spectra of all peptides were run. Peptide (10 mg) was dissolved in 1.5ml $D_2O$, and placed in an NMR tube after filtration through a cotton plug placed in a glass Pasteur pipette. All FID were analysed using the WIN-NMR software. All experiments, except those for peak identification, were performed in triplicate. Errors are expressed as the standard deviation.

### 2.3.3 NMR Identification of tetrapeptides

To assign NMR peaks, homonuclear decoupling experiments were performed using the built-in decoupler irradiating at the frequency determined by the standard instrument software.

### 2.3.4 NMR Enzymatic stability assay

The tetrapeptide (25 µmol) was dissolved in enzyme buffer (1.5ml) and placed in an NMR tube. NMR spectra without enzymes were obtained at 37$^{O}$C. In all cases, 5 activity units of the enzyme were subsequently added. The NMR sample tube was then either incubated inside the NMR machine at 37$^{O}$C for experiments requiring spectra obtained at regular time intervals or, for simpler experiments requiring one timepoint, spectra were obtained with the machine operating at room temperature, after a 1 h incubation in a 37$^{O}$C water bath. Degradation was observed by differences in the NMR spectra. Method validation and positive controls were performed using tri-glycine (Sigma) as this showed degradation under these conditions.

Quantification of the degree of degradation was taken as the mean deviation from the expected integral values for the peaks in the tetrapeptide, and from the peaks appearing as the degradation products are formed.

#### 2.3.4.1 Enzyme buffers used in stability work

The following enzyme buffers were used as they represent the conditions under which each enzyme is known to be active. As all of these buffers are pH dependent apparent pD values were measured with a standard pH metre.

i) Carboxypeptidase

A deuterated solution ($D_2O$ of NMR quality) of Tris( hydroxymethyl)methylamine (Tris) (25mM) and sodium chloride (0.5 M) at pD of 7.6 using HCl to adjust pD (pH of a

solution containing the majority $^{2}H$ - read from a standard pH meter) (Typically less than 2 ml for 10 ml of solution).

ii) Aminopeptidase

A deuterated solution of Tris (0.05mM) and manganese chloride (2.5mM) at pD 8.5.

iii) Elastase

A deuterated solution of Tris (250mM) at pD 8.8.

iv) Bromelain

A deuterated solution of sodium acetate (100mM) and sodium chloride (150mM) at pD 2.0 with HCl.

v) α-Chymotrypsin

A deuterated solution of Tris (80mM) and calcium chloride (53.3 mM) at pD of 8.8 using HCl.

### 2.3.5 Enzyme activity assay

To check that the enzymess and buffers used were active under the conditions used bovine serum albumin fraction V from heat shock (BSA) (Sigma) (10 mg) was digested in 1.5 ml buffer, with 5 units protease at 37$^{o}$C for 1 h. The resulting protein fragments were separated by SDS Page (5mg loaded per well) with uncut BSA as a control.

### 2.3.6 Total hydrolysis of tetrapeptides

Tetrapeptide (10mg) was dissolved in hydrochloric acid (6M, 1.5ml) and heated to 95$^{o}$C for 6 hs. The resulting solution was evaporated to dryness overnight in a fume hood. The powder obtained was re-dissolved in $D_2O$ and the NMR spectrum obtained.

### 2.3.7 Thermal stability studies

NMR spectra were obtained of the tetrapeptide in $D_2O$ solutions with apparent pD adjusted using HCl to 1.0, 2.5, 3.7, and 7.0. The NMR tubes were sealed and then

incubated at 80°C (oven) and spectra acquired after 1, 2, and 7 days, to maintain concentration any liquid loss was replaced by fresh $D_2O$ to the previous liquid level. Degradation was observed by changes in the NMR spectra.

### 2.3.8 Human nasal wash

Human nasal secretions were collected from a healthy human volunteer. Sterile double distilled water was administered nasally (1.25 ml per nostril) and retained in the nasal cavity as long as possible. The water and nasal secretions were collected by bringing the head forwards and allowing the water to run into a flexible plastic weighing boat. The secretions were freeze-dried, analysed by SDS-PAGE for size, and assayed using tri-glycine in the NMR protocol for enzymatic activity.

### 2.3.9 BCA Assay

Proteins were assayed using the method of Almeida (1994)

### 2.3.10 Stability of Tetrapeptides to human nasal wash.

The 5 tetrapeptide drug analogues were assayed for their stability to the collected human nasal using the NMR technique outlined previously. Lyophilised nasal wash (0.5 mg) was added to 20 mg of trial peptide and diluted to a suitable volume and concentration for NMR analysis using $D_2O$.

## 2.4 Results and discussion

### 2.4.1 Initial NMR peak assignments

Initially, $^{1}H$ spectra were run on 10mg samples of each of the five tetrapeptides, and the peak analysis is presented in tables 2.1 to 2.5. Since the peaks are used later for quantification of degradation, the peak assignments were checked by performing homonuclear decoupling experiments.

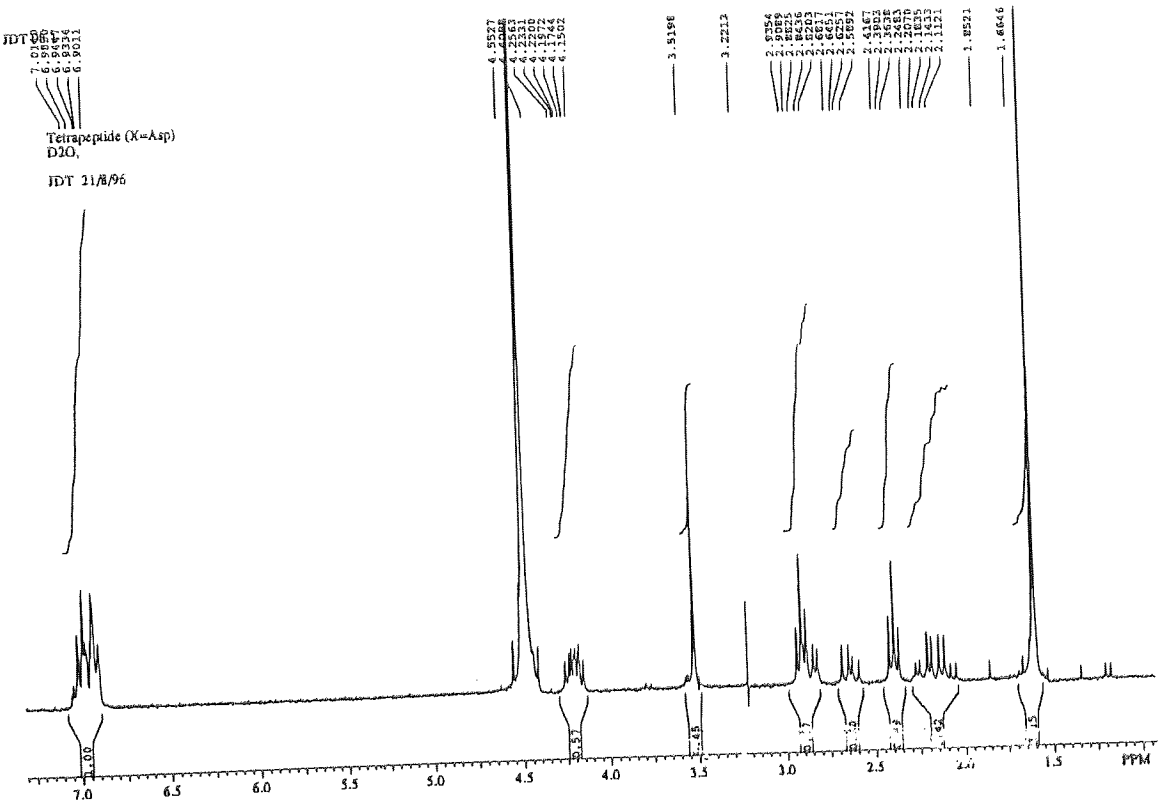


**Figure 2.6** $^{1}H$ NMR spectrum of Tetrapeptide 1, R = Asp. Referenced to δ DOH, 4.6

| Residue | Multiplicity | δ /ppm | Assignment |
|---|---|---|---|
| β Ala | Triplet | 2.91 | $CH_2$ (α or β) |
| | Triplet | 2.39 | $CH_2$ (α or β) |
| Gly | Singlet | 3.52 | $CH_2$ |
| Asp | Quartet of Doublets | 2.22 | |
| | Multiplet | 4.20 | |
| Phe-Amide | Multiplet | 6.99 | Aromatics |
| | Multiplet | 4.20 | Side Chain $CH_2$ |
| | Quartet of Doublets | 2.70 | α CH |

**Table 2.1** NMR Peak assignment, tetrapeptide 1 R = Asp

From the $^1H$ NMR of tetrapeptide 1 (R = Asp, Figure 2.6) the peak assignment above were made (Table 2.1). These were confirmed by the homonuclear decoupling experiments performed, as outlined with their results below in Tables 2.2 to 2.5.

| **Group Irradiated** | **Assignment** | **Group Affected** | **Assignment** |
|---|---|---|---|
| Triplet δ 2.39 | β ala $CH_2$ | Triplet δ 2.91 | β ala $CH_2$ |
| Triplet δ 2.91 | β ala $CH_2$ | Triplet δ 2.39 | β ala $CH_2$ |

**Table 2.2** Homonuclear decoupling to identify β ala $CH_2$

Irradiation of δ 2.39 triplet at 4245 Hz as shown in Figure 2.7 resulted in the triplet at δ 2.91 being reduced to a single peak. From the structure of the tetrapeptide there is only one possible combination that could cause this effect, the two adjacent $CH_2$ groups on the aspartate residue.

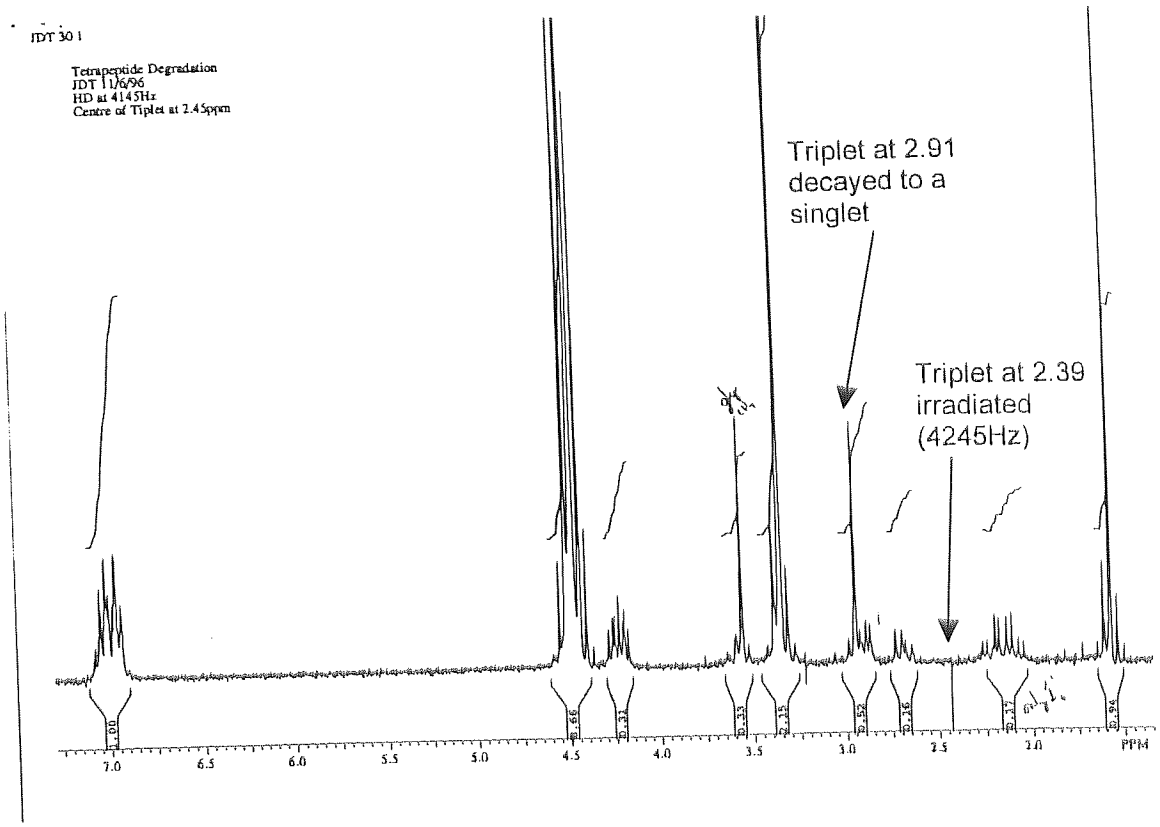


**Figure 2.7** $^1$H NMR spectrum of Tetrapeptide 1, R = Asp, homonuclear decoupled at 4245Hz. Triplet atd 2.91 has decayed to a singlet Referenced to δ DOH, 4.5

This confirms that the assignment of the two triplets is the β-ala $CH_2$-$CH_2$ system, however it does not separate them. The values of δ would suggest that the first triplet, δ 2.75, is probably the N terminal $CH_2$, whilst the 3.2 group is probably that nearer the carboxy group. This conclusion is based on the greater deshielding effect of the carboxyl group.

| Group Irradiated | Assignment | Group Affected | Assignment |
|---|---|---|---|
| Multiplet δ 7.2 | Phe aromatics | None | N/A |

**Table 2.3** Humonuclear decoupling of the multiplet δ 7.2

One might expect the multiplet at δ 7.2 to be connected to the side chain $CH_2$ group, however no coupling is seen, this is possibly due to the frequency at which the large multiplet was irradiated being sufficiently close to what it should be to colapse the multiplet, but not close enough to colapse any other group. These experiments were performed using the software supplied with the machine.

| Group Irradiated | Assignment | Group Affected | Assignment |
|---|---|---|---|
| Quartet of Doublets, δ 2.9 | Phe Side chain $CH_2$ | Multiplet δ 7.2 | Phe Aromatics |
| | | Multiplet δ 4.5 | Phe α CH |

**Table 2.4** Humonuclear decoupling of the quartet of doublets, δ 2.9

Although there was no coupling visible between the aromatic protons on the Phe ring and the side chain $CH_2$, however on irradiation of the peak that was suspected to be the side chain protons there was coupling visible with both the aromatic ring, and the α CH proton, confirming this assignment, and also that of the α CH

| Group Irradiated | Assignment | Group Affected | Assignment |
|---|---|---|---|
| Quartet of doublets δ 2.4 | Asp α CH | Multiplet δ 4.5 | Asp $CH_2$ (Side Chain) |

**Table 2.5** Humonuclear decoupling of the quartet of doublets, δ 2.4

Irradiation of the δ 2.4 quartet of doublets confirms that the multiplet at δ 4.5 contains the Asp side chain $CH_2$ protons as well as the Phe side chain $CH_2$ peaks

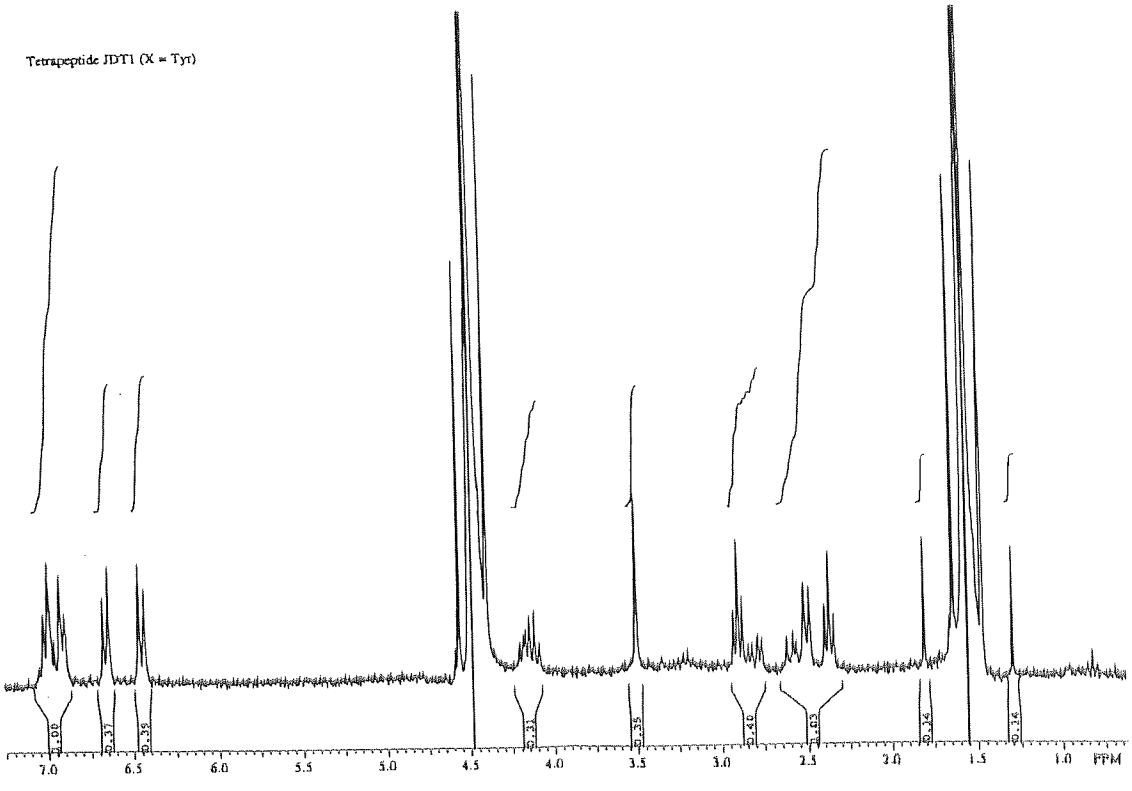


**Figure 2.8** $^1$H NMR spectrum of Tetrapeptide 2, R = Tyr. Referenced to δ DOH, 4.5

| Residue | Multiplicity | δ / ppm | Assignment |
|---|---|---|---|
| β Ala | Triplet | 2.91 | $CH_2$ |
| | Triplet | 2.39 | $CH_2$ |
| Gly | Singlet | 3.52 | α CH |
| Phe-Amide | Multiplet | 6.99 | Aromatics |
| | Quartet of Doublets | 2.70 | |
| | Multiplet | 4.20 | $CH_2$ (Side Chain) |
| **New Peaks** | | | |
| Tyr | Doublet of Doublets | 6.55 | Aromatic Ring |
| | Doublet | 2.55 | α CH |
| | Multiplet | 4.2 | Side Chain $CH_2$ |

**Table 2.6** Peak assignment tetrapeptide 2 R = Tyr

Assignment of the common backbone was performed by comparison of the $^1$H NMR spectrum (Figure 2.8) with tetrapeptide 1 (R = Asp, Figure 2.6) to produce the assignment above (Table 2.6). It should be noted that the Phe and Tyr side chain $CH_2$ groups are superimposed to produce the indecipherable multiplet.

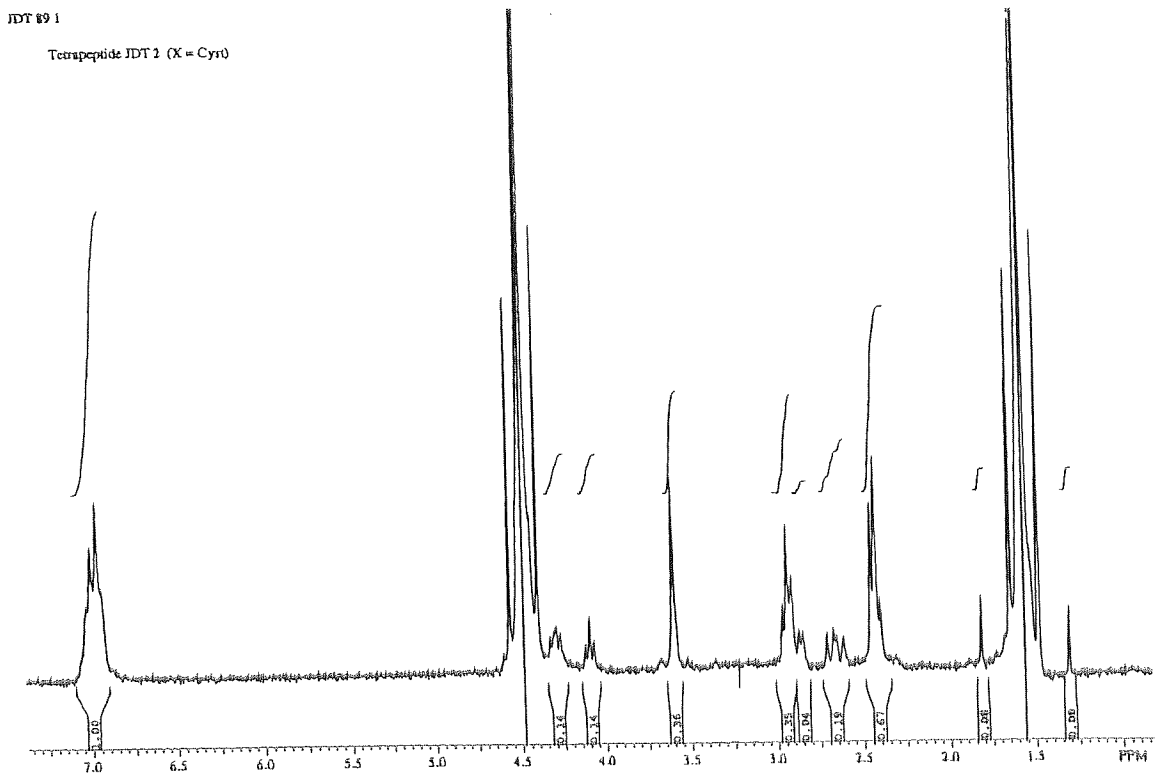


**Figure 2.9** $^{1}H$ NMR spectrum of Tetrapeptide 3, R = Cys. Referenced to δ DOH, 4.6

| Residue | Multiplicity | d / ppm | Assignment |
|---|---|---|---|
| β-Ala | Triplet | 2.95 | $CH_2$ |
| | Triplet | 2.4 | $CH_2$ |
| Gly | Singlet | 3.6 | α-CH |
| Phe-Amide | Multiplet | 7.0 | Aromatics |
| | Quartet of Doublets | 2.5 | α-CH |
| | Multiplet | 4.3 | $CH_2$ (Side Chain) |
| **New Peaks** | | | |
| | Doublet | 2.4 | α-CH |
| | Triplet | 4.2 | Side Chain $CH_2$ |

**Table 2.7** Peak assignment tetrapeptide 3 R = Cys

The assignment (Table 2.7) of δ 2.4 as both the β Ala CH2 and the Cys α CH (Figure 2.9) was confirmed by the integral of the combined peaks, as it represents 4 protons, not the two that would be expected for either peak.

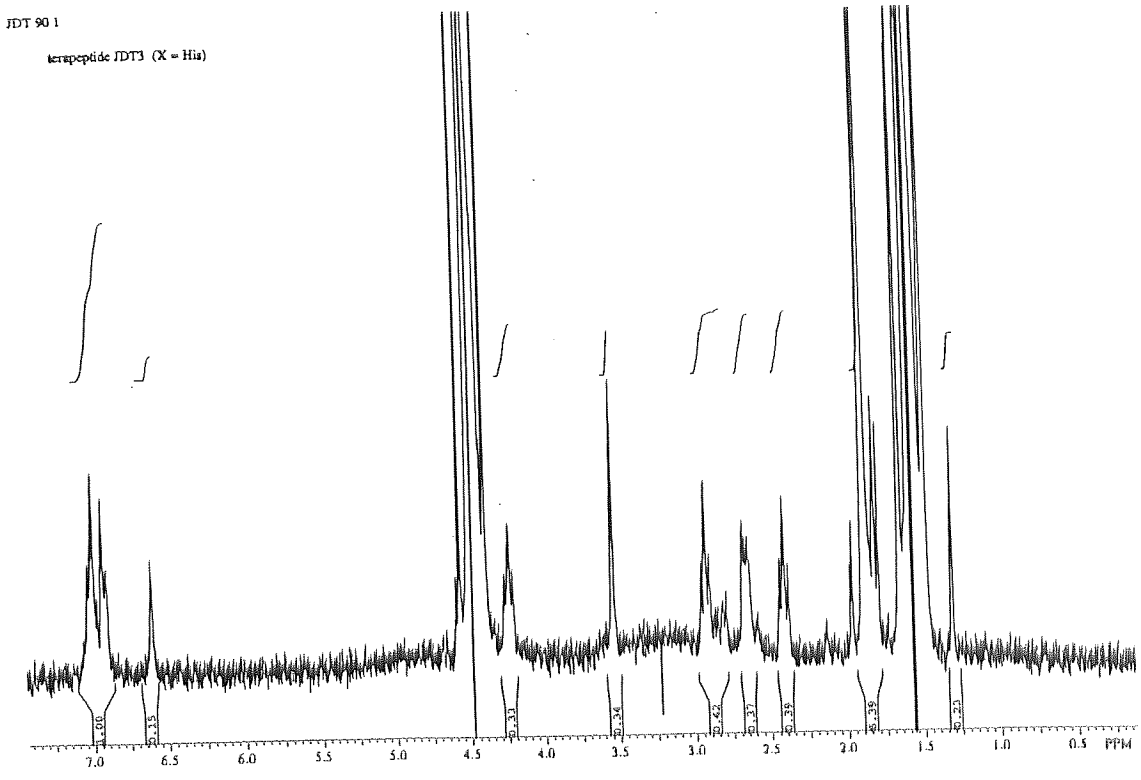


**Figure 2.10** $^{1}$H NMR spectrum of Tetrapeptide 4, R = His. Referenced to δ DOH, 4.6

| Residue | Multiplicity | δ / ppm | Assignment |
|---|---|---|---|
| β Ala | Triplet | 2.9 | $CH_2$ |
| | Triplet | 2.4 | $CH_2$ |
| Gly | Singlet | 3.6 | α CH |
| Phe-Amide | Multiplet | 7.0 | Aromatics |
| | Quartet of Doublets | 2.5 | α CH |
| | Multiplet | 4.5 | $CH_2$ (Side Chain) |
| **New Peaks** | | | |
| His | Singlet | 6.6 | 2 Aromatic ring $^{1}$H's |
| | Multiplet | 2.62 | Side Chain $CH_2$ |

**Table 2.8** Peak assignment of tetrapeptide 4 R = His

These peaks were assigned (Figure 2.10, and Table 2.8) by comparison with the tetrapeptide 1 (R = Asp).

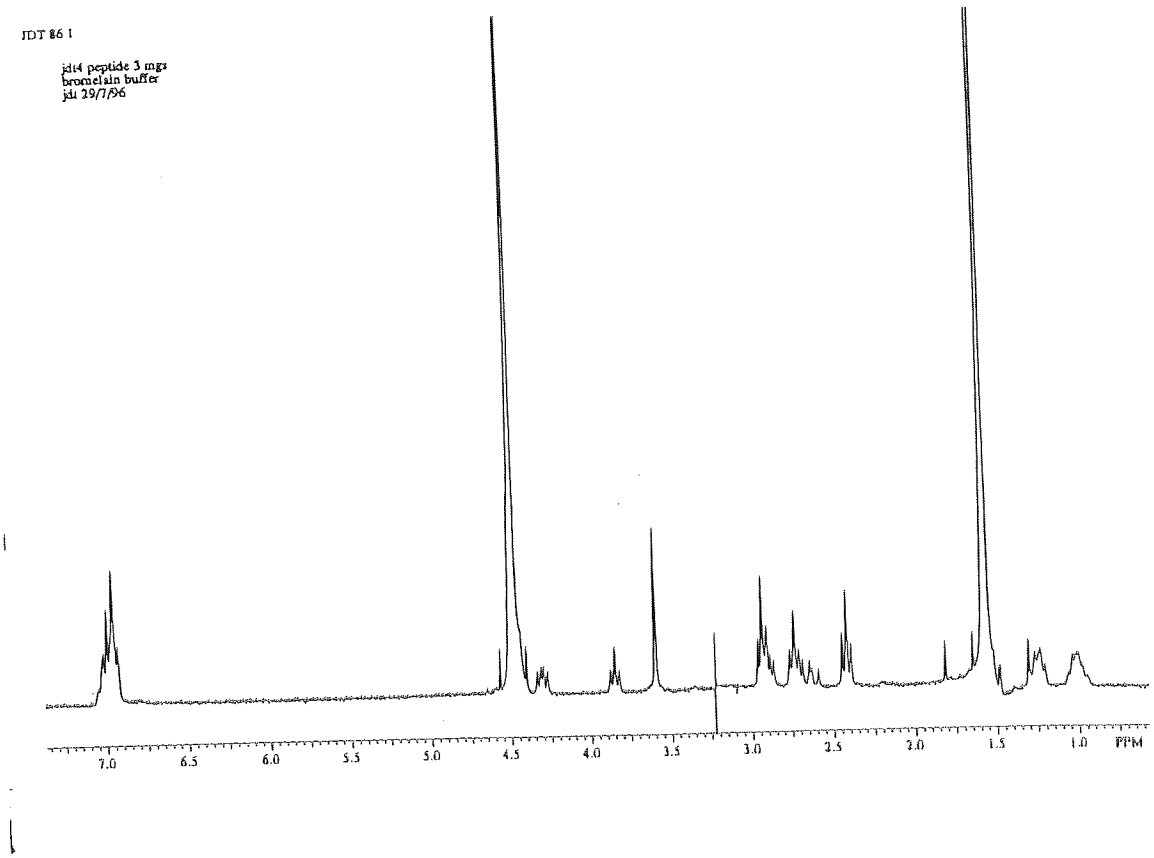


**Figure 2.11** $^{1}$H NMR spectrum of Tetrapeptide 5, R = Arg. Referenced to δ DOH, 4.5

The tetrapeptide backbone of tetrapeptide 5 (R = Arg, Figure 2.11) was assigned by comparison with tetrapeptide 1 (R = Asp, Figure 2.6). The assignment of the side chain can be seen in Figure 2.12

| Residue | Multiplicity | δ / ppm | Assignment |
|---|---|---|---|
| β Ala | Triplet | 2.9 | $CH_2$ |
| | Triplet | 2.4 | $CH_2$ |
| Gly | Singlet | 3.55 | α CH |
| Phe-Amide | Multiplet | 7.0 | Aromatics |
| | Quartet of Doublets | 2.75 | α CH |
| | Multiplet | 4.3 | $CH_2$ (Side Chain) |
| **New Peaks** | | | |
| Arg | Triplet | 2.7 | α CH |
| | Multiplet | 1.0 | Side Chain $CH_2$ (1) |
| | Multiplet | 1.25 | Side Chain $CH_2$ (2) |
| | Triplet | 3.9 | Side Chain $CH_2$ (3) |

**Table 2.9** Peak assignment Tetrapeptide 5 R = Arg

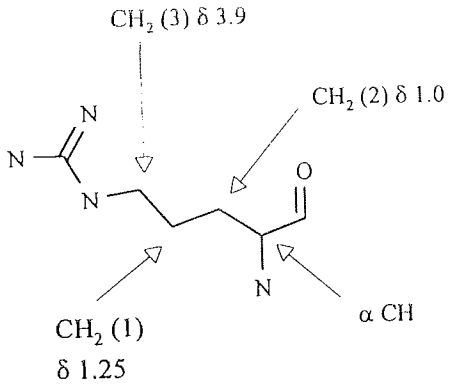


**Figure 2.12** Arginine side chain assignment

## 2.4.2 Method evaluation - positive control

As a positive control, to show that the NMR observation of peptide hydrolysis is feasable, an initial experiment was done digesting glycylglycylglycine with Carboxypeptidase A, and spectra recorded over time.

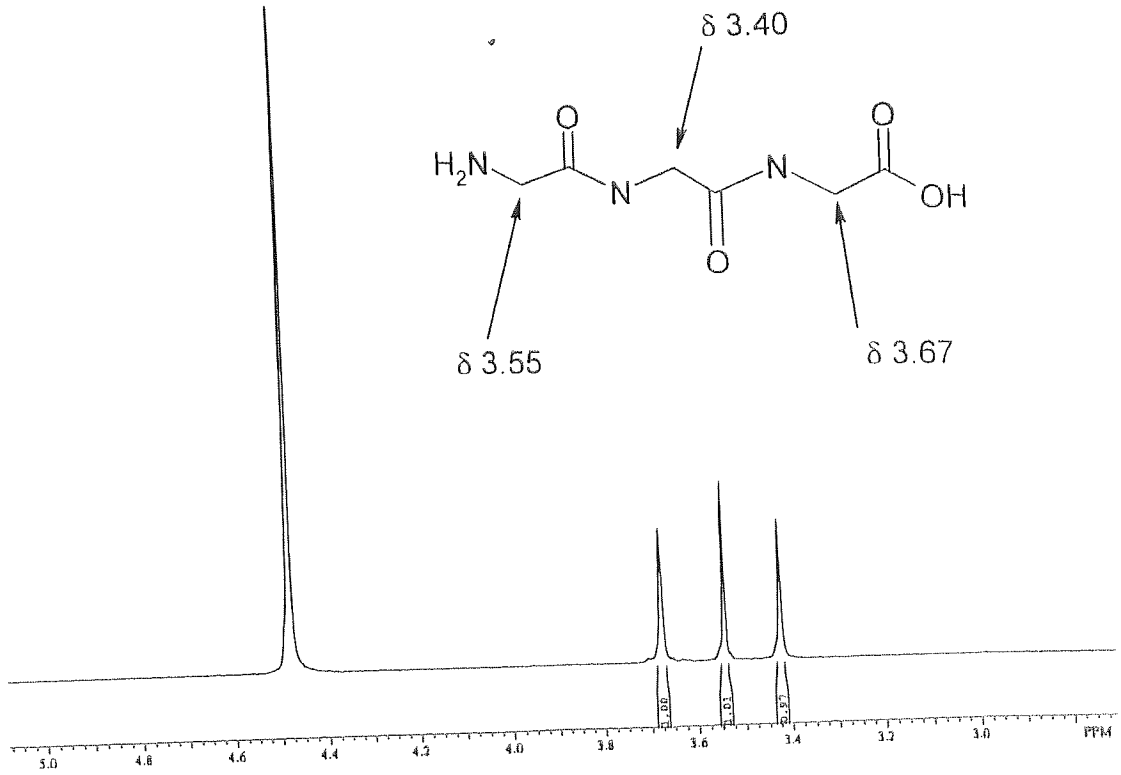


**Figure 2.13** $^{1}$H NMR spectrum of tri-glycine. Referenced to δ DOH, 4.6

As shown in Figure 2.13 triglycine (tri-glycine) has only 3 peaks, one for each of the glycyl $CH_2$ groups, as below in table 2.10,

| Peak δ/ppm | Assignment |
|---|---|
| 3.4 | Central Gly |
| 3.55 | N terminal Gly |
| 3.67 | C terminal Gly |

**Table 2.10** Peak assignment for tri-glycine

After 15 mins at 37$^{o}$ C the spectra had changed to:-

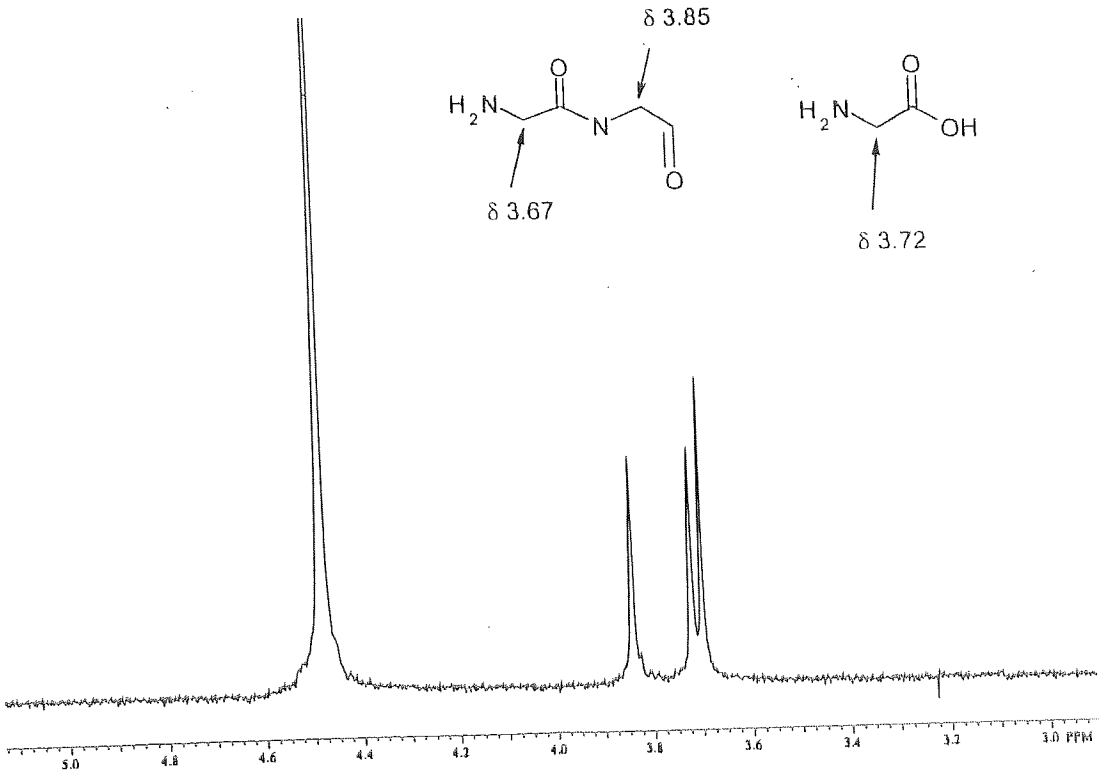


**Figure 2.14** $^1$H NMR spectrum of triglycine after 15 min incubation with Carboxypeptidase A. Referenced to δ DOH, 4.5

| Peak δ/ppm | Assignment |
|---|---|
| 3.67 | N terminal Gly (Gly-Gly) |
| 3.72 | Glycine |
| 3.85 | C terminal Gly (Gly-Gly) |

**Table 2.11** Peak assignment for triglycine after degradation be carboxypaptidase a

After 15 mins, there are significant changes in the NMR spectrum, there is the complete loss of the central gly residue peak at δ 3.4, and the appearance of the single peak corresponding to glycine at δ 3.72. Concurrently both the N- and C- terminal glycine peaks shift slightly upfield, giving the values for di-glycine. These changes can be interpreted as the tri-gly being hydrolysed to give di-gly and glycine. From the integration of the peaks, there is more than a 1:1:1 ratio for all of the peaks that would be expected if the tripeptide had been hydrolysed only once. As there is an excess of the δ 3.72 peak this would indicate that some of the gly-gly has been degraded. From this it can be concluded

that this method can shows measurable changes when the peptide bond is hydrolysed. However, it should be noted that there is no visible triglycine left at this point.

### 2.4.3 Method evaluation - total hydrolysis

After total hydrolysis of R = Asp by 6M HCl the NMR spectrum is compared to that of the tetrapeptide, and there are several changes,

| | |
|---|---|
| Gly | Singlet moves from 3.8 to 3.7 |
| Phe | Multiplet at 7.0 remains unchanged |
| | Quartet of doublets at 2.9 moves to 2.6 |
| | Multiplet at 4.6 becomes Triplet at 3.3 |
| Asp | Quartet of doublets at 2.4 remains unchanged |
| | Multiplet at 4.5 becomet Triplet at 4.0 |
| β Ala | Triplet at 2.75 remains unchanged, |
| | Triplet at 3.2 moves to 2.9 |

These changes in the NMR spectrum, although subtle are significant enough that any degradation would be seen.

### 2.4.4 Enzymatic stability of tetrapeptides

Incubation of the tetrapeptides with active enzymes as shown in Figures 2.16 to 2.21 under these model conditions have shown the tetrapeptides to be stable after a 1 h incubation with the individual enzymes. The time period chosen for these experiments was one h, in the positive controls (2.4.2 and 2.4.3) complete proteolysis was seen within 15 mins, so it is reasonable to assume that if any proteolysis was to occur it would be visible within this one h experimental time period. To verify this, one series of experiments, using Carboxypeptidase A, was extended over a 6 h period with NMR spectra being recorded every h. At the end of this extended time period no degradation was observed (Figures 2.16 and 2.17).

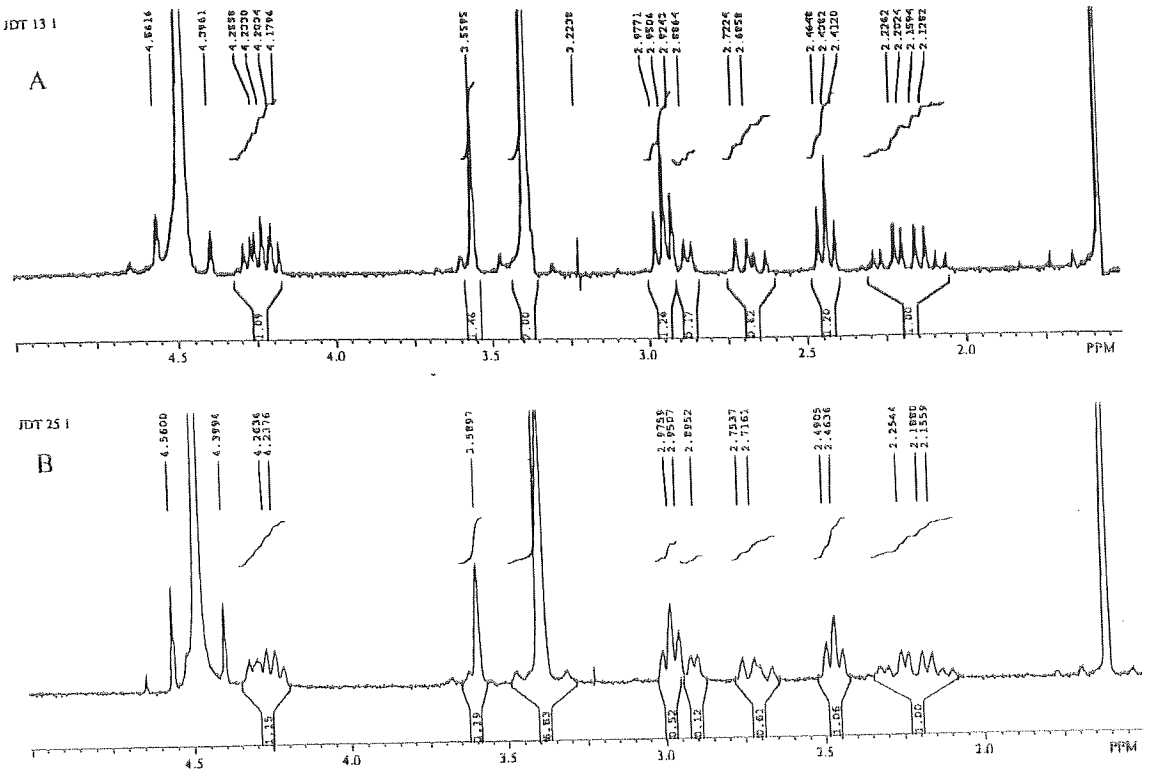


**Figure 2.15** $^1$H NMR spectrum of Tetrapeptide 1, R = Asp before (A) and after (B) a 6 h exposure to Carboxypeptidase A. Referenced to δ DOH, 4.5

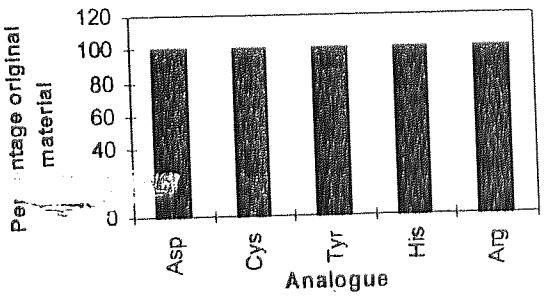


**Figure 2.16** Tetrapeptide stability towards Carboxypeptidase A. Results after 1 h incubation at 37°C, n=3, no degradation seen in any experiment.

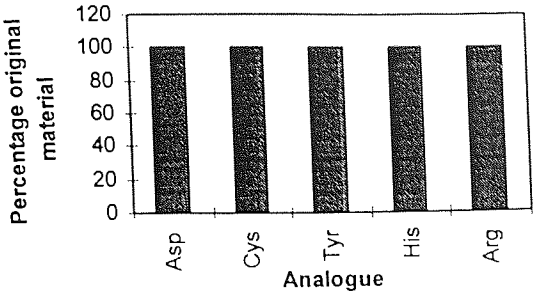


**Figure 2.17** Tetrapeptide stability towards Carboxypeptidase A. Results after a 6 h incubation at 37°C, n=3, no degradation seen in any experiment.

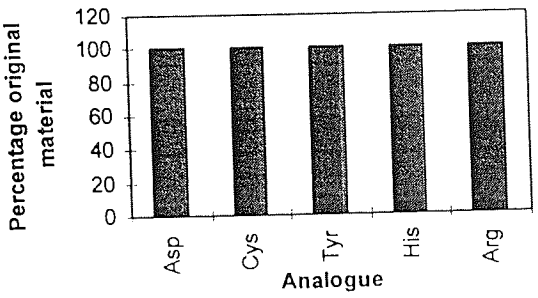


**Figure 2.18** Tetrapeptide stability towards Aminopeptidase M. Results after 1 h incubation at 37°C, n=3, no degradation seen in any experiment.

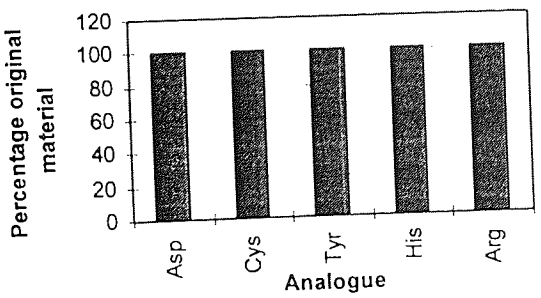


**Figure 2.19** Tetrapeptide stability towards elastase Results after 1 h incubation at 37°C, n=3, no degradation seen in any experiment.

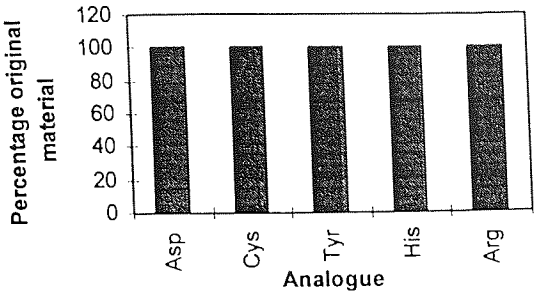


**Figure 2.20** Tetrapeptide stability towards bromelain, Results after 1 h incubation at 37°C, n=3, no degradation seen in any experiment.

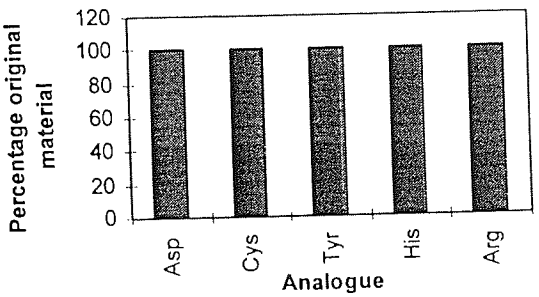


**Figure 2.21** Tetrapeptide stability towards α-Chymotrypsin, Results after 1 h incubation at 37°C, n=3, no degradation seen in any experiment.

## 2.4.5 Thermal stability of tetrapeptides

The thermal stability in aqueous solution of all the tetrapeptides at 80°C was investigated, there was no visible degradation of any of the peptides except that containing the aspartate group (Figure 2.23). Figures 2.23 to 2.28 show the thermal stability of the tetrapeptide R = Asp, there was breakdown of the peptide under the extreme conditions of 80°C for 1 week at all pH values, although most markedly at very low pH, and neutral pH. As this tetrapeptide contains the aspartic acid group, the degradation is *via* the aspartate rearrangement. The aspartate rearrangement is visible as the appearance of a triplet at δ

3.9, and the simplification of the multiplet at δ 4.5 to give a multiplet of less complicated pattern, although still not resolvable. The appearance of the triplet at δ 3.9 corresponds to the change in environment that the side chain $CH_2$ experiences as the cyclic imide is formed. The cyclic imide and the location of the triplet are shown in Figure 2.22.

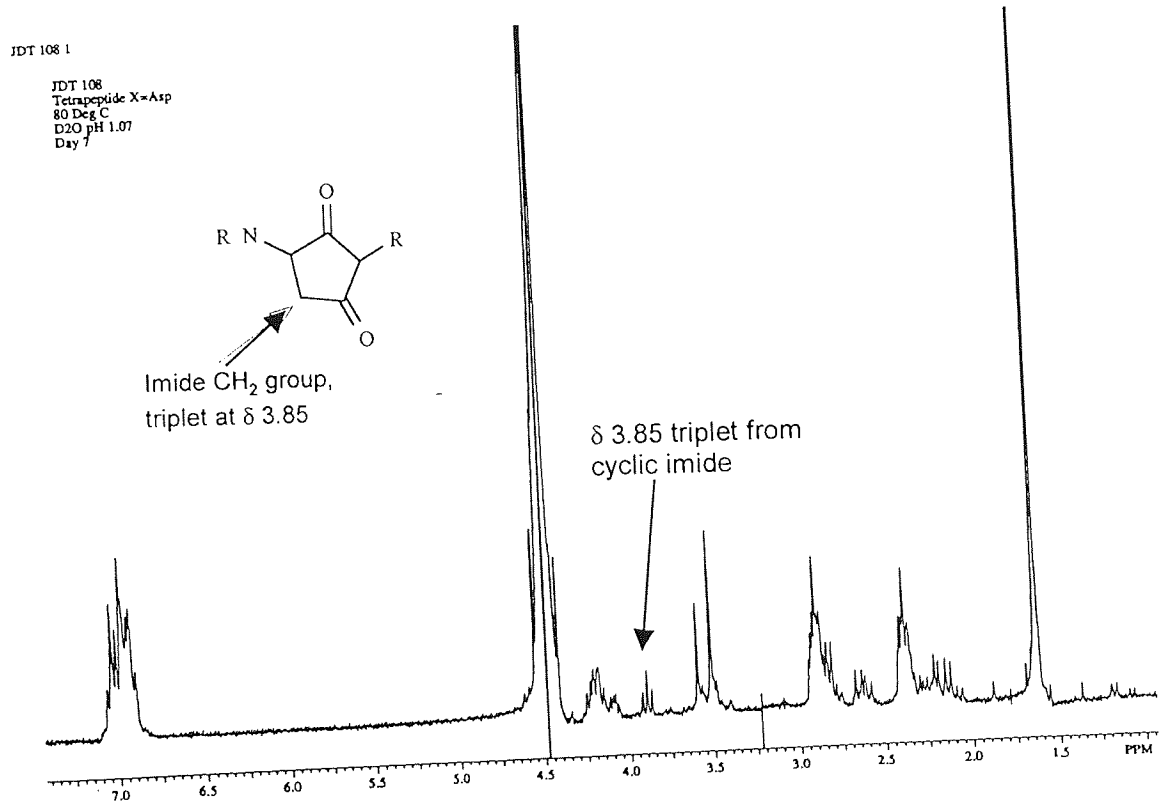


**Figure 2.22** $^1$H NMR spectrum of Tetrapeptide 1, R = Asp. Referenced to δ SOL 4.5 Cyclic imide and NMR triplet assignment resulting from tetrapeptide 1 (R = asp) degradation is highlighted.

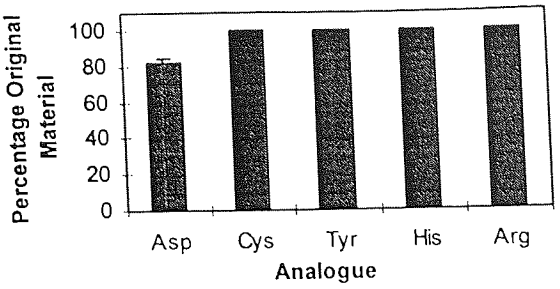


**Figure 2.23** Tetrapeptide thermal stability. Results after 7 day incubation at 80°C, n=3, degradation only seen in Asp experiments.

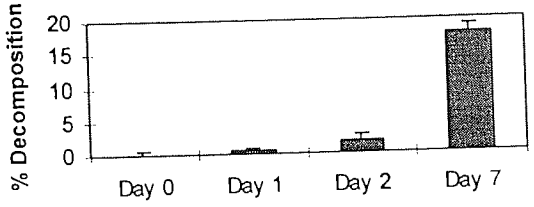


**Figure 2.24** Tetrapeptide R = Asp thermal stability pH 7.40 Results after incubation at 80°C, n=3, degradation to cyclic imide seen in all cases.

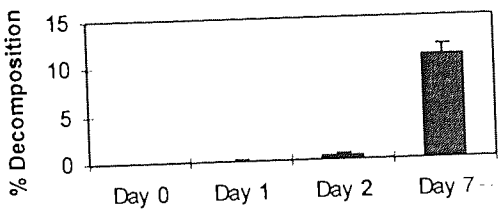


**Figure 2.25** Tetrapeptide R = Asp thermal stability pH 3.20 Results after incubation at 80°C, n=3, degradation to cyclic imide seen in all cases.

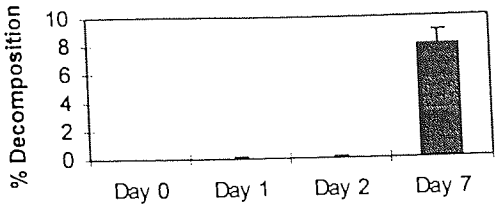


**Figure 2.26** Tetrapeptide R = Asp thermal stability pH 2.50 Results after incubation at 80°C, n=3, degradation to cyclic imide seen in all cases.

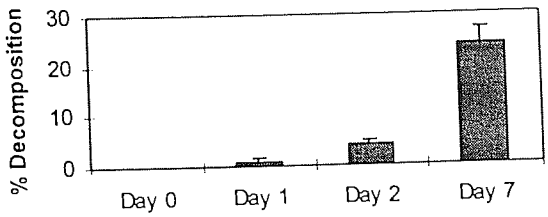


**Figure 2.27** Tetrapeptide R = Asp thermal stability pH 1.07 Results after incubation at 80°C, n=3, degradation to cyclic imide seen in all cases.

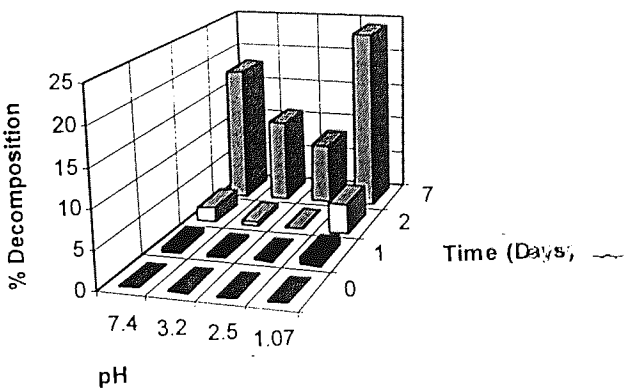


**Figure 2.28** Tetrapeptide R = Asp thermal stability, overall effect of pH at elevated temperatures.

From the enzymatic and thermal model stability work we can conclude that the tetrapeptide analogues are extremely stable, requiring 80°C for one week to produce any degradation. Figure 2.28 highlights not only the extreme conditions required to degrade the peptide, but also a peak in stability at pH 2.5 can be seen. Since these peptides are

analogues of an actual drug molecule that is known to be, and was designed to be highly stable *in vitro* and *in vivo* (Simpkin, 1996) it can be concluded that this in-vitro model provides a good indication that the analogues themselves will be extremely stable when they come into contact with a biological system.

## 2.4 6 Stability of the tetrapeptides to human nasal wash

To advance from the model system in which known enzymes are used, nasal secretions containing mucosal enzymes were collected and processed to model stability of the tetrapeptides *in vivo*. Nasal secretions were collected from a healthy volunteer, and freeze dried. The secretions were analysed for protein content using the BCA assay against bovine serum albumin as a standard, and also run on an SDS-PAGE gel to ascertain the approximate molecular weight of the proteins isolated (Figure 2.29).

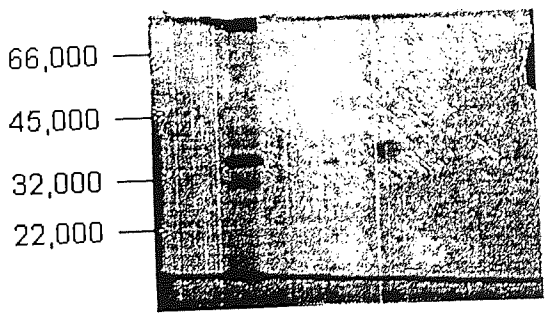


**Figure 2.29** SDS-PAGE gel of human nasal wash
12% Gel run at 15 $Vcm^{-1}$ for 2 hs.

The degradation of triglycine by the nasal wash was slow, with complete degradation taking approximately one h (Fig 2.30), compared with the complete degradation after 15 mins seen earlier. Without rigorous examination of the nasal wash, and the construction of either a Lineweaver-Burke plot, or an Eadie-Hofstee to analyse the kinetics of the degradation, it can be seen from the data obtained that proteolytically active proteinaceous secretions have been isolated, albeit at a lower activity level per mg protein

than any of the pure enzymes used in the study. Furthermore, their activity can be seen using the NMR technique. When the stability of the 5 tetrapeptide analogues was assayed using this technique (Figure 2.31) no degradation was seen.

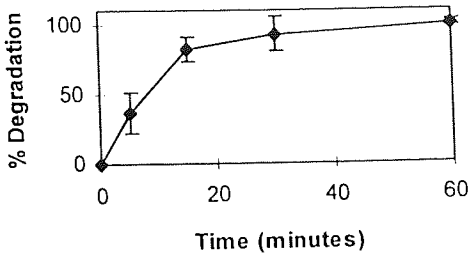


**Fig 2.30** Appearance of tri-Glycinedegradation products Degradation of tri-gly by human nasal wash, 37°C n=3 degradation to Gly and Di-Glycine.

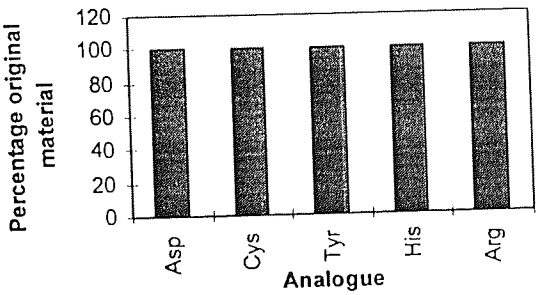


**Figure 2.31** Tetrapeptide stability towards human nasal wash. Results after 1 h incubation at 37°C, n=3, no degradation seen in any experiment.

## 2.5 Conclusions from stability work

From this stability work, it can be concluded that the NMR technique developed for this study represents a reliable and accurate method of determining the stability of small peptide molecules. There are two advantage that this technique has over other existing techniques, such as analysis by HPLC, in that the degradation can be monitored in real time (Figure 2.31). Also, for compounds of which there is only a small sample available, the ability to be able to monitor on the NMR scale, where samples as small as 2-3 mg can be used provides another advantage. However, for the tetrapeptides considered here the greatest advantage of this technique is that it is the most sensitive technique available. The tetrapeptides all have a very poor UV adsorbance and poor fluorescence, so traditional analysis by HPLC would be very insensitive, and other techniques for quantifying peptides such as the BSA and ninhydrin assays do not distinguish between complete and proteolytically degraded peptides.

The peptides themselves have proved to be particularly stable, not degraded by the proteolytic enzymes chosen, or by the nasal wash. Elevating the temperature to 80$^{o}$C caused degradation only for the tetrapeptide containing the aspartate residue. This degradation can reasonably be explained as the peptide undergoing the aspartate rearrangement. No work was performed to assess why these tetrapeptides proved so stable, further studies in which other amino acids within the peptides were changed together with molecular modelling of the interior active site of the enzymes used should provide data to answer this unknown point, however, such studies were are not within the aims of this work..

In summary:

- The NMR technique developed proved throught the positive controls to be a viable technique.
- The technique not only provided data as to the amount of degradation, but as to the exact identification of all of the degradation products.

- The use of nasal secretions proved to be successful in that they degraded the positive controls.
- The tetrapeptides used were analogues of a Rhône-Poulenc Rorer peptide that is known to be exceptionally stable, and in these systems there was no degradation seen except under extreme conditions.

# Chapter 3

## Design and evaluation of an *in vitro* tissue viability chamber for epithelial tissues.

## Overview

*In vitro* and *ex vivo* models for nasal drug delivery studies are a relatively novel area of investigation, since there has been very little work done on developing a suitable system. In this chapter an *ex vivo* system is developed to maintain the viability of excosed epithelial tissues.

## 3.1 Introduction

As already discussed in chapter 1 (introduction), *in vitro* studies for nasal delivery have until recently been limited to the vertical Ussing chamber (Östh, 1997b; Wadell *et al.*, 1999), studies have been done using the Costar Horizontal Ussing chamber, although there are several unsolved problems with this system (Östh, 1997b). The problems that were encountered included simple mechanical problems in mounting the tissue, the perfusion volume being too great, oxygenation, and circulation. All the studies that have been performed to date have been done in systems containing an aqueous phase either side of the tissue.

Work has been done on model systems for nasal delivery since Wheately *et al.* first reported the use of the vertical Ussing chamber in 1988 (Wheatley *et al.*, 1988). In this original work, the vertical Ussing chamber again had a relatively large volume of fluid on both the muosal and serosal sides of the tissue. This large perfusion volume was reduced to less than 2ml when Bechgaard *et al.* (1992) introduced a modification to the chamber system.

### 3.1.1 Measurement of viability

Experimentally, the viability of any excised nasal tissue [illegible] nsidered in two parts. Firstly the biological condition of the cells in the tissue sample, and secondly the physical integrity of the barrier. For nasal drug delivery it is thought that the most important physical barrier is the layer of epithelial cells, in measuring the viability of any tissue samples in a new chamber system it is important to be able to assess the damage to this monolayer of cells. There are two different methods that are used in tandem to assess the condition of tissue samples. Firstly, since the nasal mucosa is known to transport ions, the condition of the tissue can be monitored by measuring the electrophysiological properties of the tissue sample, and secondly, the physical integrity of the tissue is monitored by assessing the flux of a marker across the tissue.

### 3.1.2 Electrophysiological measurement of viability

For epithelial tissues and other tissues that possess ion transport mechanisms, measurement of the electrical properties of the tissue is used to assess the condition of the cells. This is done by placing two sets of Ag/AgCl electrodes in the tissue viability solution either side of the tissue. One pair of electrodes are used to monitor the voltage generated by the tissue as it transports ions from one chamber to the other, and the other pair are used to measure the current generated. Since nasal epithelial tissue generates a voltage and hence a current Ohms' Law (Equation 3.1) must apply. The voltage generated is to a large extent dependent on the ions transported by the tissue; the current and the resistance are a much better measures of the tissues' viability. To ensure accuracy, reproducibility, and reliability, standard electrophysiological conditions have been developed. The key measuruements of viability are the epithelial potential difference (voltage), short circuit current ($I_{sc}$) and resistance R. $I_{sc}$, the short circuit current is defined as the back current required to be forced through the tissue to produce a measured epithelia voltage of 0 V by an external voltage source (this is otherwise known as a 0 V voltage clamp).

**Equation 3.1** Ohms' Law

$$V=IR$$

Where V= Voltage
I = Current
R = Resistance

### 3.1.3 Marker flux

Since the major barrier is thought to be the epithelial layer, commonly used paracellular transport markers such as mannitol can be used to quantify any changes we may see in the paracellular transport route, for example changes in diffusion through the cellular junctions due to damage to the epithelial, or ideed any of the underlying tissues, as suggested by Bechgaard *et al.* (1992) for monitoring tissues in the Ussing chamber.

For the two chamber systems to have the same viability with respect to mannitol transport there has to be a method of comparing paracellular flux, the two values must be

equal within measurable experimental limmits. There are several equations used for monitoring and comparing paracellular marker flux, the first is that of Hilgers *et al.* (1990), equation 3.2. For the two systems to be equivalent we have equal values of $P_{eff}$ as in equation 3.3.

**Equation 3.2** $P_{eff}$ (Hilgers *et al.*)

$$P_{eff} = \left(\frac{dC}{dt}\right)_{ss} \frac{V}{AC_D}$$

Where
$P_{eff}$ = effective permeability
(dC/dt) = Rate of change of receiver conc.
V = receiver volume
A = permeation area
$C_D$ = initial donor concentration

**Equation 3.3**

$$P_{eff}\,(\text{Ussing}) = P_{eff}\,(\text{New chamber})$$

or less simply

$$P_{eff} = \left(\frac{dC}{dt}\right)_{ss} \frac{V}{AC_D}(\text{Ussing}) = \left(\frac{dC}{dt}\right)_{ss} \frac{V}{AC_D}(\text{New chamber})$$

Since permeability is independent of donor volume when using the $P_{eff}$ formula (equation 3.2), and we have identical receiver volumes (V) and permeation areas A for comparison of the two different chamber systems this can be simplified to equation 3.4.

**Equation 3.4**

$$\left(\frac{dC}{dt}\right)_{ss}(\text{Ussing}) = \left(\frac{dC}{dt}\right)_{ss}(\text{New chamber})$$

There are other mathematical techniques available for the comparison of the paracellular marker fluxes, most importantly $P_{app}$ the apparent permeability (equation 3.5) that is used by Bechgaard *et al.* (1992) for Ussing chamber studies.

This method gives the apparent permability of the tissue for any time point during the experiment, and as such it can be considered as an instantaneous diffusion constant for the tissue.

## Equation 3.5

$$P_{app} = \frac{X_R}{X_D}\frac{V_R}{At}$$

Where

$P_{app}$= apparent permeability
$X_R$ = receiver concentration
$V_R$ = reciever volume
$X_D$ = donor concentration
A = permeation area
t = time

Since $P_{eff}$ gives a rate constant at a steady state and $P_{app}$ gives an instantaneous value although both are dimensionally the same, the two values are not comparable. For comparative studies either $P_{app}$ or $P_{eff}$ must be used, however neither method can be used directly in the new chamber. The approach of Bechgaard *et al* ($P_{app}$) is not feasable due to the necessity to measure the mucosal (donor) concentration at each time point to obtain the instantaneous $P_{app}$. The design of the new chamber is such that with the minimal volume present this is not possible. The $P_{eff}$ method of Hilgers *et al.* (1990) can be used; however, certain assumptions have to be made.

From previous experience with tissues such as rabbit nasal tissue (Bechgaard *et al*, 1992) in chambers such as the Ussing chamber the flux of markers such as mannitol during such experiments is known to be very low (0.73 ± 0.42 ‰ $h^{-1}$). With such low permeation rates the first assumption (Assumption 1) is that the donor concentration is significantly greater than the receiver concentration at any point in the experiment. The second assumption (Assumption 2) is that since the rate of permeation is so low, there is no appreciable difference in the marker concentration in the donor chamber in either chamber

system. This is necessary due to the significantly lower ammount of marker available in the case of the new chamber if experiments at the same concentration are compared between the new and Ussing chambers.

**Assumption 1**

Where $X_D$ = donor concentration

$X_R$ = receiver concentration

$$X_D \rangle\rangle X_R$$

**Assumption 2**

$$\left(\frac{dC_D}{dt}\right)(\text{Ussing}) \approx \left(\frac{dC_D}{dt}\right)(\text{New chamber}) \approx 0$$

Where $dC_D / dt$ is the rate of change of donor compartment concentration with time.

It should be noted however, that in the literature there seems to be no standard method for calculating such quantities as $P_{app}$ for example Schipper *et al.* (1996) omit the volume term (V) from equation 3.2 ($P_{eff}$ calculation) and call the resulting value $P_{app}$. The methods for calculating $P_{app}$ and $P_{eff}$ here are both dimensionally identical, however, one is calculated from a steady state, wheras the other is calculated from an instantaneous rate.

### 3.1.4 Aims and objectives

The objective of this study is to design and develop a chamber system in which the viability of excised nasal tissue is maintained to within, or exceeds that in the existing horizontal and vertical Ussing chambers. The key design aims are:-

- Tissue mounted horizontally
- Ability to have either a dry or minimal volume on the mucosal side of the tissue
- $P_{eff}$ or $P_{app}$ must be assessed, and the assumptions in 3.1.3 validated
- Adequate tissue viability.

## 3.2 Materials and methods

### 3.2.1 Chemicals and materials

All chemicals used, were of analytical grade and obtained from Sigma (Poole, England). Carbogen (95% $O_2$/5% $CO_2$) was obtained from BOC Ltd (England). Radiolabelled $^{14}C$ mannitol (2.07 GBq $mmol^{-1}$) and $^{14}C$ PEG4000 (688MBq $g^{-1}$) were obtained from Amersham (Amersham UK).

Acrylic blocks for the fabrication of the chambers were purchased from Amari Plastics (Birmingham UK). Electronic components for the voltage modifictation circuit were obtained from RS Ltd (Birmingham UK). All tubing and other anciliary items used in the construction and operation of the chambers was obtained from Fischer Scientific.

### 3.2.2 Buffer solutions

Glucose Krebbs ringer solution (GR) consisted of $HPO_4^{2-}$ (1.6 mM), $H_2PO_4^-$ (0.4 mM), $Mg^{2+}$ (1.2 mM), $Cl^-$ (122 mM), $Ca^{2+}$ (1.2 mM), $K^+$ (5 mM), $HCO_3^-$ (25 mM), $Na^+$ (141 mM) and D-(+)-glucose (13 mM). Since glucose ringer buffer is an ideal growth medium for bacteria it was sterile filtered (0.2 μm), and then stored at 0 - 4 °C.

### 3.2.3 Dissection methods

#### 3.2.3.1 Rat ileum

Rats were sacrificed by inhalation of an increasing concentration of $CO_2$. The rat was laid upside down on a suitable disecting mat. The skin along the mid ventral line was slit, and the skin was loosened from the body wall manually and then pinned out. The abdominal wall was then cut along the mid ventral line upto the rib cage (the xiphoid cartilage), and cut around the rib cage to expose the stomach and intestines. The fat bodies were moved aside. Gently, the duodenum and colon were carefully pulled apart and then

turned over to undo the twist where the small intestine crosses the large intestine. Prior to removal of any tissue the caecum, jejunum, duodenum, and the hepatic portal vein with its chain of lymph nodes was identified. A portion on the ileum approximately 6 cm long was removed together with the attached mesentery. The freshly excised tissue was placed in warm glucose ringer solution. The tissue was prepared for mounting in the chamber by removing the mesentery, and then slitting the ileal tissue down its length where it had been joined to the mesentery. A 6 cm piece of tissue proved ample for 3 chamber runs.

### 3.2.3.2 Rabbit head

The method used for the dissection of the rabbit's head and the subsequent isolation of the nasal epithelial tissue was based on that of Bechgaard *et al.* (1992).

Male and female New Zealand White rabbits of approximately 3 kg were sacrificed by injection an overdose of 5% pentobarbitone (unless otherwise stated, Sagatal) into the marginal ear vein. After confirmation of death a longitudinal incission was made along the nasal ridge to expose the soft bone covering the nasal cavity. This was then cut through using a pair of blunt nosed disecting scissors taking care to avoid touching the sceptal epithelium. The nasal cavity was completely exposed, and then the middle and ventral conchae were removed. The nasal epithelial tissue was obtained from the exposed septum. Using a blunt-ended pair of forceps the tissue was loosened at the junction of the septum and the roof of the nasal cavity, and with great care was loosened over the entire septal area. The required tissue section was then cut out and immediately placed in cold oxygenated GR solution.

### 3.2.3.3 Pig head

Pigs heads were obtained from a local abattoir and the nasal tissue was isolated as soon as possible after sacrifice. No method has been published by the group using Pig's heads at Uppsala university (K. Östh and E. Bjork) and a method was developed based on that outlined above for the rabbit tissue, however, it is much harder to gain access to the

nasal cavity without damaging the epithelium to be used. To gain access to the nasal cavity the majority of the thickness of the bone along the nasal ridge, and arround the area where access was required was cut through using a hacksaw blade, then this was broken through using a pair of bone cutters to expose the nasal cavity. Epithelial tissue was isolated from two regions in the nasal cavity, from the septum, and from the turbinates. The technique used for isolating the different tissues was identical to that used for the rabbit tissue.

### 3.2.4 Ussing chamber operation

#### 3.2.4.1 Chamber modification

Commercial chambers (WPI stevenage, Herts UK) with a half cell volume of approximately 20ml were modified to give a design similar to that of Bechgaard *et al.* (1992) with a half cell volume of 1.5 ml.

#### 3.2.4.2 Electrical monitoring

The electrical properties were monitored using a DVC-1000 dual voltage clamp (World Precision Instruments Inc., CT, USA) and recorded using a PC30G datalogging card (Amplicon Liveline, Brighton, UK) in a 486PC (Opus Technology, UK). The output signal was amplified using a op-amp circuit as described in figure 3.1. Data analysis was performed using the waveview software (Eagle Technology Pty., Cape Town South Africa).

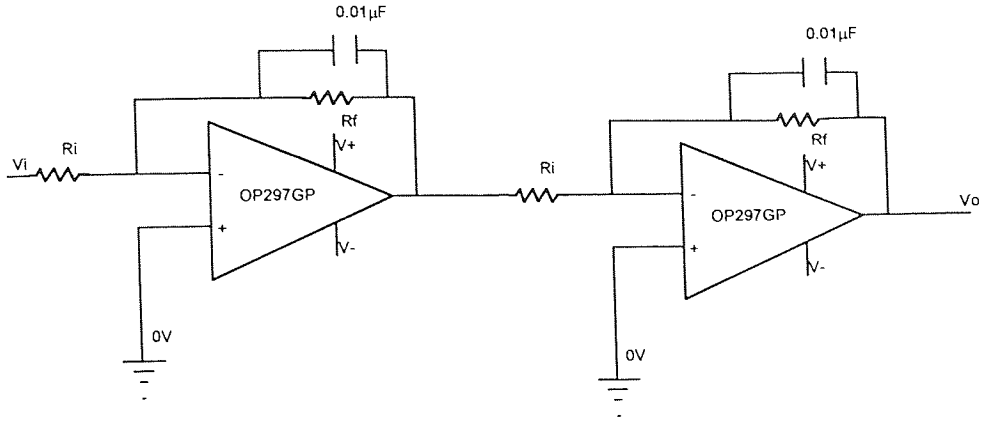


**Figure 3.1** Operational amplifier circuit for amplification of output signal from DVC1000 voltage clamp. Vi Input voltage, Vo Output voltage, Ri Input resistance, Rf Field resistance, V+ operational supply voltage, V- negative operational supply voltage. The gain of each op-amp is defined as Ri/Rf. Total gain for two series op-amps is $Gain_1$ x $Gain_2$

### 3.2.4.3 Electrode manufacture

The electrodes (WPI, UK) require agar bridges between the elecrode body and the mucosal or serosal solution. These were made from 4% agar (Bacterological Agar, Oxoid) in GR. The electrodes were held in the end of a 1ml syringe barrel, with the barrel being filled with the agar gel, as shown in Figure 3.2

Agar (2g) was added to fresh GR (50ml) and heated to 80 $^{o}$C, care was taken to ensure that the temperature did not exceed 83 $^{o}$C. On cooling the agar solidifies, using a 5 ml syringe and a suitable piece of rubber tubing, the electrode syringe body was filled. It was essential at this stage to ensure that there were no air bubbles present. The electrode ends were placed into the agar before it had completely set, and the filling syringe was then removed. Upon complete cooling the electrodes were inspected to ensure that there were no airbubbles present in the solidified agar bridge. After elecrodes had been made they required some time to equilibrate. Stored in 4$^{o}$C GR (changed daily) between 3 and 7 days were required for a steady electrical baseline to be achieved.

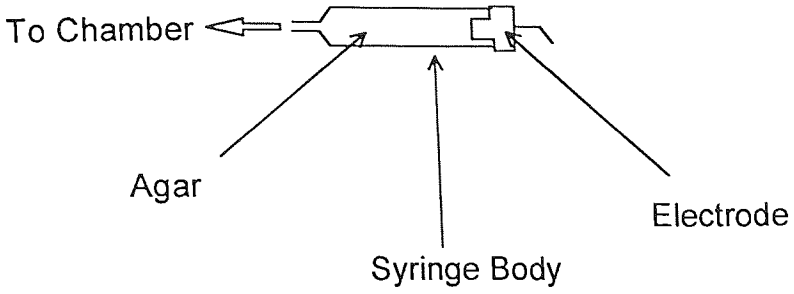


**Figure 3.2** A scematic representation of the electrode assemble for the Ussing chamber.

### 3.2.4.4 Chamber setup

Between chamber runs, the chambers were left with the electrodes in place, filled with non oxygenated glusose ringer solution, but with the thermostatted water circulator switched off. To prepare the chambers for a run the GR in the chambers was replaced and the chambers left for 45 minutes for equilibration to the experimental temperature of 37 °C. After 45 minutes the electrodes were cheched for 10 minutes to establish a solid clear baseline. After the chamber had equilibrated and the electrodes were producing a steady reading the electrodes were zeroed to account for the fluid resistance and the measured voltage. The fluid resistance is the resistance due to the agar bridges and the ionic solution. The voltage zero is to overcome any junction potential (measurable voltage across the Ag/AgCl electrode and the agar bridge). After the electrodes have been zeroed the GR was removed from the chamber. Great care has to be taken from this point on to ensure that the electrodes do not move as this invalidates the chamber zero. The chamber is then removed from the mounting clamp and separated into the two halves. At this point the tissue sample can be mounted in the chamber.

The tissue is mounted in the Ussing chamber by placing it mucosal side uppermost over the metal mounting spikes, and gently pressing the tissue down onto the spikes using the other half of the chamber.

### 3.2.5 Assessement of viability in the new chamber

Tissue viability in the new chamber was monitored by exposing the tissue in the new chamber for a fixed period of 1 h. Since it was not possible to mount an electrode on the dry upper surface of the tissue, tissue samples were then removed and placed in the Ussing chamber, where their epithelial voltage and $I_{sc}$ were monitored for a 15 minute period. As a control tissue samples were mounted in the Ussing chamber, and and after a 1h incubation the voltage was recorded in the same way as for the tissue that had been exposed in the new chamber.

### 3.2.6 Assessement of the barrier integrity, and transport kinetics

Paracellular marker experiments (mannitol or PEG 4000 in GR) were performed to assess the transport kinetics discussed in section 3.1.3, and then later to assess the integrity of the physical barrier.

Marker (100 µM, 1.5mL Ussing chamber, 50 µL new chamber) in GR was added to the mucosal side of the tissue. Serosal samples (200 µL) were removed to quantify the marker concentration, and replaced with fresh GR (200 µL). Removed serosal samples were quantified by scintillation counting in 10 mL Hisafe 2 (Wallac, UK) of a Hewlet Packard Tricarb scintillation counter.

Data obtained from marker transport experiments using scintillation counting required correction to allow for the removal of samples from the chamber and their replacement with fresh GR. A traditional cumulative total approach was used (equation 3.6).

**Equation 3.6**

$$Q = V_s\left(\sum_{n=1}^{n} C_{n-1}\right) + C_n V_t$$

where Q=total ammount of mannitol
Vs=sample volume
Vt=chamber volume
$C_{1,2.....n}$ = concentration of samples 1 to n

## 3.3 Design of new chamber

### 3.3.1 Design - description of chamber

The tissue viability ½ cell consists of a reservoir of tissue viability fluid, a source of oxygenation, and a method of clamping the tissue in place. The cell contains internal temperature control waterways, and is maintained at 37 $^{o}$C by an external thermostatted water circulator, as shown in Figure 3.3.

The chamber is constructed from acrylic blocks (Amari Plastics, Birmingham UK) in two parts, an upper part with the tissue clamping setup, and reservoirs of fluid, and a lower blanking plate with waterways machined and a lower connecting waterway between the two reservoirs according to Figures 3.4 – 3.6. After machining these blocks the mating surfaces were smothed using a face plate and 1200 grade glass paper and when the chamber was assembled they were mated with a thin layer of PTFE sealant.

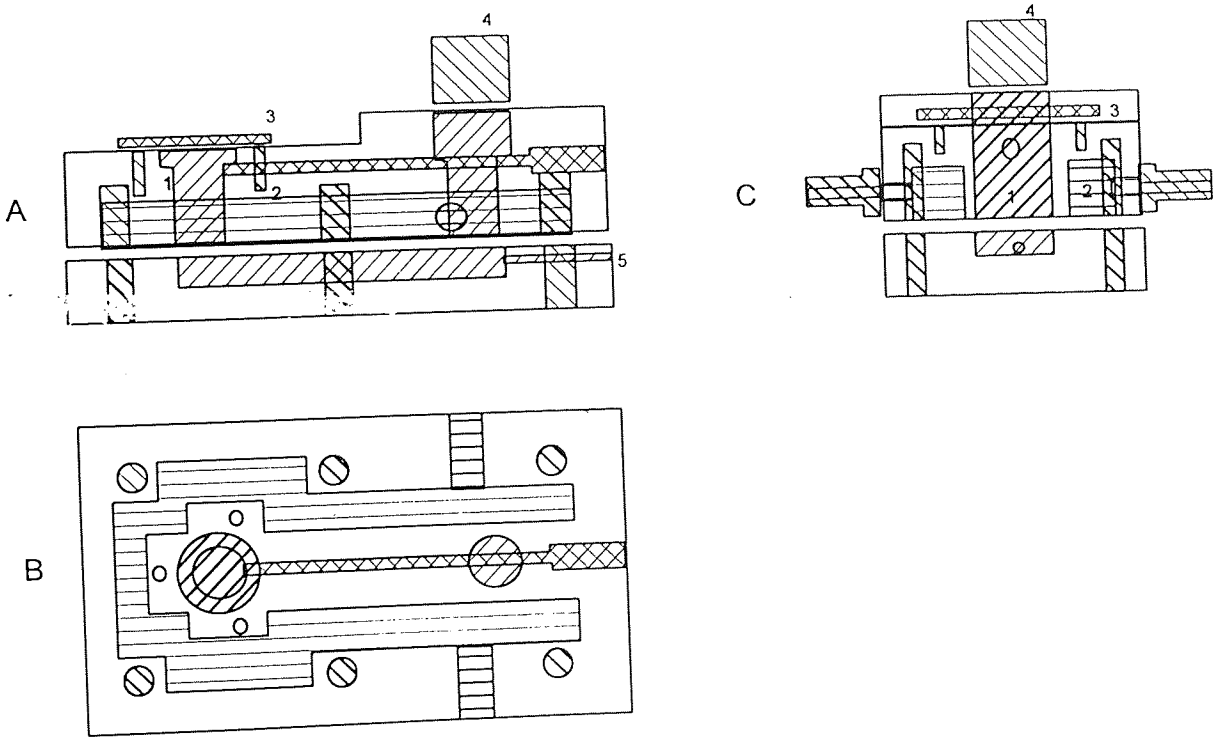


**Figure 3.3** The lower tissue viability 1/2 cell.
Cross Section (A), and side view (B) of novel chamber system. (1) Chamber (1.8 ml), (2) Water jacket (37°C), (3) Tissue mounting ring, (4) Funnel to prevent overflow due to gas lift system, (5) Gas lift system to provide circulation and oxygenation (95% $O_2$ 5% $CO_2$)

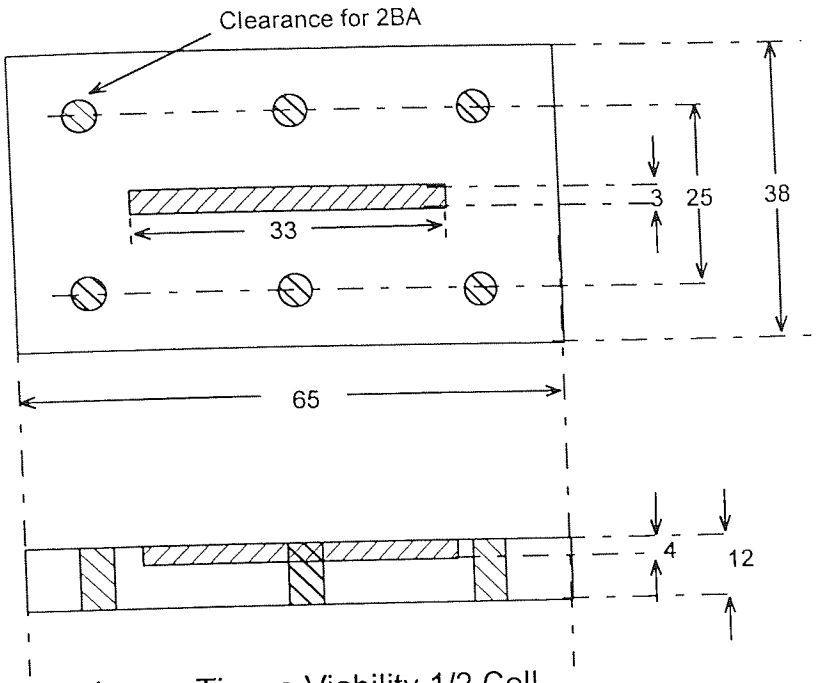


Lower Tissue Viability 1/2 Cell.
Lower Section.
Material: Acrylic
Dimensions: mm
Quantity: 1

**Figure 3.4** Engineering drawing of the chamber lower section

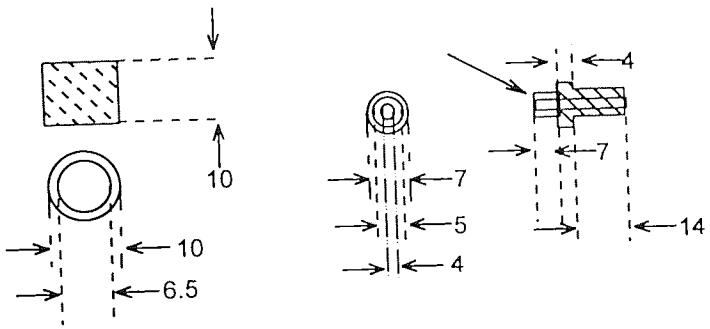


Chimney
Quantity:
Material: PTFE

Water Union
Quantity: 2
Material: Brass

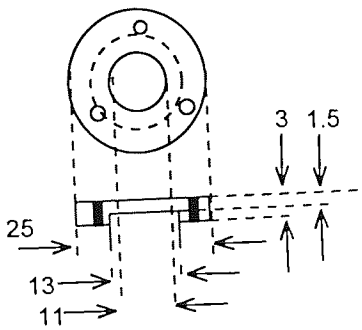


Upper Mounting Ring
Quantity: 1
Material: PTFE

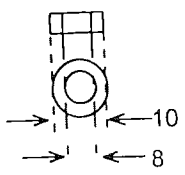


Lower Mounting Ring
Quantity: 1
Material: PTFE

Tissue Viability 1/2
Misc. Parts
Items not shown:
3 x 6 BA bolts x 10mm
6 x 2 BA bolts x 13mm

**Figure 3.5** Engineering diagram of the anciliary chamber parts.

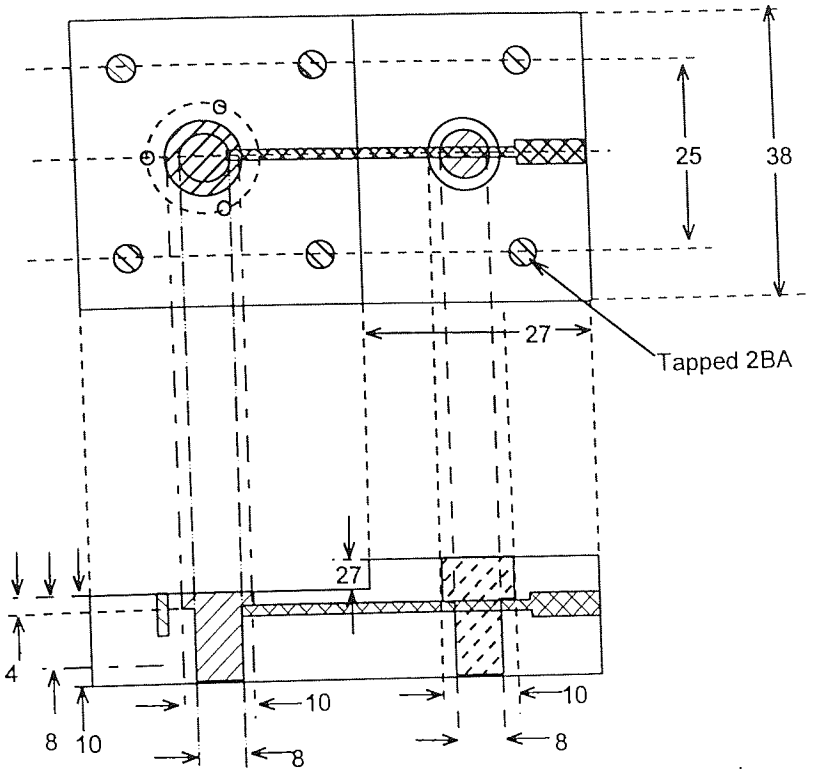


Tissue Viability 1/2 Cell
Upper Section - Excluding Thermostatting
Material: Acrylic
Dimensions: mm
Quantity: 1

**Figure 3.6** Engineering drawing of the chamber upper section.

## Macroscopic Validation of New Chamber

The chamber is designed to provide oxygenated viability buffer to the tissue, using a gas lift system to provide both the oxygenation and circulation in the underlying buffer. Before any experiments were performed with live tissue the macroscopic properties of the chamber, the internal temperature, and water flow were investigated to ensure adequate operation.

### 3.3.2.1 Circulation within the lower chamber

To assess the circulation within the lower chamber a small volume (50 µl) of a blue marker dye (trypan blue 5% in water) was added to a chamber filled with water through the chimney after circulation had been established. In the place of live tissue a silicicone membrane was placed over the lower tissue ring and held in place with the tissue mounting ring. The time taken for the blue dye to disperse around the chamber (if suitable water-flow was present) was then recorded for a series of different gasflow rates, as shown in Table 3.1

| Flow rate (bubbles / second) | Time required for circulation to be established (s) | Acceptable water flow characteristics Y / N |
|---|---|---|
| 0.2 | 100 | N |
| 0.35 | 35 | Y |
| 0.5 | 20 | Y |
| 1 | 10 | Y |
| 2 | - [a] | N |

**Table 3.1** The effect of oxygenation gasflow rates on the circulation within the lower chamber. a) circulation not achieved.

Since the gasflow rate would appear to have a major effect on the water circulation within the lower chamber the gasflow rate was standardised for all subsequent runs at a rate of 1 bubble per second, as this gasflow rate provided a reliable water flow within the chamber, and the maximum oxygenation.

### 3.3.2.2 Serosal temperature

After standardising the gasflow rate to provide suitable circulation within the chamber the temperature achieved by the internal thermostatting was investigated. As with the gasflow validation, a silicone membrane was used in place of a tissue sample, and the reservoir was filled with double-distilled water. Initially the external thermostatting was set to a temperature of 37°C, and the chamber allowed to equilibrate for 1 hour. The thermistor

probe of a Hanna instruments thermohygrometer was adapted and fitted into the chamber as shown in Figure 3.7 to measure the chamber internal temperature. Gasflow was initiated and the temperature was measured over time. The maximum temperature achieved was 31.7°C, 5.3°C lower than necessary, to compensate for this the external water thermostatting was set at successively higher temperatures until an internal temperature of 37°C was achieved. Thermostatting the internal viability solution to 37°C required the external thermostatting to be set to 42°C.

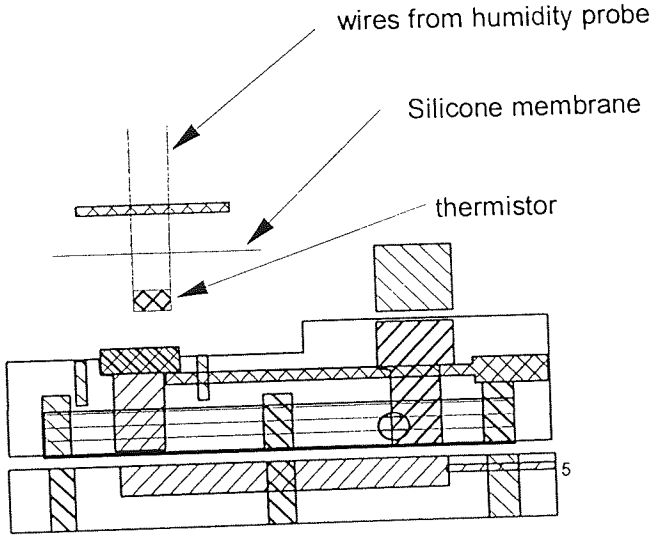


**Figure 3.7** A schematic representation of the thermistor mounted in the silicone membrane to measure the temperature of the serosal viability fluid.

### 3.3.3 Setup and operation of new chamber

#### 3.3.3.1 Tissue mounting

Tissue was mounted in the chamber by placing the underlying serosal side of the tissue over the lower tissue mounting ring. During manipulation of the tissue great care had to be taken to ensure that at no point during the procedure was the tissue surface touched, since any contact with the tissue surface that is exposed would result in damage to the epithelial and mucosal barriers. Tissue samples were manipulated using bent forceps, and after the tissue was placed on the lower mounting ring closed blunt nosed bent forceps were pushed under the tissue whilst one edge of the tissue was held to then flatten out the tissue

section, resulting in a single flat layer of tissue placed over the lower tissue mounting ring. The tissue was then clamped in place using the upper tissue mounting ring.

#### 3.3.3.2 Chamber cleaning

After each run, the tissue chamber was cleaned. The chamber was soaked in 5% Decon 90 (Decon Labs, Hove, UK) in water for a minimum of 2 hours, and then immediately prior to the following run was washed through with copious quantities of double distilled water, and finally with 100 mL glucose Krebbs ringer buffer.

## 3.4 Tissue viability results and discussion

### 3.4.1 Viability of rat ileal tissue

Rat ileal tissue was used as to investigating the versatility of the chamber in maintaining the viability of non-nasal epithelial tissues, and as a ready source for initial evaluation of the drug permeation calculations and the assumptions made. The rat was chosen since the size of the tissue obtained when an ileal section is opened out flat is ideal for mounting in the new tissue viability chamber, and it is readily available. Unlike the experiments performed with the nasal tissue in sections 3.4.2 and 3.4.3. after the the tissue sample had been mounted it was covered by a glass coverslip, since, unlike the nasal tissue, the GI tissue is not in contact with air *in vivo*.

Figures 3.8 and 3.9 show the PD generated by the tissue in the Ussing and new chamber respectively. In both cases, the voltage and short circuit current values (Table 3.2) are within the criteria setout by Hemlin *et al.* (1988) for rat intestinal tissue. Statistical analysis (single variable ANOVA) of the results in figures 3.8 and 3.9 shows that there is no statistical difference ($P < 0.05$)

| Rat ileum | Isc (μA) | PD mV |
|---|---|---|
| New chamber | 18 ± 5 | 3.2 ± 0.4 |
| Ussing chamber | 19 ± 6 | 3.4 ± 0.7 |

**Table 3.2** Isc and PD data for rat ileal tissue in both the Ussing chamber and the new chamber.

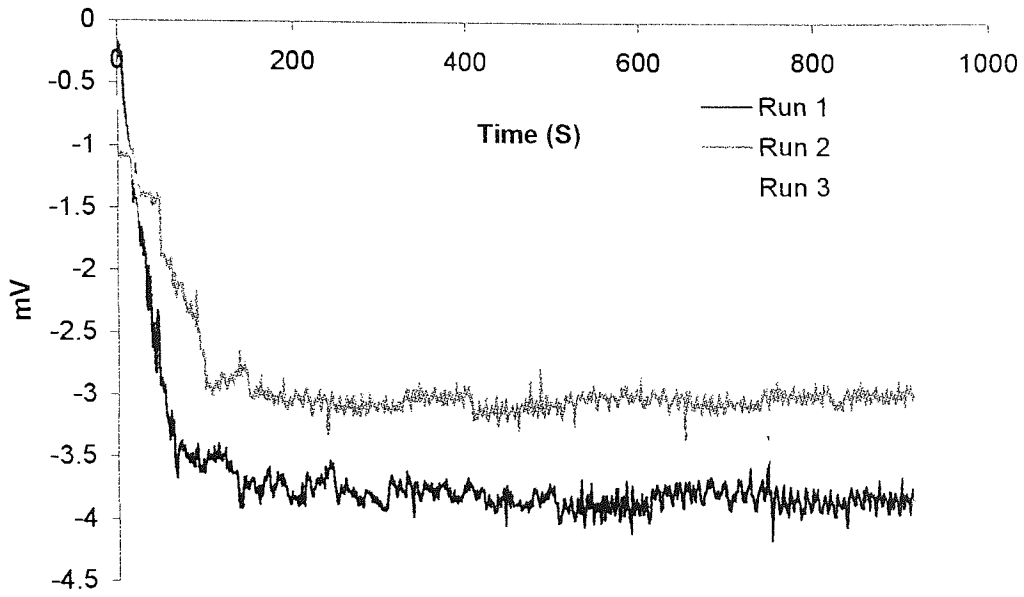


**Figure 3.8** Electrophysiological trace of epithelial PD (mV) by rat ileal tissue in the Ussing chamber without prior exposure to the ½ cell.

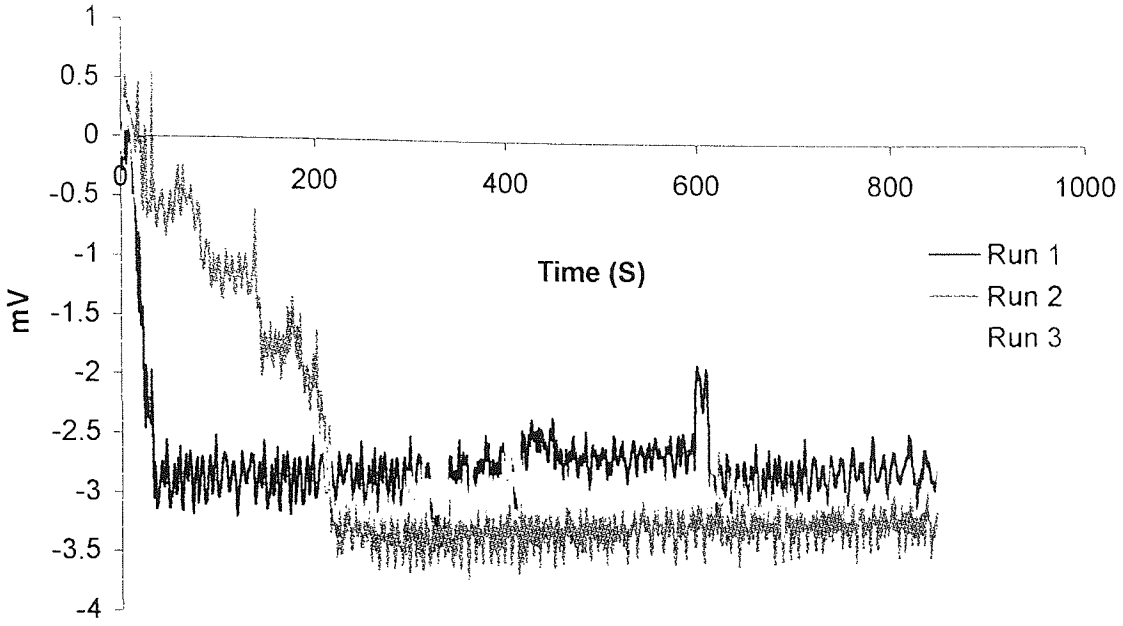


**Fig 3.9** Electrophysiological trace of epithelial PD (mV) by rat ileal tissue in the Ussing chamber after a 1h exposure to the ½ cell.

In section 3.1.3 the mathematical treatment of marker transport was considered. Two assumptions were made; firstly, that the donor concentration was significantly higher than the receiver concentration, and secondly, that the rate of change of the donor compartment concentration with time is approximately 0. From figure 3.10 it can be seen that less than 0.5 nMoles of a total amount of mucosally applied mannitol of 150 nMoles (Ussing chamber), or 5 nMoles (new chamber) reaches the lower chamber within 60 minutes; and, that less than 0.02 nMoles of a total amount of mucosally applied PEG4000 of 150 nMoles (Ussing chamber), or 5 nMoles (new chamber) reaches the lower chamber within 60 minutes. For the applied PEG4000 the two assumptions would appear to hold due to the linear nature of both permeation rates. However, for the mannitol permeation, considering the two situations up to 60 minutes, there is no statistical difference using ANOVA, ($P > 0.05$) between the serosal appearance in the two chamber situations. It is possible that after 60 minutes the second assumption (assumption 2, section 3.1.3) is no longer valid, and the mucosal concentration has changed significantly. In the early part of the experiment, it would appear that both assumptions are valid, provided that time points of 60 minutes or less are used.

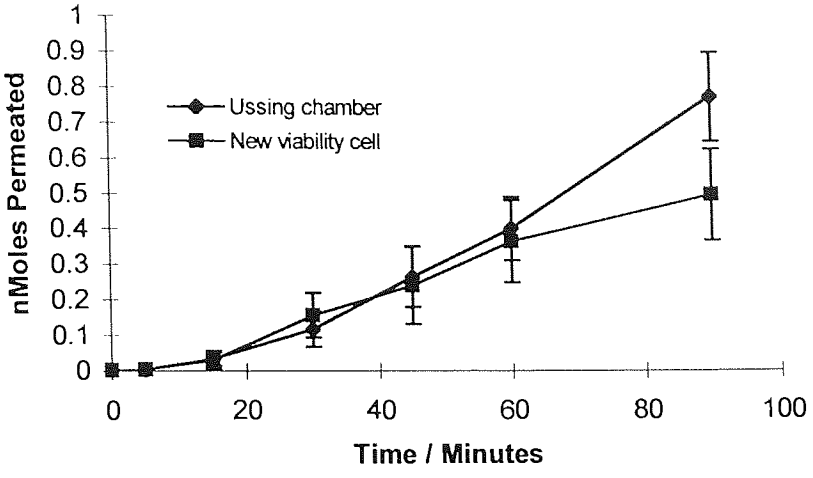


**Figure 3.10** Mannitol transport transport across rat ileal tissue expressed as nMoles permeated for both the Ussing chamber and the new tissue viability cell. (n=3)

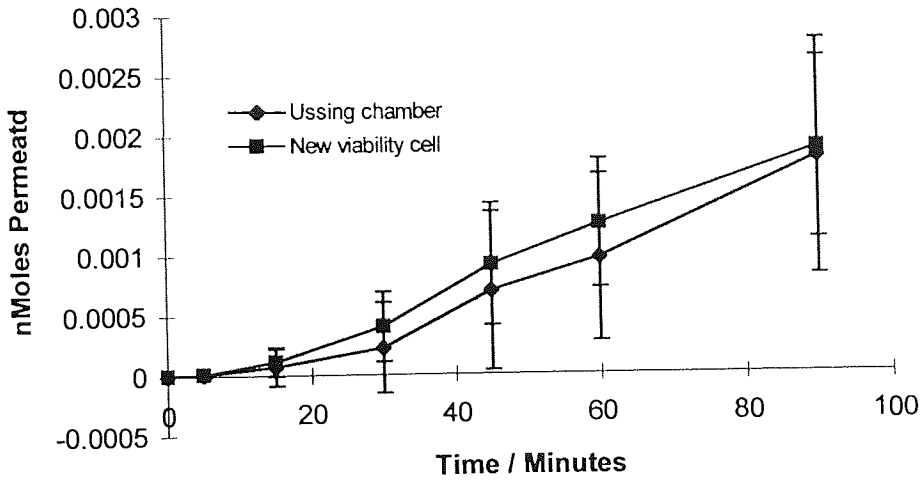


**Figure 3.11** PEG4000 transport across rat ileal tissue expressed as nMoles permeated for both the Ussing chamber and the new tissue viability cell. (n=3)

Figures 3.10 and 3.11 above, and the $P_{eff}$ values in Table 3.3 show that, since both assumptions can be held to be valid for the first 60 minutes, for the rat ileal tissue the $P_{eff}$ calculation technique described in section 3.1.3 hold for this minimal volume model, and that the new and Ussing chambers have similar marker permeation properties.

| Rat ileum | Mannitol $P_{eff}$ x $10^{-6}$ (cm $s^{-1}$) | PEG 4000 $P_{eff}$ x $10^{-9}$ (cm $s^{-1}$) |
|---|---|---|
| Ussing chamber | 2.3 | 4.1 |
| New chamber | 2.5 | 3.7 |

**Table 3.3** $P_{eff}$ values for mannitol and PEG 4000 across Rat ileum in the new chamber and the Ussing chamber.

### 3.4.2 Viability of rabbit nasal tissue

Exposure of excised rabbit nasal tissue in the Ussing chamber (Figure 3.12) resulted in a mean equilibrium voltage after 1 h for the 3 tissue samples of 6.2 ± 1.8 mV. These results are in agreement with the only available literature data for excised rabbit nasal tissue (Bechgaard *et al.*, 1992) where a mean voltage of -6.4 ± 1.5 mV was reported. This value reported by Bechgaard *et al.* was the mean value over a 10 h period, and the value obtained in Table 3.4 is the mean of a 15 minute measurement 1 h into the experiment; as such the values are not directly comparable, although it can be concluded that the voltage generated here is consistant with that previously reported. The direction of the voltage (negative or positive) is different, this is purely due to the side of the tissue that the two electrodes were placed. Reversal of the electrodes whilst collecting these data would have produce a positive voltage. $I_{sc}$ values for tissue samples exposed in both the Ussing and new chambers are shown in Table 3.2. Again, the value obtained for the $I_{sc}$ is comparable with that previously reported (Bechgaard *et al.*, 1992).

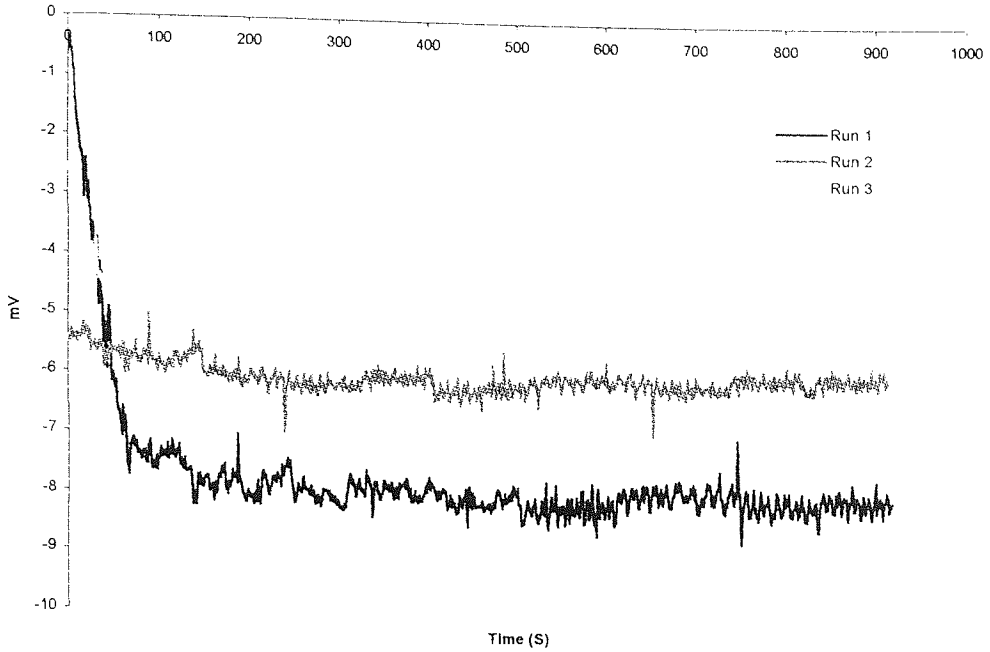


**Figure 3.12** Potential difference (mV) generated by excised rabbit nasal epithelium after a 1 h incubation in the complete Ussing chamber.

After a 1 hour exposure in the new tissue viability cell excised rabbit nasal tissue was seen to generate an equilibrium voltage potential difference of –3.2 ± 1.1 mV when transferred to the Ussing chamber (Figure 3.13). This is somewhat lower than that recorded for the tissue after 1 h Ussing chamber, indicating that after a 1 h exposure in the new chamber the tissue is not as healthy as that mainained in the Ussing chamber. Examination of the $I_{sc}$ data (Table 3.4) supports this conclusion, as the $I_{sc}$ value is significantly lower ($P < 0.05$).

| $I_{sc}$ µA | PD (mV) | Source |
|---|---|---|
| 92 ± 13 | 6.4 ± 1.5 | Bechgaard *et al.* (1992) |
| 85 ± 17 | -6.4 ± 1.5 | Ussing chamber |
| 53 ± 9 | –3.2 ± 1.1 | New viability cell |

**Table 3.4** $I_{sc}$ and PD values for rabbit nasal tissue

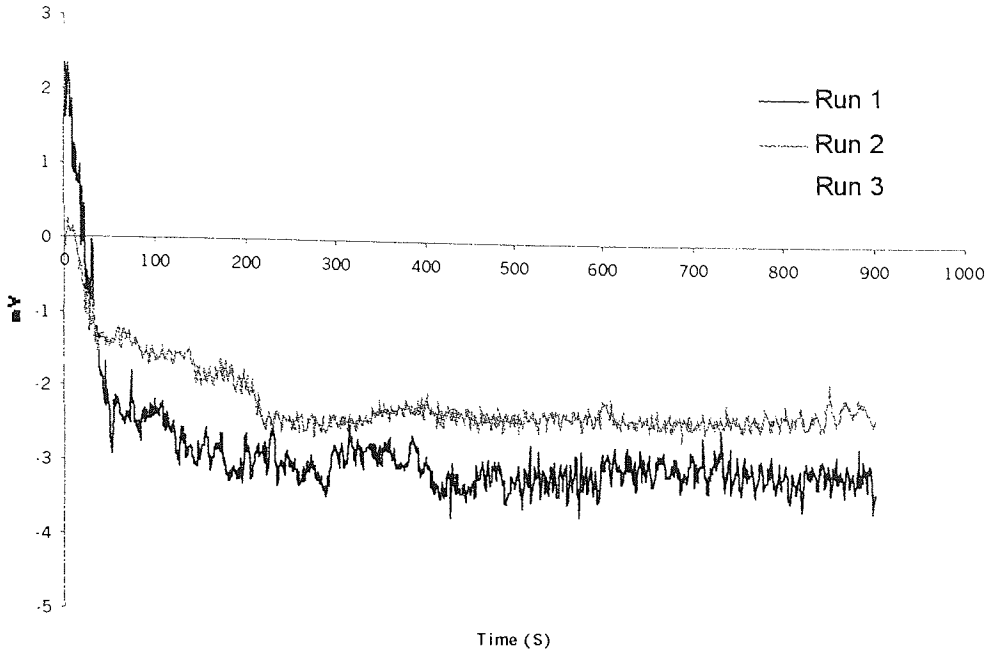


**Figure 3.13** Potential difference (mV) generated by excised rabbit nasal epithelium in the complete Ussing chamber after a 1 hour exposure in the new tissue viability cell.

Examination of the mannitol transport data (Figure 3.14) for the two chamber systems shows that there is no statistical difference ($P > 0.05$) when analysed using a single variable ANOVA test. When the $P_{app}$ for the mannitol transport in the Ussing chamber is calculated using the method of Bechgaard *et al.* (1992) a value of $5.1 \times 10^{-7}$ cm $s^{-1}$ is obtained. This is in direct agreement with the value of $0.4 \times 10^{-6}$ cm $s^{-1}$ reported by Bechgaard *et al.* (1992). $P_{eff}$ calculations for tissue in both the new and Ussing chamber give the values shown in Table 3.5. In was stated in Equation 3.3 that for the two chambers to be equivalent, the $P_{eff}$ values should be equivalent. The values obtained are not identical, but ANOVA analysis on the ammount of the total applied marker transported suggests that the two data sets are from the same population, and the closeness of the $P_{eff}$ values suggests that the two chamber systems provide adequate viability, and that the barrier function, as indicated by the paracellular transport is not different between the two systems for the rabbit nasal tissue.

| Chamber | $P_{eff}$ / $10^{-6}$ (cm $s^{-1}$) |
|---|---|
| Ussing Chamber | 1.09 ± 0.18 |
| New Chamber | 0.99 ± 0.20 |

**Table 3.5** $P_{eff}$ values calculated for mannitol in both the new and Ussing chambers

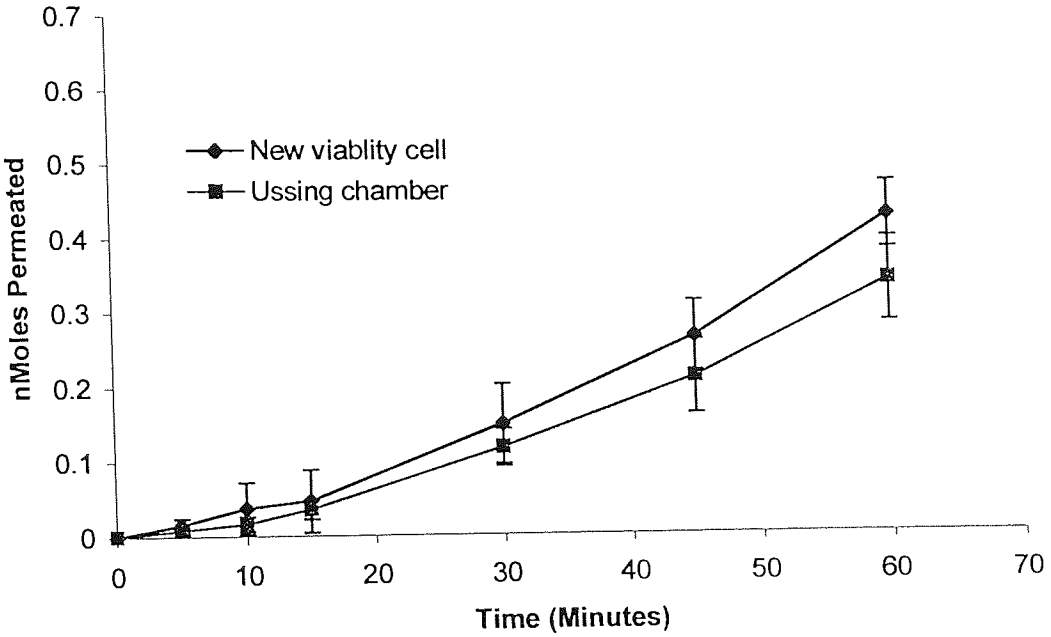


**Figure 3.14** Mannitol transport across excised rabbit nasal tissue both in the Ussing chamber and in the new tissue viability cell (n=3)

The mannitol, epithelial PD, and $I_{sc}$ data show that the Ussing chamber is maintaining the viability of the tissue, and that during the dissection procedure there is no mechanical damage to the tissue. Compartison of these factors for the Ussing chamber and the new chamber show that there is no mechanical damage to the tissue, although the new chamber is not as effective in maintaining the viability of the excised tissue.

### 3.4.3 Viability of pig nasal tissue

The viability of excised porcine nasal tissue was investigated by Wadell *et al.* (1999), they proposed from their work certain minimum values for $I_{sc}$ and epithelial PD (Table 3.6) as being necessary to define the tissue as viable. Resistivity is quoted as $\Omega$ cm$^2$, since resistance is proportional to surface area, the resistance value divided by the surface area of the tissue should be constant between different chamber types with different exposed tissue surface areas.



**Table 3.6** Minimum electrophysiological values proposed by Wadell *et al.* (1999) for excised porcine septal epithelial tissue.

The potential difference data shown in Figure 3.15 and the $I_{sc}$ data in Table 3.6 for excised porcine nasal mucosa (obtained from the septum) in the Ussing chamber all meet the minimum electrophysiological criteria outlined above. The values obtained for the voltage (mean PD –3.3 ± 0.7) and $I_{sc}$ (54 ± 22 μA) are somewhat lower than those reported by Wadell *et al.* The system used by Wadell *et al.* is a Costar horizontal Ussing chamber, it is well known that as well as wide intra laboratory and inter laboratory differences in electrophysiological values the system used has a significant effect on the values obtained (Wadell *et al.*, 1999).

| | Isc (μA) | PD (mV) |
|---|---|---|
| Ussing chamber | 54 ± 22 μA | –3.3 ± 0.7 |
| New chamber | 34 ± 10 μA | -1.03 ± 0.3 |

**Table 3.7** Isc (μA) and PD (mV) for porcine nasal epithelium in both the new and Ussing chambers after a 1 h incubation.

After a 1h exposure in the new tissue viability chamber, the epithelial potential difference (Figure 3.16) and $I_{sc}$ (Table 3.7) are significantly lower than those reported for the control exposure in the Ussing chamber, however, they are still above the minimum limits setout by Wadell *et al.* (Table 3.6)

The transport of the paracellular marker, mannitol, across the porcine epithelial tissue (Figure 3.17) proved to be not statistically different from the baseline readings - suggesting that the tissue represents an impenetrable barrier. Conversely, Wadell *et al.* (1999) reported a relatively high $P_{app}$ value of 3.9 ± 2.2 x$10^{-6}$ cm $s^{-1}$. This difference could be due to any number

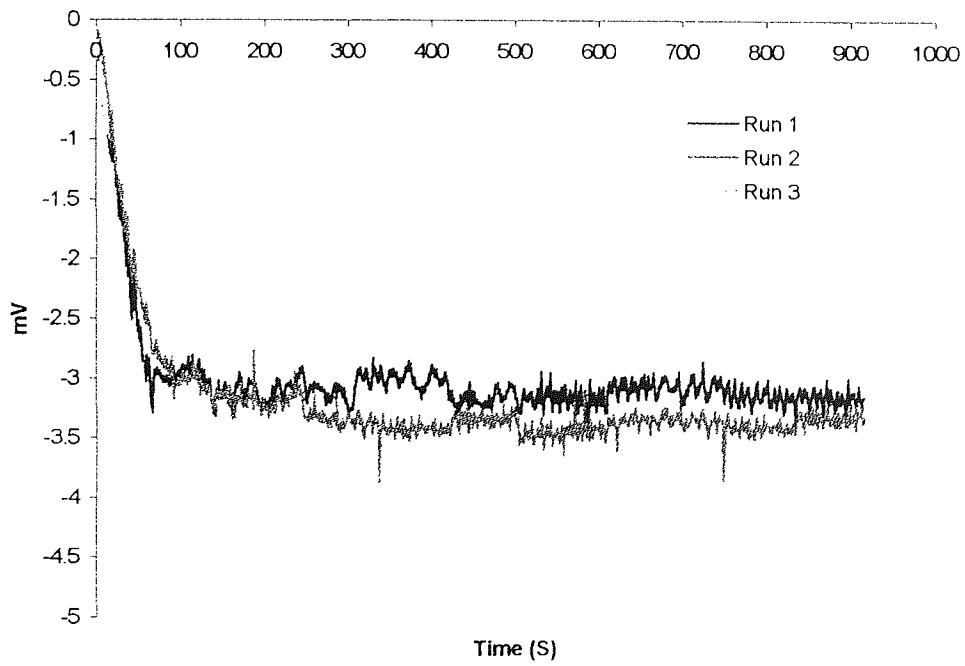


**Figure 3.15** Electrophysiological trace of epithelial PD (mV) generated by pig nasal tissue in Ussing chamber without prior exposure to the ½ cell.

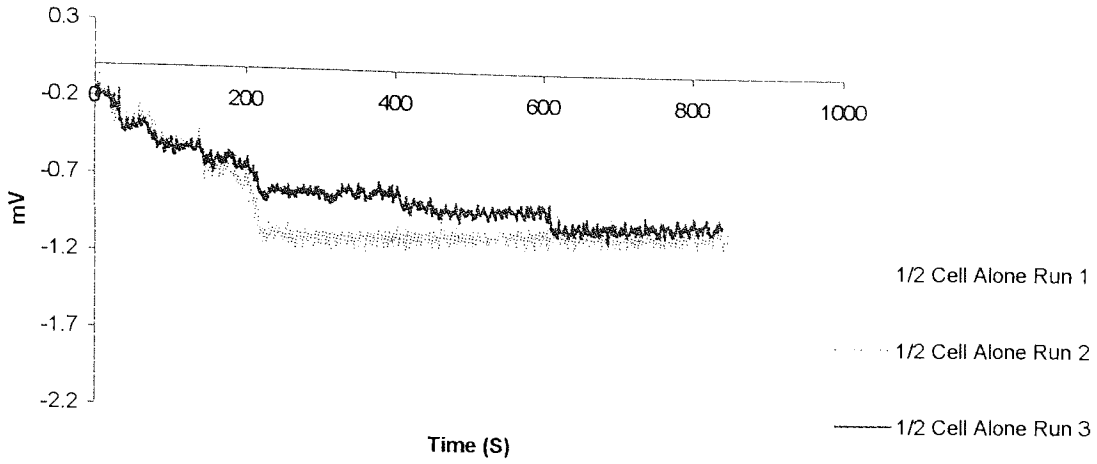


**Figure 3.16** Electrophysiological trace of epithelial PD (mV) generated by pig nasal tissue in Ussing chamber after 1 hour exposure in the lower ½ cell alone and in the Ussing chamber without prior exposure.

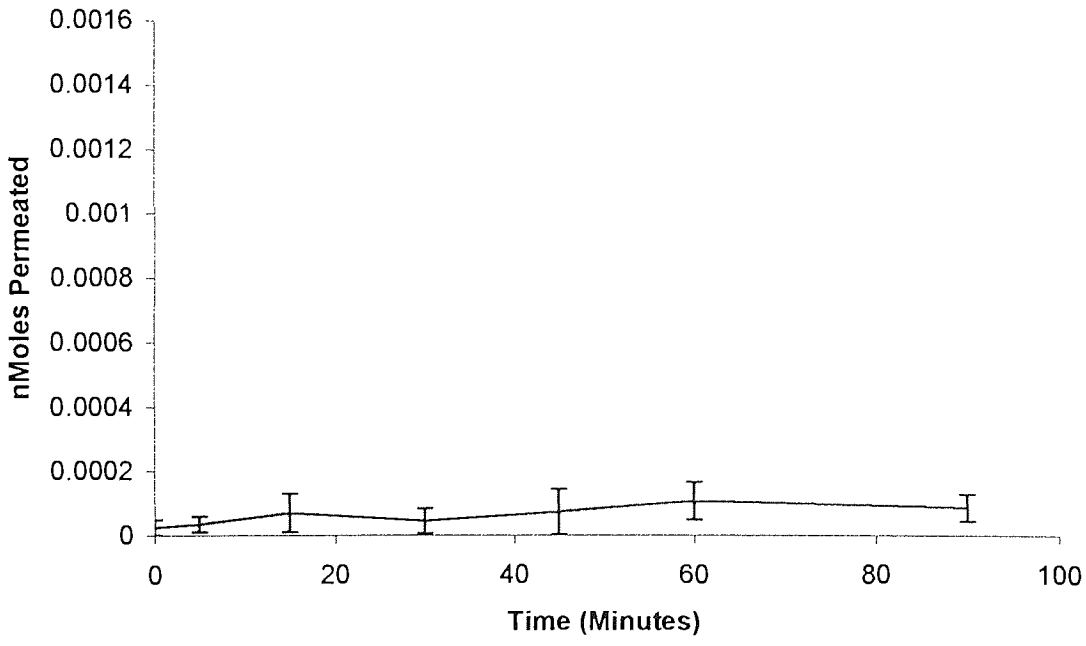


**Figure 3.17** Mannitol transport across excised porcine nasal tissue both in the Ussing chamber and in the new tissue viability cell (n=3).

of factors, including the sub-species, age, sex, of the donor, as well as experimental techniques such as the tissue isolation method. A potentially greater factor is the method in which the donor was sacrificed. In the United Kingdom, animals are stunned and then either shot or have their throats cut, wheras, in Sweden where the work of Wadell *et al.* was performed the preferred method of sacrificing by inhalation of an increasing concentration of

carbon dioxide. The inhalation method of sacrifice may have an effect on the tissue, since the use of inhalation anaesthetics has already been proved to have an effect on drug permeability across the nasal epithelium (Section 1.5.1.3).

From the data in Table 3.7 and Figures 3.15 and 3.16, it can be concluded that the new tissue viability chamber maintains the tissue to above the minimum requirement, however, as with the excised rabbit nasal tissue, the new chamber did not perform as well as the traditional Ussing chamber.

## 3.5 Discussion and conclusions on viability of tissues within 1/2 chamber.

The new chamber system described here proved able to provide warm, oxygenated, tissue viability buffer to the tissues serosal surface. The external thermostatting together with the internal waterways in the chamber kept the serosal buffer solution at a temperature of 37 °C. The oxygenation system proved acceptable at generating a suitable water flow within the inside of the chamber. Standard operating procedures for the mounting of tissues in the new chamber were developed, together with protocols for operating the chamber system.

With a dry upper surface to the tissue, it proved impossible to measure the epithelial electrical characteristics directly. Tissue samples are mounted in the the new chamber where then transferred to the Ussing chamber to measure these electrical properties. This proved possible since the new chamber was designed with the same size aperture as the Ussing chamber. If, in future, smaller chambers are produced, for example for the use of mouse GI tissues, or nasal tissue from smaller species, this approach may not be feasible, since the Ussing chambers used were the smallest currently available.

From the data presented in sections 3.4.1 to 3.4.3 it can be seen that the new chamber provides adequately for the viability of the rat ileal tissue when it is kept under a glass coverslip; similarly, with the rabbit nasal tissue the viability is maintained when the tissue is under a glass coverslip. However, for the nasal tissue samples exposed to the

ambient atmosphere there is a significant reduction in the potential difference that the tissue generates, although in all cases the tissue is still viable, and above the minimum values acceptable as an indication of viability.

To measure the physical barrier properties two markers, mannitol and PEG4000 were applied to the epithelial surface of rat ileal tissue. Experiments in both chamber systems had the same molar concentration of marker applied, with the difference being in the volume that was used. Volumes of 1.5 mL and 50 µL were used for the Ussing chamber and the new chamber respectively. From the data in section 3.4.1 the mathematical assumptions made (assumptions 1 and 2, section 3.1.3) were proved to be valid for these two compounds within a limited time period.. Using the $P_{eff}$ technique for measuring marker flux within this 60 minute time period the physical barrier properties of all the tissues were shown to be statistically non significant when data from tissue in either the Ussing chamber or the new chamber are compared.

Taking into account the increase in epithelial potential difference when the tissue is kept under a glass coverslip significant changes can be made to the chamber system to improve the viability of the tissue. These changes are described in chapter 4.

# Chapter 4

## The upper environmental chamber – design, development, and, validation.

## Overview

In the previous chapter an *in vitro* system for maintaining the viability of epithelial tissues was developed. The work done highlighted the potential for improving the environment that the nasal tissues investigated experienced. In this chapter the chamber system is modified so that the environment that the nasal tissue experiences *in vitro* is much closer to the *in vivo* situation.

## 4.1 Introduction with aims in designing nasal chamber

In chapter 3, a tissue viability cell was developed with the specific aim of using an aqueous phase only on the serosal side of the tissue. As previously outlined, there are various disadvantages to this system, mainly the lack of control over the atmosphere experienced by the tissue; also, for nasal delivery studies, any system should provide an atmosphere as close as possible to that found in the nasal cavity. The aim of the work in this chapter is to modify the chamber system to produce one that mimics the nasal cavity more closely. Once the correct atmosphere above the tissue has been incorporated, this represents an ideal opportunity to develop a system that can be used to investigate the effects of the atmosphere on nasal delivery devices.

## 4.2 Modelling the nasal cavity

The nose has an important physiological function, and any model of the cavity must also be able to reproduce reliably these characteristics. The nasal modification of inspired air by filtration, humidification and warming (Proctor, 1977) are considered to be the main functions of the human nose, providing a constant stream of air in a precisely controlled condition. Equally the chamber should be able to provide such a controlled, reproducible environment whatever the ambient laboratory conditions are.

Any model of the nasal cavity must model the temperature, humidity and air-flow rates found *in vivo*.

### 4.2.1 Temperature

The function of the nose is to warm and humidify inhaled air. Air enters the nose at ambient conditions. Ambient temperature can vary widely (temperatures ranging from -20 to +40 °C can be experienced). This air is warmed to a temperature that is not harmful to the lungs, and at the nasopharynx, some 12-14 cm into the adult human nasal cavity, the air temperature approaches 37 °C (Proctor, 1977).

The design of the lower chamber precludes using the tissue, or the lower viability 1/2 cell to provide the warming of the air, so the chamber design must accommodate this, supplying the chamber with pre-warmed air at a temperature that is somewhere between the ambient laboratory conditions and 37 °C

### 4.2.2 Humidity

The nose supplies the inhaled air with vast quantities of water to ensure that as the air leaves the nasal cavity at the nasopharynx, where the septum ends and the two halves of the nasal cavity merge into one, the air has a suitable level of moisture. By the time the inhaled air reaches the nasopharynx, the humidity has risen so that it is close to 100%.

As with warming the air in the nasal chamber, the design of the lower chamber precludes using the tissue, or the lower viability ½ cell, to provide the moisture to raise the humidity of the inhaled air, so the chamber design must accommodate this, supplying the chamber with pre-warmed, pre-humidified air at a temperature that is somewhere between the ambient laboratory conditions and 37 °C, and at as high a humidity as possible.

### 4.2.3 Airflow

In the adult male the mean tidal volume (the volume of each breath whilst the individual is relaxed) is 500ml, and the average breathing rate is 7.5 breaths per minute, equal to one every eight seconds. This represents a typical flow of 3.75 L $min^{-1}$ per nostril, although as a pulsatile rather than uniform flow (Lippman, 1990). There is no current monograph on testing for nasal delivery, although currently for pulmonary delivery the monograph stipulates a flow rate of 60 L $min^{-1}$ (BP 1993) which is in stark contrast to that above.

From this observed anomaly flow rate data was obtained from 15 healthy postgraduate students. Each student was asked to breathe through the apparatus shown in

Figure 4.1. For each subject the maximum flow rate was recorded on 10 successive inhalations and exhalations. This results in a mean peak inhalation rate of 4.02 L $min^{-1}$, and a peak exhalation rate of 4.8 L $min^{-1}$. This would suggest that an air-flow rate significantly lower than that currently used in the BP would more suitable in the new chamber. In all experiments flow rates of 4 L $min^{-1}$, together with 10 L $min^{-1}$ as a higher more forceful rate were used.

The linear velocity of the air can be considered as the volume flow divided by the cross sectional area of the vessel through which the air-flows. The BP specified apparatus (techniques A, B, and C) has a range of linear flow values of 3.1 – 5.3 L $min^{-1}$ $cm^{-2}$ at the inlet. Calculation of the linear flow rate for the above students, making the assumption that their nostrils were circular gives a flow rate of 4.2 ± 1.3 L $min^{-1}$ $cm^{-2}$. When the calculations were performed for the design proposed in section 4.3 the linear velocity was 5.1 L $min^{-1}$ $cm^{-2}$ for the flow rate of 4 L $min^{-1}$, and 12.8 L $min^{-1}$ $cm^{-2}$ for the 10 L $min^{-1}$ suggesting that for normal breathing the airflow values chosen are suitable and relevant to the *in vivo* situation.

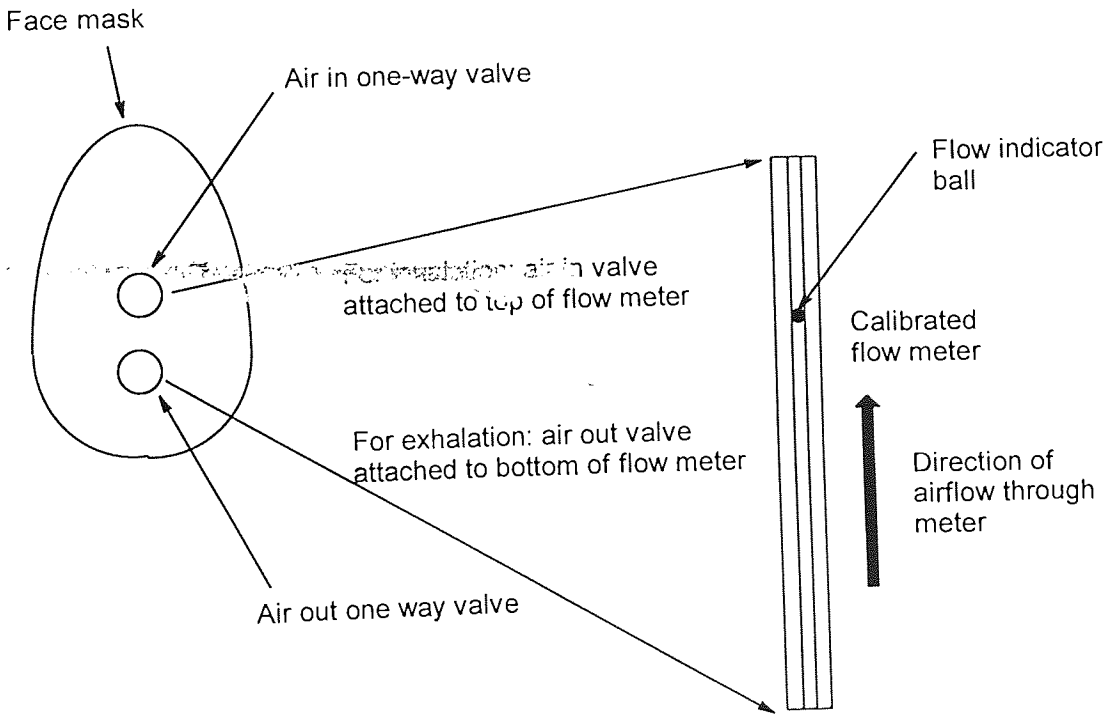


**Figure 4.1** Apparatus used to measure flow rate at rest

## 4.3 Design of new chamber

The design criteria for the new chamber have been outlined in section 4.2, essentially an area must be created over the lower tissue viability 1/2 cell in which a controlled atmosphere can be generated. After unsuccessful experimentation, a chamber that fitted over the lower chamber and was supplied with pre-warmed and humidified air was decided upon. This has the advantage that the lower cell can be removed and used by itself as and when circumstances dictate, making the chamber more flexible.

### 4.3.1 Design - description of chamber

The principle of the upper chamber mounted onto the lower tissue viability ½ cell is illustrated in Figure 4.2, and the overall layout of the complete system with the air supply is shown in Figure 4.3. The complete system consists of the ½ cell with the upper chamber attached supplied with pre-warmed humidified air. The air warming and humidification is described in 4.3.2. Unlike the *in vivo* situation, this system is a continuous flow model. Airflow is provided by attaching the upper chamber to a vacuum source This pressure difference provides the flow of warm humid air from its source through the chamber and out to the moisture trap. The air-flow rate was controlled by means of a flow-control valve placed between the vacuum pump and the flow meter.

The nasal chamber is a simple perspex box with an inlet designed to mimic a nostril and an outlet to the vacuum source *via* a 0-15 L $min^{-1}$ air-flow meter (ball in tube type). The aim of the simple perspex box is to contain the modified environment above the tissue surface. Since the lower chamber has a large surface compared to the size of the tissue surface, the "nostril" is placed directly over the tissue. The flow patterns of the air introduced into the chamber are then modified by placing a number of baffles in the upper chamber. These baffles were moved around the chamber until satisfactory air-flow was achieved.

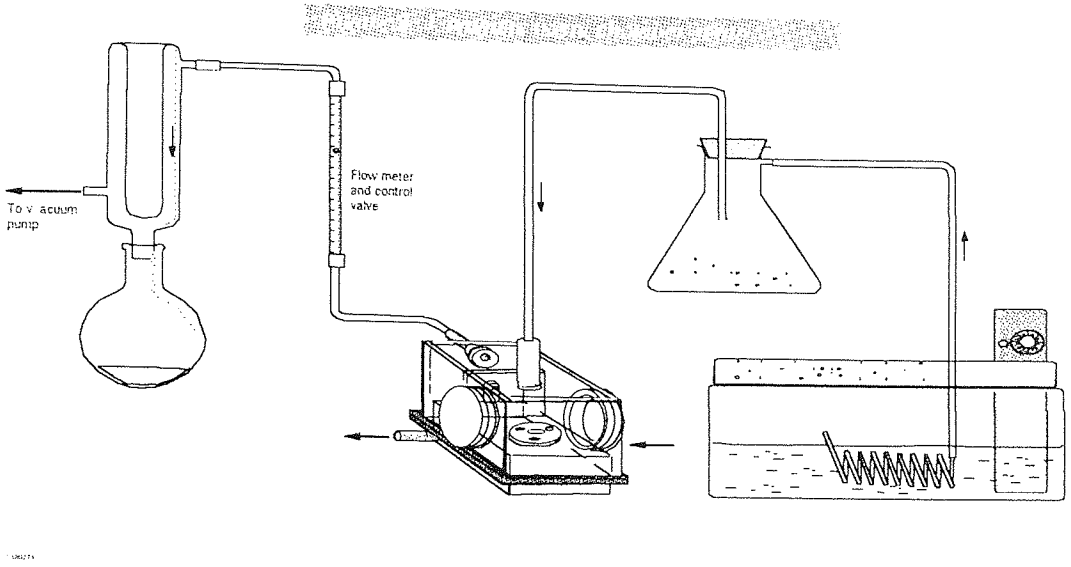


**Figure 4.2** Complete nasal chamber setup. (From Turner *et al., 1999*)

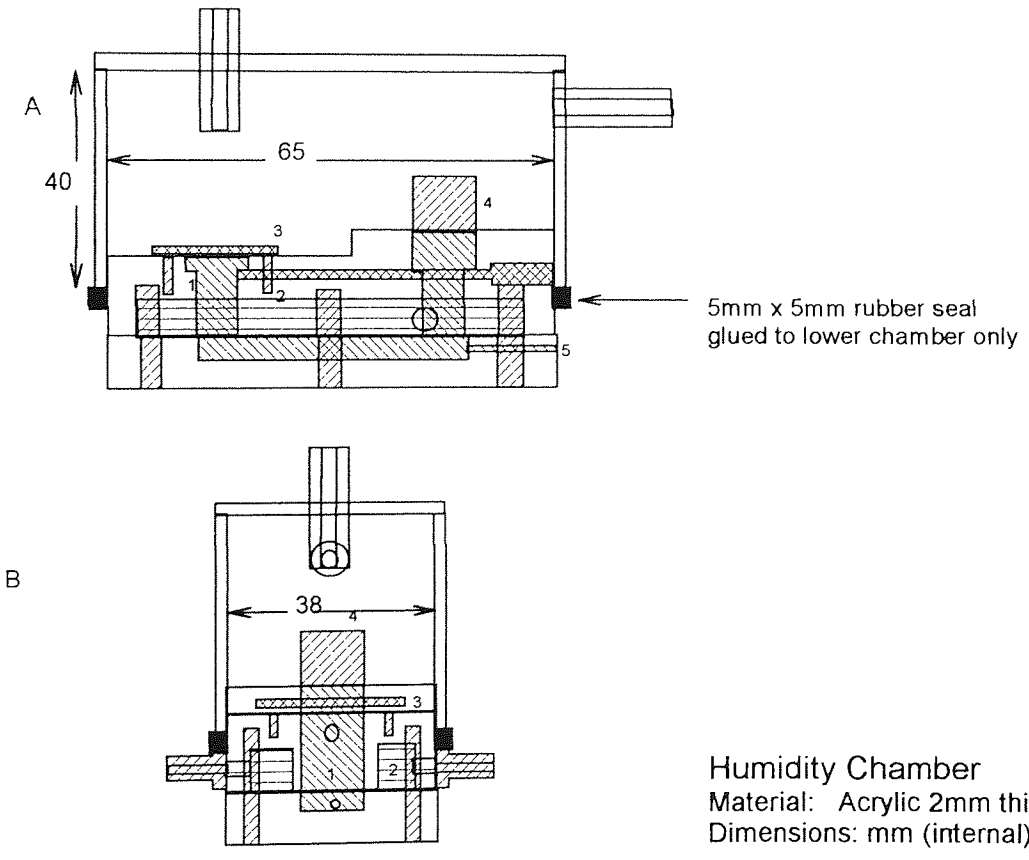


**Figure 4.3** Layout of the upper chamber on top of the lower tissue viability ½ cell. A) side view, and B) end view. 1) Lower reservoir, 2) Thermostatting waterways, 3) Tissue mounting rings, 4) Anti-splash chimney, 5) Carbogen inlet.

### 4.3.2 Advantages / disadvantages of design

This particular design of the upper chamber was settled upon after considerable thought, the upper chamber is an enclosed environment that represents the environment in the nasal cavity. The function of the nose includes modification of the inspired air; the upper chamber, unlike the nose, is supplied with pre-warmed, pre-humidified air as there is only a small fraction of the nasal epithelium, whose function is to provide the warming and humidification, present in the chamber.

Humidity can be controlled in two ways; either the air can have small amounts of water introduced in a controlled manner, or an excess of water can be introduced into the air and then the humidity reduced to the level required. In choosing the latter system, the humidity and air-flow rates required were considered. Chemical systems of controlling humidity are considered good for low flow rates, and low humidities. The conditions required (10 L $min^{-1}$ and >95% RH) would suggest that it would be better to generate large volumes of saturated air and then correct the humidity and temperature. As can be seen later, this method proved to be reliable, reproducible and, most importantly, simple. In the final design, steam generated by a very hot water-bath (80 °C) is collected. This saturated air is then pulled through a heating column in the 80°C water bath, to a 500ml Büchner flask. The Büchner flask is warmed in a second water-bath set to the desired air temperature.

The major departure from the *in vivo* situation in this particular design is that the warm humid air is drawn in directly onto the tissue. In the human nasal cavity, the air-flow is parallel, not perpendicular to the direction of flow. Consideration was given to producing a system in which the air-flow was parallel rather than perpendicular to the tissue surface. The major disadvantage of a system of this type is the mounting of the tissue. Arrangements were considered where the air-flow was horizontal, over the tissue surface. Any mounting device (in the design chosen it is a PTFE ring) in such a system must in no way interfere with the air:surface interface, the mounting device must be below the final tissue surface to allow uninterrupted air-flow from the nostril, over the tissue surface, and

then to the outlet. The final arrangement chosen does have the advantage that any drug or applied substance entering from the nostril does have an uninterrupted passage to the tissue surface, and impacts the tissue in a controlled manner.

In designing the chamber, the final use has to be considered. Deposition models of the nasal cavity are available (Chien *et al.* 1989). This chamber is not designed as a deposition model, but primarily to enhance the viability of the excised nasal tissue by providing a controlled environment on the mucosal side. With these considerations, it was decided that having the air-flow perpendicular to the tissue surface was not a major drawback to the system.

## 4.4 Macroscopic validation of chamber - Methods

Before any studies can be performed in the chamber, the design must be validated with respect to its macroscopic properties, the air-flow pattern, humidity and air temperature experienced by the tissue.

Characterisation of the atmosphere experienced by the tissue surface in terms of temperature and humidity was performed by manufacturing a false lower chamber fitted with temperature and humidity probes from a Hanna Instruments Thermohygrometer (Model HI8564, [illegible]). In this false base, the temperature and humidity probes were placed just above the nominal tissue surface. The actual tissue surface position varied with the thickness of the excised tissue samples. In the false chamber, the bottom of the temperature and humidity sensors (at the very end of the probe) were placed at the level of the serosal side of the tissue as shown in Figures 4.4 and 4.5. The advantage of making an artificial base is that it can readily be swapped with the lower tissue viability cell for monitoring air temperature before and after experimental runs.

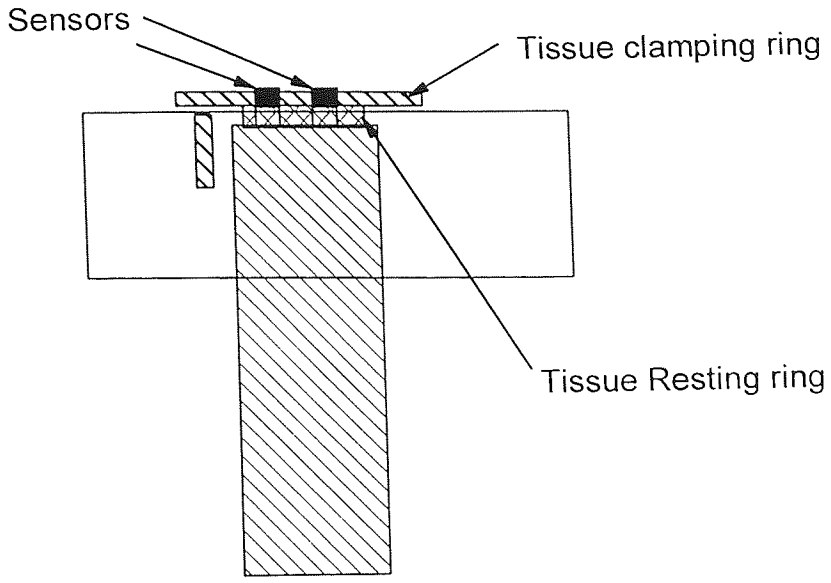


**Figure 4.4** Arrangement of the temperature and humidity probes in the artificial lower base.

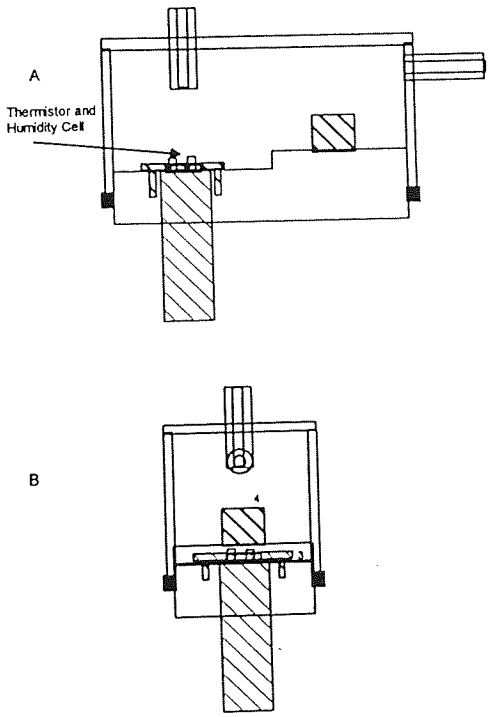


**Figure 4.5** Arrangement of the temperature probe in the complete chamber system. A) side view, B) end view.

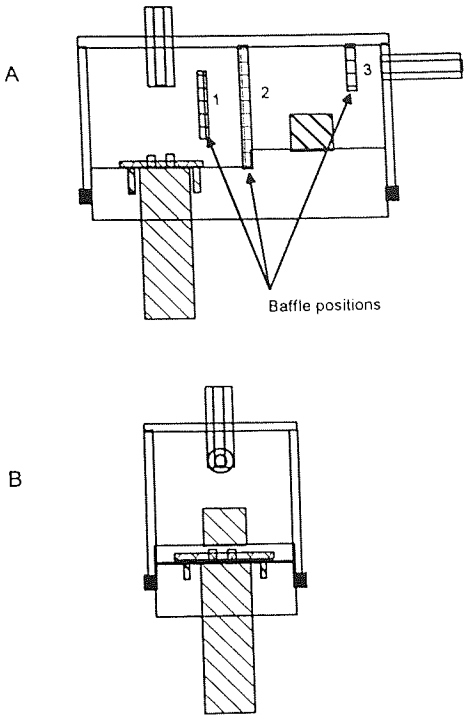


**Figure 4.6** Arrangement of the internal baffles within the upper chamber. A) side view, B) end view. Numbers represent baffle positions referred to in Figures 4.8 to 4.12.

### 4.4.1 Airflow

Smoke was introduced into the complete chamber as a method of visualising the air-flow within the complete setup. Smoke was generated by removing the air warming and humidifying apparatus and replacing this with a smoke source. In this case, a lit cigarette was used as the smoke source ("Marlboro", BAT, Leicester UK), and the cigarette placed in the artificial nostril. After the air-flow was started, the resulting smoke patterns were monitored by video capture (Panasonic CCD-12 camera) and recorded for analysis. Video was analysed by digitising the picture using the Adobe Premier™ software (Adobe Systems Europe BV, Amsterdam, The Netherlands) on an Apple Macintosh fitted with a miroMotion DC30 card (miroComputer Products AG, Braunschweig, Germany). After digitisation, the video image was de-interlaced and still frames were removed from the video clips.

The air-flow round the chamber was modified by placing a number of baffles in different places around the upper chamber. The baffles (Figure 4.7) were of various sizes and shapes, although all manufactured from 3mm perspex. The smoke flow was visualised

with a number of different baffle arrangements, five of which are shown in Figures 4.8 to 4.12

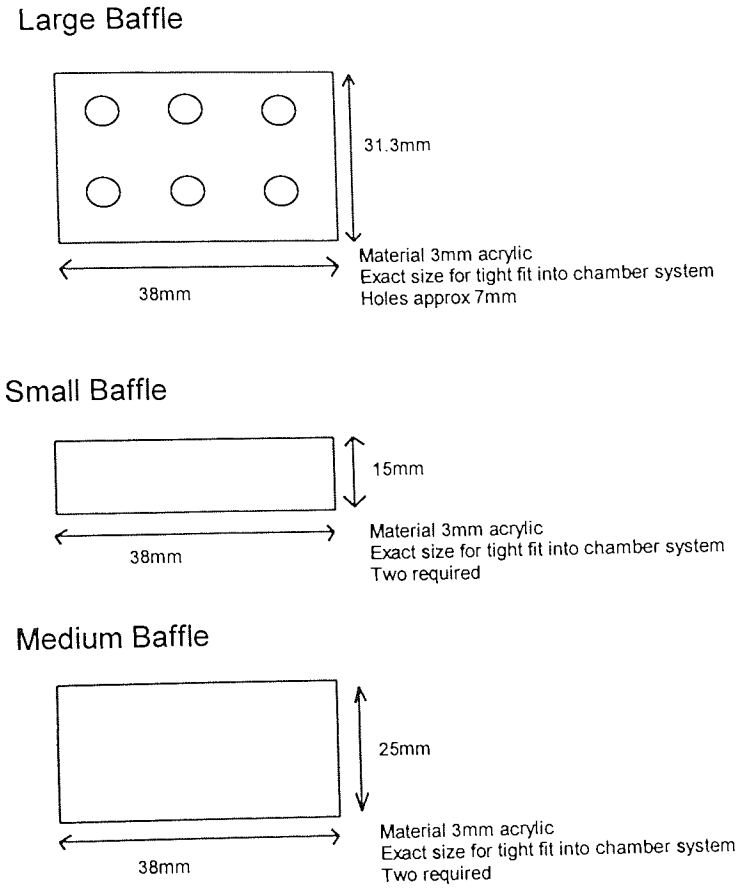


**Figure 4.7** Engineering diagram for internal baffles

From Figures 4.8 to 4.12, the various different air-flow patterns around the chamber can be seen. Under the low flow rate conditions, several of the arrangements gave a layer of modified air "hugging" the bottom of the chamber, covering the tissue area. However, as soon as the air-flow rate was increased to the higher rate (10 L $min^{-1}$) this layer did not form. When the medium-sized baffle (2/3 of the upper chamber height) was placed in position 2 (Figure 4.12), this layer of modified air covered the tissue adequately. The smoke was seen to fill the well formed by the baffle, and then overflow into the rest of the chamber and to the outlet. The use of smoke to visualise the air-flow around the chamber relies on the smoke having similar flow patterns to the warmed humid air. If the flow of the smoke and that of the humidified, warmed air is similar as has been assumed, these experiments indicate that the air-flow in the chamber produces a suitable layer of modified air above the tissue.

a)

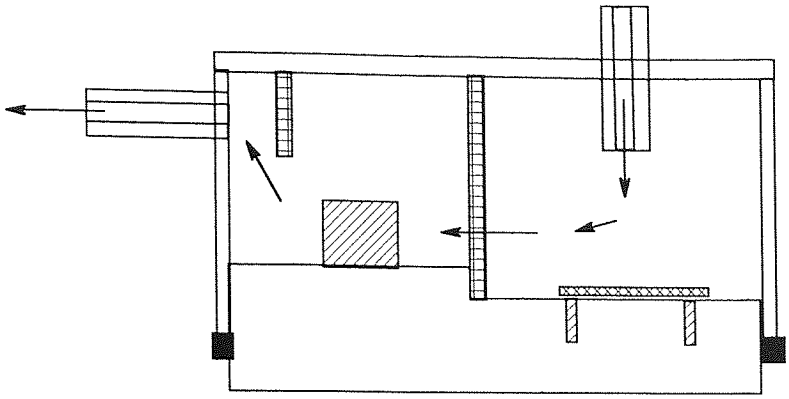

b)

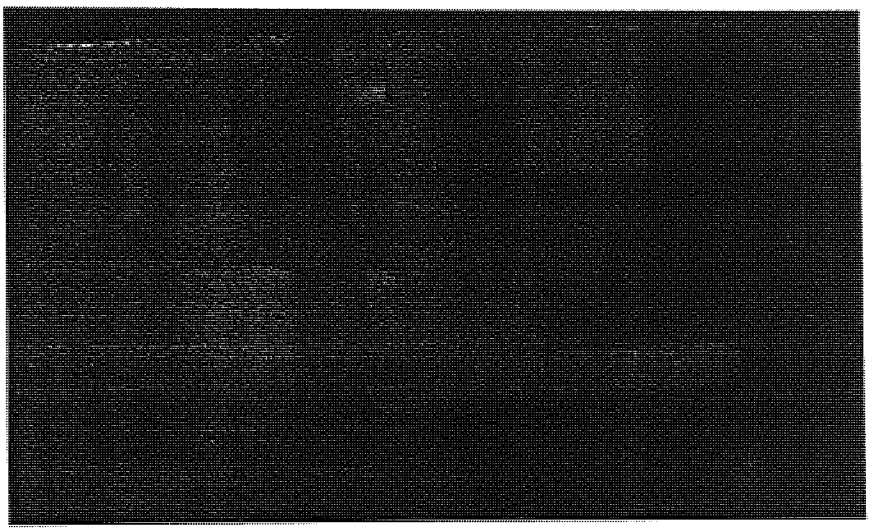

c)

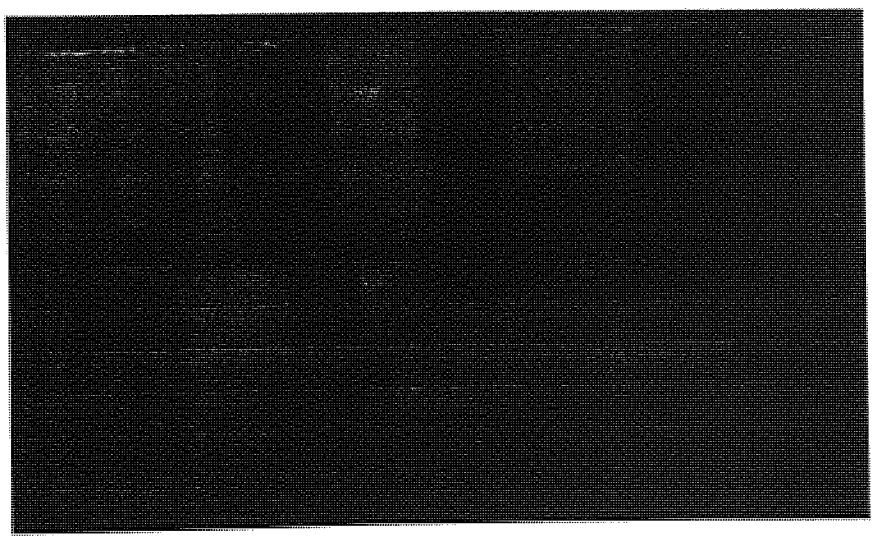

**Figure 4.8** Smoke flow patterns within complete nasal chamber. Large baffle in position 1, and small baffle in position 3. a) diagramatic representation of air-flow b) smoke flow at an air-flow rate of 10 L $min^{-1}$, and c) air-flow rate of 4 L $min^{-1}$

a)

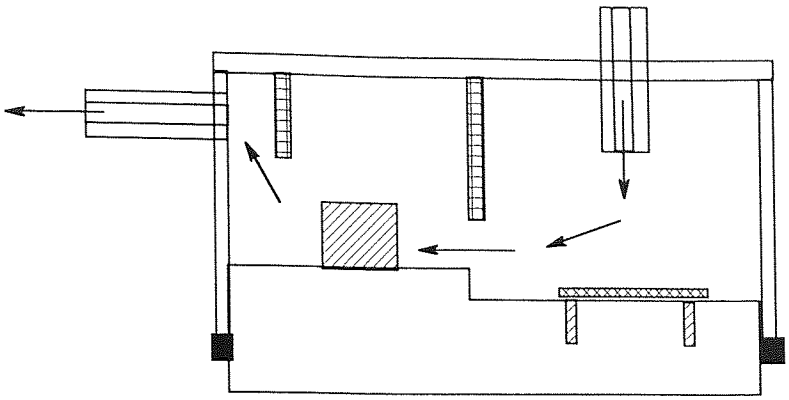

b)

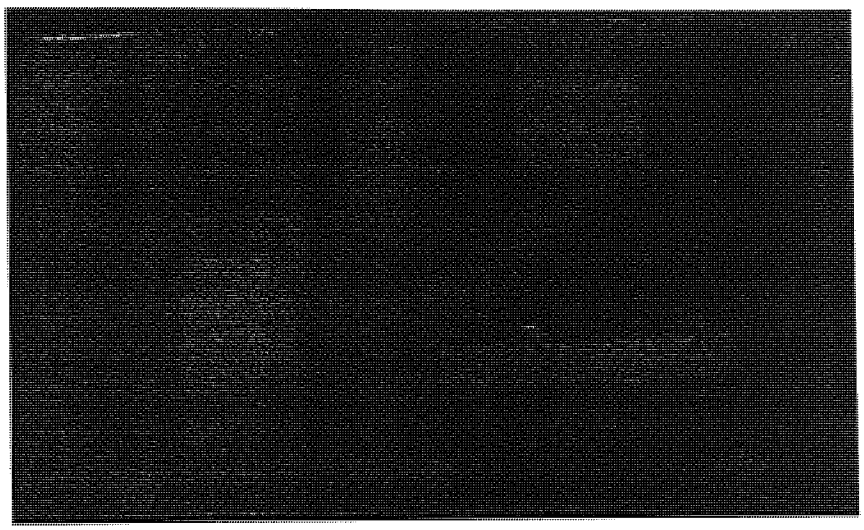

c)

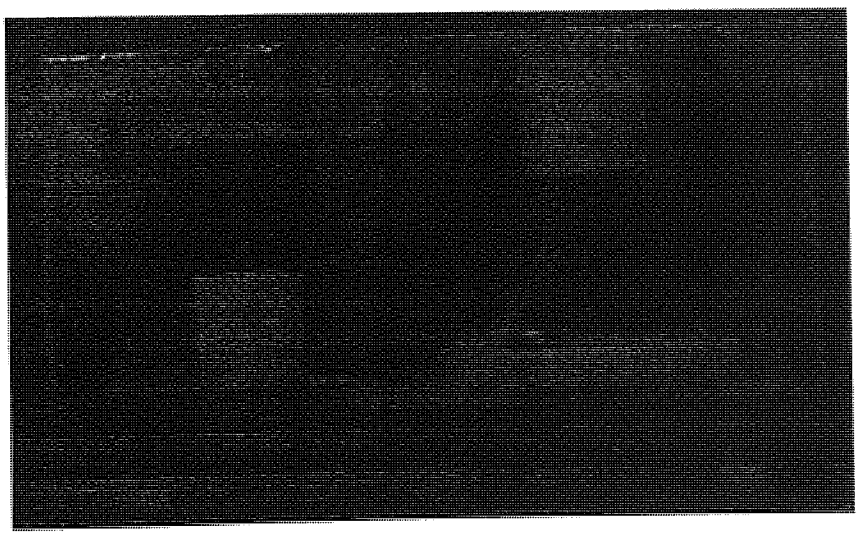

**Figure 4.9** Smoke flow patterns within complete nasal chamber. Small baffle in position 1 only. a) diagramatic representation of air-flow b) smoke flow at an air-flow rate of 10 L $min^{-1}$, and c) air-flow rate of 4 L $min^{-1}$

a)

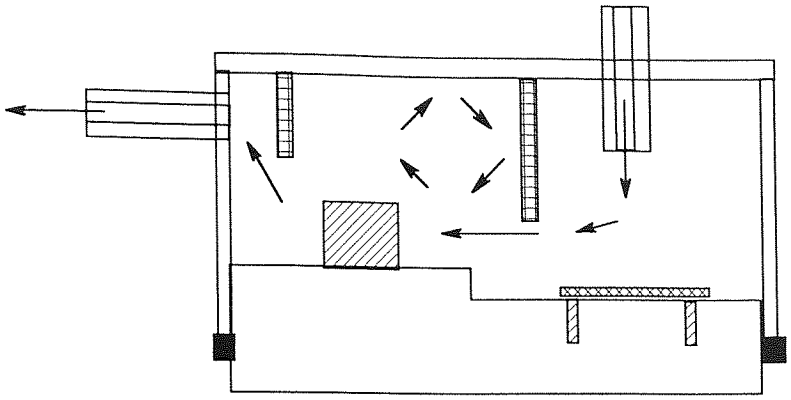

b)

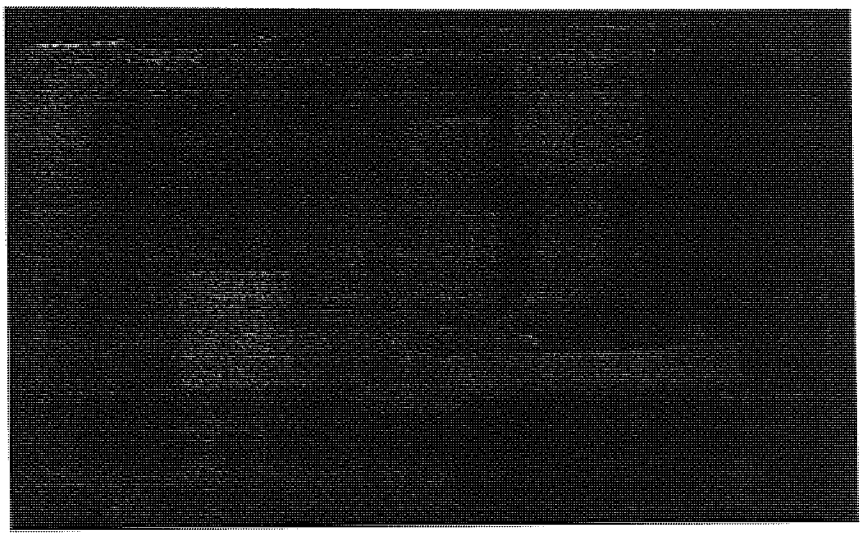

c)

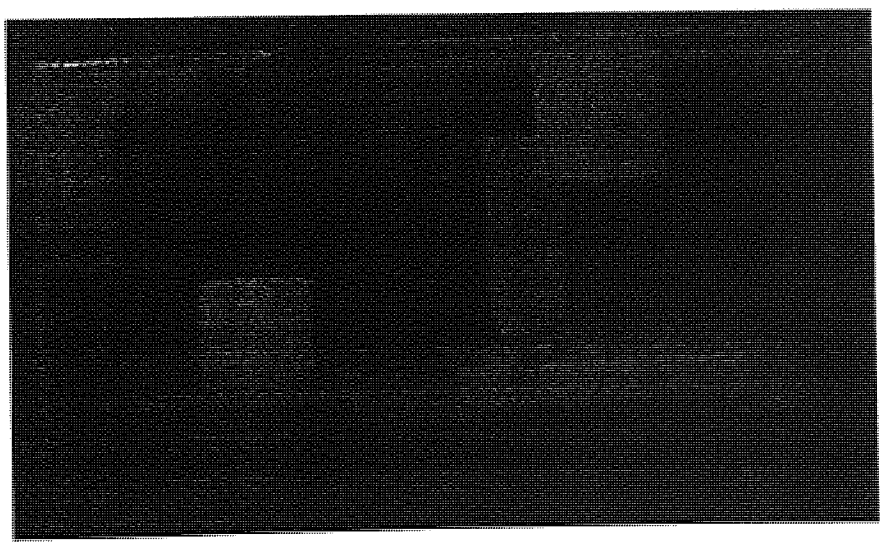

**Figure 4.10** Smoke flow patterns within complete nasal chamber. Medium baffle in position 2 only. a) diagramatic representation of air-flow b) smoke flow at an air-flow rate of 10 L $min^{-1}$, and c) air-flow rate of 4 L $min^{-1}$

a)

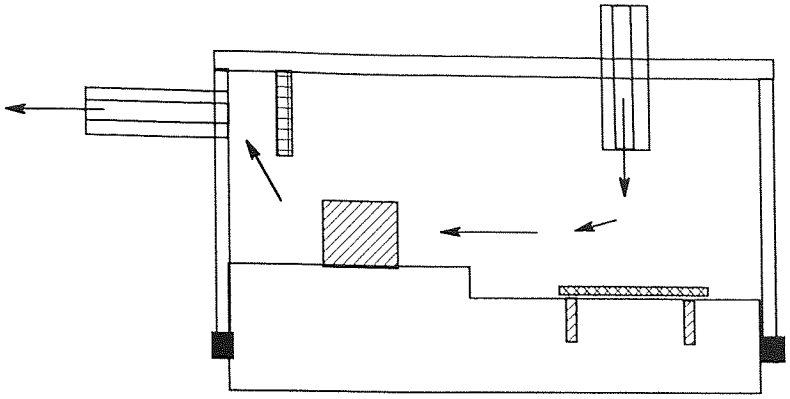

b)

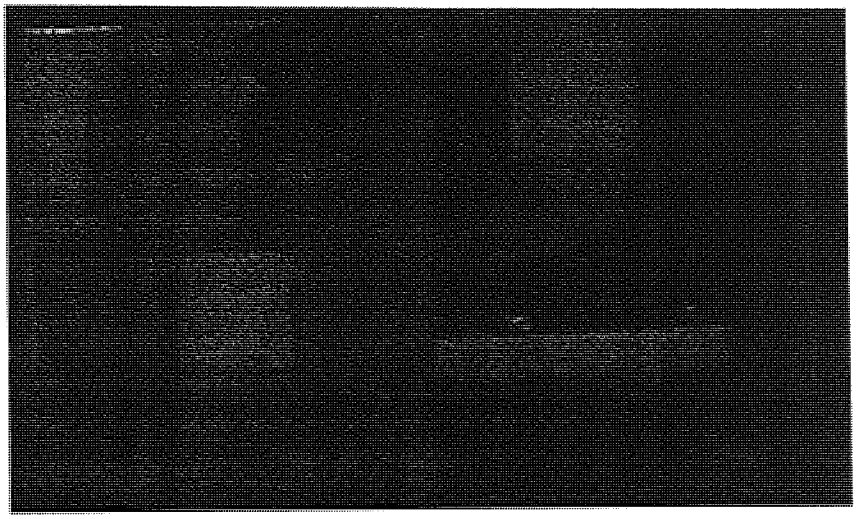

c)

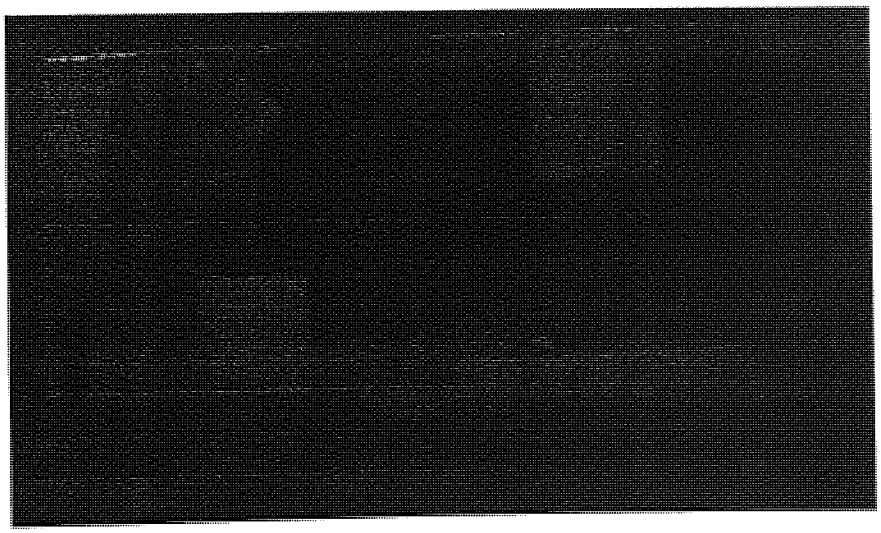

**Figure 4.11** Smoke flow patterns within complete nasal chamber. Small baffle in position 3 only. a) diagramatic representation of air-flow b) smoke flow at an air-flow rate of 10 L $min^{-1}$, and c) air-flow rate of 4 L $min^{-1}$

a)

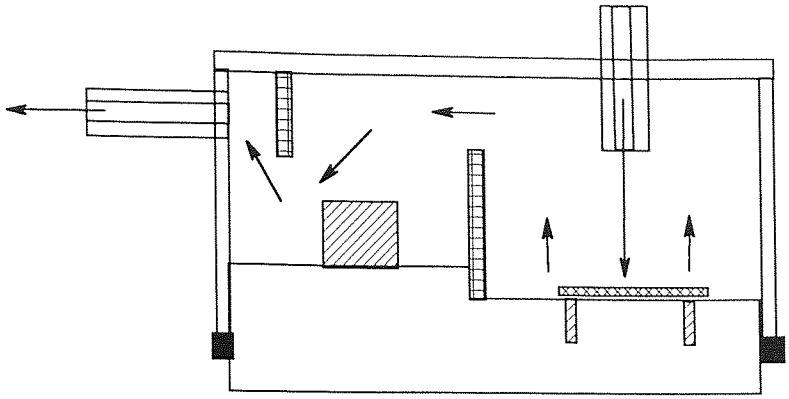

b)

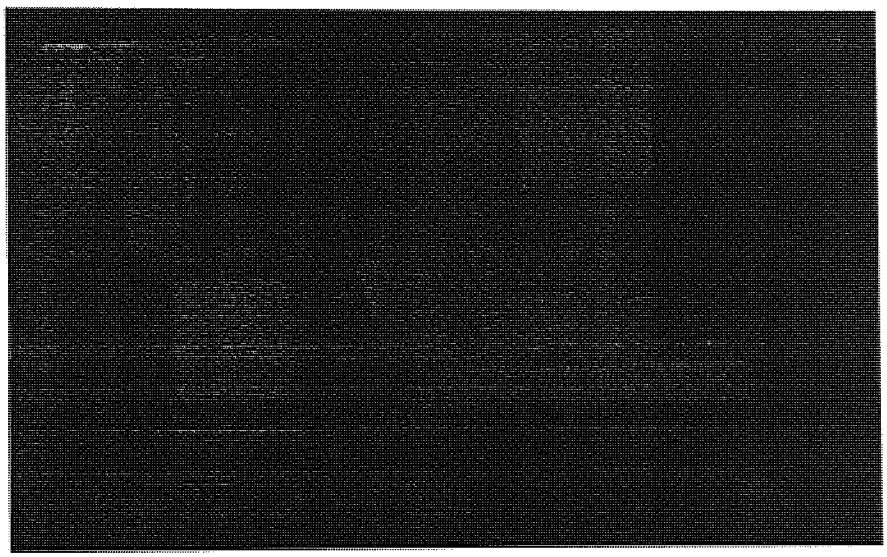

c)

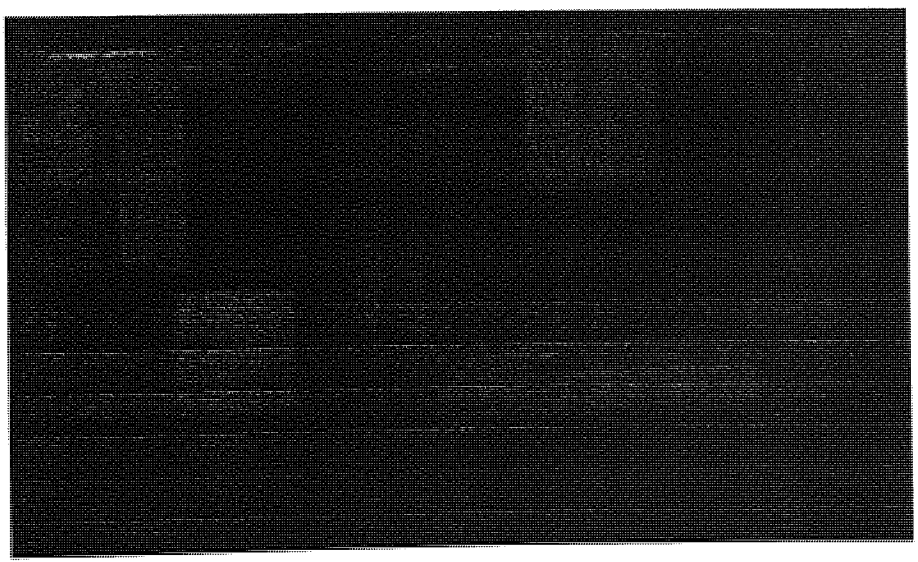

**Figure 4.12** Smoke flow patterns within complete nasal chamber. Medium baffle in position 1, small baffle position 3. a) diagramatic representation of air-flow b) smoke flow at an air-flow rate of 10 L $min^{-1}$, and c) air-flow rate of 4 L $min^{-1}$

### 4.4.2 Temperature

The temperature of the air directly above the tissue surface was measured using the replacement base previously described (section 4.4). As can be seen from Figure 4.13, the temperature of the air above the tissue surface was successfully measured. There are three items of interest in investigating the air temperature: firstly, the increase in temperature from a "cold start"; secondly, the point at which thermal equilibrium is reached, together with the equilibrium temperature; and, thirdly, the effect of disturbing the established equilibrium. As previously discussed, physiologically relevant air-flow rates of 4 L $min^{-1}$ and 10 L $min^{-1}$ were used for all experiments.

To examine the time to equilibrium and the equilibrium temperature values, the air-flow is started at t=0 after the initial water bath had reached its final operating temperature (80°C) and the system then allowed to equilibrate. These data are shown in Figure 4.13 for both 4 L $min^{-1}$ and 10 L $min^{-1}$ and these gave equilibrium (constant) air temperatures of 32 ± 2.3 and 29 ± 2.4°C respectively after between 30 and 45 minutes air-flow. Although there is no strict statistical difference between the temperature of the two air-flow rates ($p > 0.05$), it would seem that the lower flow rate of 4 L $min^{-1}$ give a slightly higher temperature. In both cases, thermal equilibrium had been reached within 45 minutes although, due to humidity considerations (section 4.4.3), in all subsequent experiments 60 minutes was allowed for thermal equilibration.

To allow for administration of drugs, or other substances to the tissue surface, the effect of removing the air source for a short period of time was investigated. In these experiments, the chamber was equilibrated for 1 hour, and then the temperature monitored for 30 minutes to establish the equilibrium temperature. After 30 minutes, the air supply was remove for either 30 second or 60 seconds, and the change in the air temperature monitored with time.

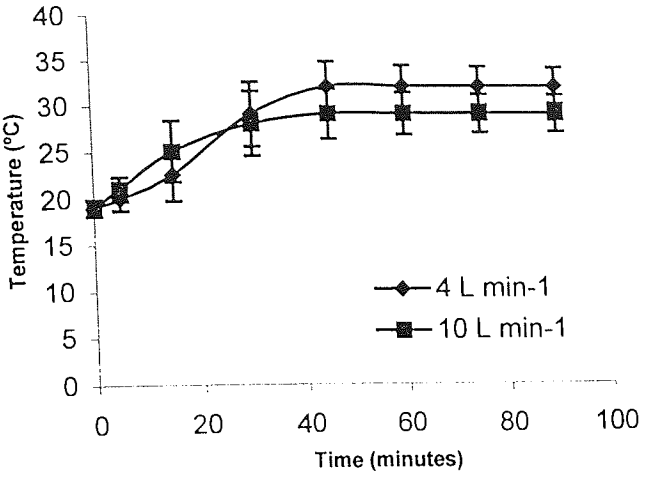


**Figure 4.13** Temperature profile at the tissue surface as the upper chamber is warmed. (n=5)

After removal of the air-flow for either 30 or 60 seconds (Figures 4.14 and 4.15) very little difference in temperature was seen; statistically differences were not significant. For the flow rate of 4 L $min^{-1}$ 1 minute after removal of the air source for 30 seconds, the temperature had fallen from 32 ±2.3 to 31 ±2.5 °C when analysed using the students t-test gave $P > 0.05$. For the higher flow rate of 10 L $min^{-1}$ after a 30 second disruption in the air-flow, the temperature above the tissue surface fell from 29 ± 2.4 to 28 ± 2.2°C, again a statistically insignificant result ($P > 0.05$).

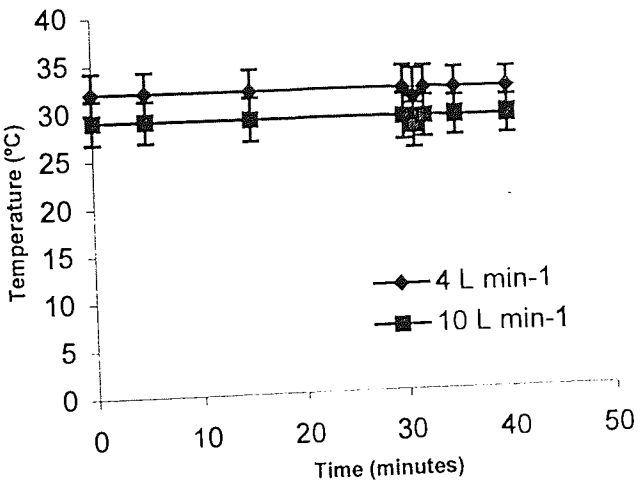


**Figure 4.14** Effect of a 30 second disruption in air-flow on the temperature of the air measured at the tissue surface. (n=5)

Longer disruptions in the air-flow gave similar results to those obtained for the flow rate of 4 L $min^{-1}$. Sixty seconds after the removal of the air source for 60 seconds (the temperature immediately prior to re connecting the air-flow) the temperature had fallen from 32 ± 2.3 to 30 ± 2.6 °C when analysed using the students-t test gave $P > 0.05$ . For the higher flow rate of 10 L $min^{-1}$ after a sixty second disruption in the air-flow, the temperature above the tissue surface fell from 29 ± 2.4 to 27 ± 2.3°C, again giving a statistically insignificant result ($P > 0.05$).

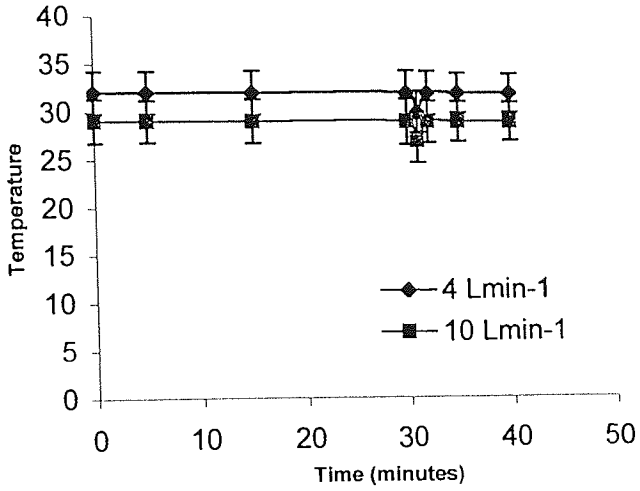


**Figure 4.15** Effect of a 60 second disruption in air-flow on the temperature of the air measured at the tissue surface. (n=5)

Analysis of all the individual runs for each of these experiments indicates that the errors are introduced not from time-point to time-point in each run, but from each run reaching thermal equilibrium at a slightly different temperature. Each run for Figure 4.13 was from a "cold start", i.e. all the system, except the 80 °C water-bath and flask, was dry and at ambient laboratory temperature. The effect of the ambient temperature on the air temperature above the tissue has to be considered. As the combined thermo-hygrometer probe was designed as an easy swap-in for the tissue viability ½ cell, in all subsequent experiments, the air temperature was monitored to ensure that the equilibrium level obtained was suitable.

### 4.4.3 Humidity

Humidity was measured in exactly the same manner as the air temperature was, using the combined thermo-hygrometer probe. Again with humidity, as with the temperature study, there are three areas of interest; firstly, the increase in humidity from a "cold start"; secondly, the point at which we obtain a humidity equilibrium, together with the equilibrium humidity level; and, thirdly, the effect of disturbing the established equilibrium.

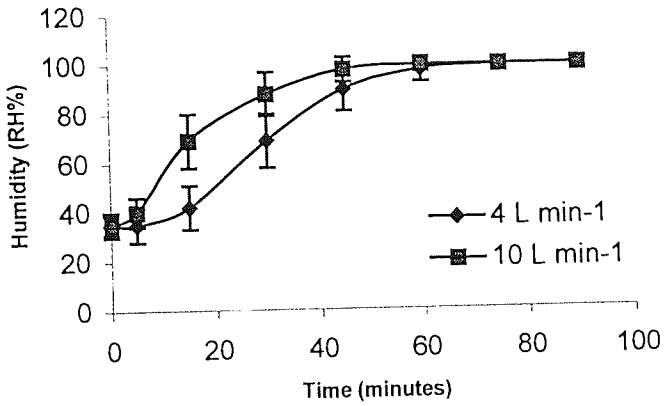


**Figure 4.16** Humidity profile at the tissue surface as the upper chamber is warmed and humidified. (n=5)

Figure 4.16 shows the increase in humidity with time. Humidity in both flow-rate cases establishes itself at 95% some time between the 45 and 60 minute time-points, this compares with the temperature reaching its equilibrium value between the 30 and 45 minute time-points. Again, comparing with the temperature data (Figure 4.13), where the higher flow rate equilibrates at a lower temperature, although the initial rise is much greater, we see the same initial rise in humidity for the higher flow rate. The high humidity values, approaching 100% present problems in measurement. Water condenses on the hygrometer probe, before any readings were taken the probe was examined for signs of condensation. If enough condensation to cover the electrodes in the humidity meter developed the equipment must be dismantled, dried, and the run re-started.

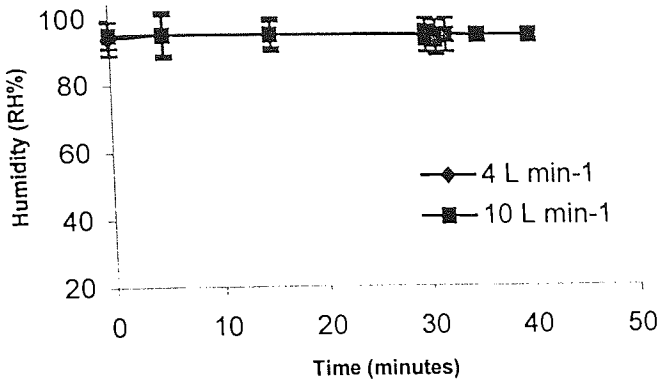


**Figure 4.17** Humidity profile at the tissue surface after a 30 second interruption to the air supply. (n=5)

After removal of the air-flow for either 30 or 60 seconds (Figures 4.17 and 4.18), very little difference in humidity was seen; statistically, the difference in humidity was not significant. For the flow rate of 4 L $min^{-1}$ 1 minute after removal of the air source for 30 seconds, the humidity had fallen from 95 ± 4% to 94.5 ± 5%RH when analysed using the students t-test gave $P > 0.05$. For the higher flow rate of 10 L $min^{-1}$ after a 30 second disruption in the air-flow, the humidity above the tissue surface fell from 95 ± 4% to 93 ± 5% RH giving a statistically significant result ($P > 0.05$).

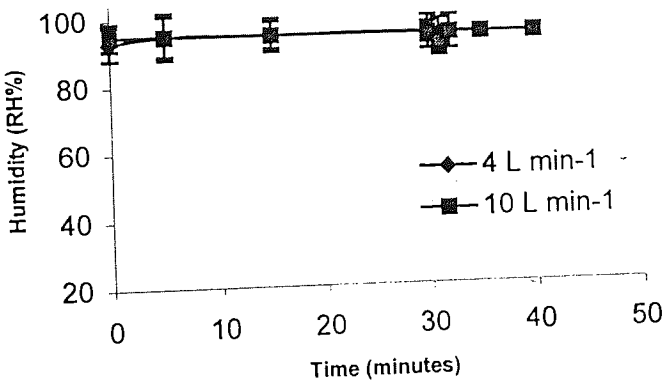


**Figure 4.18** Humidity profile at the tissue surface after a 1 minute interruption to the air supply. (n=5)

Longer disruptions in the air-flow gives similar results. For the flow-rate of 4 L $min^{-1}$, 1 minute after removal of the air source for 60 seconds (the temperature immediately prior to re connecting the air-flow), the humidity had fallen from 95 ± 4% to 94 ± 5%RH when analysed using the students t-test gave $P > 0.05$. For the higher flow-rate of 10 L $min^{-1}$,

after a 60 second disruption in the air-flow the temperature above the tissue surface fell from 95 ± 4% to 92 ± 5%RH again giving a statistically insignificant result ($P > 0.05$).

Looking at the air-flow, humidity and temperature data it can be concluded that the upper chamber provides an atmosphere above the tissue that is suitable, reproducible, and able to withstand minor interruptions in the supply, such as with administration of drugs through the "nostril". In both the temperature and humidity cases, the air-flow disruption caused statistically insignificant changes in the atmosphere, changes which lasted for less than five minutes. Macroscopic validation of the upper chamber from the data here indicates that the chamber was functioning as it was designed to do.

## 4.5 Tissue viability within chamber

Tissue viability in the complete chamber was analysed using the Ussing chamber technique previously described (Section 3.2.5).

### 4.5.1 Viability of excised Pig nasal Tissue

Figure 4.19 shows the electrophysiological trace obtained for excised pig nasal tissue after one hours exposure in the complete nasal chamber, together with the data collected in section 3.4.3 in which the upper humidity chamber was not present. These electrophysiological traces clearly show that there is a difference in voltage generated by the tissue, with the greater (-ve) voltage being generated by the tissue exposed in the complete chamber system. The data were collected using the computerised system (section 3.2.4.2) every second the epithelial voltage is measured (Figure 4.18). By inspection the tissue exposed to the complete chamber system can be seen to have a significantly improved PD over that obtained from the chamber alone. Comparison of these values with those reported (Östh 1997a, Östh 1997b) would suggest that the tissue viability is as good as that obtained in the horizontal Ussing chamber.

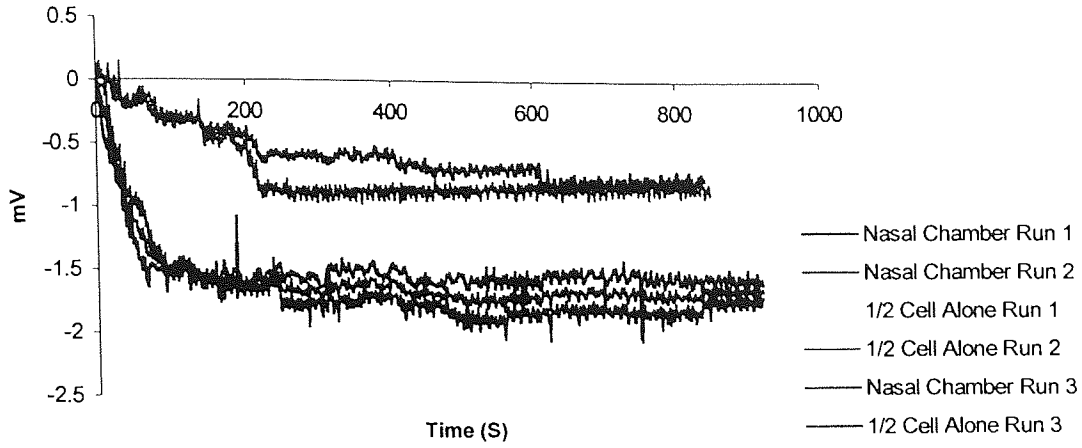


**Figure 4.19** Electrophysiological trace of epithelial PD (mV) generated by pig nasal tissue in Ussing chamber after 1 hour exposure in either the complete nasal chamber, or the lower ½ cell alone.

As previously noted (3.4.3) work by Waddell *et al.* (1999) give significantly higher PD's for their tissue samples. However, taking into account all the data available on epithelial PDs, these values obtained here can be considered to be indicative of a viable epithelial tissue sample. Despite being an uncontrolled, qualitative observation, the colour of the tissue after a 1 hour exposure, to the chamber is a good reflection of the tissue condition. After the 1 hour exposure, the tissue removed was seen to be a healthy pink colour, looking 'pinker and healthier' than tissue removed after exposure to the ambient atmosphere.

## 4.6 Trial deliveries to new chamber

As an initial assessment of deliveries to epithelial tissue in the complete chamber, small volumes of radiolabelled mannitol were delivered using a Gilson pipette. The effect of the volume delivered, humidity, and air-flow rate were investigated. For the chamber to be effective, it is desirable that simple deliveries from devices such as a Gilson pipette (section 4.6.2) are not effected by any of these variables. For more complicated devices such as the pump spray (section 4.6.3) that is commonly used for nasal delivery of liquids, the chamber system should however be able to determine any differences observed.

### 4.6.1 Methods

To assess the delivery of drugs into the complete chamber, silicone membrane was mounted in the lower tissue viability ½ cell. The silicone membrane is hydrophobic, allowing for the easy collection of the delivered mannitol, ensuring that none is lost by absorption to the artificial membrane. The artificial membrane also ensures that no marker enters the underlying parts of the chamber, and that valuable tissue samples are not wasted on validation experiments.

All experimental deliveries to the chamber were visually recorded using the apparatus previously described for recording the smoke flow patterns around the complete chamber (section 4.4). These data were represented as a series of pictures each separated by 1/25 second.

A fixed activity (2 kBq) of $^{14}C$ mannitol marker introduced into the chamber to determine the fate of delivered doses. The mannitol was diluted to the required volume with double distilled water. Delivered doses were immediately collected from the artificial tissue, chamber walls, and tissue mounting ring using the minimum water (approximately 3ml) to wash areas affected by the delivery into the scintillation fluid. The activity present was analysed by scintigraphy (Packard Instruments, USA) using 10ml Hisafe2 (Fischer Scientific, UK)

### 4.6.2 Delivery from Gilson micropippette

#### 4.6.2.1 Effect of volume

The fate of the applied marker is shown in Figure 4.20 for two delivery volumes, 50 and 200 µL. In both of these cases, the delivery landed on the artificial tissue surface with a minimum of loss to the surrounding mounting ring, or chamber sides. The volume had no statistically significant effect of the amount of marker deposited on the tissue surface ($P < 0.05$).

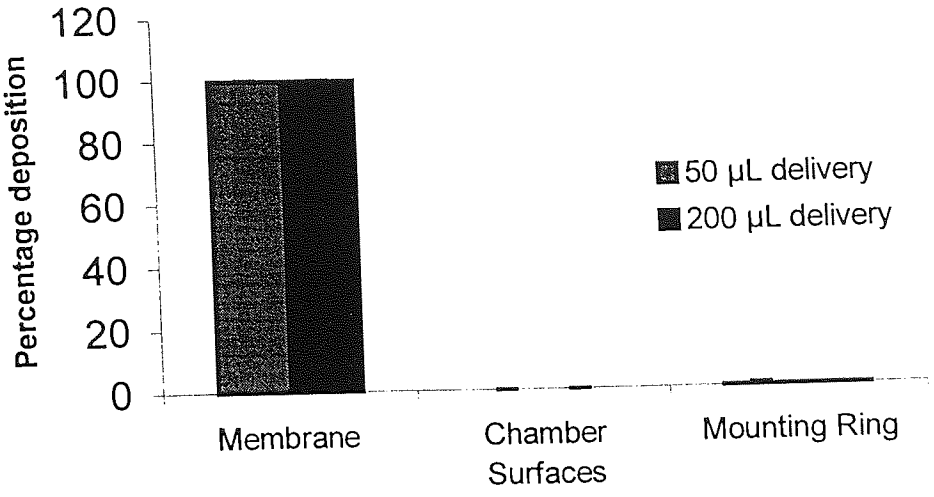


**Figure 4.20** Effect of delivery volume on dispersion around the nasal chamber. Ambient humidity, air-flow rate of 4 L $min^{-1}$ (n=3, ±SD)

Video recording of deliveries from a micropipette (Figures 4.21 and 4.22) show that, during delivery from such a simple device, there is no observable loss of marker due to it not landing on the artificial tissue surface.

### 4.6.2.2 Effect of air-flow rate

Similarly to the effect described previously for delivery volume, the effect of the air-flow rate on the fate of the delivered marker was considered for two volumes (50 and 200 µL, 2 kBq per delivery). For the small (50 µL) delivery (Figure 4.24), the air-flow rate has a statistically insignificant effect ($P > 0.05$) on the distribution of the marker. However, for the much larger volume of 200 µL (Figure 4.23), the difference in the amount hitting the tissue surface is statistically significant ($P < 0.05$). The amount hitting the surface is reduced at increased flow-rates.

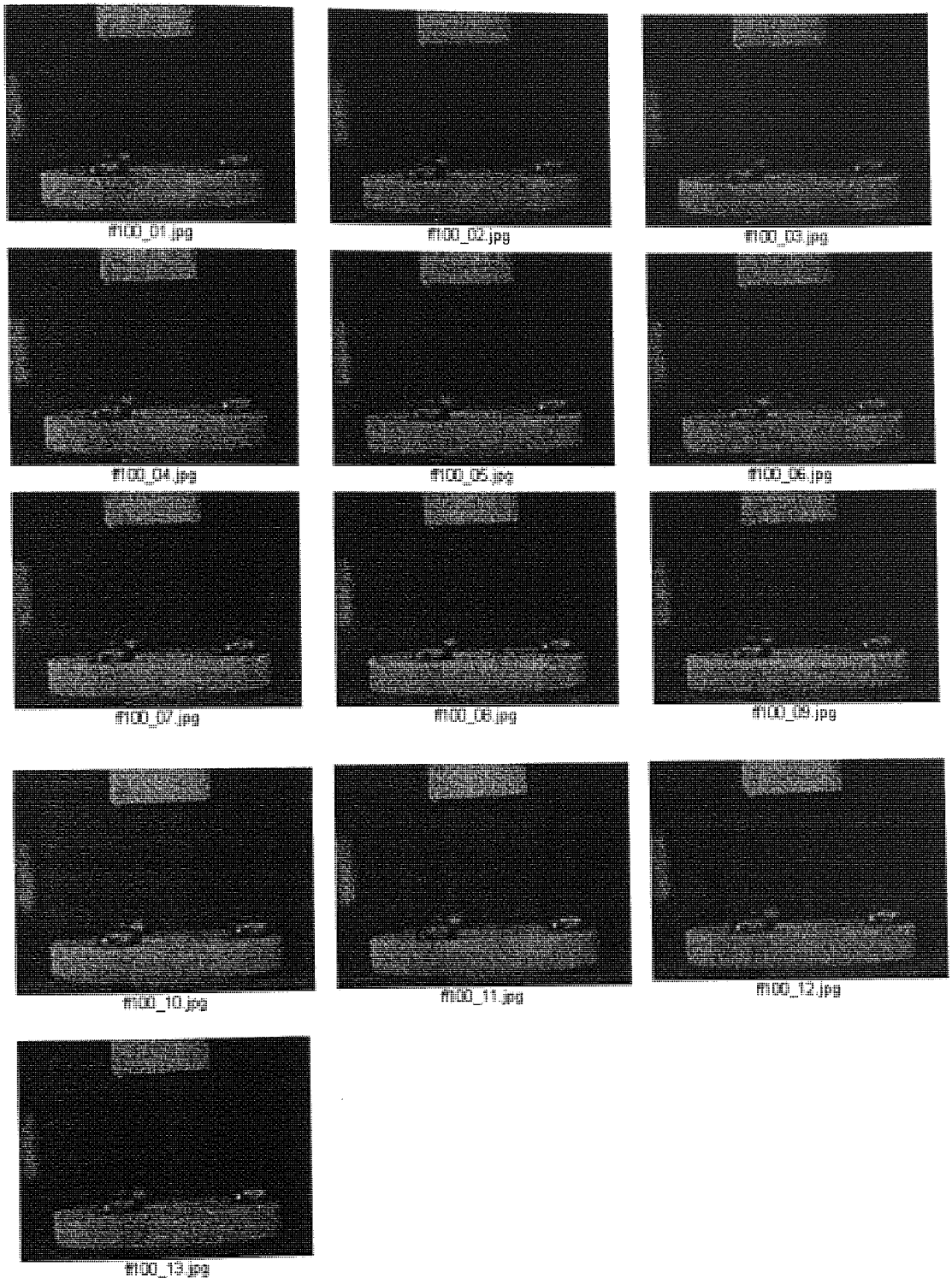

**Figure 4.21** Frame-by-frame videography of a 200 µL delivery from a Gilson pipette into complete chamber setup. Airflow-rate of 10 L $min^{-1}$, ambient humidity.

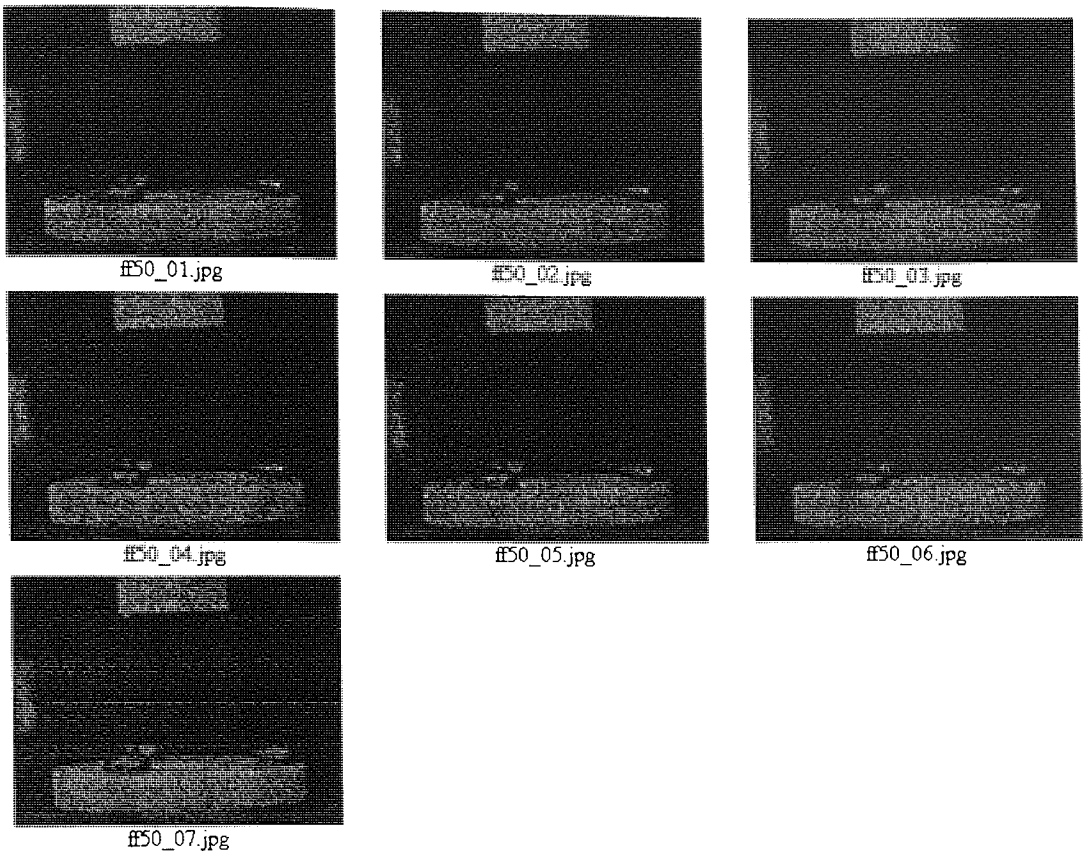


**Figure 4.22** Frame-by-frame videography of a 50 µL delivery from a Gilson pipette into the complete chamber setup. Airflow-rate of 10 L $min^{-1}$, ambient humidity.

As previously discussed, the delivery volume of 50 µL is that for which the chamber is designed. A delivery of 200 µL results in a reservoir forming over the tissue, held in place by the mounting ring. Considering this, and the statistically insignificant difference in the amount deposited on the tissue surface for the more relevant 50 µL delivery, the differences seen with the 200 µL delivery need not be seen as major flaw in the system, provided this is borne in mind when larger deliveries are considered.

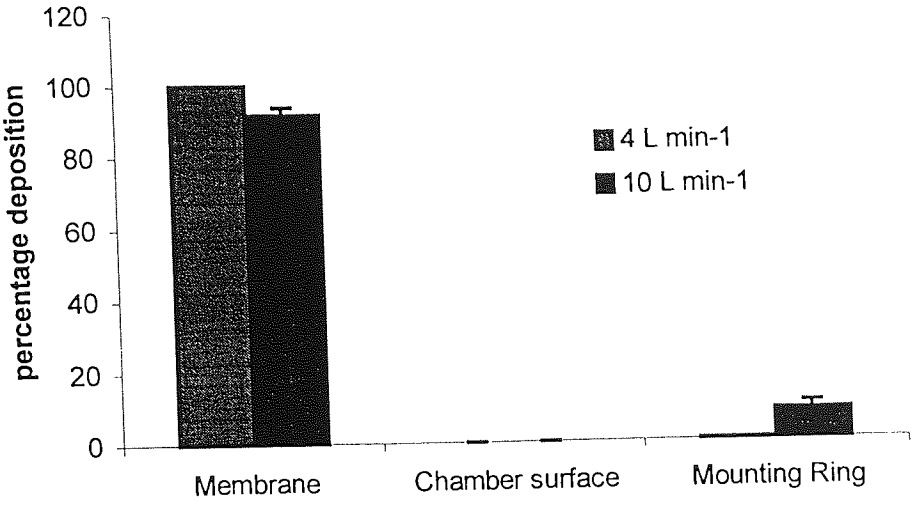


**Figure 4.23** Deposition of a 200 µL delivery of $^{14}C$ mannitol after delivery into chamber as a function of air-flow rate. (n=3, ±SD)

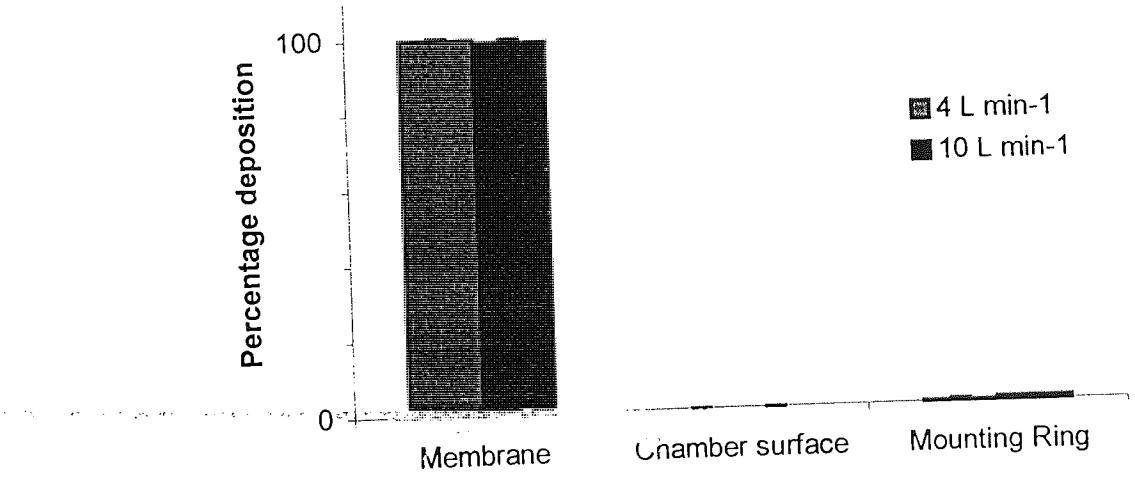


**Figure 4.24** Dispersion of a 50 µL delivery of $^{14}C$ mannitol around the chamber under constant (ambient) humidity as a function of flow rate. (n=3, ±SD)

### 4.6.2.3 Effect of humidity

At ambient humidity, the flow rate is seen to effect the deposition of the large (200 µL) delivery, but not that of the smaller (50 µL) delivery. This was repeated at 95% humidity. At elevated humidity, the same pattern is seen (Figures 4.25, and 4.26). Similarly to the ambient humidity result above, there is no statistically significant difference between the amount deposited on the tissue surface at the two different flow rates. The larger

volume delivery again has a statistically insignificant difference on the amount of marker deposited on the tissue surface ($P > 0.05$).

Comparison of the amount of marker hitting the tissue surface for the 200 µL delivery at high flow rates (10 L $min^{-1}$) yields a statistically insignificant difference ($P > 0.05$) between that obtained at ambient (section 4.6.2.2) and 95% humidity. This would indicate that the effect is due to the air-flow rate only, and not one of the humidity. Humidity would

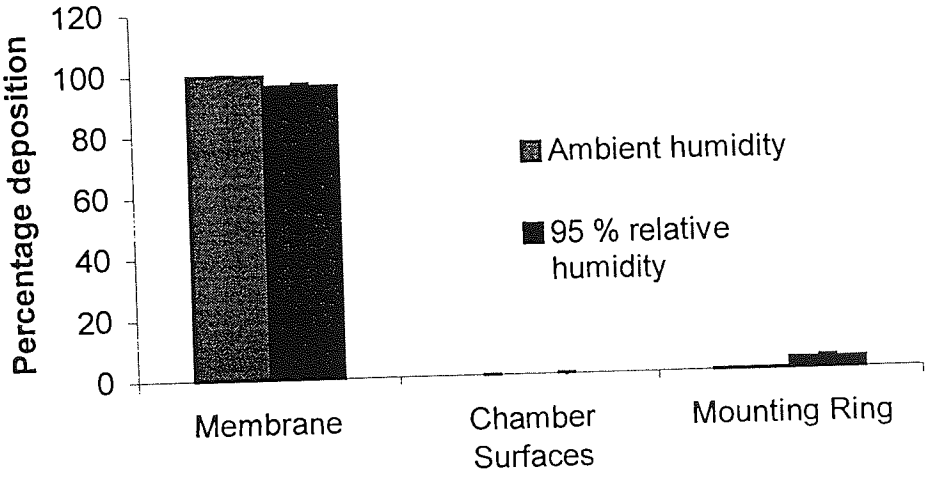


**Figure 4.25** Effect of humidity on the deposition of a 200 µL delivery at 4 L $min^{-1}$ flow rate

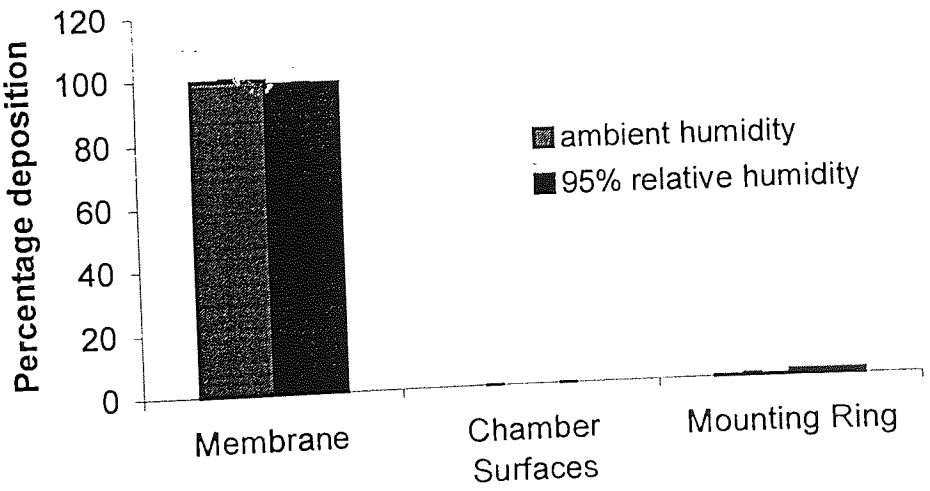


**Figure 4.26** Effect of humidity on the deposition of a 50 µL delivery at 4 L $min^{-1}$ flow rate

appear to have no significant effect on the fate of the applied dose for simple deliveries. Figure 4.27, which shows the delivery of 50 µL at 95% humidity would seem to emphasise this point, as there is no visible difference from that seen in Figure 4.22, where a similar volume (50 µL) was delivered at ambient humidity.

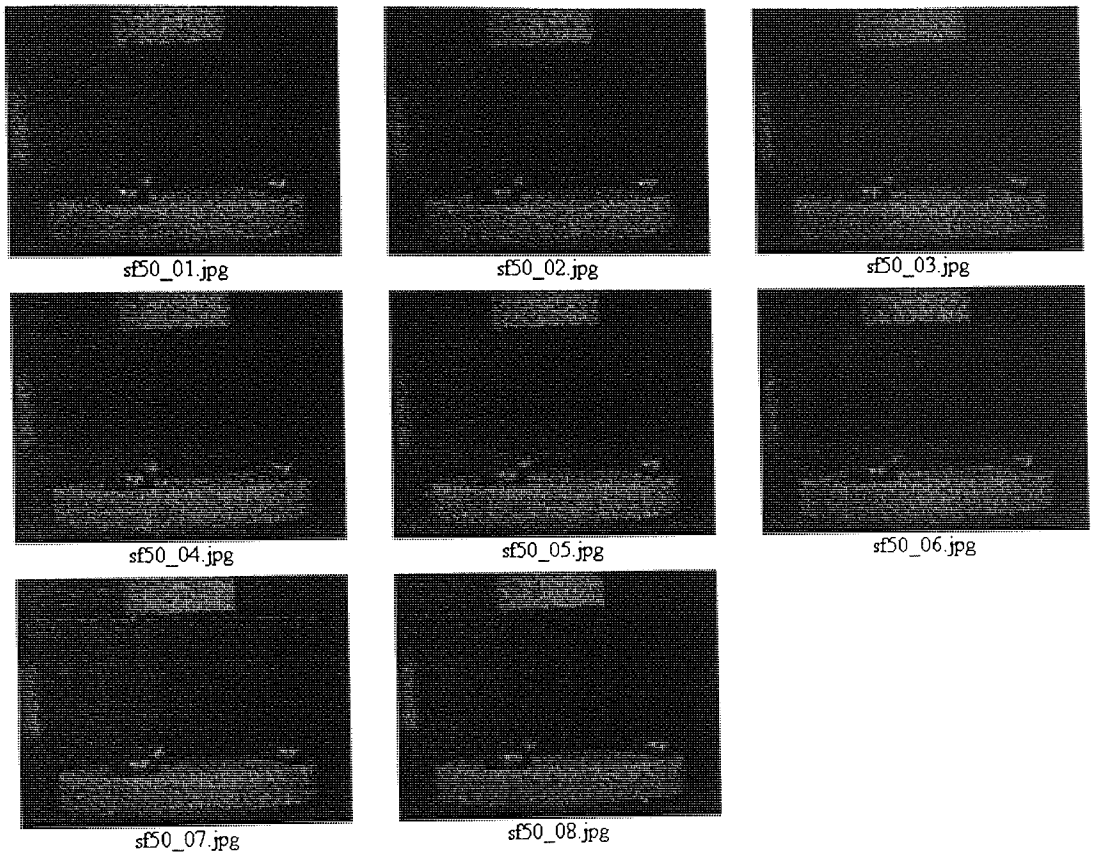


**Figure 4.27** Frame-by-frame videography of a 50 µL delivery to the complete nasal chamber at 95% RH.

### 4.6.3 Nasal spray pump delivery

The Gilson micropipette represents the most basic delivery device, progressing from this a more clinically relevant device was investigated. A 140 µL delivery pump spray designed for locally delivered agents (Rhinolast®, Boots Plc, Nottingham UK) was acquired. This is a simple pump device of the type illustrated in Figure 4.28. This was investigated in the same manner as previously described (2 kBq marker per delivery) for the Gilson pipette. These experiments were performed under identical conditions to those described in sections 4.6.2.1 to 4.6.2.3.

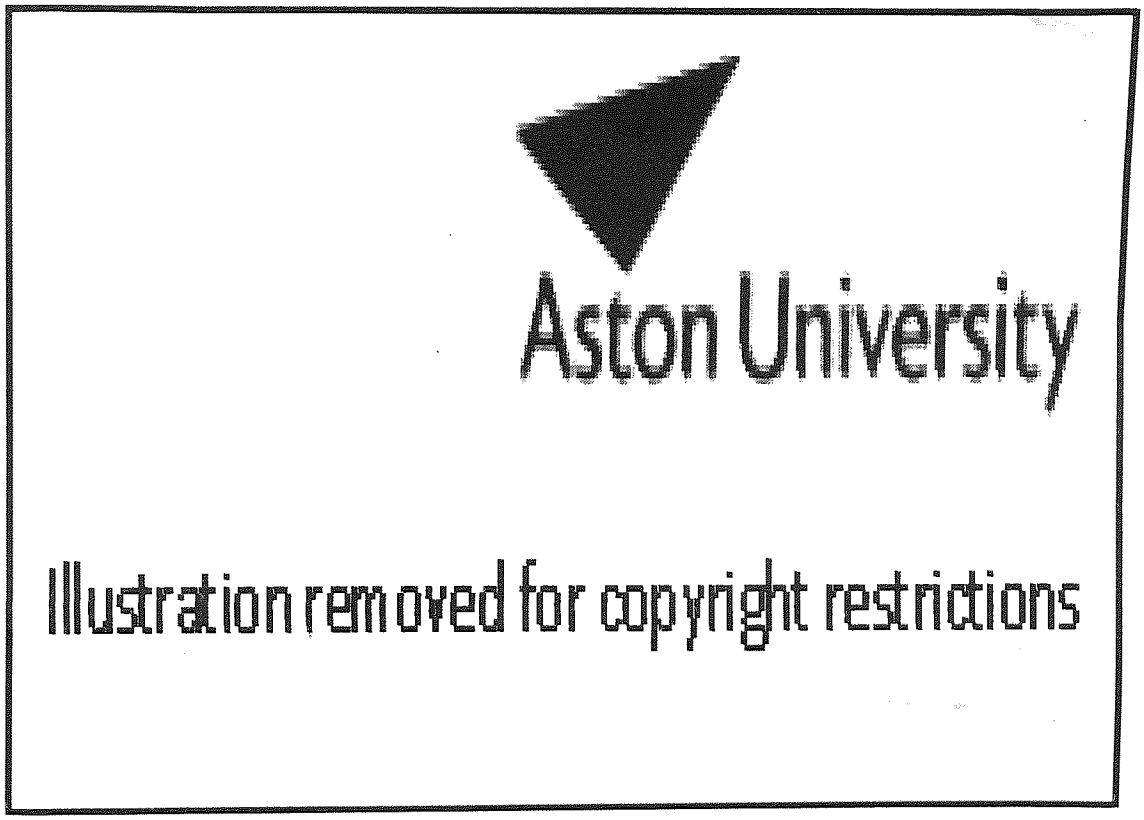


**Figure 4.28** The Pfeiffer nasal pump (Pfeiffer, Radolfzell, Germany), Kublik and Vidgren (1998)

### 4.6.3.1 Effect of flow rate on nasal pump

Airflow-rate would appear to have a significant effect on the deposition of aerosolised droplets around the chamber surface ($P < 0.05$ between 4 and 10 L $min^{-1}$, for chamber surfaces only). The major difference would appear to be in the amount of marker that hits the chamber surfaces rather than the membrane surface. Although the change in marker hitting the membrane is statistically insignificant it would appear from Figure 4.29 that the membrane is the area that loses marker to the chamber surface. As the air-flow speed is increased the percentage of the marker hitting the chamber surface is increased, with the corresponding decrease in that hitting the membrane surface.

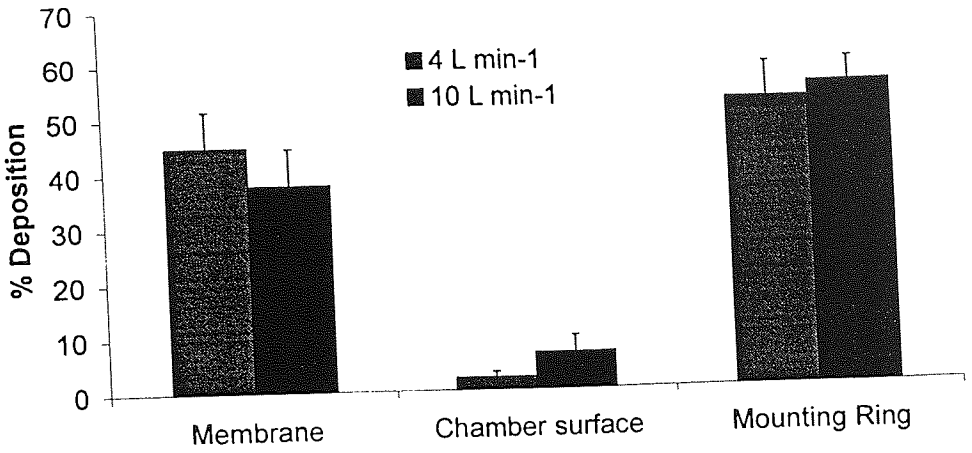


**Figure 4.29** Effect of flow rate on spray delivery (140 µL) at ambient humidity. (n=3, ± SD)

Videography of the delivery at different air-flow rates (Figures 4.30 and 4.31) yields inconclusive results. There is no apparent difference between the results obtained for the 10 and 4 L $min^{-1}$ runs (n=5). This discrepancy between the dispersion, and visible delivery from the spray would suggest that the effect seen on the dispersion might be due to the increased air-flow having a slightly different flow pattern around the chamber, resulting in the droplets landing in a different area.

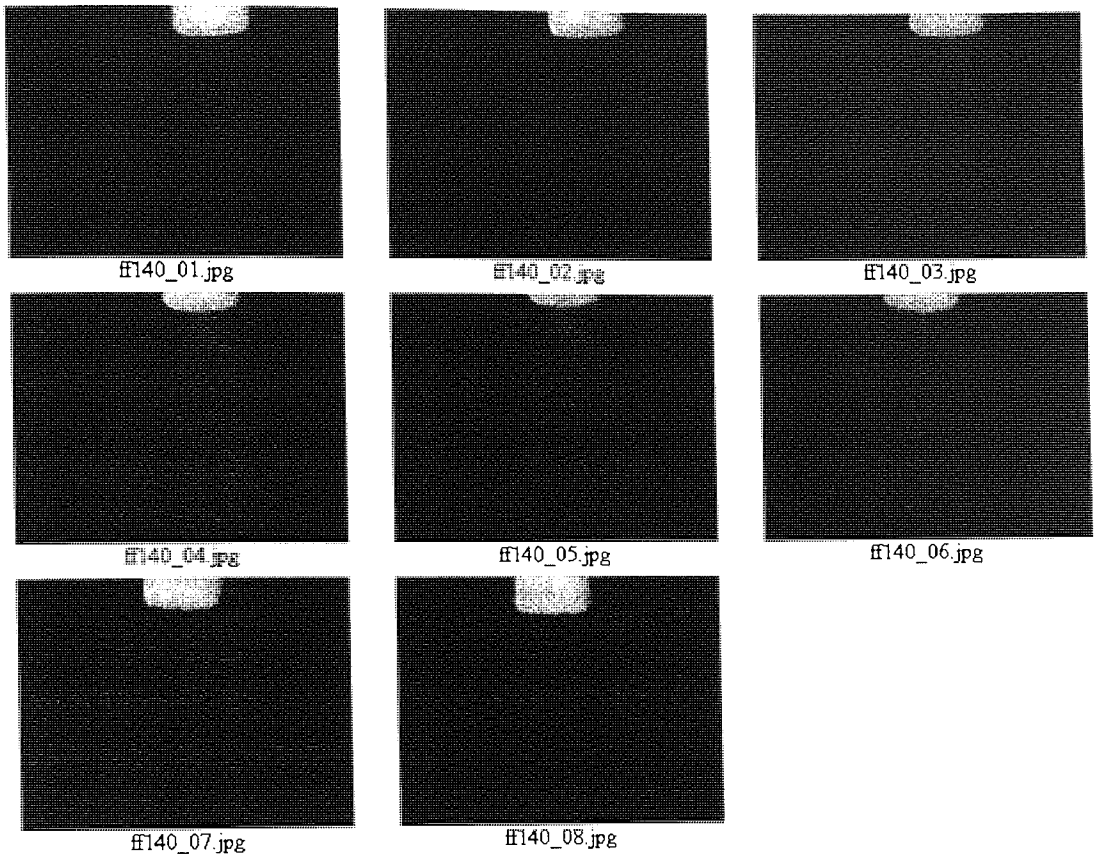


**Figure 4.30** Frame-by-frame videography of the delivery from a 140 µL nasal spray into the complete nasal chamber. Airflow-rate 10 L $min^{-1}$, ambient humidity.

### 4.6.3.2 Effect of humidity on nasal pump delivery.

Video recording of the pump delivery shows significant differences between the spray dispersion at elevated, and ambient humidity (Figures 4.30 and 4.33). The presence of humidity results in a narrow cone of droplets from the spray, whereas, at ambient humidity, the cone of droplets is visibly larger. Interpretation of such data is always subjective; however, it would appear that differences between the different conditions are visible. Repetition of the videography reveals that such differences are visible over a number of experimental runs (n=5). When the videography was repeated at a lower magnification, where the tissue mounting ring and lower chamber surfaces are visible, at high humidity the spray would appear to be deflected back up

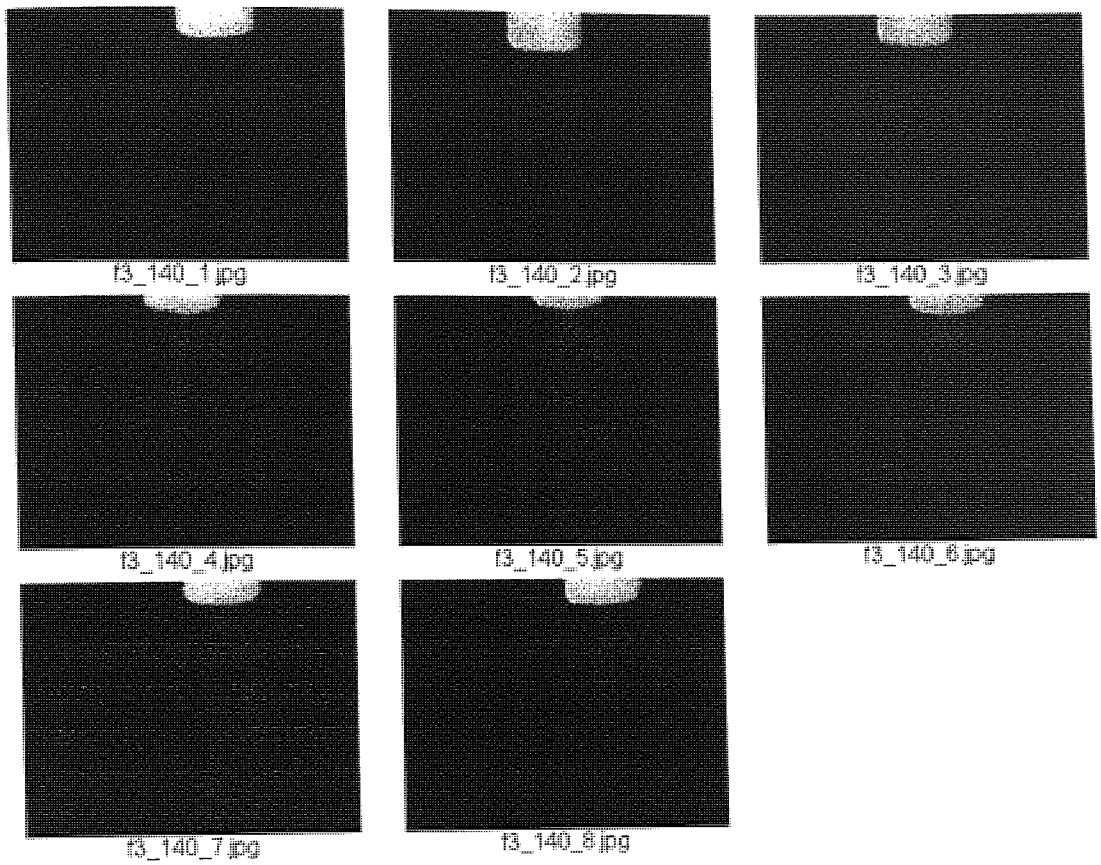


**Figure 4.31** Frame-by-frame videography of the delivery from a 140 µL nasal spray into the complete nasal chamber. Airflow-rate 4 L $min^{-1}$, ambient humidity.

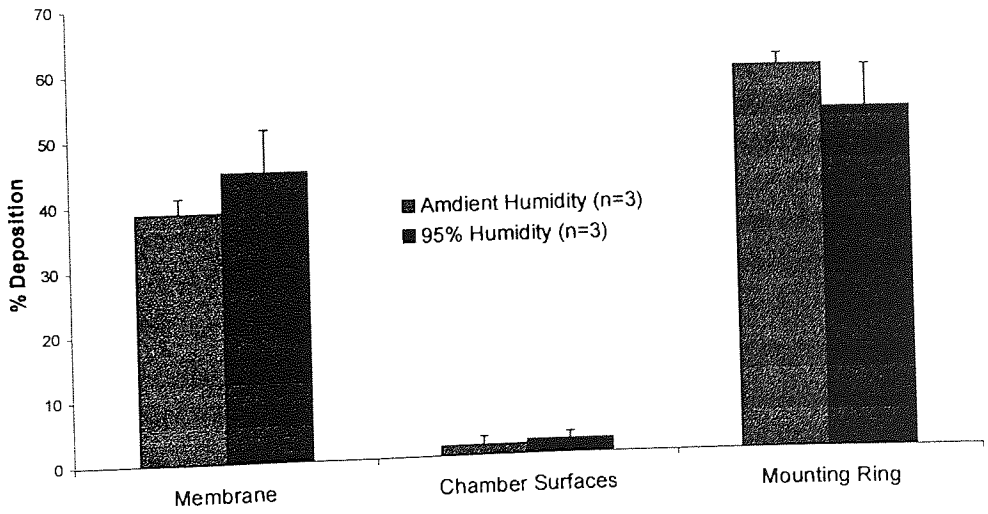


**Figure 4.32** Effect of humidity on spray (140 µL) at a flow rate of 4 L $min^{-1}$

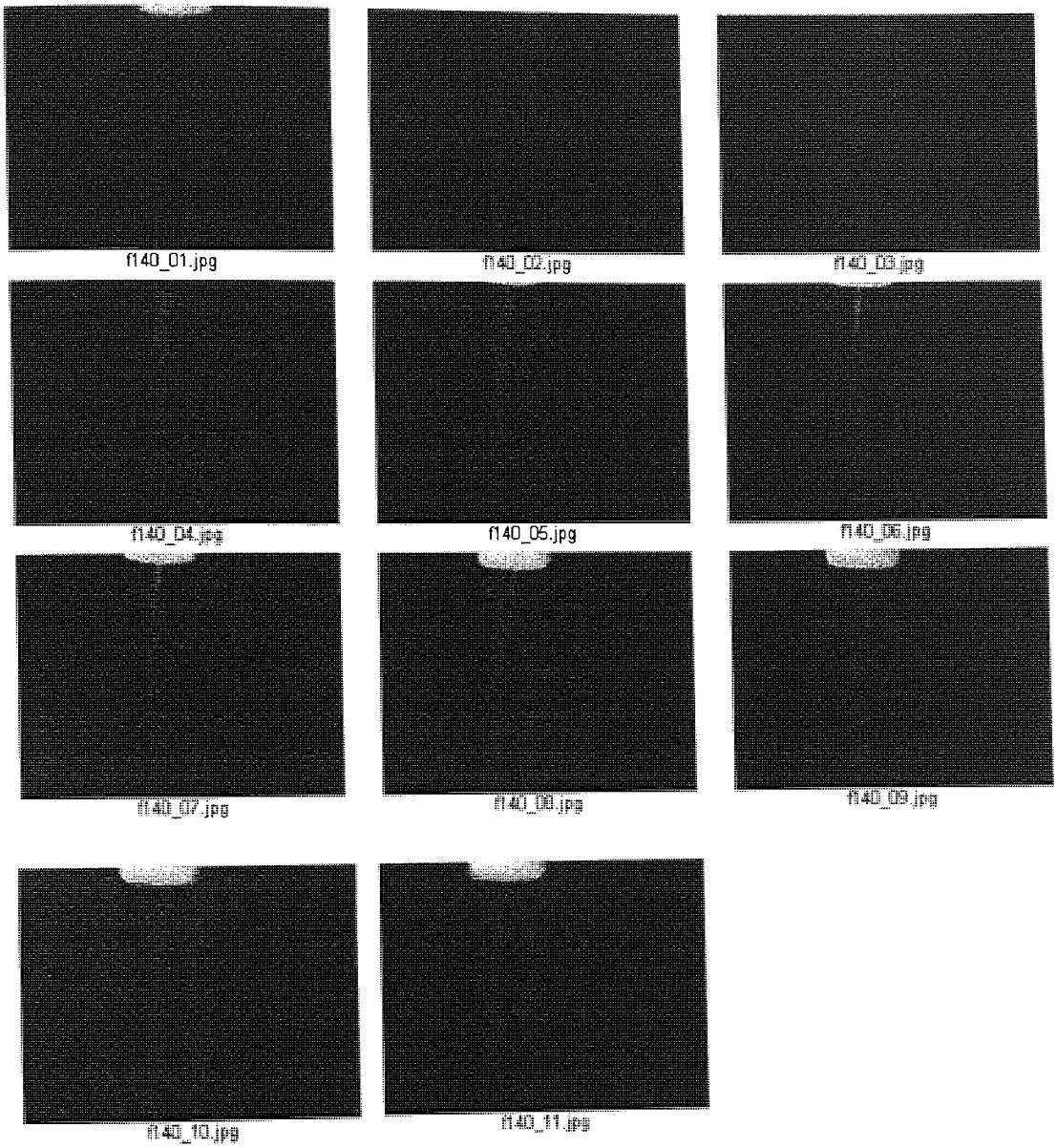


**Figure 4.33** Frame-by-frame videography of the delivery from a 140 µL spray into the complete chamber. Airflow-rate 10 L $min^{-1}$, 95 % RH

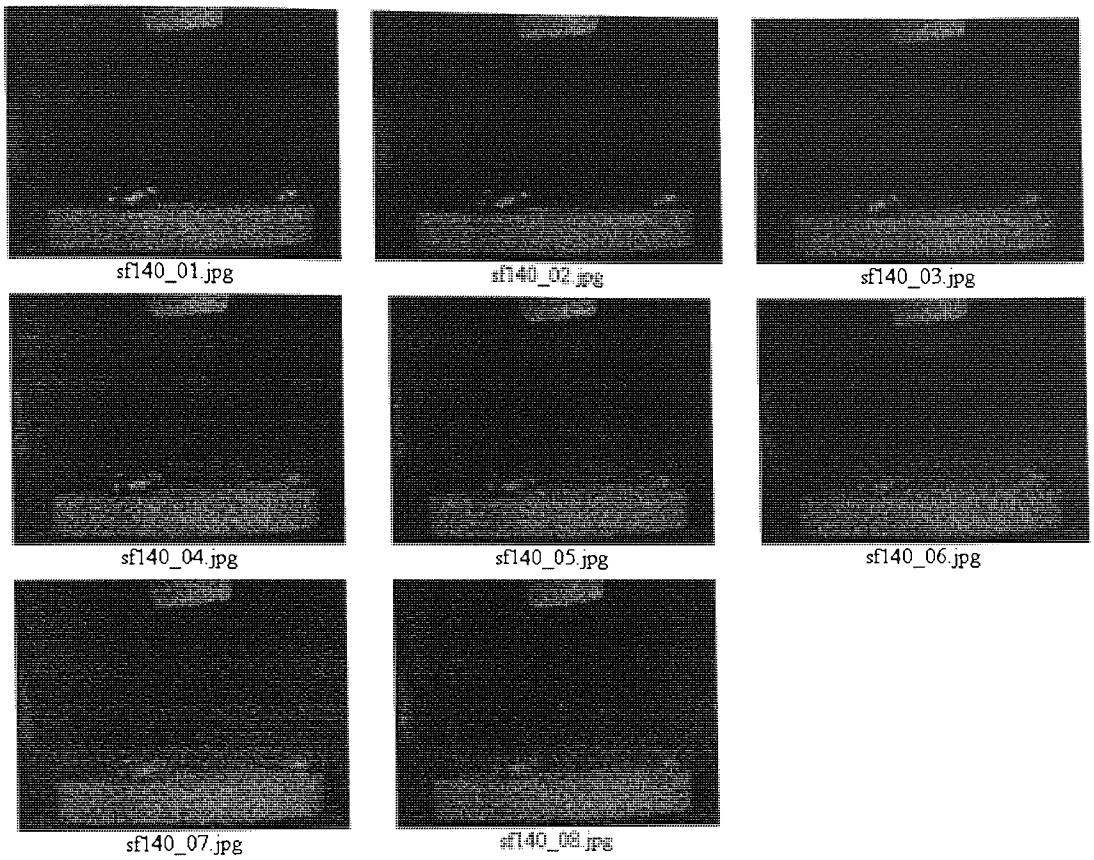


**Figure 4.34** Frame-by-frame videography of delivery from a 140 µL spray, lower magnification that Figure 4.31, highlighting loss on chamber walls. Airflow-rate 10 L $min^{-1}$, ambient humidity.

from the tissue. The increase in marker lost to the chamber surface is also seen on the chamber surface in front of the lens.

The dispersion of the marker around the chamber (Figure 4.32) shows that there is no statistically significant difference between the ambient and elevated humidity values for any region within the chamber.

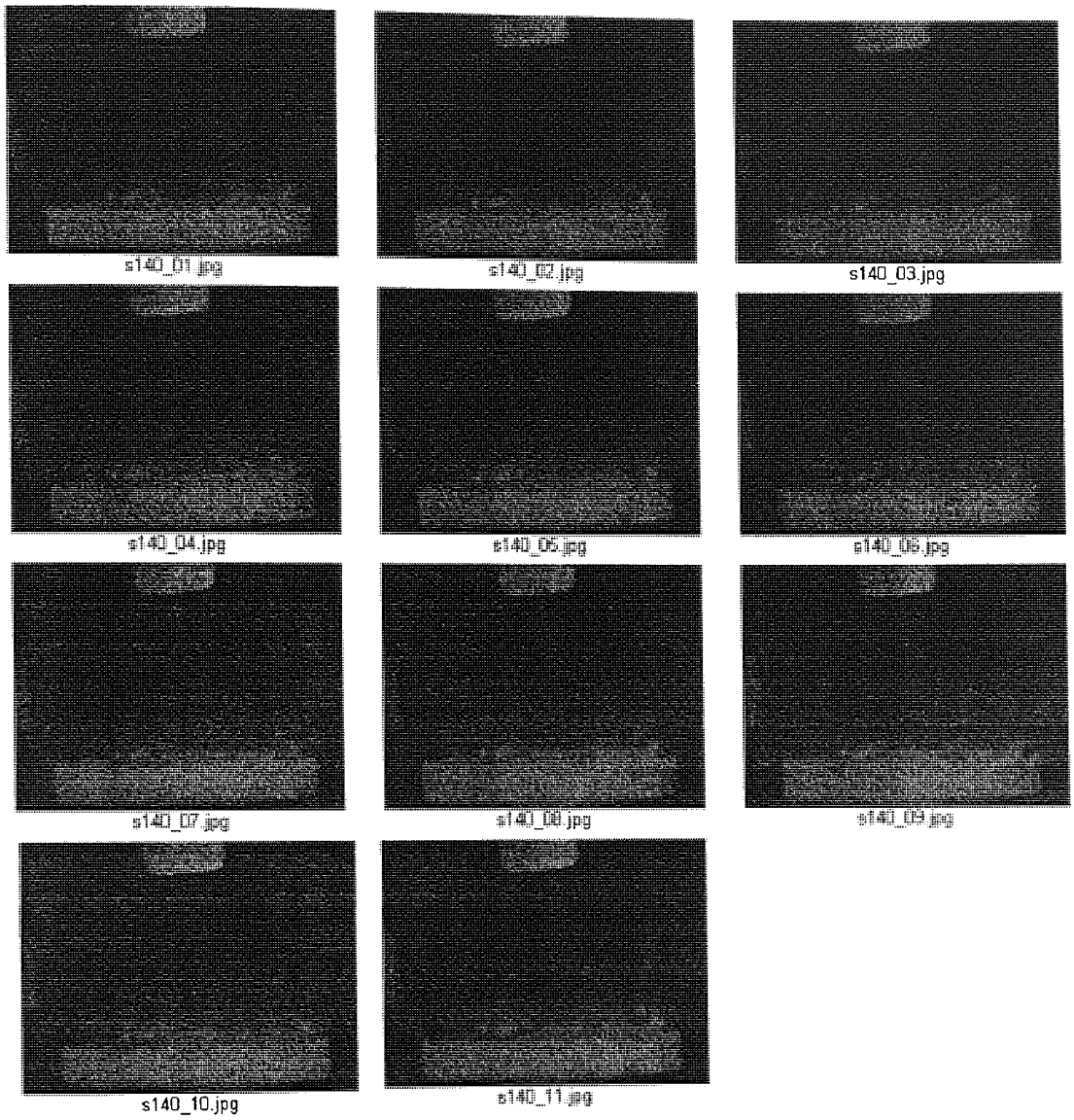


**Figure 4.35** Frame-by-frame videography of delivery from a 140 µL spray, lower magnification that Figure 4.33, highlighting loss on chamber walls. Airflow-rate 10 L $min^{-1}$, 95% RH.

## 4.7 Adaption of nasal chamber to Malvern Mastersizer

Visually humidity was seen to affect the delivery from a 140 µL pump spray (Figures 4.30 vs 4.33, and 4.34 vs 4.35). In this section, the nasal chamber was adapted to fit into a particle-sizing instrument (Mastersizer, Malvern Instruments, Malvern, UK) to provide quantitative data to supplement the qualitative data obtained from the video analysis. Although there are methods available for sizing aerosols and particles after delivery, the nasal chamber constructed offers the opportunity to add two further variables into any investigation, humidity and air-flow rate.

### 4.7.1 Chamber modifications

The lower tissue viability ½ cell was not altered in any way to fit into the mastersizer, however, during regular use the acrylic (perspex) of the upper chamber becomes significantly scratched. To overcome problems that these scratches produce when obtaining background readings, windows of unscratched perspex were made. A second and possibly more important factor is locating the chamber in the instrument in a reproducible manner. The production of removable perspex windows to overcome the problem of the scratched perspex also allows removable opaque perspex windows to be produced. This allows the chamber to be positioned in the mastersizer such that the laser is aimed at a specific point in the chamber, the opaque windows can then be replaced with the unscratched ones to allow measurement. The removable windows (Figure 4.36) consist of the unscratched perspex lens glued to a PTFE lens holder. In operation, the lens and ring fit into a second ring permanently mounted in the chamber. This results in a flush internal surface to the chamber wall.

The chamber windows were designed according to the light trace in Figure 4.37. Incident light arrives at the first chamber window as a tight beam, passing through the chamber and the aerosol the beam is scattered. The exit window is then sized to provide a cone of light 110% times that of the measurement lens, providing [illegible] in the designed-light path of the machine.

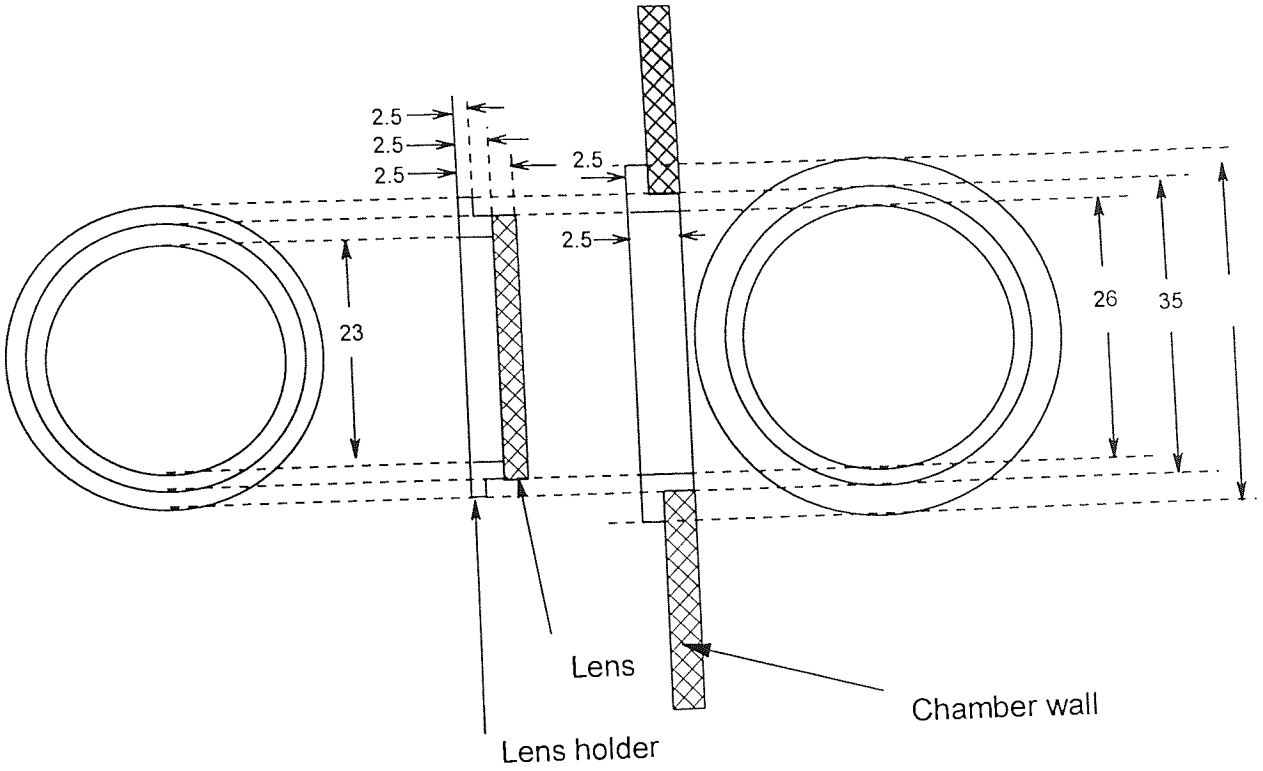


**Figure 4.36** Lens modifications to the upper humidity chamber.

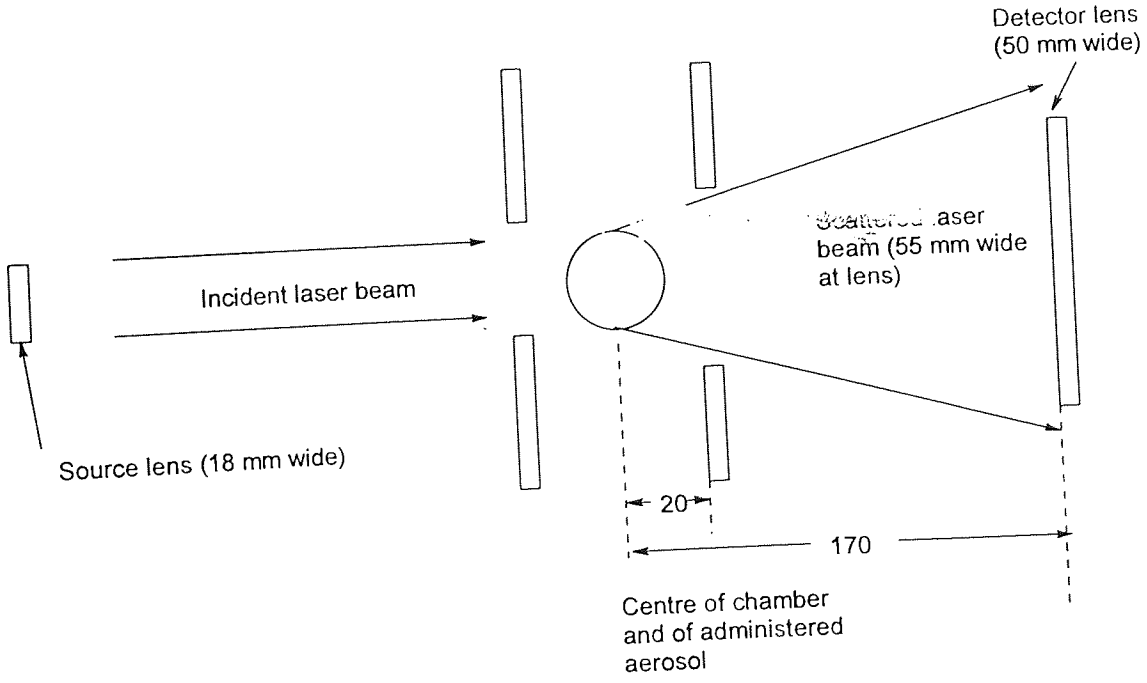


**Figure 4.37** Optical arrangement of the chamber set-up in the mastersizer.

**Figure 4.38** Diagramatic representation of the complete chamber assembled in the Malvern Instruments Mastersizer S (From Turner *et al., 1999*).

### 4.7.1 Validation of chamber modifications

The only modification made was to the internal surface of the upper chamber walls. Using the smoke methods previously described (section 4.4) the air-flow around the chamber was re-evaluated. This method proved that the modifications made had no effect on the internal air-flow patterns.

### 4.7.3 Chamber mounting

The complete chamber was mounted in the Mastersizer (Figure 4.38) using an adaptation of a Malvern Instruments metered-dose inhaler (MDI) bracket system. This system consists of a base-plate that mounts onto the machine with a moveable stand attached. The stand is capable of moving in the Y direction only (perpendicular to the direction of the laser beam), and is fixed 170 mm away from both the source lens and the detector lens. The complete chamber was mounted to this stand using a standard boss and clamp. With the opaque lenses mounted in the chamber the chamber was then aligned with the laser beam. Repeated mounting of the chamber within the Mastersizer proved this to be a suitable technique for repeated relocation of the chamber within the system. After

successful location of the chamber the lenses were then replaced by the unscratched perspex lenses.

### 4.7.4 Sizer operation

Operation of the Mastersizer is split into two operations; background reading, and experimental reading. Background reading is performed at the start of an experimental session, as with the normal operation of such a machine, however, in this case the background is obtained with the chamber present, together with required air-flow and humidity. To prevent any accidental exposure to errant scattered light, and to reduce the measured background, the centre section of the chamber was covered with a layer of heavy cloth.

For data analysis, a water-in-air aerosol presentation matrix was developed using the software supplied by Malvern Instruments. The presentation matrix provides the instrument with the data on the refractive index of the particles (water), and the solvent (air) required for the analysis of the particle size from the angles of diffraction obtained during the experimental run.

Measuring experimental samples was performed in a manner almost identical to that used as standard practice. The source of warm and humid air was removed, data collection was manually started from the controlling PC, the nasal delivery device fired, and then data collection stopped manually. In all cases data was analysed and presented as a volume mean. From the work done on the effect of interrupting the air-flow (sections 4.4.2, and 4.4.3), a one-minute interruption in the air-flow supply has an almost negligible effect on the conditions within the chamber. Providing the administration was performed in a competent and efficient manner, the overall disruption to the air-flow (after practice) was measured at 9.5 seconds (n=5, ± 1.3 seconds), and the mean data collection time was 3.8 seconds (n=5 ± 0.8 seconds).

### 4.7.5 Measurement of particle size, effect of air-flow rate.

The effect of the air-flow rate on the droplet size distribution obtained from the nasal pump previously described (4.6.3) was investigated using this mastersizer technique at air-flow rates from 0 to 15 L $min^{-1}$. The results for all the 0 and 15 L $min^{-1}$ individual runs performed are shown in Figure 4.39. It can be seen that the effect of air-flow is to reduce the mean particle size. The distribution produced by the spray is visibly mono-modal at high flow rates, and multi- modal when the air-flow is not present. In all cases shown

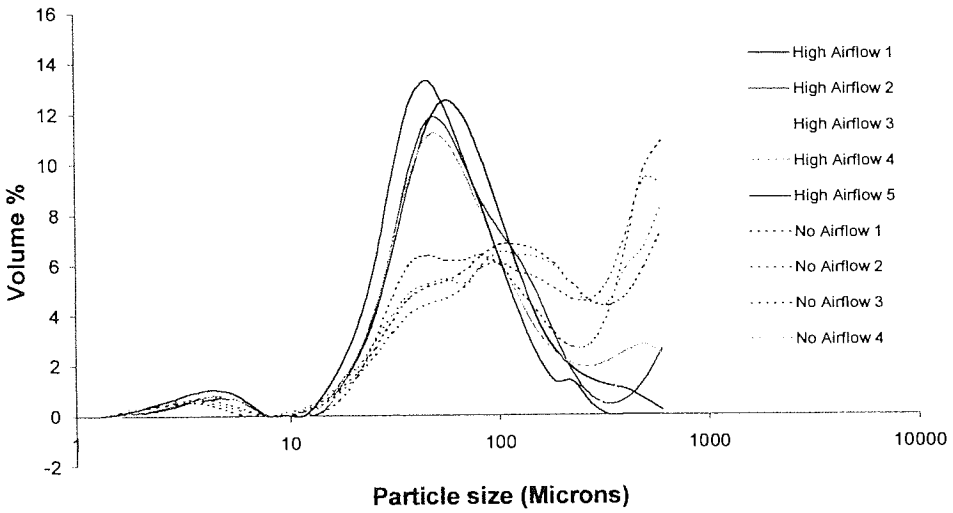


**Figure 4.39** Comparison of mean particle size, and particle distribution as a function of air-flow.

in Figure 4.39 at the higher end of the measured scale (>350 μm) the volume percentage of droplets increases. Figures 4.34 and 4.35 highlighted the appearance of droplets on the chamber walls, it was assumed that these droplets were those measured at the higher sizes. To investigate this, the deliveries where air-flow was absent were repeated in the chamber without the lenses present (Figure 4.40). It can be clearly seen from these data that, in the absence of the windows, there are no large particles present.

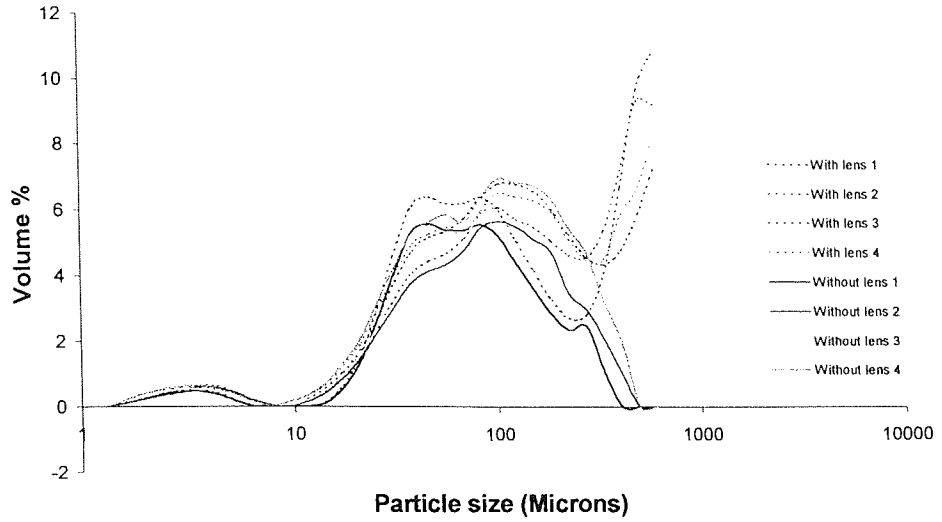


**Figure 4.40** Comparison of particle size distribution in the presence and absence of the chamber windows. No air-flow, ambient humidity.

This aggregation of droplets on the window surface to produce larger droplets imposes a limitation on the system in that values for particles above 350 µm can not be considered. This arises since there is no way to know what percentage of the larger particles seen are genuine particles, or are aggregates on the chamber lenses. In all further studies, the size range considered was from 1.06 to 331.77 µm . A value of 331.77 µm was chosen since this is a discrete measurement value for the Malvern Mastersizer, and the machine can be set to remove data from this point upwards.

The effect of the air-flow rate on the mean particle size generated is shown in Figure 4.41, single factor analysis of vaiance (ANOVA) of these data gives P = 5.11E-06, and a critical F value of 5.317645 indicating a statistically significant difference as well as the visibly different profile as the airflow is increased to 10 L $min^{-1}$.

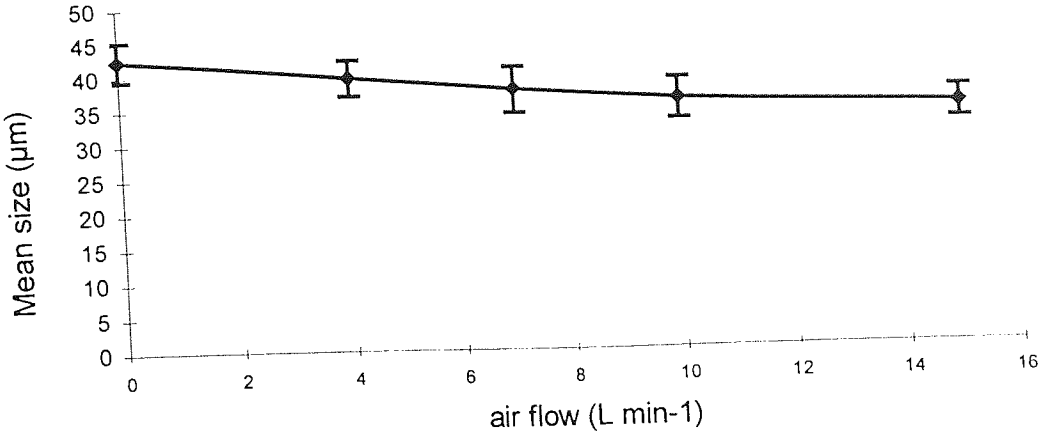


**Figure 4.41** Variation of mean particle size with air-flow. (n=5)

### 4.7.6 Measurement of particle size, effect of humidity.

As with the measurement of the resultant particle size with the change in air-flow, operation of the complete chamber in the presence and absence of humidity allowed the investigation of the effect of humidity on the resulting particle size. Figure 4.42 illustrates the increase in particle size with the concurrent increase in humidity. As the humidity increases from the ambient laboratory value to >95% the mean particle size increases from 42.3 ± 6.5 to 125.8 ±15.4 µm. The particle size data obtained agrees with the videography if the mass and energy of the droplets is considered. Since the internal volume of the droplets is proportional to the cube of the radius, the larger particles will have a significantly larger mass, as well as there being significantly fewer droplets formed. This increased mass will result in the droplets having a greater amount of kinetic energy for the same velocity, and concurrently greater momentum. Provided the droplets leave the delivery pump at the same velocity, and with similar sizes, fewer, larger heavier droplets would be expected to have a narrower, less disperse profile than more, smaller particles if only due to the reduced probability of droplets colliding.

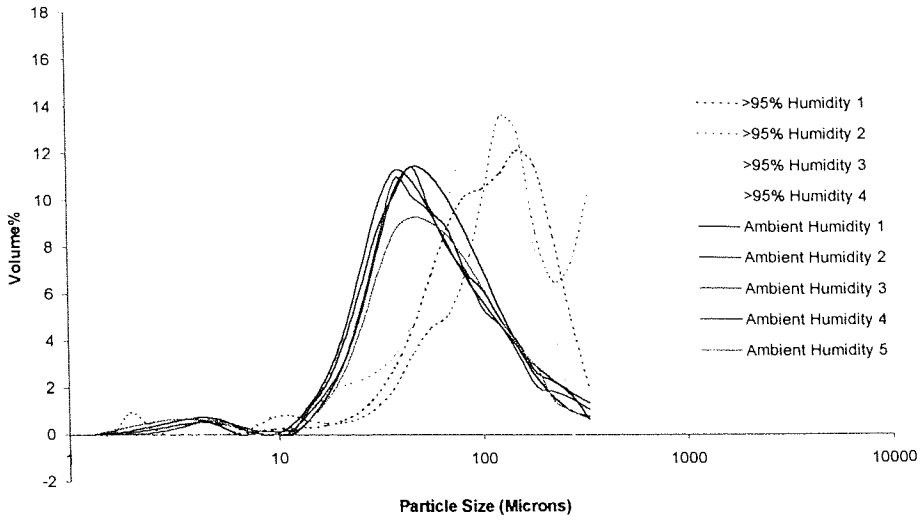


**Figure 4.42** The effect of humidity on droplet size, air-flow rate 10 L $min^{-1}$.

## 4.8 Conclusions

The prime aim of this chapter was the production of an upper chamber that not only enhances the viability of excised nasal tissues, but can provide data suitable for the evaluation of nasal delivery devices. From the electrophysiology of the pig nasal tissue, the first part of this aim, the enhancement of the viability, has been achieved, increasing the epithelial PD from 0.73 to 1.78 mV after a 1 hour incubation in the complete chamber. As previously discussed (3.5) the values obtained for the epithelial PD are in line with those reported for other species. The complete chamber even exceeding the PD values obtained by Östh *et al.* (1997a and b).

The internal configuration and the behaviour of the chamber was exhaustively investigated with respect to its air-flow, humidity, and temperature. The design reported here provides the tissue surface with a suitable environment within which to allow the investigation of drug delivery whilst controlling three more variables than currently available, the air-flow, the air temperature, and the humidity above the tissue surface. Perturbation in the supply of warmed humid air for short periods of time, such as those that would be encountered during normal experimentation proved to have a very minimal effect on the condition of the environment immediately above the tissue surface.

The ability of the complete chamber system to provide data on the performance of nasal delivery devices was then investigated. Initially, a Gilson micropipette was used as a model delivery device. Humidity and air-flow proved to have no effect on the distribution of the marker around the chamber, although the delivery of a very large dose (200 µL) did prove to increase the percentage lost to the tissue mounting ring, almost certainly due to the greater percentage in contact with the mounting ring than to any other effect. When the Gilson micropipette was replaced by a commercially available nasal pump spray, physical differences due to humidity and air-flow rate were seen in both the video and dispersion data. As a means of explaining these differences, the chamber was then further adapted. The adaptation of the chamber to work in the Malvern Mastersizer yielded interesting droplet size data when either humidity or air-flow were investigated. As the air-flow was increased, there was a slight decrease in particle size from a mean size of 42.4 ± 2.6 µm (no air-flow) to a mean size of 37.8 ± 2.1 µm (15 L $min^{-1}$), however, the larger effect was seen when the humidity was increased from ambient to >95% when the mean particle size rose from 42.3 ± 6.5 to 125.8 ±15.4 µm. It is thought that the increase in humidity causes the droplets to aggregate, and the fewer resulting particles either through their lower numbers, or their increased kinetic energy and momentum result in the significantly narrower cone seen on the videographic data.

In conclusion, the aims set out in section 4.1 were met, providing a system capable of enhancing the viability of the excised nasal tissue, and investigating the effects of nasal drug delivery devices.

# Chapter 5

## Ex-vivo confocal microscopy of nasal tissue – investigation of the penetration of latex microspheres into excised rabbit nasal epithelium

### Overview

In this chapter the chamber described in the two preceding chapters has been adapted and developed for use in conjunction with a BioRad MRC 600 confocal microscope. After successful adaptation, viable excised rabbit nasal tissue was used to study the uptake kinetics of fluorescent labelled latex microspheres. FITC labelled latex microspheres were used as a model system since they are non-biodegradable and, readily available fluorescently labelled. Histological techniques were used a comparison to the chamber techniques developed here.

## 5.1 Introduction

The complete nasal chamber is a device that maintains the viability of excised epithelial tissues and the absence of a mucosal aqueous phase presents a with useful system to investigate delivery from non-liquid formulations, for example dry powders, or resuspended micro- and nano- particles. Traditionally drug delivery from such formulations to epithelial tissues has involved *in vivo* experiments. The delivery sites have then been investigated by sectioning and subsequent histological examination. When particulate delivery systems such as microspheres are applied and the tissue sectioned there is always an element of doubt as to whether the resulting section with its particles represents the true distribution. The possibility exists that knife drag compromises the experiment.

Confocal microscopy offers the advantage that tissue can be imaged in three dimensions in a non-destructive way. Since confocal microscopy is a non-invasive technique a significant bonus is that a single experiment can hopefully reveal data not just about penetration depth, but about depth changes with time. The aim of this work is to adapt the chamber so that it can be used in a confocal microscope; this should be done in such a way that live tissue can be imaged in real-time, providing a clear three-dimensional picture of the tissue. Hopefully, this should result in a technique capable of monitoring the changes in the tissue due to the applied formulation over time (figure 5.1 and 5.2).

### 5.1.1 Confocal microscopy

Confocal Laser Scanning Microscopy (CLSM or confocal microscopy) is a modern imaging technique based on fluorescence microscopy. The device consists of a standard fluorescence microscope, with a scanning laser source and electronic detector fitted.

The scanning laser source provides the excitation illumination; this is directed through the objective lens to the tissue as in fluorescence microscopy. The emitted light is then monitored using the electronic detector (photomultiplier) in the position usually occupied by a camera in a fluorescence microscope. Since both the laser excitation beam and emission travel through the objective, there is a beam splitter, usually a dichroic

reflector to separate the two beams. The main feature of a confocal microscope is the confocal aperture below the detector (photomultiplier). The confocal aperture separates out the light from the plane of focus of interest and rejects all other emissions. Unlike normal fluorescence microscopy, where the eye tries to build a three-dimensional image itself the image produced is from a very narrow focal plane and is the result of numerous scans. After recording the required number of scans the individual scans are averaged by the controlling computer software to produce a mean image value. This provides for the increase in the signal:noise ratio, and hence an increase in the sensitivity of the device. From experience, the most common number of scans performed on the BioRad MRC 600 confocal microscope, and that used in this study is 7 scans per image.

Since each image is from a very narrow focal plane confocal microscopy is a powerful tool for gaining three-dimensional data from a biological sample. To gain these data, a series of images at fixed depth intervals in the tissue under investigation are taken. These electronic images are then processed into a three-dimensional image electronically. As each image is at a known depth, the three-dimensional image is produced by placing one image below the previous one and the intervening space is filled by calculating the mean optical density of the layer above and the layer below. This interpolation process can be used to produce a three-dimensional image with any separation between the layers within reason.

### 5.1.2 *In vivo* confocal microscopy

*In vivo* confocal microscopy was introduced by Jester *et al* (1988) for the purpose of investigating the effects of substances on the eye, for which until currently this technique has had limited use (Jester *et al.* 1988, Jester *et al.* 1996, Li *et al.* 1997, Maurer *et al.* 1997, Maurer *et al.* 1999), almost always for testing cosmetic components. In this particular technique, an anaesthetised rabbit is mounted on the microscope, and the objective lens placed above the cornea. The data obtained from this particular type of work was aimed at

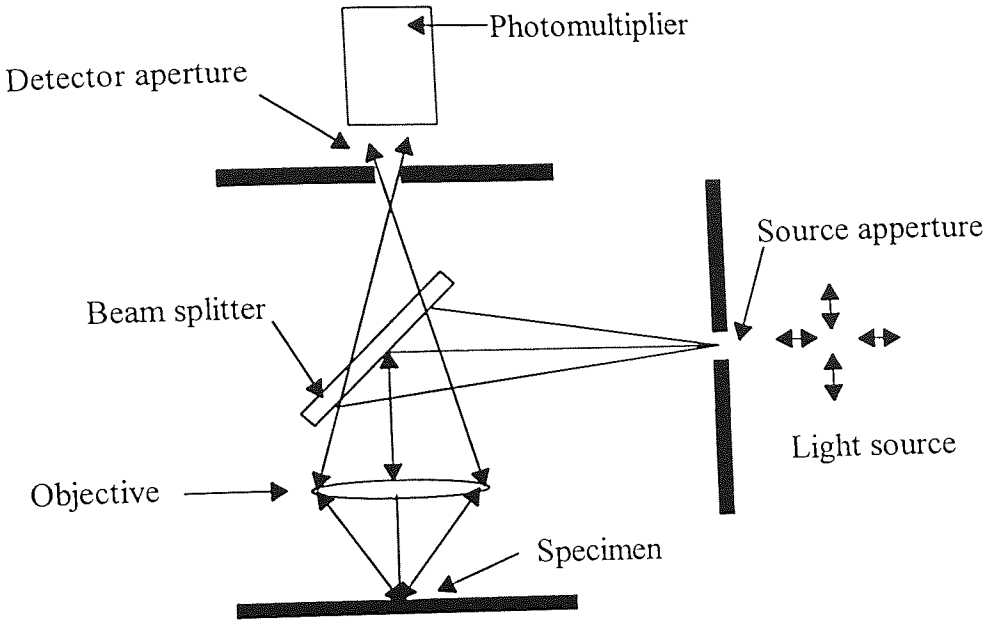


**Figure 5.1** Layout of confocal microscope.

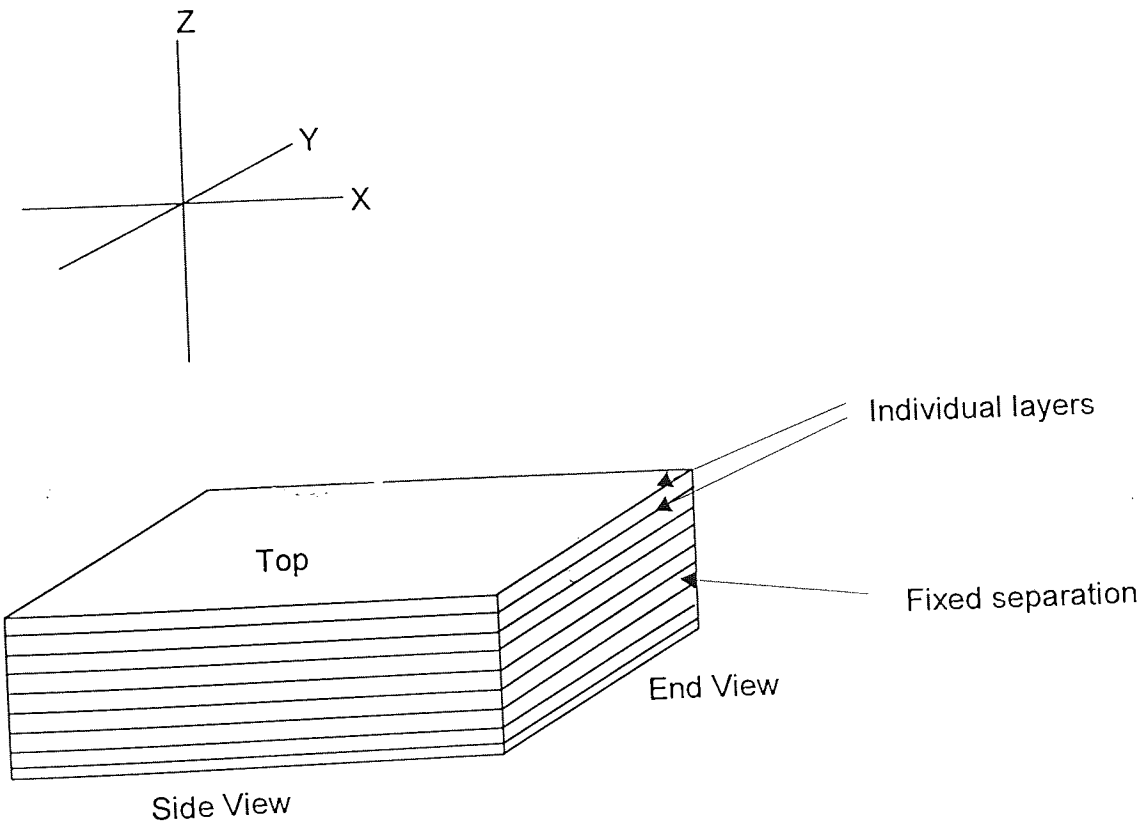


**Figure 5.2** Illustration of a confocal series made up of a number of individual pictures at a fixed interval, and the conventional designation of the axies

looking at the macroscopic changes in the cornea with intervals of 50 μm between successive layers in each Z series.

The higher specification hardware required for *in vivo* confocal microscopy was then above that commonly available. The equipment initially described by the group at Johnson & Johnson Inc. that developed the system (including Maurer, Jester, and Petroll) used a tandem scanning confocal microscope together with a then high-end computer such as a DEC Micro VAX II computer. Recently this was updated to a Silicon Graphics INDY computer fitted with a VINO image acquisition board. This systems requires an expensive video camera to capture and record confocal images rather than the more conventional confocal scanning head (Petroll 1996a, Petroll 1996b).

### 5.1.3 Aims of this chapter

The use of confocal microscopy in living tissue has previously been demonstrated. The aim of the work presented here is to develop the nasal chamber system so that, in conjunction with confocal microscopy, it can be used as a quantitative technique for analysing the uptake of particles, and potentially other suitably labelled delivery systems

## 5.2 Adaption of chamber to confocal microscope.

The chambers produced for the earlier work were initially tried under a BioRad MRC 600 attached to a Leitz microscope. This initial work failed since the table could not be lowered enough to fit the chamber under the objective lens, even using the physically smallest (10 x objective) lens.

To overcome this problem, the chamber system was re-designed with a significantly lower profile shown in figures 5.3–5.7. There were no gross changes to the chamber layout; upon completion the water-flow round the chamber was assessed to compare the new design with that previously discussed. No other properties were assessed since the overall principle of the chamber remains unchanged, together with the vast majority of the key dimensions.

### 5.2.1 Chamber construction

As with the system described in section 3.3, the upper section of the lower chamber was constructed from an acrylic block (Amari Plastics, Birmingham UK). The lower blanking plate was made from a sheet of 3.5mm acrylic. After machining these blocks, the mating surfaces were smoothed using a faceplate and 1200 grade glass paper and when the chamber was assembled they were mated with a thin layer of PTFE sealant

### 5.2.2 Chamber operation

The mounting of the tissue in the chamber, and everyday operation of the new chamber is the same as that described previously for the full height chamber in section 3.3.3 . All tissue samples in this study were covered with a 15mm glass coverslip before putting the chamber under the confocal microscope.

### 5.2.3 Initial assessment of chamber system on CLSM

After the macroscopic properties of the chamber had been assessed, the chamber was mounted on the confocal microscope. Even though the reduced profile chamber fitted easily under the microscope lens, further problems in mounting the tissue arose. After mounting the tissue chamber on the microscope table in a similar way to that used for an ordinary microscope slide, any slight movement of the table resulted in the chamber moving on the table. This was partly due to the shape and orientation of the chamber on the table, and partly due to the number of tubes attaching the chamber to equipment away from the microscope, ($O_2$ supply, thermostatting). For mounting on the confocal microscope, a special aluminium base was devised. This base is simply a piece of aluminium that is of similar size to a standard microscope slide, but with a special cut-out to mount the chamber at 90° to the direction that the slide holder is designed for, as shown in figures 5.9 and 5.10.

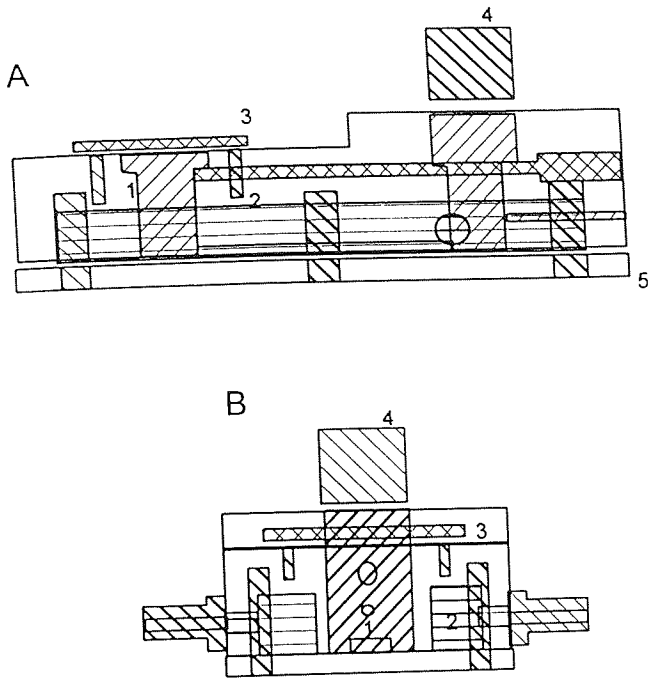


**Figure 5.3** The lower tissue viability 1/2 cell.
Cross Section (A), and side view (B) of novel chamber system. (1) Chamber (1.8 ml), (2) Water jacket (37°C), (3) Tissue mounting ring, (4) Funnel to prevent overflow due to gas lift system, (5) Gas lift system to provide circulation and oxygenation (95% $O_2$ 5% $CO_2$)

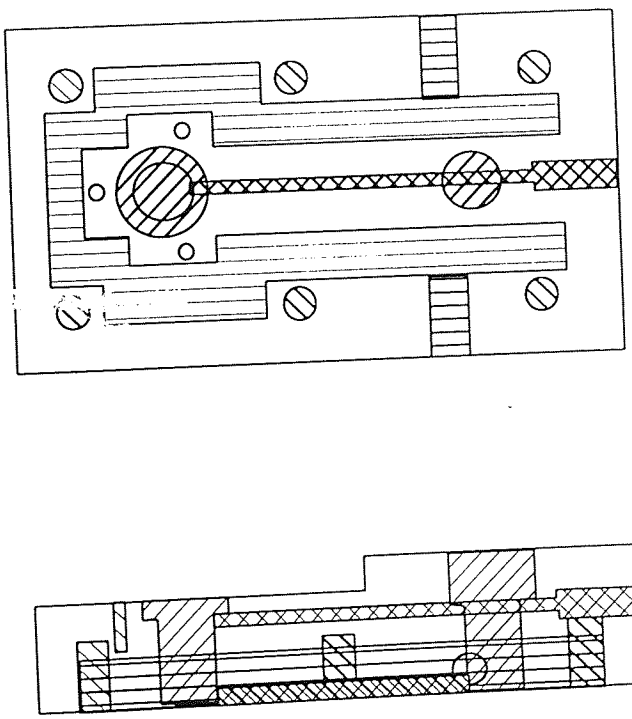



Tissue Viability 1/2 Cell
Upper Section
General Layout.

**Figure 5.4** General layout of the lower tissue viability chamber.

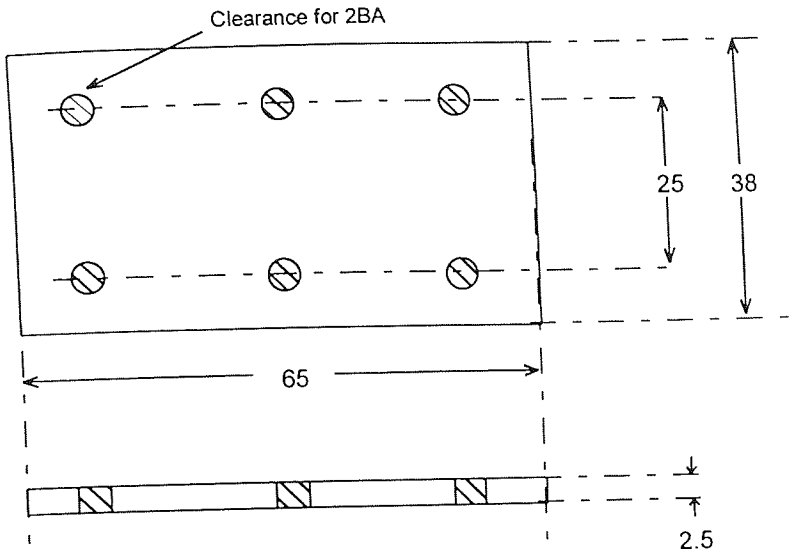


Lower Tissue Viability 1/2 Cell.
Lower Section.
Material: Acrylic
Dimensions: mm
Quantity: 1

**Figure 5.5** Engineering drawing of the lower section of the tissue viability ½ Cell

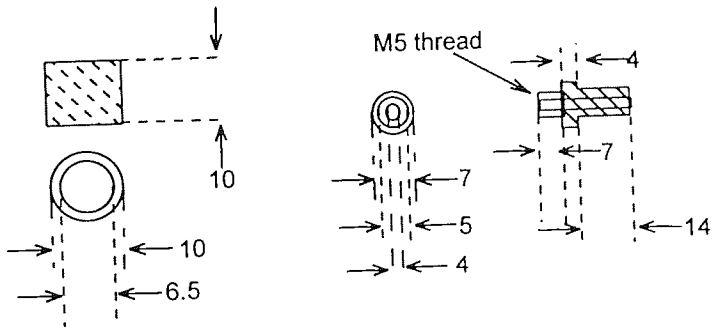


Chimney
Quantity: 1
Material: PTFE

Water Union
Quantity: 2
Material: Brass

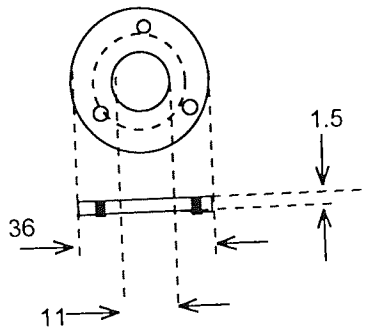


Upper Mounting Ring
Quantity: 1
Material: PTFE

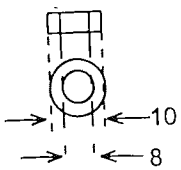


Lower Mounting Ring
Quantity: 1
Material: PTFE

Tissue Viability 1/2
Misc. Parts
Items not shown:
3 x 6 BA bolts x 10mm
6 x 2 BA bolts x 13mm

**Figure 5.6** Engineering drawing for tissue viability ½ cell miscellaneous parts.

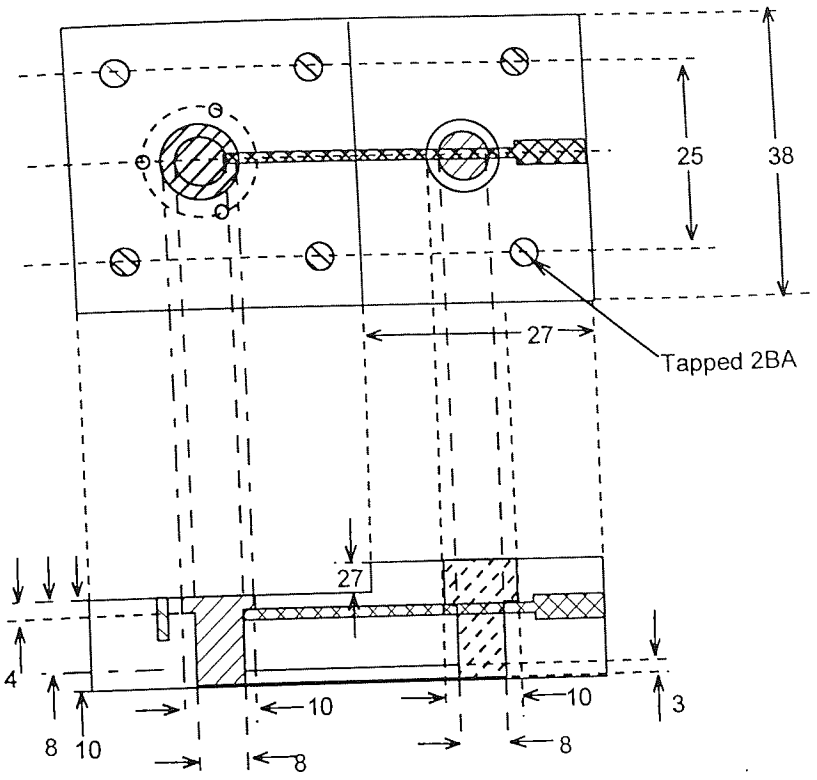


Tissue Viability 1/2 Cell
Upper Section - Excluding Thermostatting
Material: Acrylic
Dimensions: mm
Quantity: 1

**Figure 5.7** Engineering drawing for the upper section of the tissue viability chamber

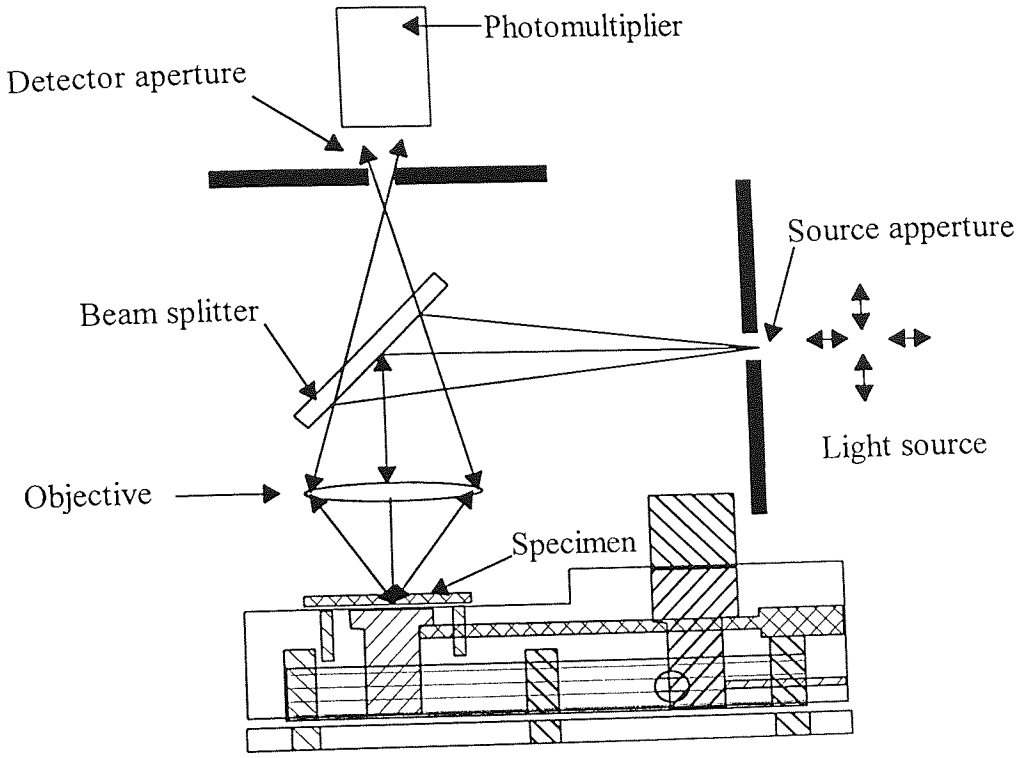


**Figure 5.8** Layout of confocal microscope with new chamber.

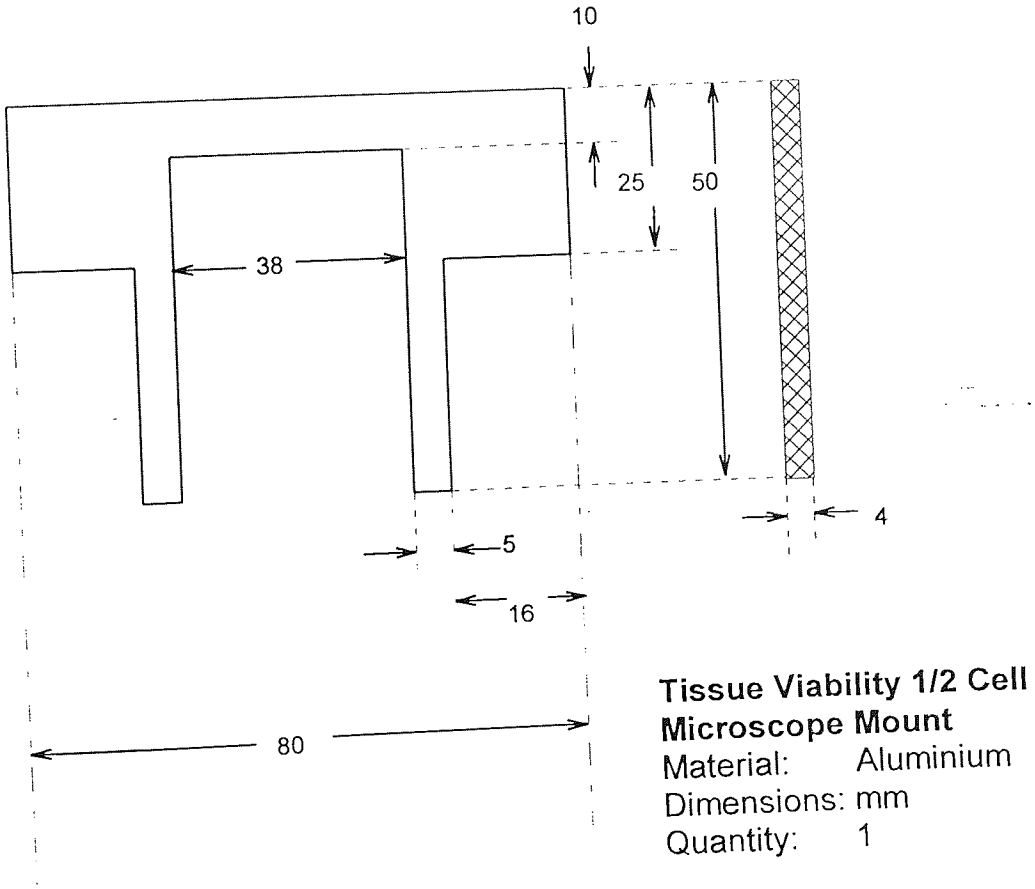


**Figure 5.9** Aluminium base for mounting chamber on microscope table.

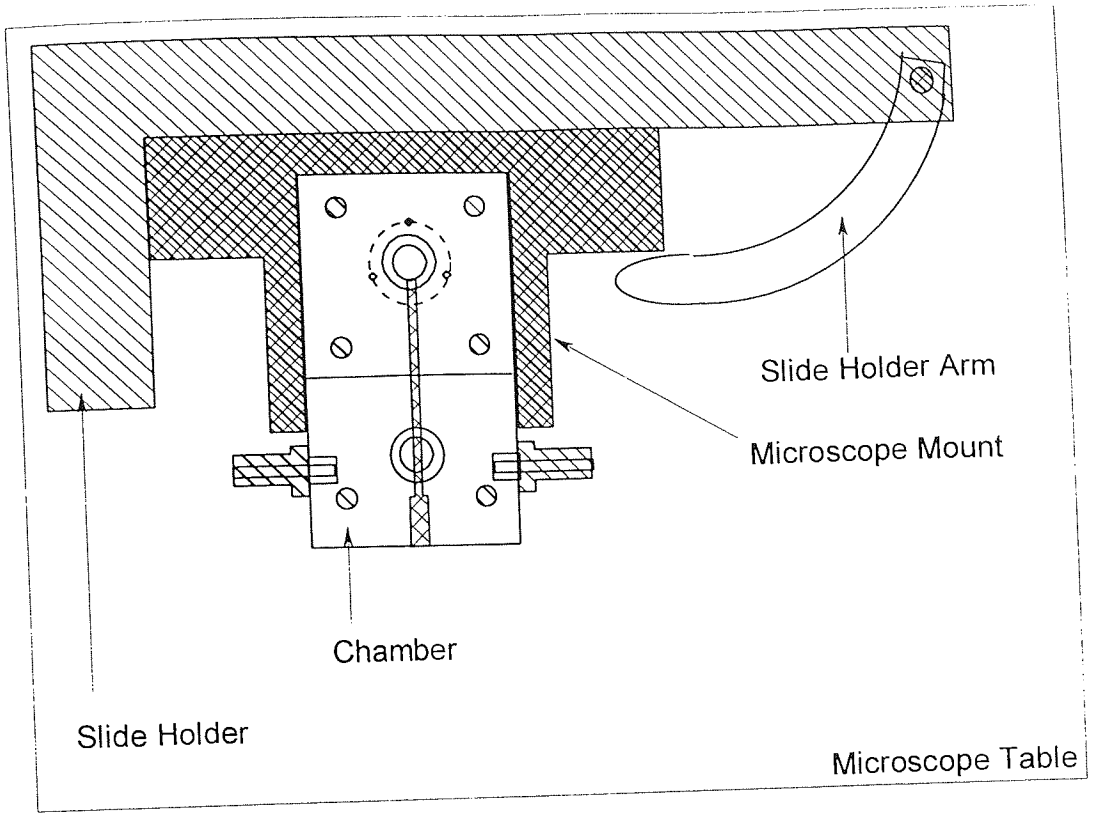


**Figure 5.10** Setup of chamber on microscope table.

### 5.2.4 Water flow in confocal chamber

The only macroscopic property that was investigated in the new chamber, since the internal design was altered to such a minimal extent was the water flow properties. These were assessed as described previously (section 3.3.2.1). At gas-flow rates of more than 1 bubble/second, the internal flow was seen to stop, remaining unchanged from those previously established.

## 5.3 Confocal methods

### 5.3.1 Confocal Microscope operation

Operation of the confocal microscope is very similar to an ordinary fluorescence microscope. The chamber is mounted on the microscope table using a special aluminium base designed to fit onto the table as a normal microscope slide would (figures 5.9 and 5.10). This base provides the chamber with sufficient rigidity on the table that when the table moves (to move the focal plane) the chamber is not moved because of the attached thermostatting equipment and carbogen supply.

Initially the tissue is viewed using the microscope as a standard fluorescence microscope. An ultraviolet (UV) source provides the illumination for this initial observation. The microscope is brought to the focus region of interest manually using the UV excitation, and then switched to confocal imaging. For the experiments performed in the mucin matrix the focus was manually set to the top of the mucus, and the series performed under computer control. The methods used for the live tissue experiments are much more complicated, and discussed in some detail later (section 5.5).

#### 5.3.1.1 Standardised Z section parameters

To enable easier comparison between experiments, a number of key parameters were defined, and unless otherwise stated remained constant throughout the study. These key parameters included magnification, sectioning interval, aperture controls and the number of scans per layer. These were set as follows:

| | |
|---|---|
| Magnification | 16x objective |
| Sectioning interval | 1 μm |
| Aperture control | Minimum setting |
| Scans | 7 scans per image |

### 5.3.2 Image analysis

Images were obtained on the BioRad MRC600 microscope and saved in BioRad's proprietary "name.PIC" format, for later off-site analysis. All picture analysis was performed using either the Confocal Assistant, or Scion Image software.

### 5.3.2.1 Three-dimensional analysis

After recording the Z series, the data were analysed using the Confocal Assistant software (Confocal Assistant –V4.02 Build 101, by Todd Clark Brelje). For simple graphical analysis, Z section views at the side and end of the section were generated using the 'project' command. These two images together with a view from above the 3D section give a good visual representation of the tissue surface, however, they do not give the complete picture. For complete analysis of the 3D section, a 3D rotating image of the tissue section is generated, however this can obviously not be adequately represented pictorially. 3D rotating images were generated of all the tissue sections, and analysed for unevenness of the tissue surface. Whilst this is less important in the time course experiment, as the same tissue section is continually being re-examined, it becomes far more important when comparing the results obtained from different tissue samples.

### 5.3.2.2 Measuring mean OD

As well as the visual non-quantitative assessment of the change in fluorescence over time, the mean OD of the individual layer images can be quantified using the Scion Image software package to provide an accurate indication of the change in fluorescence with depth. The total area of the image being analysed was selected using the select rectangular area tool. The mean OD was then calculated using the measure command from the analyse menu. This gives the mean OD on a scale of 0 (pure white) to 255 (pure black). This is the opposite of the conventional RGB and Greyscale scaling where 255 is pure white and 0 is pure colour absence (black). Since the data are presented graphically as a value relative to the t=0 value, this is not of any significance, however, it should be noted that values obtained are different from traditional OD values. In this case, when OD=0, there is a maximum of fluorescence, and an OD=255 is a complete absence of fluorescence.

### 5.3.2.3 Writing Scion Image macros

ScionImage is the IBM PC version of the popular Image analysis software NIH-Image (NIMH, Bethesda Maryland USA, www.nimh.gov), and it contains its own macro language, that can be considered to be based on Pascal. There is very little documentation available about this macro language, however several macros were written to assist in this work. The most important macro written was that to take a selected area on one layer of a Bio-Rad confocal image, measure the mean OD, close that layer, select the next layer, select the same region, measure the OD from that region through the complete Z series, and then to continue the process through individual layers in subsequent Z-series files at later time points.

This macro is incredibly important in the picture analysis as it allows exactly the same point to be selected and analysed at each recorded depth and each time point. This removes the inevitable errors that would occur if each layer (24 layers per Z section, 6 time points per experiment, 144 images in total) was to examined individually. The macro written is included in Appendix 1.

## 5.4 Initial confocal validation

As an initial assessment of the chamber system mounted on the confocal microscope, particles made from either latex or PLA were studied in a viscous matrix. The aim of these initial experiments was to prove that the chamber system did not interfere with the workings of the microscope, and to provide loading, concentration, size, and label data for the microspheric system.

### 5.4.1 Assessment of confocal imaging

As an initial experiment, FITC-labelled latex microspheres (80 nm) (Fluoresbrite®, ) were immobilised in a 5% mucin matrix. The 5% solution of Mucus Proteins (Sigma) in double-distilled water was made by stirring overnight to facilitate the wetting process. This solution was then loaded with microspheres from stock to 0.027% w/v. The resulting

suspension of microspheres was placed on a blank silicone membrane held in the place of the tissue in the lower chamber. The matrix was covered by a 15mm round glass cover slip (the silicone membrane was in effect the tissue, with the mucus placed above, where it would be *in vivo*). This was then observed under the confocal microscope.

The confocal system used relies on taking several pictures at each section depth and averaging these to produce the final image. For these initial experiments only 2 scans were taken for each image. Z sectioning was performed with a distance of 0.5 μm between each section, and a total sectioned depth of 4 μm. Laser confocal micrograph images (CMi's) are electronically produced images and are naturally greyscale images. Artificial colours were applied using the confocal assistant software.

For single-layer Z sections, artificial colour has not been added. In these CMi's the white areas represent the particles (fluorescence sources). From these sets of pictures it is difficult to get any real indication of what is happening.

To assist in interpretation, single-layer images have been overlaid. In these images, artificial colours have been applied to the two images. The uppermost image (layer 1) has coloured red, and the lowermost image has been coloured green. In the instances where there is overlap these two colours merge to form yellow. Two types of image have been processed, those with two adjacent layers (layers 1 and 2) and those with the top and bottom layers (layers 1 and 9).

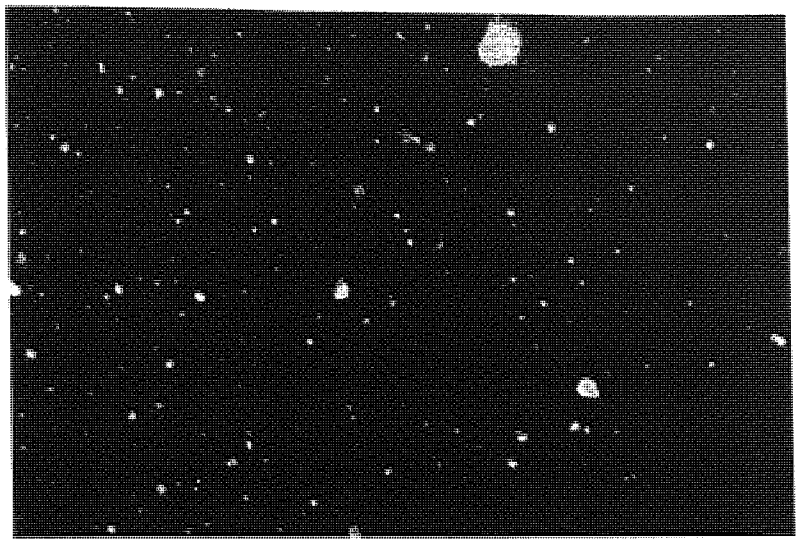

**Figure 5.11** CMi's taken at 0.5 μm interval. FITC labelled Latex microparticles, 0.08 μm mean diameter. Overlay of layers 1 and 2. Red - Layer 1. Green - Layer 2. Yellow - Both layers.

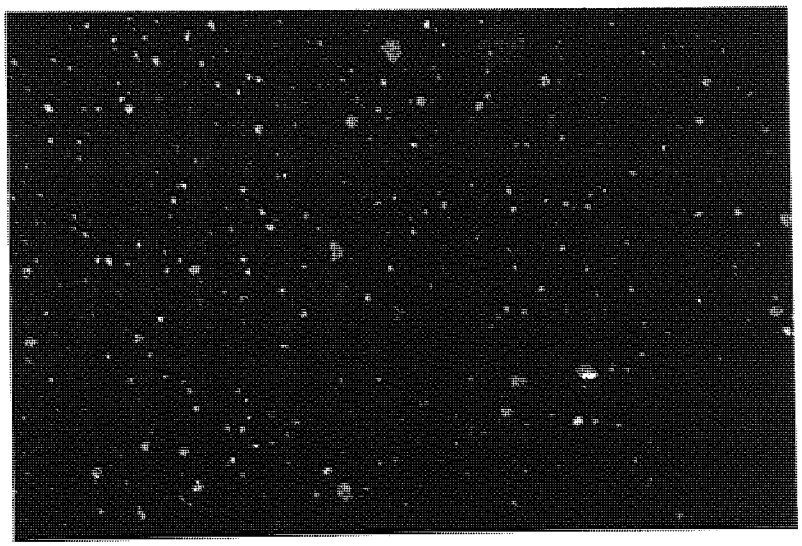

**Figure 5.12** CMi's taken at 0.5 μm depth. FITC labelled Latex microparticles, 0.08 μm mean diameter. Overlay of layers 1 and 9. Red - Layer 1. Green - Layer 2. Yellow - Both layers.

Looking at the overlayed images for these FITC-Latex particles, it is very difficult to see the differences between the layers (figures 5.11 and 5.12). The latex particles are very small (0.08 μm mean diameter), and each layer in the section is 0.5 μm below the previous; in the picture of two layers superimposed there is very little yellow, mostly discrete particles. Where there is yellow it is due to large aggregations of the particles that are big enough to appear in at least two levels. From these initial scans it would appear that the presence of the chamber has very little effect on the working of the confocal microscope.

### 5.4.2 Particle concentration

As an initial experiment 1 μm nominal diameter particles, labelled with FITC (Fluoresbrite® Latex microspheres, Park Scientific, Warrington, UK) were observed supported in a mucin matrix under the confocal microscope. A 5% solution of Mucin Proteins (Sigma) in double distilled water was made by stiring overnight. This solution was then loaded with microspheres to the desired concentrations, 0.0027% w/v, 0.027% w/v and 0.27% w/v. These were then observed under the confocal microscope. The mean OD was measured from the whole-image

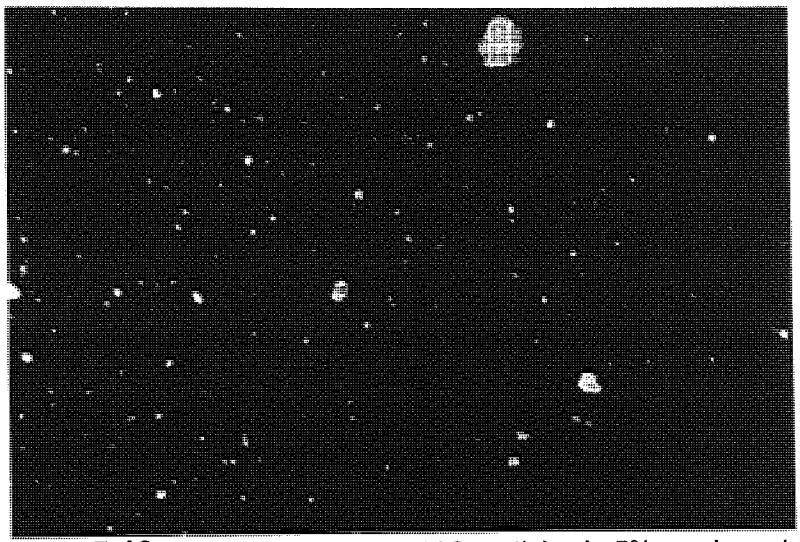

**Figure 5.13** 0.0027% w/v 1 μm FITC particles in 5% mucin matrix.

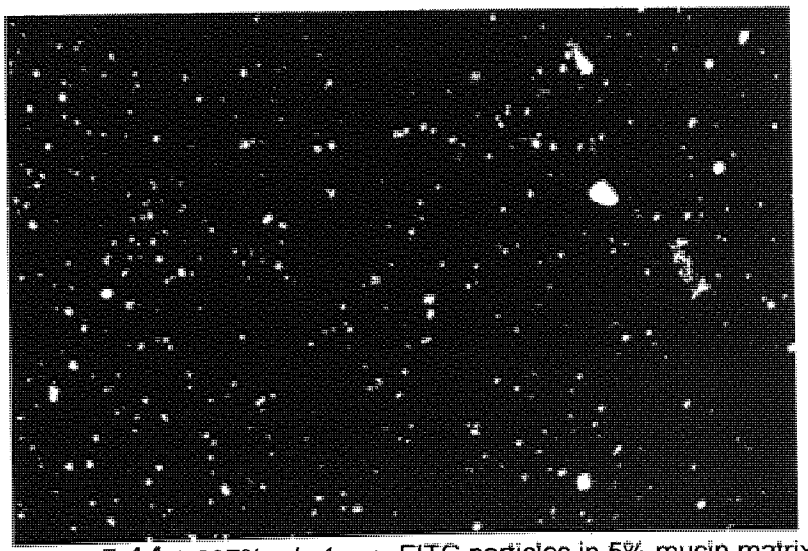

**Figure 5.14** 0.027% w/v 1 μm FITC particles in 5% mucin matrix.

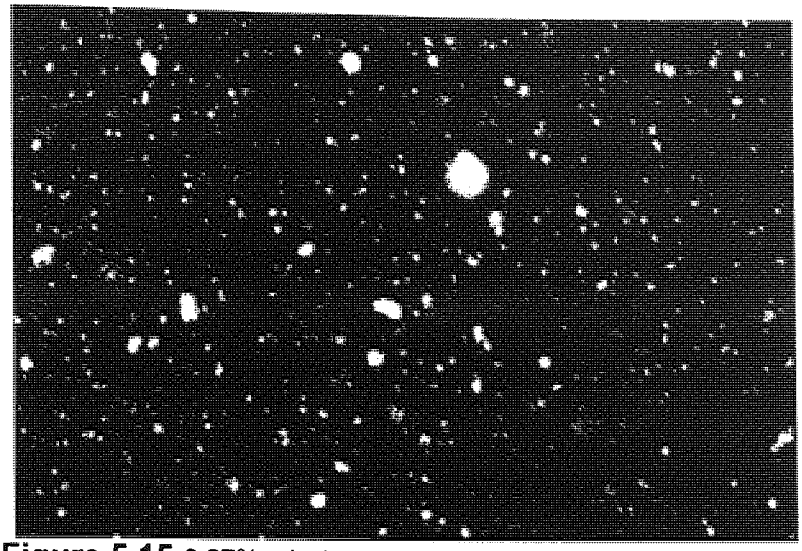

**Figure 5.15** 0.27% w/v 1 μm FITC particles in 5% mucin matrix.

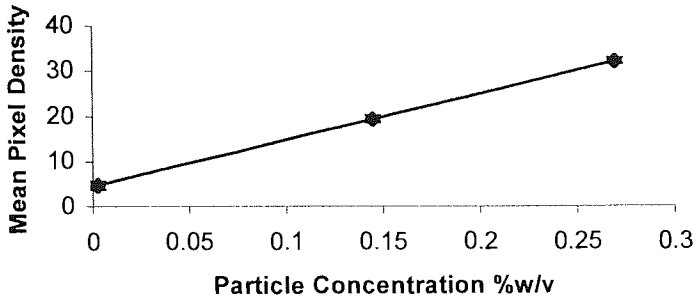


**Figure 5.16** Mean pixel OD as a function of particle concentration, suspended in a 5% mucin matrix. Mean pixel density was measured using the small-square method. N=5

### 5.4.3 Fluorescent label used

As an initial experiment particles labelled with similar amounts of rhodamine and FITC were observed supported in a 5% mucin matrix under the confocal microscope. This solution was then loaded with microspheres to the concentrations of 0.27% w/v and 0.027%

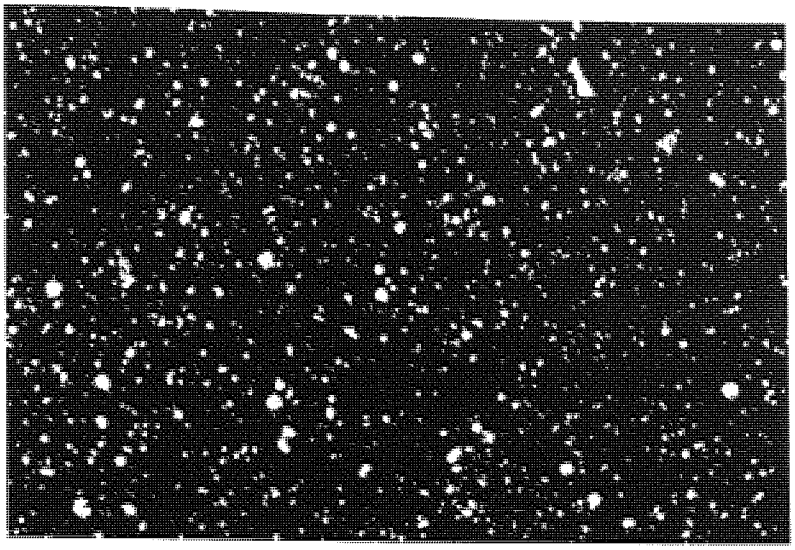

**Figure 5.17** 0.27% w/v Fluoresbrite® Latex microspheres in 5% mucin matrix

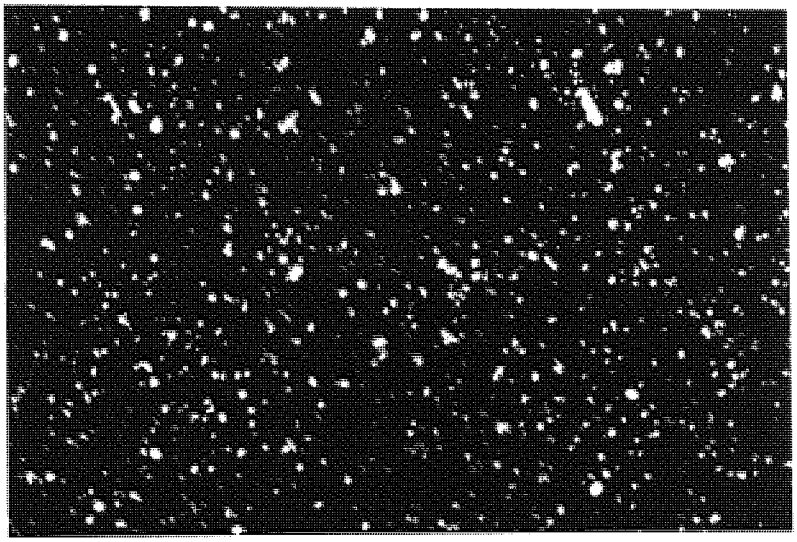

**Figure 5.18** 0.27% w/v rhodamine labelled PLA particles in 5% mucin matrix

Analysis by measurement of mean OD from the entire picture gave very similar results for the two labels used, FITC and rhodamine, with mean pixel densities of 24.07 (± 1.3, n=6) and 22.25 (±2.0, n=6) respectively for 0.27% w/v particles in the matrix. For 0.027% w/v particles in matrix the OD was 8.91 (± 0.5, n=6) and 9.33 (±0.6, n=6) respectively. Since both these sets of results are statistically insignificant ($p>0.05$), both dyes used provide linear responses against particle concentration. This is somewhat unexpected, as it would be expected that the two dyes have different adsorption/emission characteristics, however, over the limited particle concentration range being considered they proved to have very similar characteristics.

### 5.4.4 Particle size

Analysis of the effect of particle size on the system was performed using FITC-labelled Fluoresbrite® Latex particles with a size-range from 50 nm to 1000 nm (1 μm) in a 5% mucin matrix. The 1 μm particles are much clearer in the confocal images obtained (Figures 5.19 and 5.20). From the Z sectioning result, it can be seen that the nominally 1 μm particle that was chosen in this particular Z section is much closer to 8 μm in size, since each layer in the Z section was taken at an interval of 1 μm. The nominally 1 μm particle can be seen in great detail, whereas by contrast the 50 nm particles are simply indistinguishable dots.

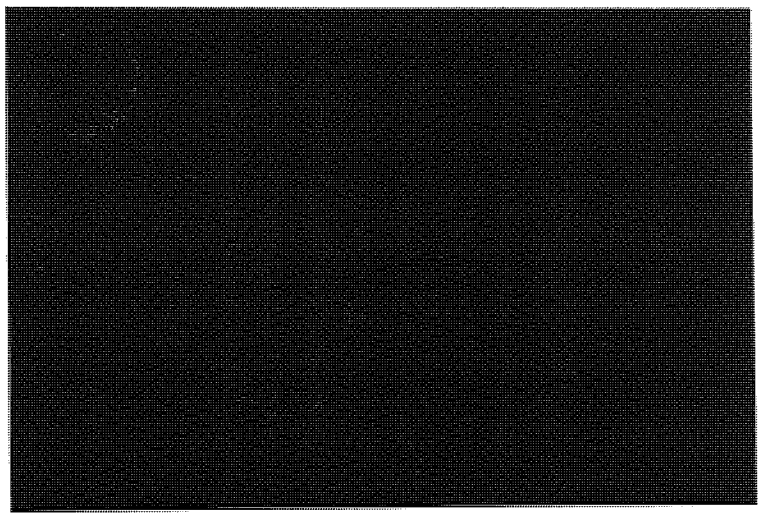

**Figure 5.19** 1 μm Nominal particle size

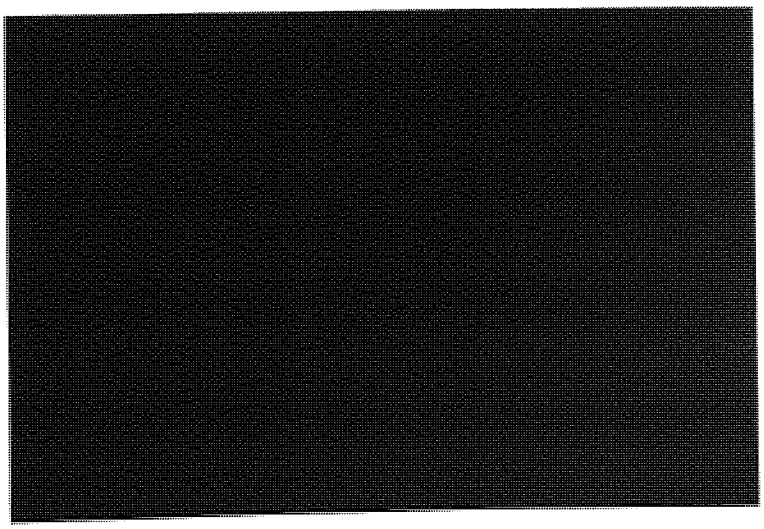

**Figure 5.20** 50 nm Nominal particle size

If we extend this to Z sectioning of the particles suspended in a mucin matrix we would expect to see the larger particles covering more than one layer, and the significantly smaller particles only appearing in one layer unless there has been significant aggregation. To this end, suspensions of particles in a 5% mucin matrix were made, and Z sectioning was performed on the resulting suspension. For analysis, layers 1 and 2 were overlaid, and false coloured, the upper layer (layer 1) was coloured red, and the lower layer (layer 2) was coloured green. Fluorescence in both layers results in a yellow area. If we look at the separate layers for the 0.08 μm Latex particles, it is very difficult to see the differences between the layers. The latex particles are very small (0.08μm) and the sections are 0.5 μm, so in the picture of two layers superimposed, there is very little yellow, mostly discrete particles. Where there is yellow, it is due to large aggregations of the particles that are big enough to appear in at least two levels.

This can be contrasted with the image obtained from the two consecutive layers containing the larger particles. These particles have a nominal mean diameter of 1 μm and as such they appear in many levels. The superimposed images have a large amount of yellow indicating that many of the particles appear in both layers, and that what is being seen is the same particle but imaged at a lower point in the particle.

Conversely when two images obtained from the top and bottom layers, are examined there is very little yellow and that present as exceptionally large aggregates of particles in the system.

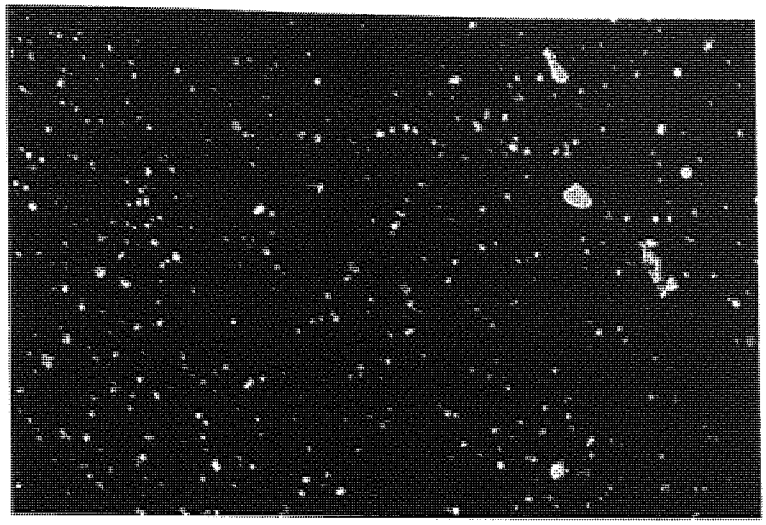

**Figure 5.21** CMi's taken at 0.5 µm depth separation. Rhodamine labelled PLA microparticles, 8 µm mean diameter. Overlay of layers 1 and 2. Red - Layer 1. Green - Layer 2. Yellow - Both layers.

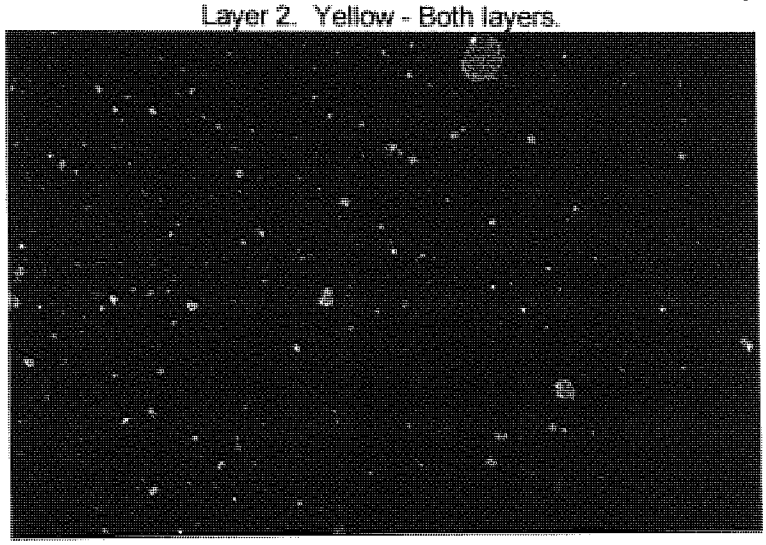

**Figure 5.22** CMi's taken at 0.5 µm depth separation. FITC labelled Latex microparticles, 0.08 µm mean diameter. Note the significant aggregation of the particles. . Overlay of layers 1 and 2. Red - Layer 1. Green - Layer 2. Yellow - Both layers.

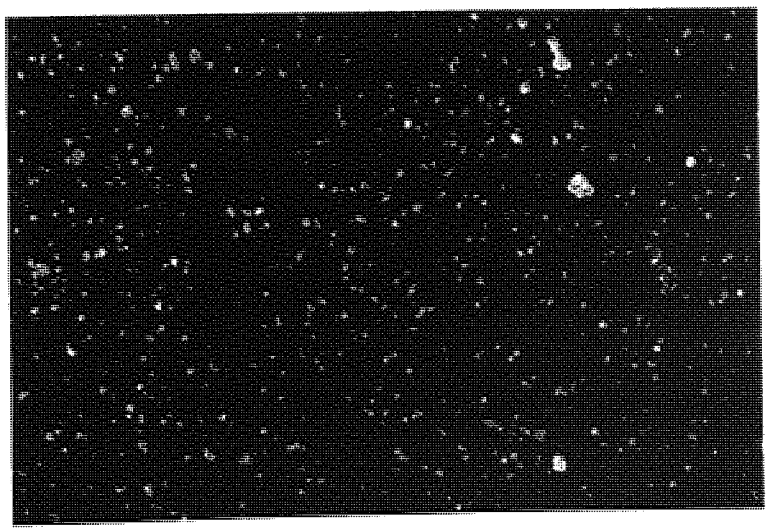

**Figure 5.23** CMi's taken at 0.5 µm depth. Rhodamine labelled 8 µm mean diameter PLA particles. Overlay of layers 1 and 9. Red - Layer 1. Green - Layer 9. Yellow - Both layers.

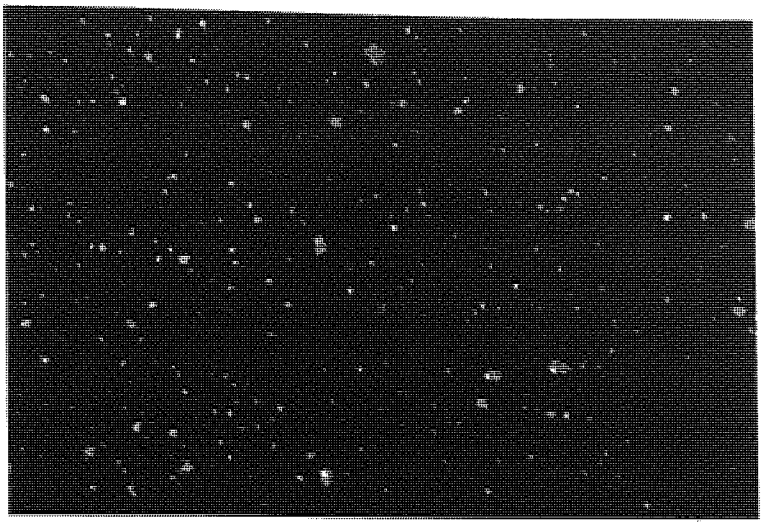

**Figure 5.24** CMi's taken at 0.5 μm depth. 8 μm mean diameter particles. Overlay of layers 1 and 9. Red - Layer 1. Green - Layer 9. Yellow - Both layers.

## 5.5 Confocal imaging of live tissue

The aim of the confocal work is to develop a system in which live tissue can be investigated over time in a non destructive way. Tissues such as skin, which can be readily mounted on the confocal microscope, are regularly investigated in this way (McCrossin, 1999; Yu 1999). There are major problems in mounting live epithelial tissues on the confocal microscope. In this section, the problems encountered and the solutions that were developed to overcome them are discussed. Since this work is centred around the development of the confocal system, scarce rabbit or pig nasal epithelial tissue was not used; in its place, gut tissue was used. The chamber is known to give more than adequate viability to excised ileal tissue and, as rat epithelial tissue is easy to obtain this was used as the developmental model. Rabbit nasal tissue was used at the end of the developmental work and also as a comparison with nasal tissue sectioned using traditional histological techniques.

### 5.5.1 Initial studies

As an initial study live rat ileal tissue was placed in the chamber under the confocal microscope. The gut tissue was covered with a glass coverslip and the chamber operated as in section 3.3.3. Initially, the tissue was left for 15 minutes before observation for the particles to settle into the mucus and to allow the viscous mucus to slow down any motion of

the particles. Since the mucus layer consists of several layers, including the upper moving layer and the lower unstirred water layer (UWL) (Holbrook, 1991), the particles were left in anticipation of them reaching the UWL and settling on the epithelial surface. If we consider the structure of the nasal epithelium (Figure 1.3) and the location of the UWL, the particles in the UWL will be within a few microns of the surface of the epithelial villi.

There was one important initial observation: the objective lens (16x) used in the developmental work could not be used to focus on the emitted fluorescence. This was due to the distance from the lens surface to the focal plane of interest being less than the distance available due to the thickness of the mucus layer and the glass coverslip. This could easily be overcome if any decrease in magnification was acceptable by using a lens with a smaller magnification (10x objective), requiring a larger distance between the surface of the objective lens and the focal plane. From the developmental work, the objective lens used provided only adequate magnification for visualisation of microspheres that were in the micron range. At the cost of the available resolution the computer analysis / control software could be used to increase the magnification with the 10x objective back to that of the 16x objective lens.

On initial focusing of the microscope, movement of the fluorescent particles was seen to the extent that particles were moving some 50-60 μm, approximately ¼ of the picture area. Observation of the tissue after this 15 - minute incubation showed that the particles at the lowest point of fluorescence which, although not stationary, were moving significantly less than those higher up. Their motion was limited to a simple oscillation. This layer of particles, below the particles being moved by the cilliary motion of the live tissue is in this study called the point of lowest movement. The surface of the epithelial tissue was then defined as being 2 microns below this point, as shown in figure 5.25. From work previously done it is known that the UWL is about 5 microns thick (Chien *et al.* 1989). The point of lowest movement could be either the particles actually on the tissue surface, or they could only just have reached the UWL. The assumption that the tissue surface is 2 microns below the lowest movement is taking this uncertainty into consideration and although the surface definition is arbitrary from the data obtained it would appear that this provides a workable solution to the problem of identifying the tissue surface level. This definition is

entirely arbitrary, and it does carry with it the risk that the surface is incorrectly identified. However, with practice the identification of the tissue surface can be done such that reproducible depth penetration results can be obtained. After incubation of the particles on the tissue surface Z sections were obtained every 15 minutes for one hour. Confocal images were analysed using both the whole-image method and the small-square method described below (figures 5.27 and 5.28). Since only small amounts of particles are thought to be taken up, the concentration of particles above the tissue can be expected to remain constant throughout the time of the experiment as it acts as a reservoir. The level of fluorescence at the arbitrarily defined surface is taken as a reference point. In all subsequent analyses the mean OD at each depth layer is expressed as a percentage of the mean OD of the top most layer in that series. Exposure of viable rat ileal tissue under standard conditions to 50 nm Fluoresbrite® plain particles (50 µl 2.7% solution in water) under a glass coverslip for one hour was performed to test the reservoir hypothesis. The mean OD was obtained by analysing the confocal image of the top layer using ScionImage. From figure 5.26 we see that the reservoir hypothesis holds for the duration of the experiment.

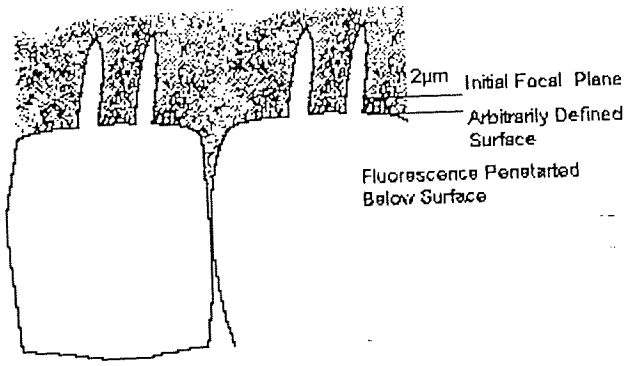


**Figure 5.25** Diagramatic representation of epithelial surface after the application of Fluoresbrite® microspheres showing the initial focal plane, and the arbitrarily defined tissue surface.

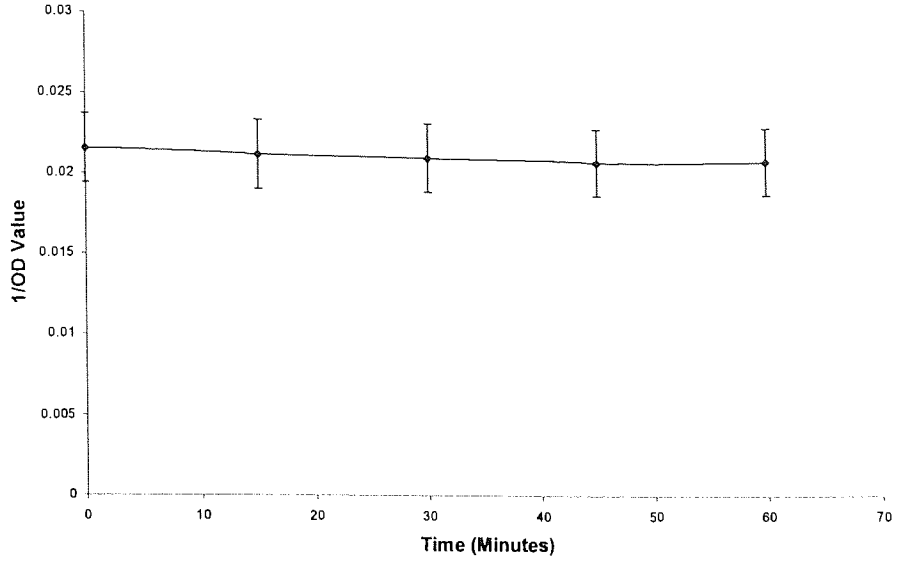


**Figure 5.26** 1/OD (corrected OD value) at arbitrarily defined epithelial surface. 50 nm plain Fluoresbrite® particles on Rat ileal tissue (n=3).

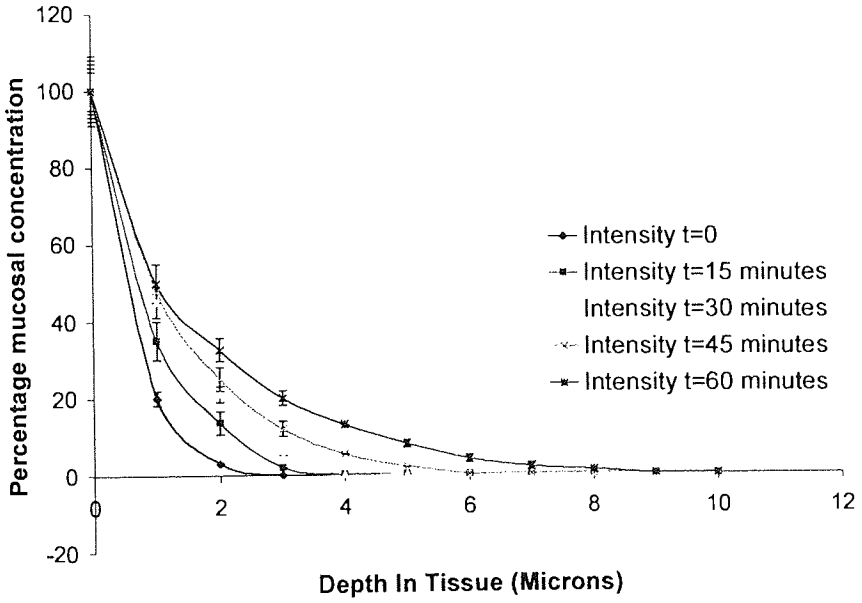


**Figure 5.27** OD expressed as a percentage of the surface level as a function of depth in excised viable rat ileal tissue. Data analysis was performed using the small-square method

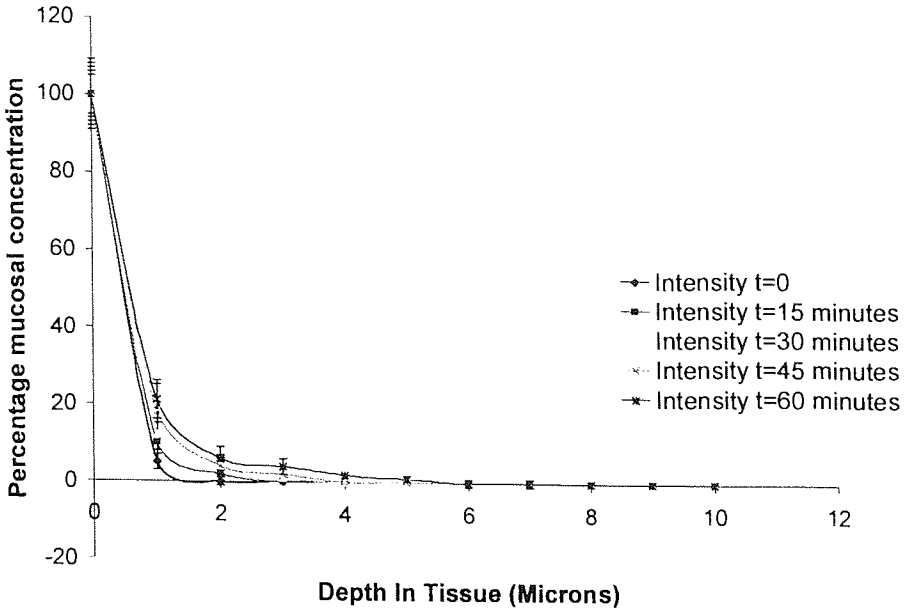


**Figure 5.28** OD expressed as a percentage of the surface level as a function of depth in excised viable rat ileal tissue. Data analysis was performed using the whole-image method (n=3)

Previously the development of ScionImage macros was discussed (5.3.2.3) together with the analysis of mean OD (5.4.2.1). The technique previously described for image analysis has a significant drawback; the image being analysed has large areas where there are no particles being taken up. To give a much more reliable picture of the particle uptake characteristics, the image analysis was repeated using a different technique. A smaller area of the image was chosen to included almost exclusively areas where uptake was occuring, rather than the large areas that contain no label in the full image. Using the ScionImage software, the particular area is carefully chosen and then marked. A macro was written (described in section 5.3.4.3) so that after measuring OD, the chosen area could be transferred between not only different depth of each time point, but to be in an identical position in subsequent time points where the data series were saved in separate files. After measuring the mean OD values, the data were analysed in the same way as for the whole-image.

To assess the effect of the analysis technique, 50 μm mean size Fluoresbrite® particles (50 μl 2.7% solution in water) were applied to freshly excised rat nasal tissue in the modified lower tissue viability ½ cell covered by a 15mm diameter cover-slip. From figures 5.27 and 5.28 the differences between the two analysis methods can easily be appreciated. If we compare this with a confocal image taken just below the cell surface (figure 5.29) we

can see that there are definite areas where microspheres are present, and distinct areas of absence. Using the small-square technique an area where uptake is occurring can be analysed, whereas, using the whole-image method, both the areas of uptake/penetration and the areas where nothing is observed to be happening are included. However, analysis by the whole-image method can not easily quantify the very small quantities of microparticles that have penetrated below the surface. The small number that reach 4 μm below the surface in figure 5.27 (where the fluorescence level is 18% of the surface value) is reduced in figure 5.28 to a minimal 3%. Both methods of analysis have their advantages and disadvantages. The major drawback of the whole-image method is that epithelial surfaces are not flat, they consist of folds, so any uptake in a whole-image analysis can be either genuine uptake/permeation, or movement of particles within folds in the tissue. Equally, this argument can be applied to using the small-square analysis method. In this method care has to be taken so that conclusions are not drawn from analysing particles moving to geographically lower areas of the tissue surface. Both analysis techniques have their uses. In the work here the small-square method was used exclusively, however, the 3D-image of the tissue was assessed to see if there was any obvious reasons for not using it. Without significant development work, beyond the scope of this study, a definitive analysis method is not possible. For this study, one method was used so that results could be compared between experiments, however, it should be remembered that these results are calculated on a relatively small area where uptake was seen.

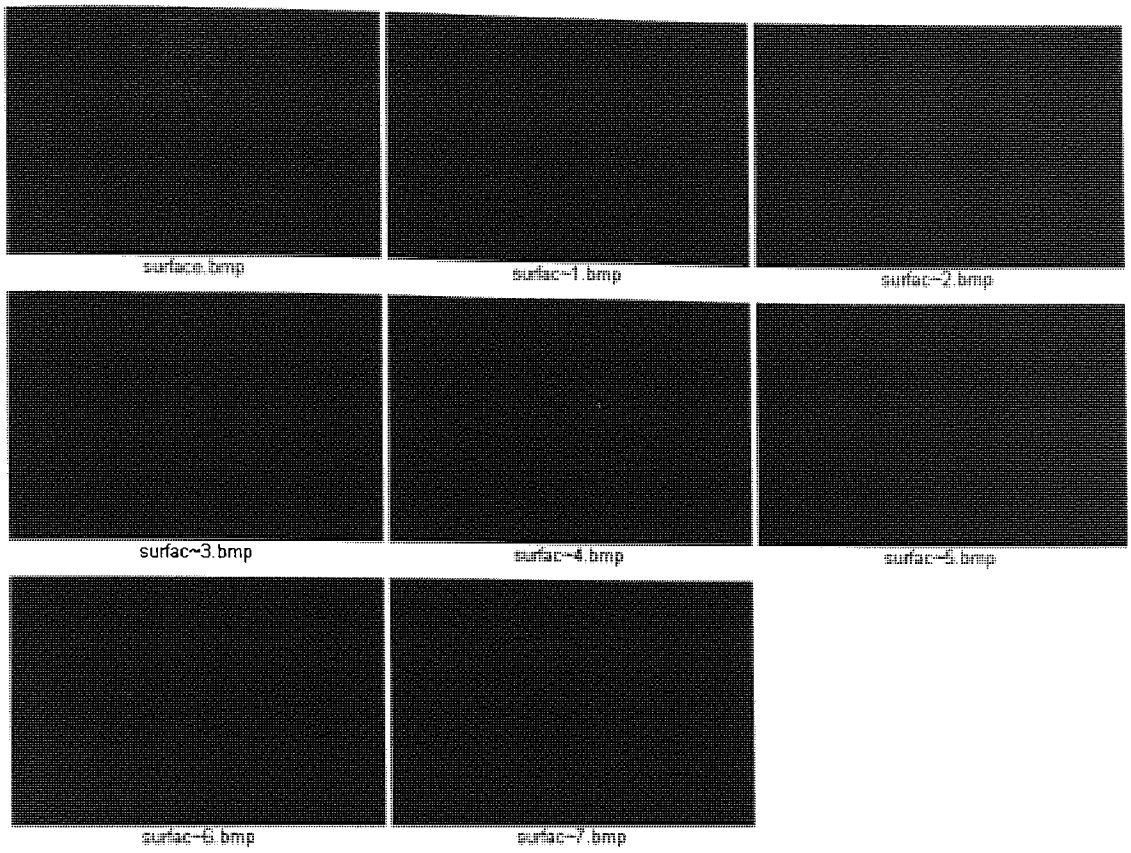


**Figure 5.29** CMi's showing a region of uptake. 50 nm plain Fluoresbrite® particles in rabbit nasal tissue. Individual images separated by 1 μm.

## 5.5.2 Effect of particle size on uptake

Many *in vivo* studies have reported that particle size plays an Important role in determining the uptake and eventual fate of any applied microparticle (Eyles *et al.* 2000). Here, plain Fluoresbrite® latex microparticles (50 μl 2.7% solution in water) were placed on the surface of viable, excised rabbit nasal tissue and examined in the way described in the previous section (5.5.1). Figures 5.30, 5.31 and 5.32 show the penetration/transport of 200, 100 and 50 nm particles, each of these figures represents a number of experimental time-points. We can see that particles of all three sizes were taken up to some extent. From the fluorescence-depth profile (fixed time point-60 minutes, figure 5.33) the significant differences between the 50 nm and both the 100 and 200 nm particles ($p<0.05$ between two points at fixed depths below 3 μm) becomes apparent. The 50 nm particles have an appreciably greater depth of penetration. From existing vaccine work it is known that the smaller particles induce a greater immune response. There was, however no significant difference when looking at the fluorescence-depth profile for the larger particles ($P > 0.05$

between any two points of fixed depths for 100 nm and 200 nm particles, except for at a depth of 4 μm).

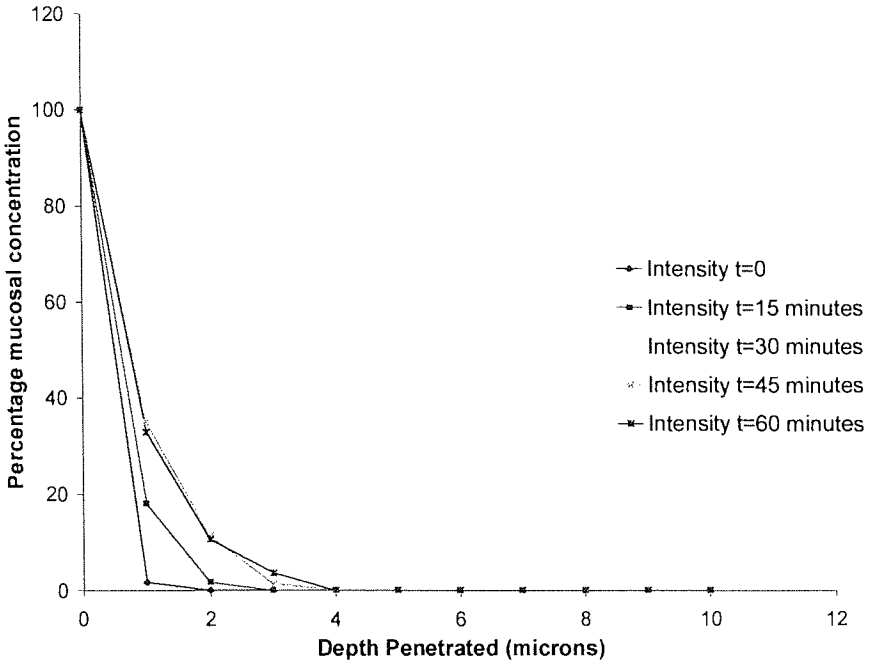


**Figure 5.30** Mean OD of confocal images expressed as a percentage of the surface level as a function of depth in excised viable rabbit nasal tissue. Data analysis was performed using the small-square method. Fluoresbrite® plain particles 200 nm nominal diameter.

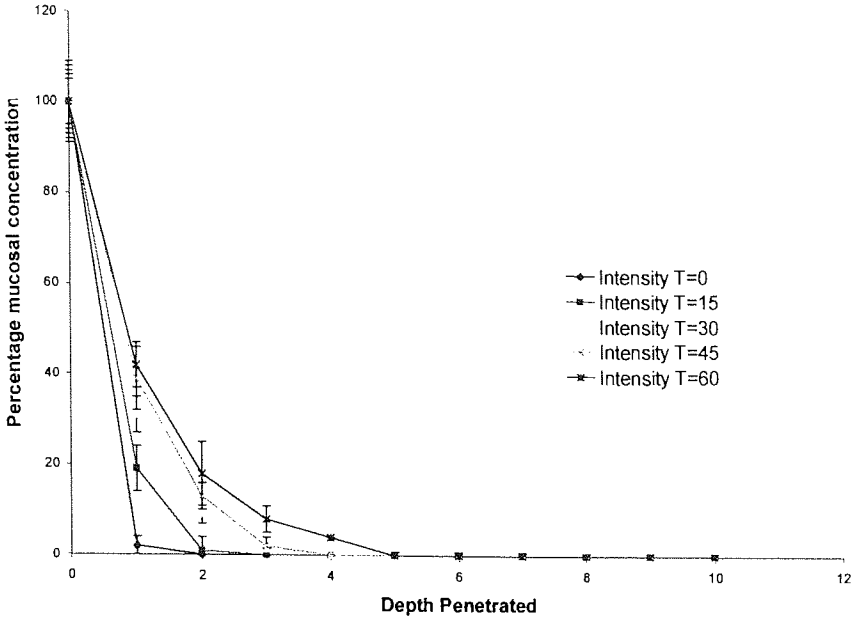


**Figure 5.31** Mean OD of confocal images expressed as a percentage of the surface level as a function of depth in excised viable rabbit nasal tissue. Data analysis was performed using the small-square method. Fluoresbrite® plain particles 100 nm nominal diameter.

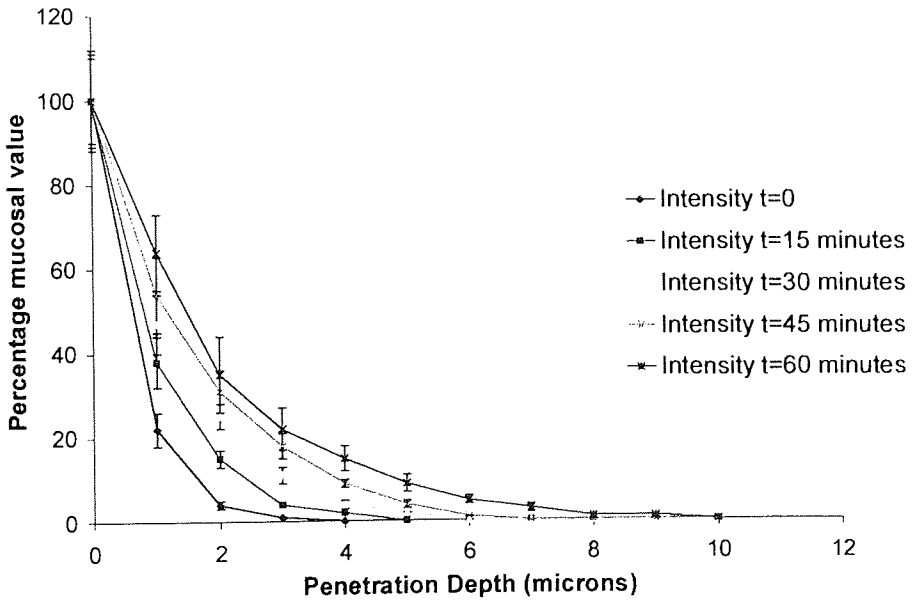


**Figure 5.32** Mean OD of confocal images expressed as a percentage of the surface level as a function of depth in excised viable rabbit nasal tissue. Data analysis was performed using the small-square method. Fluoresbrite® plain particles 50 nm nominal diameter.

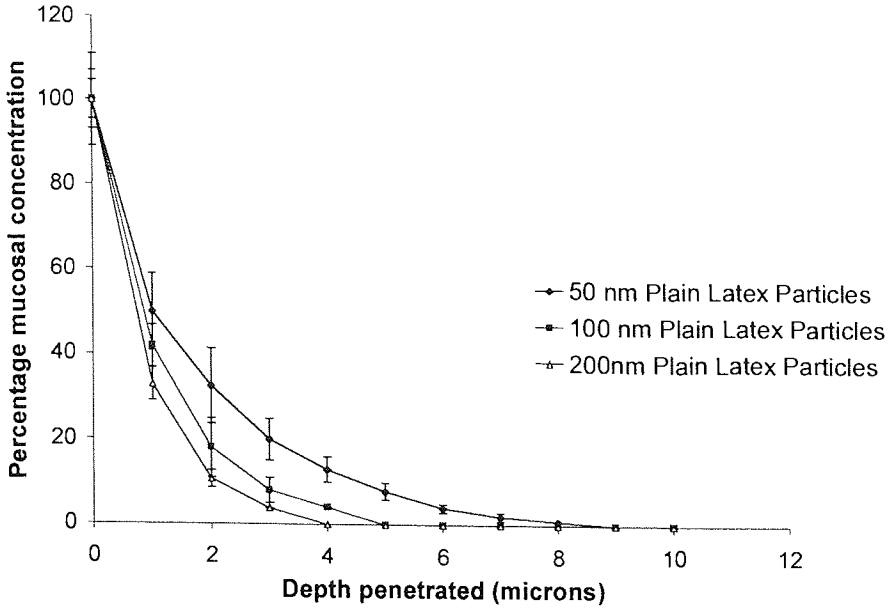


**Figure 5.33** Mean OD of confocal images expressed as a percentage of the surface level as a function of depth in excised viable rabbit nasal tissue. Comparison of T=60 data for 50 nm and 100 nm mean diameter Fluoresbrite® particles. Data analysis was performed using the small-square method.

From the fluorescence-depth plots (figures 5.30 to 5.32) it is possible to calculate the maximum depth of penetration for each particle type at each experimental time-point. This is shown in figure 5.34. The errors associated with this are that in determining the depth of penetration. There are two possible source of error, those in defining the tissue surface, and those is measuring the distance that the particles have been taken up into the tissue. The error due to the measurement of depth is easily quantifiable from the error inherent in the microscope operation, and that in between images. The accuracy to which the microscope table can be moved is quoted as ± 0.1 μm. Successive confocal layers are separated by 1 μm, the implicit assumption is that each image represents not an area, but the volume from 0.5 μm above the focal plane, to 0.5 μm below the focal plane. Since both these errors are errors in the same axis, and they are additive, the overall error due to the depth measurement can easily be quantified as a fixed error of ±0.6 μm. The error in defining the tissue surface is much harder to quantify. The error is almost certainly non-zero; however, there is no easy method of measuring this error. By inspection of all the available data, the error in defining the tissue surface would appear to be quite small as from n=3 experiments the overall error is small. Without accurate knowledge of this error, a fixed error of 0.6 μm is quoted for the maximum depth determination.

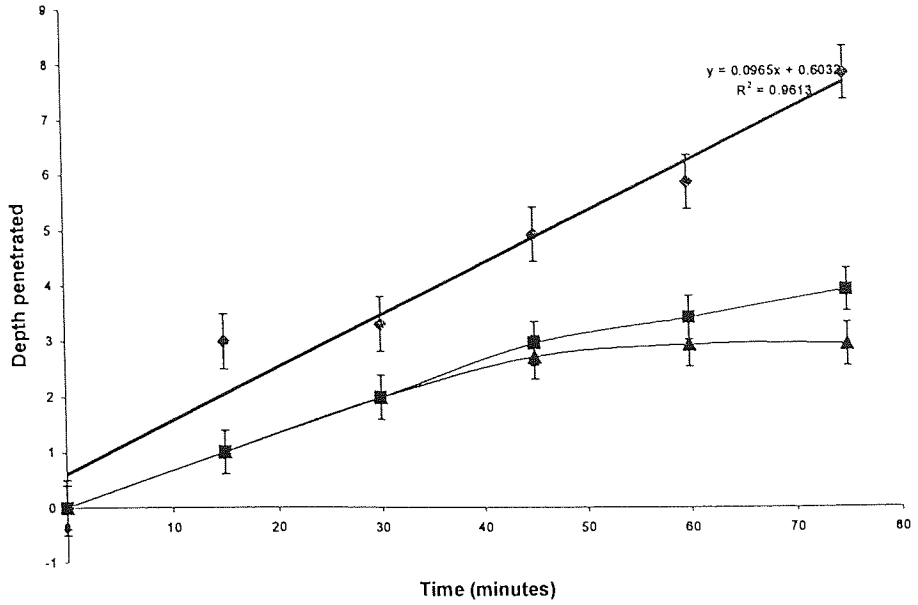


**Figure 5.34** Depth-Time profile for the maximum penetration of 200 (—▲—), 100 (—■—), and 50 (—●—) nm plain latex microspheres into viable rabbit nasal epithelium. A 1% surface OD was used as the cut-off value for determining maximum depth of penetration. For 50 nm particles linear regression analysis produces y = 0.0965x + 0.6032 with $R^2$ = 0.9613, approximately 1μm in 10 minutes.

Analysis of the depth–time profile (maximum depth) for the different size plain microspheres (figure 5.34) shows the rate of diffusion for the different particle sizes. The small (50 nm) particles giving a linear depth-time profile (y=0.0965x+0.6032 $R^2$ = 0.9613). The linear nature of the profile is indicative of a passive diffusional mechanism for uptake/penetration that follows Ficks' first law of diffusion (section 1.3.3.1). The larger particles would appear to have a more complicated uptake pattern, with an initial 30-45 minute linear period, after which their penetration rate is reduced.

From the available maximum depth and particle-size data (figure 5.36), it can be see that there is a non-linear relationship between particle size and maximum penetration depth. The non-linearity of this result would suggest that there is some more complicated mechanism occurring for the larger particles. The most obvious analysis of this result would suggest that there is a size cut-off between the 50 and 100 nm particles. However, this must remain a supposition until further results are available for a larger range of particle sizes. This analysis does not take into consideration any effects due to the difference in fluorescence of the different size particles, however, if the reservoir assumption is held true, this should take into account any major difference in fluorescence.

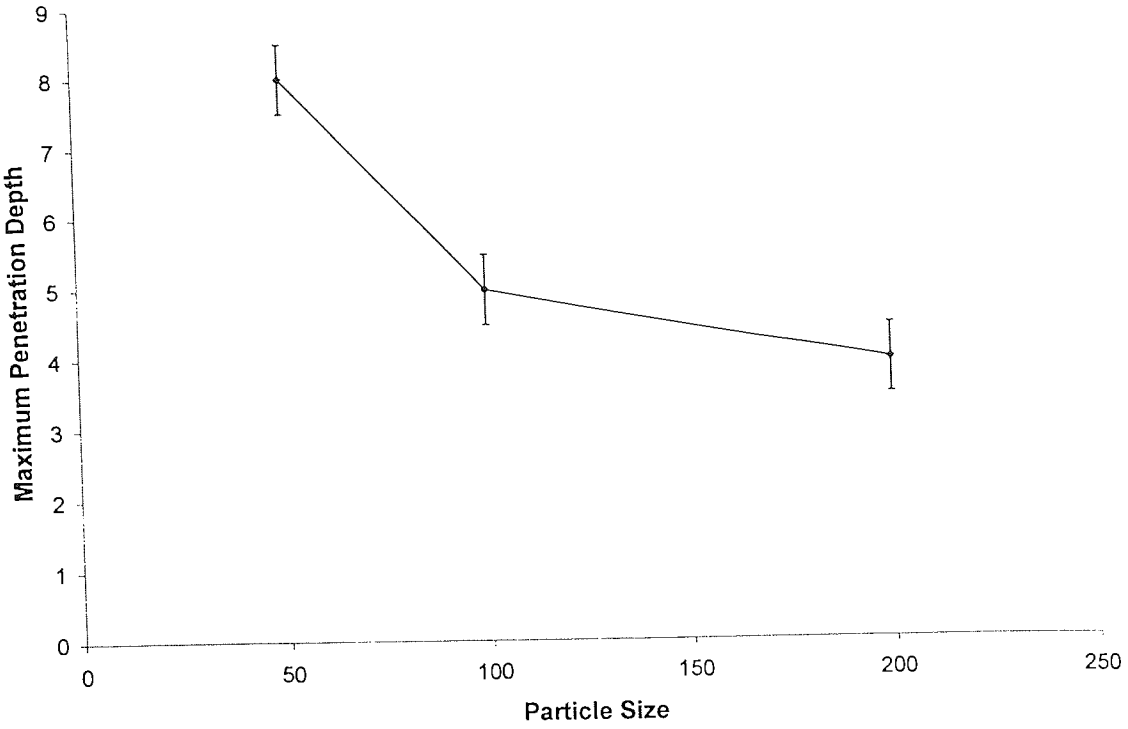


**Figure 5.35** Size-Depth plot for plain Fluoresbrite® latex particles penetration into rabbit nasal epithelium.

### 5.5.3 Effect of particle surface on uptake

Latex particles are only available in their carboxylated or plain form. As a result studying the effect of surface charge is difficult as there are only two surface conditions available. This is an obvious limitation on the experiments that were performed to investigate the relative uptake/penetration as a result of surface charge. The 50 nm plain particles (Figure 5.32) were compared with 50 nm carboxylated particles (Figure 5.36) that have a net negative charge. The differences after 60 minutes exposure is highlighted in Figure 5.37. The penetration of the carboxylated microspheres is significantly less ($P < 0.05$, comparison of the two points at each fixed depth) than that of the plain microspheres at depths below 1 μm.

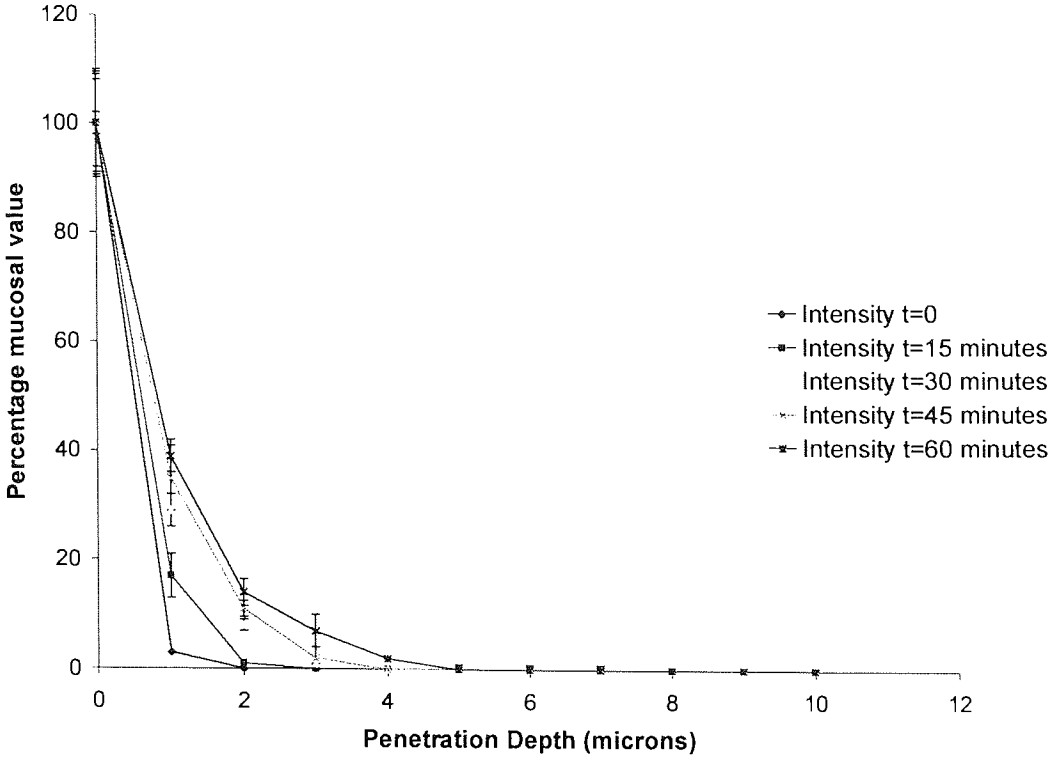


**Figure 5.36** Mean OD of confocal images expressed as a percentage of the surface level as a function of depth in excised viable rabbit nasal tissue. Data for 50 nm mean diameter carboxylated Fluoresbrite® particles. Data analysis was performed using the small-square method.

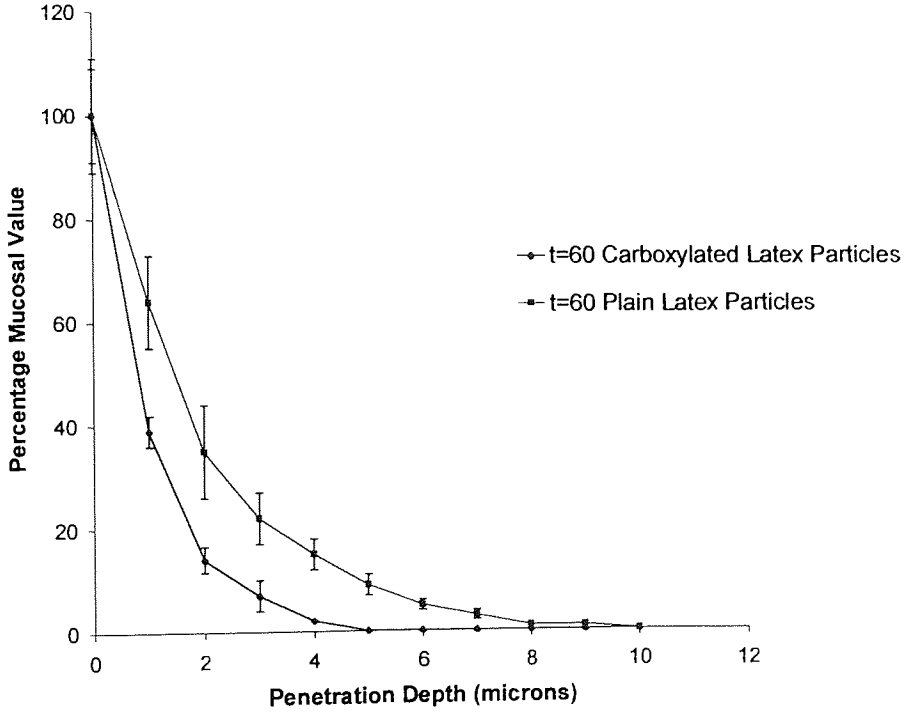


**Figure 5.37** Mean OD of confocal images expressed as a percentage of the surface level as a function of depth in excised viable rabbit nasal tissue. Comparison of T=60 data for 50 nm plain and carboxylated Fluoresbrite® particles. Data analysis was performed using the small-square method.

## 5.6 Histological investigation

Excised rabbit nasal mucosa was mounted in the complete nasal chamber. One hour after delivery of fluorescent latex particles, the tissue was removed and sectioned as a comparison to the confocal method. Unfortunately, due to the requirements imposed by the technique there was not sufficient nasal tissue available to perform histological examinations after 0, 15, 30, 45, 60 and 75 minutes, unless each experiment was performed only once.

### 5.6.1 Histology

After exposure in the nasal chamber tissue sections were removed for histological examination. The protocol of Allan (1992) was followed to stain the tissue samples. Samples were stained using heamotoxylin and eosin together with Alcian blue, a stain specific for mucus.

#### 5.6.1.1 Tissue sectioning

Tissue samples were sectioned at -20 °C using a Pierce cryostat to a thickness between 5 and 7 μm. Prior to manipulation tissue sections were flash frozen in liquid nitrogen, and the cryostat chuck was cooled to -70 °C in a long term storage freezer. The flash frozen tissue sections were attached to the cryostat chuck using OCT compound. OCT compound was applied to build up the area around the tissue and frozen using liquid nitrogen, and a cryospray as and when necessary. The tissue sample so encapsulated was then left in the cryostat for approximately 3 hours to equilibrate to the chamber temperature. After equilibration the chuck was mounted in the cryostat and tissue sections were obtained. Cutting produced a ribbon of sections. Single tissue sections were isolated and transferred to poly-Lysine coated microscope slides.

#### 5.6.1.2 Tissue staining

After sectioning tissue sections were stained using the protocol outlined in Table 5.1. This tissue staining protocol was developed to give both contrast in the cells sectioned,

and to stain the mucus that is present in each tissue section. Alcian blue stain (Sigma, UK) was used as a 1% w/v solution in $ddH_20$ adjusted to a pH of 2.5 with 1M HCl. Eosin and haematoxylin (Sigma, UK) were used as supplied.

After staining tissue samples were fixed using 10% glutaraldehyde in PBS for 30 minutes.

| | Stage |
|---|---|
| 1 | Sectioning |
| 2 | Transfer sections using $ddH_2O$ |
| 3 | Rapid Haematoxylin stain |
| 4 | Rinse in $ddH_2O$ |
| 5 | Increase haematoxylin colour using tap water |
| 6 | 1%Alcian Blue |
| 7 | Rinse in $ddH_20$ |
| 8 | Eosin stain |
| 9 | Rinse in $ddH_2O$ |
| 10 | Fixing |
| 11 | Dehydration |

**Table 5.1** Tissue sample preparation protocol.

Before mounting coverslips on the tissue section, tissue sections were dehydrated using an ascending ethanol series. Ethanol Concentrations of 25%, 50%, 75% and 100% were used for 10 minutes each. Slides were dried overnight before being mounted using DPX mounting solution.

### 5.6.4 Microscopy

Fixed, stained, and dehydrated tissue sections obtained after exposure to microparticles in the new chamber system were examined under a fluorescence microscope (Zeiss Axioscope. Zeiss Gmbh, Germany). A photographic record of combined fluorescent and light microscopy was made of all sections using a Nikon F3 camera, using Kodak Gold film (200ASA).

## 5.6.2 Results and discussion

Histological examination was performed on tissue after exposure to latex particles as previously described (5.5). Plain and carboxylated particles with a nominal size of 50 nm were investigated.

Examination of the resulting sections indicates that although great care was taken the sectioning results are not comparable to those obtained from the confocal technique. In all the sections it is not easy to identify internal structures within the tissue and, when there is significant fluorescence at the tissue surface, the location of the surface is difficult to determine. This is highlighted in figure 5.38. In the upper part of this figure the tissue surface is easy to identify, however, lower down it becomes almost impossible to determine with any accuracy the surface location. There is considerable uncertainty as to whether the large fluorescent area represents particles in the mucus, the epithelial layer, or an artifact of

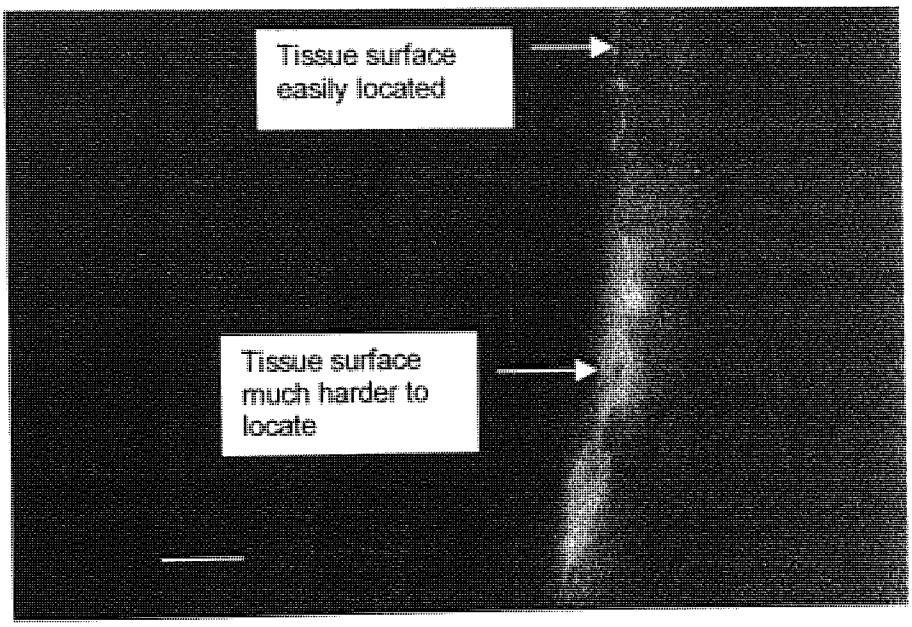


**Figure 5.38** Dual Fluorescent-white light microscopy of 5 µm section H-E-A stained rabbit nasal tissue after 60 minutes exposure to 50 nm carboxylated microspheres. Scale bar represents 100 µm

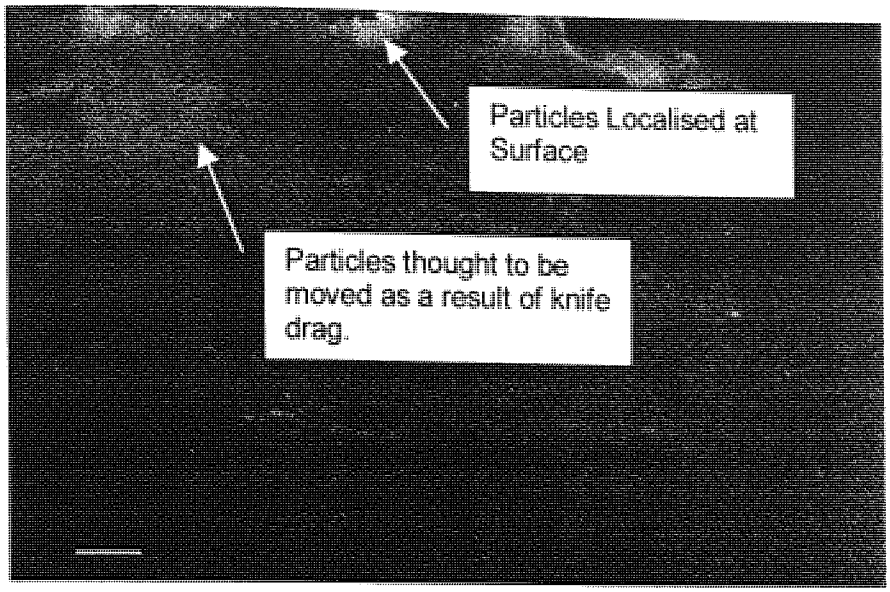


**Figure 5.39** Dual Fluorescent-white light microscopy of 5 μm section H-E-A stained rabbit nasal tissue after 60 minutes exposure to 50 nm plain microspheres. Scale bar represents 50 μm

sectioning the tissue. This area could not be investigated under greater magnification because the fluorescence levels of the particles embedded in the tissue proved to be too great. Figure 5.39 highlights another difficulty in interpreting data from sectioning work. Particles can be clearly seen at the surface, where they would appear to be localised, however, some distance below them there is another patch of fluorescence that is thought to be the result of knife-drag. If this micrograph is compared to the 50 nm plain microsphere uptake data from the confocal study where the maximum depth of penetration was measured as 9.0 ± 0.6 μm, whereas the fluorescence penetrates some 100-150 μm into the tissue using the sectioning technique.

From the photographs of the sections taken after delivery of the particles to the tissue, the difficulties in interpreting and relying on such data become instantly visible and the experiment must be performed by an expert regularly performing histological examinations. In comparison to the confocal data obtained, histological examination provides no method of gaining reliable quantitative data such as the depth-time profile previously obtained (Figure 5.34). This section has highlighted problems such as knife-drag that are experienced when performing histological examinations. The biggest disadvantage that this brief histological examination has shown is that the key element in obtaining good results is the skill of the operator.

## 5.7 General Discussion

The work in this chapter was performed with the overall aim of adapting the tissue viability chamber to the confocal microscope, producing a non- invasive technique that is able to monitor the fate of applied substances in epithelial tissues. The technique developed is also compared with the traditional histological investigation of the tissue. The most importantly the chamber was adapted to fit under the microscope; initial problems such as the chamber moving as the microscope table moved were overcome by the manufacture of the aluminium base, and the rotation of the chamber by 90° with respect to the layout of a traditional microscope slide. Parameters such as particle density (% w/w in the matrix), label used, particle size and loading were investigated, leading up to the delivery of suitable particles *in vitro* to excised tissue.

The problems that were encountered in the delivery to live epithelial tissue were somewhat harder to overcome. The simplest problem was the inability to focus down deep enough into the tissue (below the mucus, unstirred water layer and the cilia). This could have been overcome in two ways, the first was to wash off the mucus and have the epithelial cells at the surface under the coverslip. However, this method was rejected as it removed one of the key reasons for using the complete tissue model, having everything present from the apical mucus layer to the basal membrane. The second potential method was to simply use a smaller magnification objective lens, but to use the software controlling the detector and initial image processing to regain the lost magnification.

A more intractable problem was that of movement in the sample. The BioRad MRC 600 microscope is not one of the most advanced confocal systems available (The MRC 600 was available new from 1989 to 1991) and each scan taken per image layer takes several seconds, with each layer taking about half a minute. Fundamental properties of epithelial tissues such as mucocilliary clearance mean that if the tissue is alive there should be movement present. If the tissue is viable there should be detectable movement of the mucus and any fluorescent particles present at the surface move in one direction, and those lower down in the UWL move backwards and forwards making no net position change. This problem was overcome by examining and defining the surface 15 minutes after delivery of

the particles. This allowed the particles to reach the unstirred water layer and their backwards and forwards motion was visible. The microscope was then focused 2 μm below the lowest point of movement. The assumption taken at this point is that the backwards and forwards motion does actually represent the particles in the UWL and that once they enter the UWL they readily fall to the tissue surface. When using this technique there are several concerns, although the main one is that the surface of the tissue was not suitable defined. After considering the lack of available alternatives to the focusing below the lower limit of movement this was decided on as being the most practical solution.

This work then progressed beyond what has previously been done investigating the fate of applied microparticulates; suggesting that, due to the linear nature of the depth-time profile for the smallest particles, they are experiencing a passive diffusional penetration mechanism. These data also indicate that there is a non-linear relationship between particle size and penetration depth possibly indicates a size cut-off between the 50 and 100 nm particle sizes. The work of many groups including that of Alpar (Almaida and Alpar, 1996; Eyles *et al.* 1998a) Over many years has shown the effect of particle size and surface charge on physiological responses to microparticulates. This work has taken the physiological and histochemical work previously performed and progressed it producing a system which can provide basic kinetic data describing the penetration of these particulate systems into viable tissue.

The work reported here represents the beginning of an interesting field of research. This work proves that the confocal microscope can be used in conjunction with a horizontal tissue viability chamber and give accurate data not only about the penetration or uptake of particles, but also about their uptake/penetration mechanisms. These are all data that would be very difficult to obtain by the traditional histological techniques described in section 5.6.1.

# Chapter 6

## An *in vitro* investigation of the effects of potential vaccine formulations developed for mucosal delivery on excised tissues from the mucosal immune system

### Overview

*Ex vivo* models for vaccine development studies are a relatively novel area of investigation as the majority of formulation efficacy models involve *in vivo* measurements of classically assayed markers such as blood IgG levels. Investigation of the effect of candidate vaccine formulations on excised tissue has been made feasible by the development of the *ex vivo* tissue viability system (chapters 3 and 4).

The secreted protein response to microspheric delivery systems designed for mucosal antigen delivery was investigated both in this system, using viable excised rat Peyer's patches, and *in vivo*. The model vaccine formulations investigated included BSA, and Diphtheria Toxoid (DT) encapsulated in 100kDa PLA microspheres. A number of novel proteins were detected but SDS-PAGE, 2D electrophoresis, Western blotting, and proteomics have not identified them at this stage.

## 6.1 Introduction

In the previous chapter, the nasal chamber was adapted for use with a confocal microscope as a non-invasive method for investigating the fate of microparticulate matter applied to the tissue surface. In the case of particulate formulations that either encapsulate or are coated with antigenic material, their effect on the tissue is of great interest. Currently, vaccine formulations are investigated almost exclusively *in vivo*. The reason for this is that the immune system is highly complicated and there is currently no *in vitro* technique suitable for screening vaccine formulations.

### 6.1.1 The mucosal immune system

Over the past few years it has been successfully shown that application of suitable vaccine formulations to mucosal tissues that are regularly exposed to challenges *in vivo* generates local immunity and also significant systemic immunity (Williamson *et al.*, 1996; Eyles *et al.*, 1998; Eyles *et al.*, 2000). These regularly exposed mucosal tissues include the nasal, the bronchial, and the GIT epithelial tissues. The most important feature of these immunogenic structures is that challenge and successful generation of an immune response results in not just a systemic and local response, but a response at all the other mucosal sites, although not all of these express a response of the same magnitude (Kiyono *et al*, 1992). As such, these mucosal tissues are all classed as part of the common mucosal immune system (Almeida and Alpar,1996 ). This mucosal system is otherwise known as the mucosal-associated lymphoid tissue (MALT). Specifically, these tissues are the bronchus-associated lymphoid tissue (BALT), gut-associated lymphoid tissue (GALT), and the nasal-associated lymphoid tissue (NALT). Recent work on transdermal vaccination using delivery devices such as the BioRad Gene-Gun™, and the PowderJect™ transdermal delivery device has also suggested that the skin itself might be part of the MALT, or interact with it in some way (McCrossin, 1999).

## 6.1.2 Immune induction and effector sites

At the most basic level, the common mucosal immune system can be considered as several compartments. Tissues such as the MALT can be considered as the immune induction sites, this is where the body actually experiences the challenge and the initial response is mounted; and tissues such as the *Lamina Propria* (LP) can be seen as the immune effector sites. Immune effector sites are much larger areas of tissue where the immune system generates IgA antibodies. Since the mucosal tissues secrete this IgA, the IgA is classified as s-IgA (Secretory IgA). Figure 6.1 shows the induction and effector sites after oral immunisation, with the subsequent generation of a protective immune response by the MALT. Of all the immune induction sites the NALT and GALT are the most easily obtained immunological tissues. Of all the tissues in the MALT system perhaps the most well known is the GALT. The GALT tissue is mostly made up of the intestinal Peyer's patches.

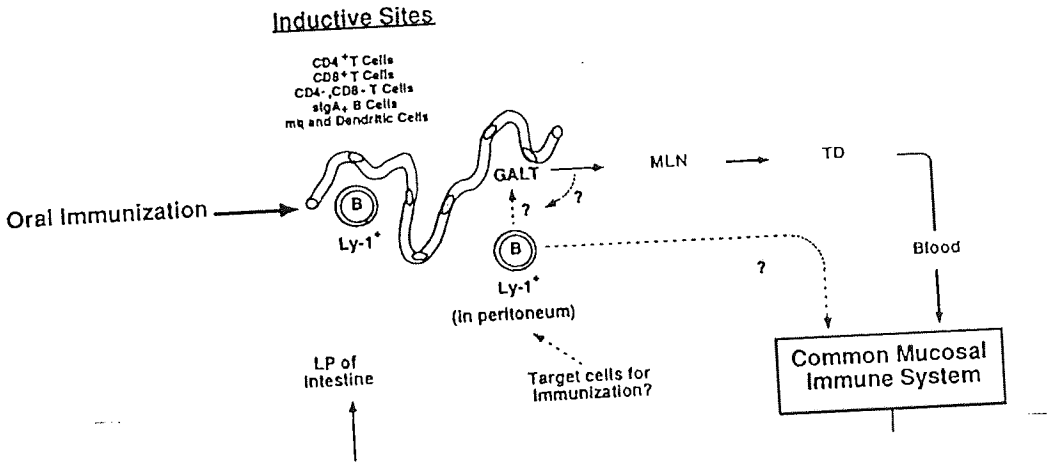


**Figure 6.1** The common mucosal immune system for mucosal vaccines. The priming of antigen specific IgA committed B cells in the classical IgA inductive sites (in this case the GALT) and alternative target B cells ($LY\text{-}1^+$ B cells) for the induction of IgA responses at mucosal effector tissues. LG: lacrimonal gland; LP: lamina propria; MG: mammary gland; MLN: mesenteric lymph node; SG: salivary gland; TD: thoracic duct. From Kiyono *et al.*, (1992)

### 6.1.3 Cytokines and chemokines as immune messengers

For the immune system to operate in the way described with induction and effector sites, effective communication between these different tissues becomes paramount. Cytokines are immune-system proteins that are biological response modifiers, co-ordinating antibody, T cell, and other immune system interactions. They are used to amplify immune reactivity, acting as promoters for various parts of the immune system. They do not have specific effects on one type of target cell, with most cytokines having a wide variety of biological effects, acting on a number of different cell and tissue types. Over the 30 or so years of cytokine research, various cytokines have been discovered. There are currently 17 interleukins (a cytokine sub-class), and numerous other chemokines and other cytokines. Often their name is of little use in finding their true purpose, for example tumour necrosis factor $\alpha$ (TNF-$\alpha$) is more correctly an immuno-modulator or pro-inflammatory cytokine.

By definition (Cruse and Lewis, 1999), cytokines are immune system proteins that are biological response modifiers. This covers a variety of different classes of compounds, including monokines, lymphokines, and cytokines. Monokines are chemical messengers produced by monocytes, lymphokines are produced by activated T lymphocytes and natural killer cells (NK cells). Chemokines are different in that they are chemokinetic and chemotactic, stimulating and directing leukocyte movement. However, as well as being [illegible]okines can be classified by the receptors they bind to. The most important feature of all the cytokines is that their effects are pleiotropic and redundant, and no cytokine acts on one cell type alone.

### 6.1.4 Inflammation as an immune response to formulations

One common side-effect found in the development of vaccine formulations is inflammation. The process leading up to inflammation is complicated, although reasonably well understood. Any number of factors, either endogenous or exogenous that cause tissue damage, can initiate inflammation. The inflammation response is mounted quickly, usually within minutes of the initial attack. The first stage of the inflammation is the induction or

increase in the concentration of the acute-phase proteins. In the case of inflammation caused by a micro-organism, the most important of the induced proteins is the C-reactive protein, a protein that binds to the micro-organism and causes activation of the compliment system, with the end result of the micro-organism being lysed or phagocytosed.

The second system that is activated upon damage to the tissue is the Kinin system, however the Kinin system is more concerned with mechanical damage, and using such chemotactic markers as clotting factor XII (the Hageman factor) which is part of the clotting cascade.

Cytokines also play a major role in the regulation of the inflammatory response. The three most important cytokines involved are interleukin 1 (IL-1), IL-6, and TNF-α. Also involved, but to a lesser extent, are IL-8 and Interferon γ. IL-1 exists as two forms IL-1-α and -β. IL-1-α exists as a cell surface associated cytokine, whereas IL1 β exists as the free form in plasma. IL-1, IL-6, and TNF-α are released by activated macrophages; their purpose is to induce adhesion molecules on the surface of endothelial cells to which neutrophils, monocytes and lymphocytes adhere before undergoing extravasation to the affected tissue. Extravasation is where the bound neutrophil, monocyte, or lymphocyte is transported across the endothelium to the challenged tissue. All of the chemotactic markers act together to enhance the chemotaxis of leukocytes and increasing phagocytosis.

### 6.1.5 Potential cytokines for vaccine screening

In this study, 5 cytokines were chosen partly for their usefulness in a vaccine screen, but also taking into account availability of suitable antibodies for their easy detection. The five chosen cytokines are IL-1-β, TNF-α, Interferon-γ, MCP-1, and MIP-1α.

As previously described, IL-1-β is the free form of IL-1 (whereas IL-1-α is the surface-bound form) which is a potent immuno-modulator, mediating a wide range of immune and inflammatory responses; these include the activation of B and T cells. Rat IL-1-β is a 17.3 kDa protein containing 152 amino-acid residues.

TNF-α is technically a lymphoid factor; it has cytotoxic effects on tumour and other cells, but is also like IL-1-β a potent immuno-modulator, and a pro-inflammatory cytokine. Rat TNF-α is a 17kDa protein containing 157 amino-acid residues.

Interferon γ (IFN-γ), like TNF-α, is a lymphoid factor. It possesses significant anti-viral activity, but it also stimulates macrophage and NK cells. Rat IFN-γ is a 15.6 kDa protein containing 135 amino-acid residues.

Macrophage / monocyte chemo-attractant protein-1 (MCP-1) is a major cytokine in the inflammatory response of blood monocytes and tissue macrophages. Rat MCP-1 is a 14 kDa protein containing 125 amino-acid residues.

Macrophage inflammatory protein-1 (MIP-1) like MCP-1 is a major cytokine in the inflammatory response of blood monocytes and tissue macrophages. Rat MCP-1 is an 8.0 kDa protein containing 69 amino-acid residues.

The poor commercial availability of rat cytokines and their antibodies limited this choice of cytokines. However, from those described above, the key areas of inflammation and a protective response are covered.

### 6.1.6 Aims in tissue viability chamber used as a vaccine screen

Mucosal delivery of vaccine formulations has proved to be an effective method of inducing immunity. Good immunity has been conferred, nasally, orally and by using the intra-tracheal route of administration (Almeida and Alpar, 1996). However, for research to continue and newer, more effective, mucosal vaccine delivery systems to be developed some method of screening adjuvants and potential delivery systems *in vitro* is required. Such a screen ought to be able to distinguish between an adjuvant or delivery system that will cause an inflammatory response, no response, and one that starts the process that will successfully induce an effective immune response.

Of special interest in developing mucosal vaccines are the NALT and GALT; both exist in tissues that can be readily acquired. The GALT, for example, consists of the Peyer's patches found in intestinal areas such as the ileum. These can easily be seen and dissected out. The tissue viability chamber previously described has been shown to keep both nasal and gut epithelia alive. At this point, it must be assumed that after administration of an antigenic substance, there must be some form of chemical messenger system that "talks" to both the other sites in the MALT and the immune effector sites. This assumption *per se* is legitimate since cytokines and chemokines would be expected to be produced in response to any challenge. Mounting tissue in the novel chamber system, identifying and monitoring the release of any chemotactic markers would represent the first stage in investigating the MALT on a molecular level. Nasal tissue has proved hard to obtain in any regular, predictable, manner and, with tissue such as rat Peyer's patches being readily available in almost every laboratory world-wide, GALT tissue represents an ideal starting point to model *in vitro* the initial response to vaccine formulations. If, after this initial work, this proves to be an effective method of investigating the effect of formulations on the MALT then the work can be easily repeated using NALT tissue as and when tissue supply permits.

The aim of this work is to assess the effect of several vaccine formulations and controls on excised viable immune induction sites, to observe and identify any secretions due to the formulations applied, and then to develop a method of screening potential formulations. To do this, the cytokines in the previous section were selected, representing both inflammatory and protective responses to the formulation, and after separation of any secreted proteins immunoblotting techniques will be used to identify the presence of any of these cytokines.

## 6.2 Materials and methods

For the work presented in this chapter, all the materials and equipment used, unless otherwise stated, were from BioRad Laboratories Ltd (Hemel Hempstead, UK), and of

suitable electrophoresis grade. All antibodies used were obtained from Peprotech EC Ltd (London, UK). Krebb's Ringer and phosphate-buffered saline (PBS) tablets were obtained from Sigma (Poole, UK). TBS buffer (1.21 g $L^{-1}$ Tris base, 8.5 g $L^{-1}$ sodium chloride, pH 7.4), TBS-Tween (1.21 g $L^{-1}$ Tris base, 8.5 g $L^{-1}$ sodium chloride, 3.0 mL $L^{-1}$ Tween 20, pH 7.4) and Western blotting transfer buffer (15 g $L^{-1}$ Tris base, 72 g $L^{-1}$ glycine in 25% methanol) prepared weekly and stored at +4°C. SDS PAGE running buffer was prepared as a 5x stock (15.1 g $L^{-1}$ Tris Base, 94 g $L^{-1}$ glycine, 50 mL $L^{-1}$ 10% SDS) and diluted as necessary. Pre-stained molecular weight markers were obtained from NEN Biolabs (Cambridge, UK), and silver stain molecular weight markers were obtained from BioRad Laboratories Ltd.

### 6.2.1 Chamber operation

The chamber system was operated as previously describe in chapter 3. Rat ileal Peyer's patches were excised immediately after sacrifice of a male Wistar rat (250 – 350g). The dissection method used was that outlined in section 3.2.3.1, except that the ileal area chosen for mounting in the chamber was carefully chosen to include a Peyer's patch. The Peyer's patches were instantly visible, and it proved very easy to mount the Peyer's patches in the novel tissue chamber.

After mounting the tissue in the chamber, the underlying reservoir was filled with glucose Krebb's Ringer buffer as previously described, 1 mg samples of the formulation under test were suspended in 30 µl glucose Krebb's Ringer, and applied to the mucosal tissue surface. As with all other gut tissue experiments, the mucosal side of the tissue was then covered with a 15 mm diameter glass coverslip. The tissue was left for 6 h, and at the end of the exposure period the serosal buffer solution was filtered through a 2.0 µm filter and freeze-dried overnight. (Virtis AdVantage). After lyophilisation, each sample was re-dissolved in 100 µL double distilled water, and analysed for protein content by BCA assay. Each tissue section was used for one 6-h experiment.

### 6.2.2 Vaccine formulations

For this study, two formulations from the laboratory of Dr H.O. Alpar (Aston University, Birmingham, UK) were used. The two formulations used were based on a 100 kDa PLA microsphere system either loaded with BSA (Dr I.D. Spiers, formulation AP9) or an effective oral formulation loaded with Diphtheria Toxoid (S. Somavarapu, formulation SomaDTOral)

### 6.2.3 SDS PAGE electrophoresis

SDS PAGE electrophoresis was performed on a mini-Protean electrophoresis apparatus using BioRad Ltd pre-cast 8 – 16% gradient Tris-HCl SDS PAGE gels with a 4% loading gel, and 10 x 30 µl loading wells. Before loading onto the gel the samples were mixed with an equal volume of sample loading buffer and then de-natured by heating to 95° C for 3 mins. 20 µl samples were run at 100 V for 40 mins in SDS PAGE running buffer.

Gels that were to be silver stained were loaded in one lane with BioRad silver stain molecular weight markers covering 14.4 to 97 kDa. For gels that were subsequently immuno-blotted pre-stained molecular weight markers covering the range 6.5-175 kDa were used (New England Biolabs, MA, USA). Since pre-staining changes the molecular weight at which the markers appear on the gel, the weights quoted are manufacturers' apparent molecular weights.

### 6.2.4 Silver staining

To visualise proteins after SDS-PAGE, the BioRad Silver Stain Plus visualisation kit was used. This is a four-stage process, involving fixing, rinsing, developing and finally stopping. The kit was used in accordance with the manufacturer's instructions.

### 6.2.5 Two-dimension electrophoresis

Two dimensional (2D) gel electrophoresis was performed using the BioRad mini 2D cell system. In this system, a capillary iso-electric focusing experiment is performed, and then the resulting gel is removed from the capillary and placed into the gel for the second (molecular weight) dimension. The overall result being iso-electric point in one dimension (horizontal) and molecular weight in the second (vertical) dimension as shown in figure 6.2

The first (IEF) dimension was performed on 10 µl sample (diluted to 400 µg / mL, 4 µg *per* sample) on a home cast gel according to the manufacturers recommended method. The gel was run on a stepped voltage programme, 500 V for 10 mins, followed by 750 V for 6 h. Upon completion of the IEF, the capillary gel was removed from the glass capillary and placed in the well of a BioRad pre-cast 8-16% Tris-HCl ready gel with 1 single 450 µl well. The second (MWt) dimension was then run as standard SDS PAGE.

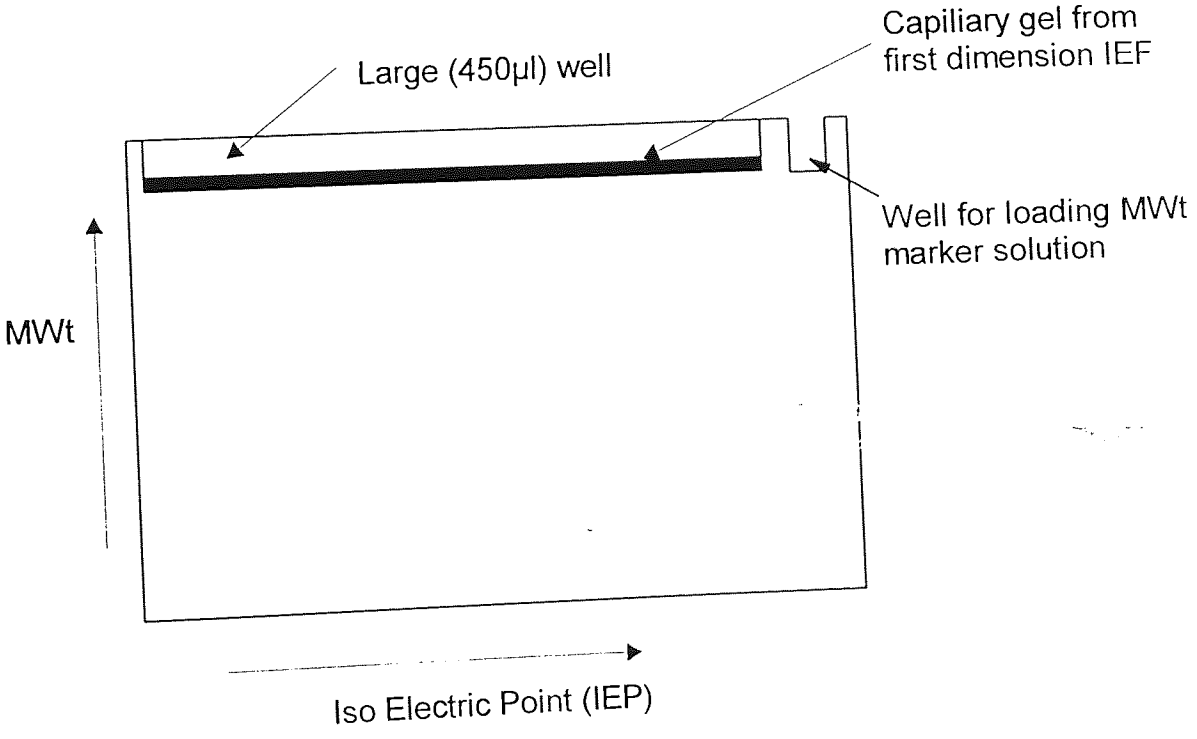


**Figure 6.2** Diagrammatic representation of 2D gel electrophoresis

### 6.2.6 Optimising and running Western blots

Immunoblotting was carried out in an effort to determine the composition of the protein bands seen in the initial vaccine screen experiment. Immunoblotting was performed on both single-dimension (MWt) and 2D gels. In both cases the technique used was identical. After running the separating gel, the proteins were blotted onto a nitro-cellulose membrane (0.45 µm pore size) using a BioRad mini trans-blot electrophoresis system. The transfer system was set up as shown in figure 6.3.

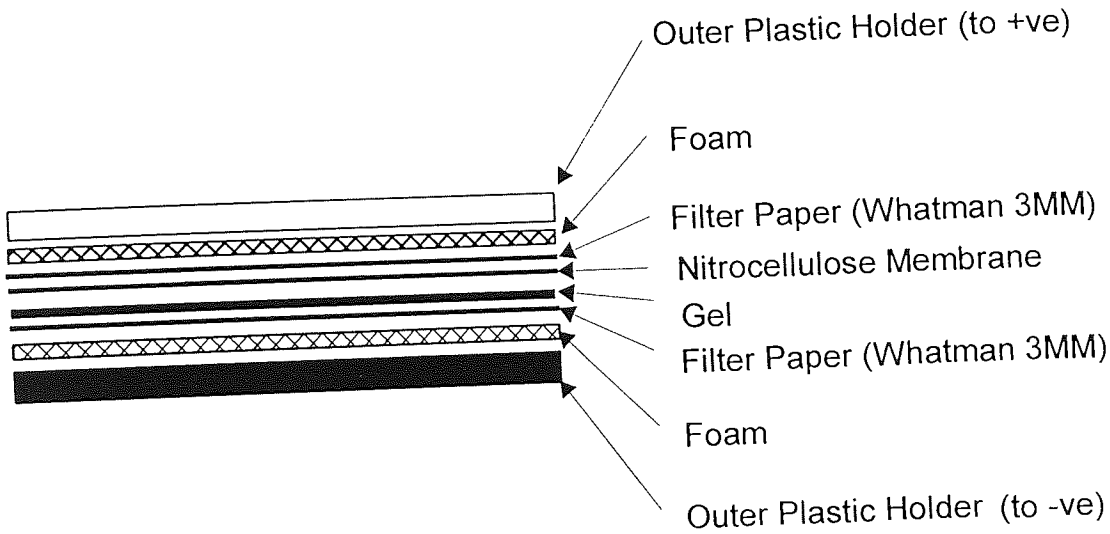


**Figure 6.3** Western blotting set-up.

Proteins were transferred from the gel to the nitro-cellulose membrane by blotting for 1 h at 100 V in transfer buffer. The transfer buffer was maintained below room temperature by using the frozen water-cooling block supplied with the apparatus.

After transfer of the proteins, the nitro-cellulose membrane was blocked using a 3% solution of bovine serum albumin (BSA) in TBS for 1 h. The blocking solution was washed with 3 five-minute washes of 10mL TBS-Tween. After washing, the primary antibody was applied in TBS for 1 h. The nitro-cellulose membrane was then washed as before in TBS-Tween. The secondary antibody was then applied in TBS for one h, and after this the membrane was again washed in TBS-Tween as before. The blot was then visualised using 3 DAB (3,3' diaminobenzidine tetrahydrochloride) Sigma Fast™ tablets in 36 mL PBS and

36 µl hydrogen peroxide. The visualising solution was left on the nitro-cellulose membrane for 30 mins. In all blots from single-dimension electrophoresis, 200 ng of the correct positive control (rat IL-1-β for western blots using the anti rat IL-1-β antibody) was also run on the gel.

Initial Western blots were run at primary and secondary antibody dilutions of 1:500. In all the Western blots performed a 1:500 dilution of secondary antibody proved more than adequate. Primary antibody dilutions of 1:500 were used for TNF-α, IL-1-β, IFN-γ, and dilutions of 1:250 were found to be necessary for MIP1α and MCP1.

### 6.2.7 *In vivo* vaccine delivery protocol

Experimental groups of 2 male Wistar rats (250-300g) were starved overnight prior to experimentation. Formulations previously described (6.2.2) were administered by gavage after dispersion (100 mg/mL) in PBS. In all cases 1 mL of formulation or control was administered. Blood was obtained from the tail vein of each animal prior to and, 2 and 4 h after dosing. The experiment was terminated after 6 h when the animals were exsanguinated under terminal anaesthesia, as large a volume of blood was collected as possible by cardiac puncture. The protocol of Eyles *et al.* (1997) was followed for the collection of plasma. All blood samples were collected in non-heparinised tubes, and allowed to clot overnight at 4°C. Plasma was then collected after centrifugation of the clotted whole blood samples at 10,000 rpm for 10 mins. Plasma samples were stored for analysis at –20°C.

## 6.3 *Ex-vivo* exposure of rat Peyer's patches to formulations

After exposure of the tissue to the formulation, the serosal solution was lyophilised and the protein content analysed by using the BCA assay. The total secreted protein is shown in table 6.1. No viability measurement were taken on the tissue after exposure for this time period, since of prime importance in this experiment was the induction of any response, rather than the effect on the tissue viability *per se*.

| Formulation | Mean secreted protein (mg) | SD |
|---|---|---|
| Control | 0.82 | 0.12 |
| BSA Loaded | 0.93 | 0.23 |
| DT-loaded | 1.12 | 0.19 |

**Table 6.1** Serosal secreted protein (mg) from rat Peyer's patch after exposure in the novel tissue viability chamber. Mean and SD are from 3 determinations of each of 2 experimental samples

### 6.3.1 SDS PAGE analysis of secreted proteins

After lyophilisation, rehydration and assay of the secreted protein the resulting solution was diluted to 100 µg $mL^{-1}$. 10 µl samples of this were analysed by SDS PAGE (figure 6.4). From this gel we can see significant differences between the control (no formulation applied), the working Diphtheria toxoid formulation and the BSA loaded microspheres. The most important difference from the point of view of developing the chambers as a technique for vaccine formulation development is the appearance of several bands of very low molecular weight. These bands proved to be reproducible when the experiment was repeated and the results analysed.

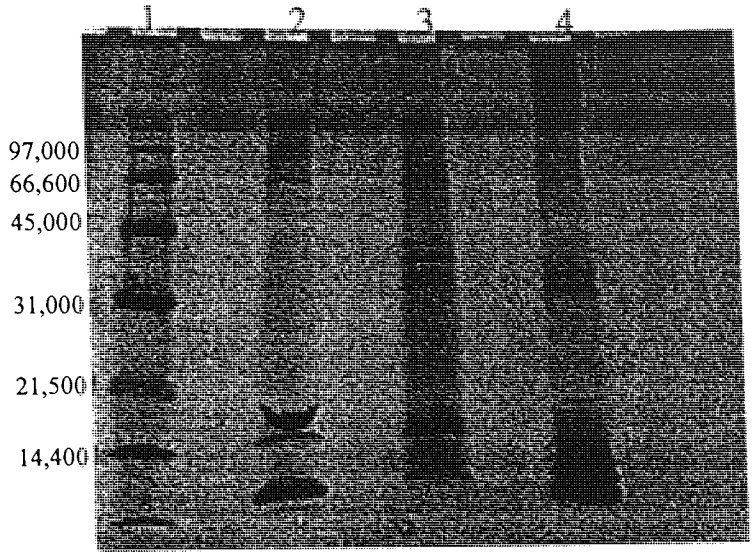


1. Marker Lane
2. Control, 6hr no particles
3. AP9 (IDS 100K, BSA loaded)
4. Soma (100K DT working Vaccine - Oral)

**Figure 6.4** SDS PAGE (8-16%) analysis of secreted protein from vaccine screen trial. (MWt in Da)

From this initial experiment there are obvious differences in composition of the serosal fluid. There are two possible explanations for this, firstly that that this is a genuine result due to the formulations applied, and secondly that this is an artefact of the particles delivered, for example release of antigenic, or control material.

To assess the second of these two alternatives, a release experiment into glucose-Krebb's Ringer buffer was performed. Each sample (20 mg) was suspended in 200 µl buffer. After 30 mins, 1 h, 2 h and 6 h, the suspension was pulsed in a bench top centrifuge and 20 µl of the supernatant solution withdrawn for analysis by SDS-PAGE. All samples were frozen immediately after collection. From the results (figure 6.5), it can be seen that, for the Diphtheria toxoid formulation, although the gel has significant background staining, there was no protein detected below 60 kDa. The large numbers of bands that had appeared in the tissue experiment did not appear in the release experiment performed.

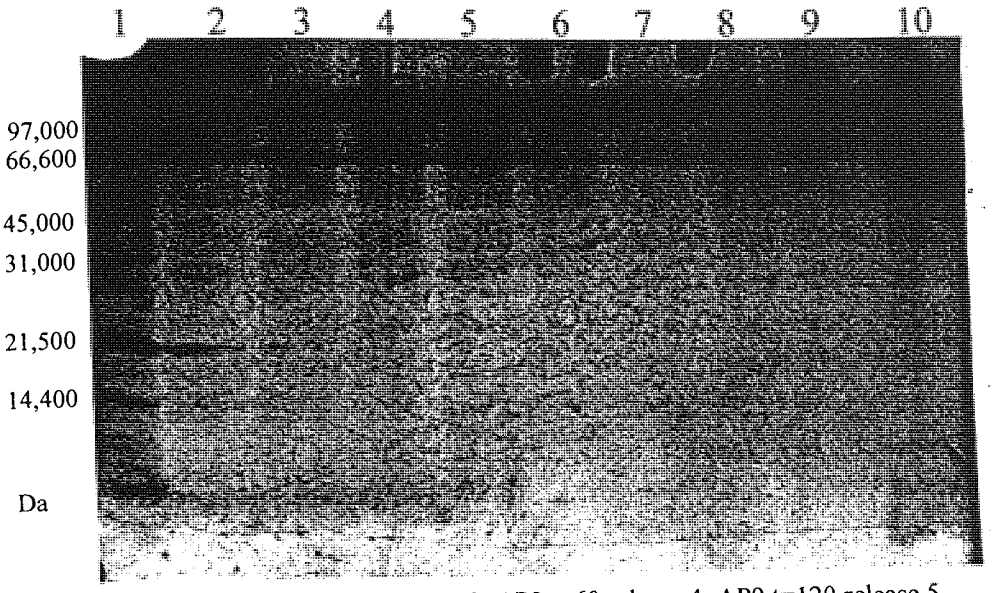


1. Marker Lane. 2 AP9 t=30 release. 3. AP9 t=60 release 4. AP9 t=120 release 5. AP9 t=6 hours release 6 Soma t=30 release. 7. Soma t=60 release 8. Soma t=120 release 9. Soma t=6 h release 10. DT

**Figure 6.5** BSA and DT release (6H) from 100K PLA microspheres.

### 6.3.2 Western blotting of *in vitro* secreted proteins

The reconstituted serosal fluid from the three tissue experiments was blotted. From the five blots (figures 6.6 to 6.10), it becomes immediately apparent that little has reacted with the primary antibody. It should be remembered that the primary antibody in each case was a polyclonal antibody. For the definite identification of a protein band using the polyclonal antibody, it is important that any band seen after blotting is at the same molecular weight as the positive control band. From the five Western blots, no bands can be confirmed as being a positive reaction to the antibodies used simply because those bands seen are of the wrong molecular weight. There remains the possibility that, as the bands seen are of much larger molecular weight, they are multimers of the target cytokine, however, without the target monomer being seen this is an unlikely proposition. With none of the cytokine antibodies identifying their target proteins identifying the bands becomes more difficult. The antibodies used were chosen partly by their function, but equally as they are anti-rat antibodies we were significantly limited in our antibody choice. At this point before acquiring or producing *in vivo* further antibodies more information about the protein

bands seen in the initial gel is required. The most useful piece of information required at this point is the isoelectric point (IEP) of each protein, since each proteins molecular weight and IEP are almost unique. The isoelectric point is the pH at which the number of negative and positive charges are equal giving the protein no net charge.

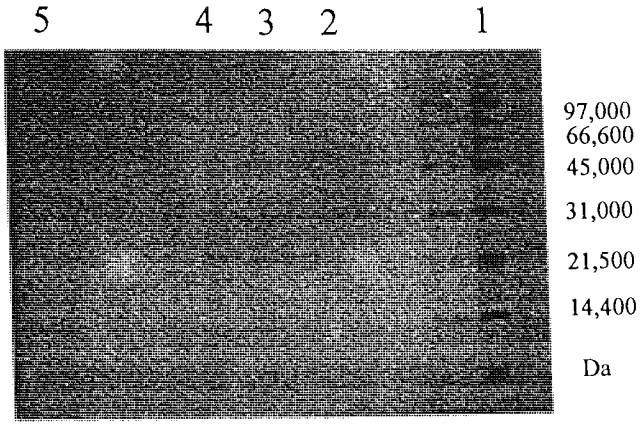


**Figure 6.6** Western blot for IFN-γ. Serosal fluid 6 h after administration. Lane 1, weight marker; lane 2, Control sample; lane 3, BSA loaded microspheres; lane 4 DT-loaded microspheres; lane 5, positive control.

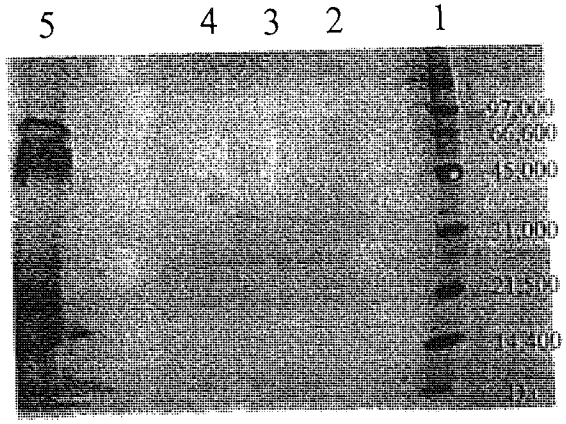


**Figure 6.7** Wester Blot for Il-1-βõ Serosal fluid 6 h after administration. Lane 1, weight marker; lane 2, Control sample; lane 3, BSA loaded microspheres; lane 4 DT-loaded microspheres; lane 5, positive control.

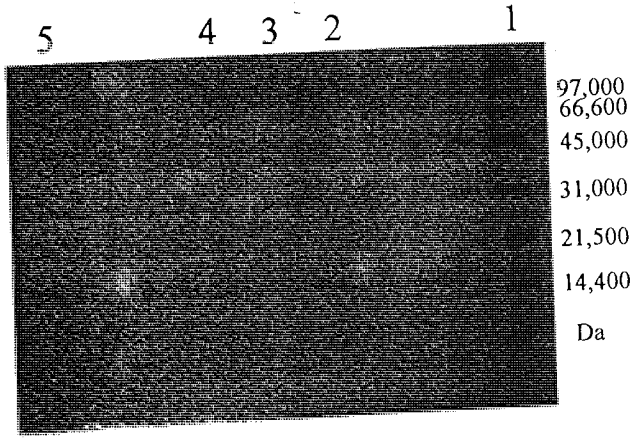


**Figure 6.8** Wester blot for MCP 1 Serosal fluid 6 h after administration. Lane 1, weight marker; lane 2, Control sample; lane 3, BSA loaded microspheres; lane 4 DT-loaded microspheres; lane 5, positive control.

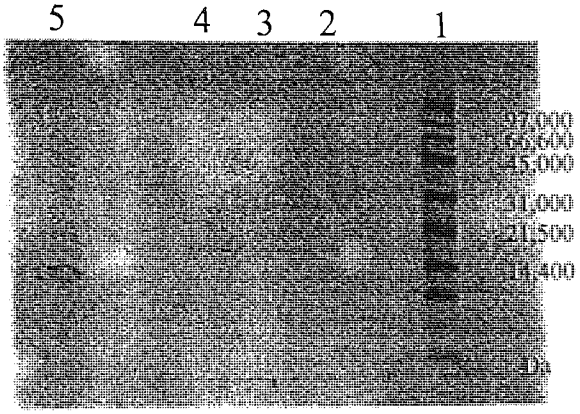


**Figure 6.9** MIP 1α Serosal fluid 6 h afteradministration. Lane 1, weight marker; lane 2, Control sample; lane 3, BSA loaded microspheres; lane 4 DT-loaded microspheres; lane 5, positive control.

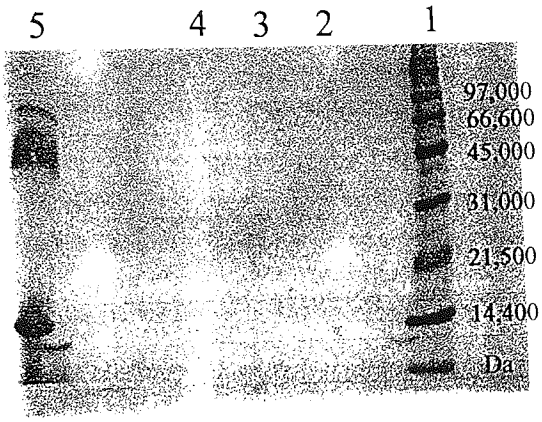


**Figure 6.10** Western Blot for TNFα Serosal fluid 6 h after administration. Lane 1, weight marker; lane 2, Control sample; lane 3, BSA loaded microspheres; lane 4 DT-loaded microspheres; lane 5, positive control.

### 6.3.3 Two-dimensional electrophoresis of secreted proteins

With the failure of the Western blotting to identify the protein bands seen, 2D electrophoresis was performed to give extra information about each of the unknown protein bands. The results of the 2D electrophoresis (figure 6.11) show that there is a series of proteins between pI =3 and 6.5. Literature searching for rat proteins matching the molecular weights of those seen in figure 6.11 yielded no positive identification for any of the spots. With these observations, the chamber work was then repeated as a limited *in vivo* study to investigate whether these proteins could be identified *in vivo.*

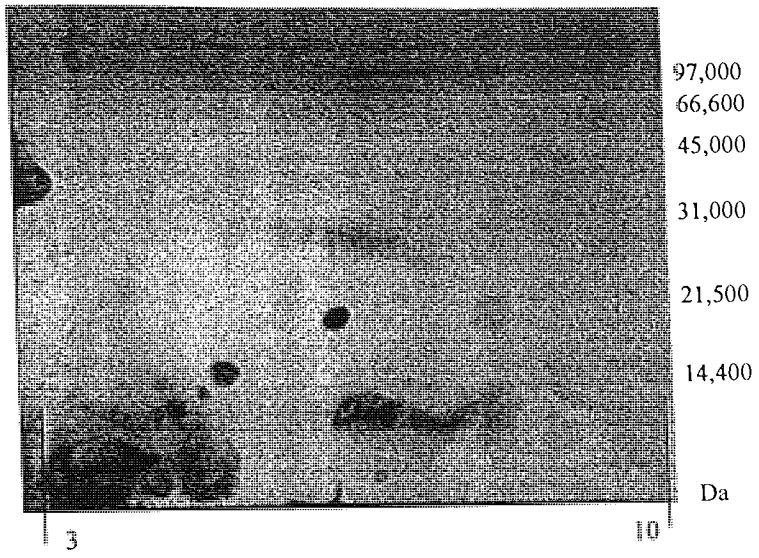


**Figure 6.11** 2D Electrophoresis of serosal sample after 6 h exposure to DT-containing formulation

## 6.4 *In vivo* delivery of formulations

Analysis of the collected plasma samples was initially performed by SDS PAGE electrophoresis, however, plasma is a much more complicated biological fluid than the serosal fluid obtained from the chamber studies, and this proved to be inappropriate due to the number of proteins present. 2D electrophoresis was used in an attempt to simplify the identification of the proteins present.

### 6.4.1Two-dimensional electrophoresis of plasma

Electrophoretic analysis of the secreted proteins can be seen in figures 6.12 to 6.13. From these 2D electrophoresis results there is only one major visible difference between the different experimental groups, which is in the group dosed with the DT-loaded microspheres. The most apparent difference is the appearance of the group of proteins at a molecular weight of 16 kDa, and with a pI of approximately 7. This particular group of proteins does not appear in any of the other experimental groups for any of the animals treated.

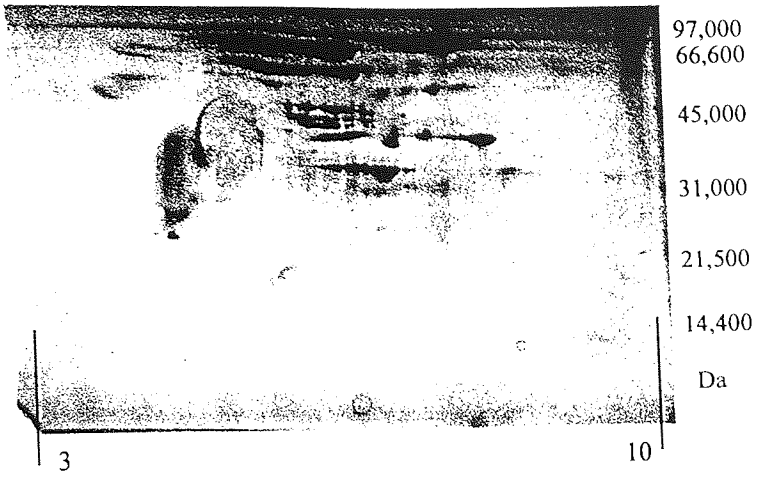


**Figure 6.12** 2D electrophoresis of control plasma, 6 h after gavage, pI 3 to 10 (x axis) MWt 14-97 kDa (y axis)

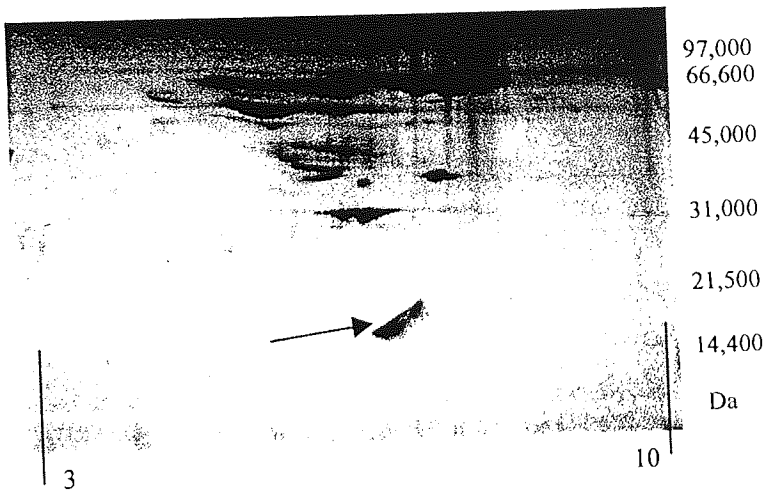


**Figure 6.13** 2D electrophoresis of plasma 6 h after oral administration of DT containing PLA microspheres, pI 3 to 10 (x axis) MWt 14-97 kDa (y axis)

Comparison of the 2D electrophoresis results for the *in vivo* study with those obtained from the *ex vivo* chamber experiment suggests that one of the proteins (MWt ≈ 16 kDa, pI ≈ 7) is seen in both of these experiments. However, gel electrophoresis and IEF experiments can not be relied upon to provide accurate MWt and pI values and comparisons.

## 6.4.2 Western blotting of plasma

As with the *in vitro* samples, the *in vivo* samples were analysed by Western blotting for the presence of inflammatory or immune regulating cytokines. Western blots were performed for the same reason as for the *in vitro* study, rather than an more sensitive technique such as an ELISA method. Like the results obtained for the *in vitro* part of the study, where there were no positive results whatsoever, there were no bands visible in any of the 6 h Western blots (figures 6.14, to 6.18). In all the cases where bands were seen, the MWt at which they were seen does not correspond to that of the positive control. This may be due to them either being a false positive due to the polyclonal antibody reacting with a completely unrelated species, or they could be due to the positive controls being of the incorrect molecular weight. The positive controls obtained were recombinant proteins obtained after expression in *E. coli*, thus introducing the difference in glycosylation between their natural (eukaryotic) and the bacterial (prokaryotic) system in which the positive control proteins were expressed. For all 5 of the cytokines examined using the Western blot system, there are precise literature MWt values available (Cruse and Lewis, 1999). In none of the cases in which bands were seen were they in the correct molecular weight region. This would support the conclusion that none of the cytokines investigated were found to be present in any detectable quantity.

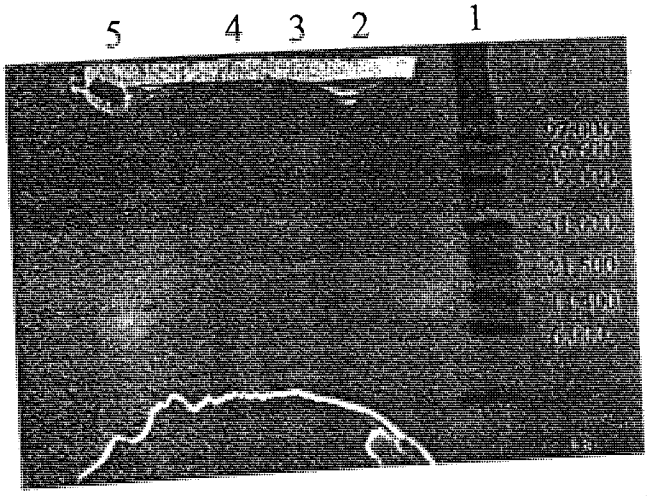


**Figure 6.14** Western blot for IFN-γ. Rat plasma 6 h after administration. Lane 1, weight marker; lane 2, control plasma; lane 3, BSA loaded microspheres; lane 4 DT-loaded microspheres; lane 5, positive control.

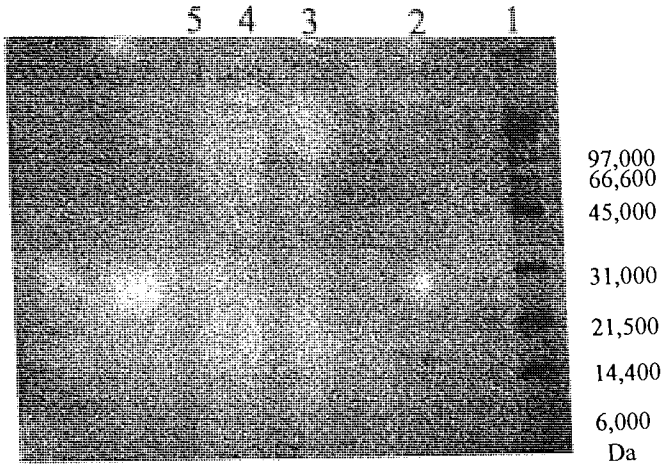


**Figure 6.15** Western blot for MCP-1 Rat plasma 6 h after administration. Lane 1, weight marker; lane 2, positive control; lane 3, BSA-loaded microspheres; lane 4 DT-loaded microspheres; lane 5, control plasma.

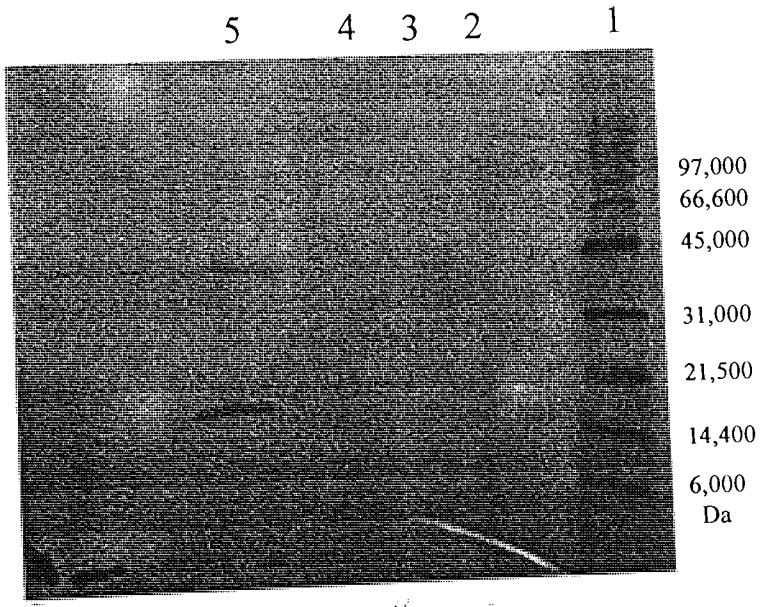


**Figure 6.16** Western Blot for TNF-α Rat plasma 6 h after administration. Lane 1, weight marker; lane 2, Control plasma; lane 3, BSA-loaded microspheres; lane 4 DT-loaded microspheres; lane 5, positive control.

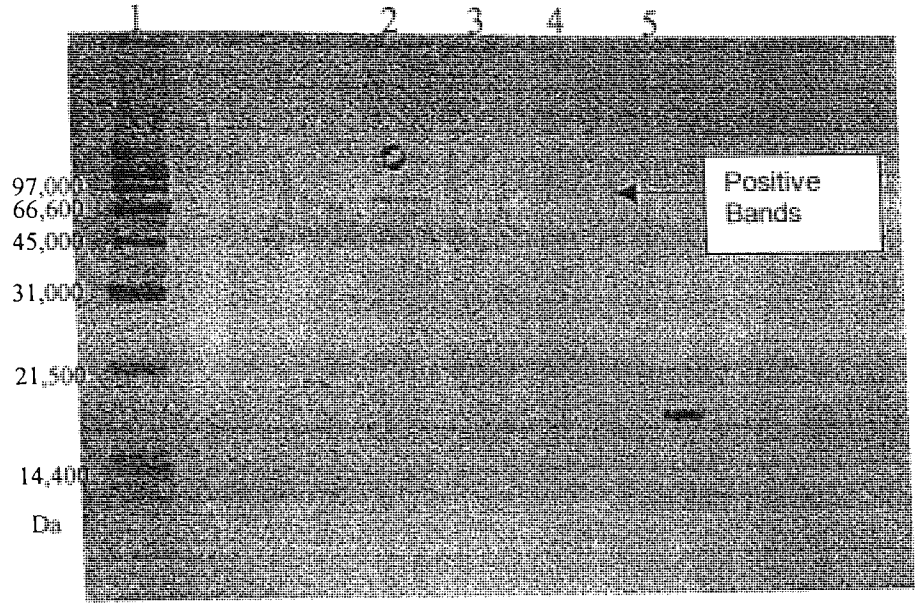


**Figure 6.17** Western blot for MIP1α Rat plasma 6 h after administration. Lane 1, weight marker; lane 2, Control plasma; lane 3, BSA loaded microspheres; lane 4 DT-loaded microspheres; lane 5, positive control.

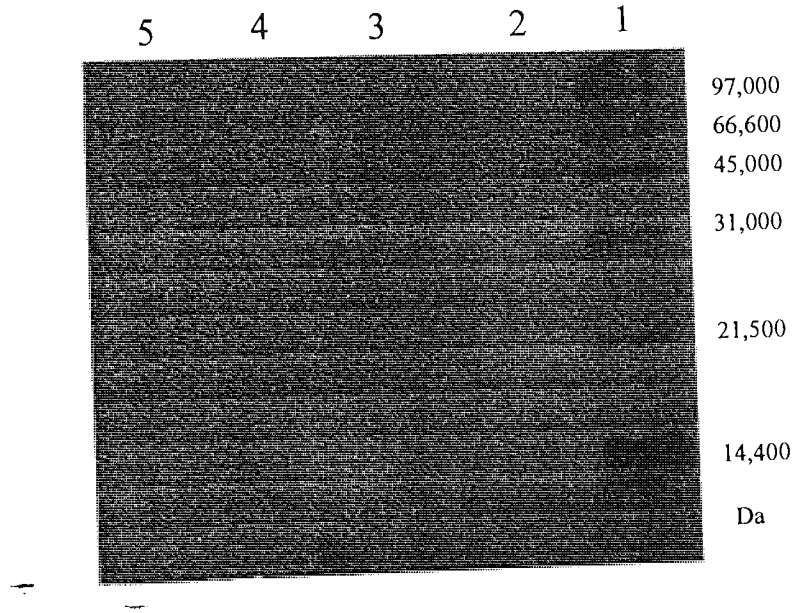


**Figure 6.18** Western blot for IL-1β rat plasma 6 h after administration. Lane 1, weight marker; lane 2, positive control; lane 3, BSA loaded microspheres; lane 4 DT-loaded microspheres; lane 5, Control plasma.

## 6.5 Proteomic investigation of secreted proteins

A basic proteomic investigation of the proteins seen in both the *in vitro* and *in vivo* study was performed. Standard rat plasma 2D gels were not available from the SwissProt database. As a starting point, the 2D gels were compared with the standard human 2D gel (figure 6.19) stored on the SwissProt database. The region of the 2D gel of interest is

highlighted by the box in Figure 6.19. There are no identified proteins in this region, however, there is one protein just outside this region, MWt 16 kDa, and with a pI of 6.6, although this currently remains unidentified on the SwissProt database. Without knowledge of the physiological function of the proteins that have been observed, it is not possible to investigate human proteins with a similar function in the hope of finding an analogous protein, for which there exists data in the literature including its MWt and pI. Without knowing the identity of this protein, it not possible to draw any conclusions about the rat proteins we have seen in this range.

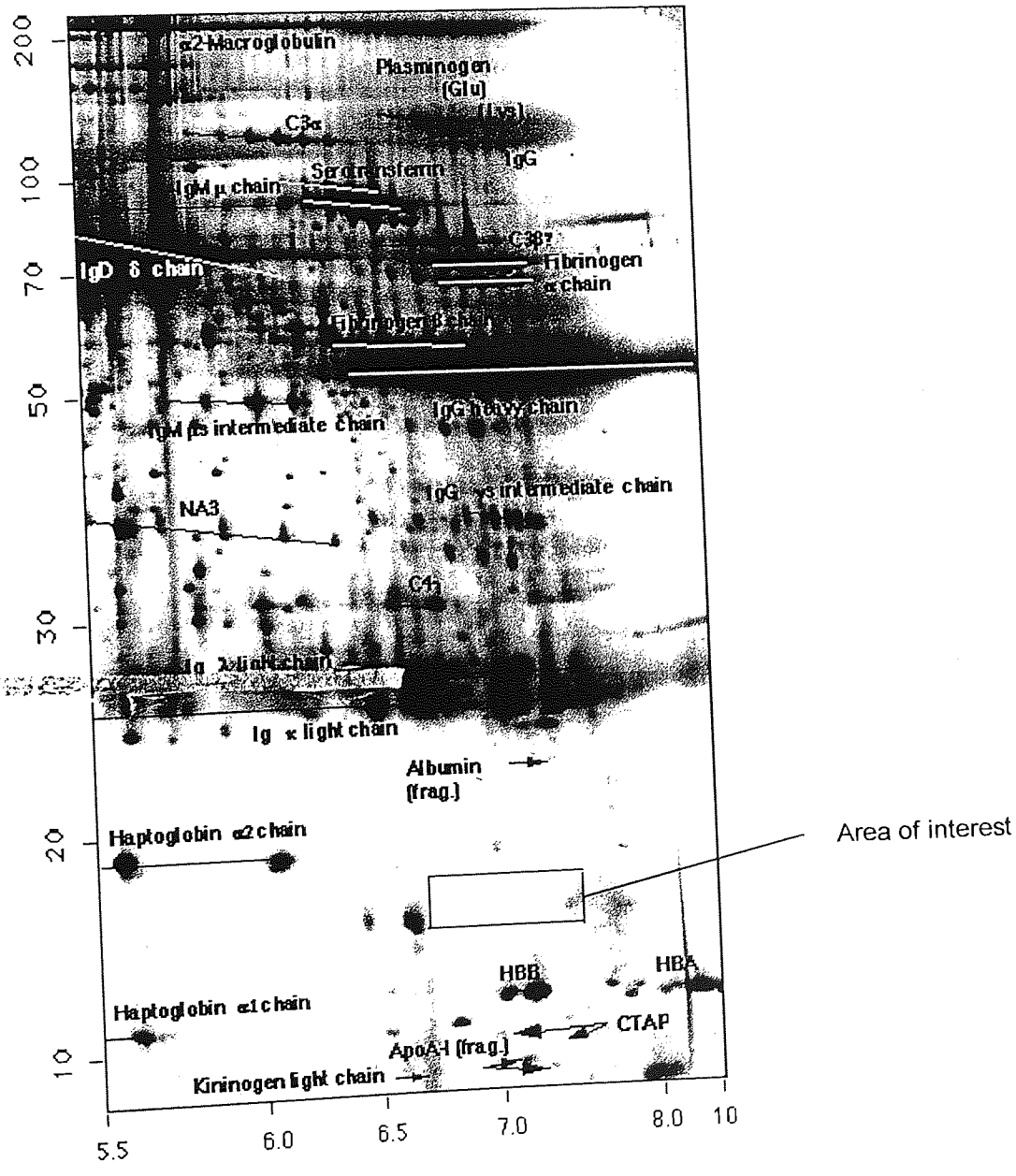


**Figure 6.19** SwissProt standard human plasma 2D electrophoresis map.

There does exist a 2D electrophoresis gel of rat plasma in the literature, that of Innanen *et al.*, (1988). However, in this gel the proteins that we have observed in this limited study are also noticeable by their absence

## 6.6 Discussion and conclusions

Both the *in vitro* and *in vivo* work described here would suggest that the chamber has a use as a vaccine screening tool, however, there is still significant work to be done investigating the chamber as a potential system for screening mucosal vaccine formulations. In both systems, differences were seen in the response from the tissue / animal between different formulations. From the work performed to date, it is not possible to identify what these differences are since the attempts at identifying a number of key cytokines that would be expected to be involved in any immune response to the delivery of such antigenic material were not successful. None of the cytokines could be found either *in vivo* or *in vitro*. The absence of suitable monoclonal antibodies proved to be the largest factor in this, with the *in vivo* work highlighting just how important it is to know what the antibodies are reacting with. The Western blots proved effective with the polyclonal antibodies that were available. However, the detection limits are much higher than those obtainable if suitable monoclonal antibodies were available to allow more sensitive techniques such as ELISA's to be performed. Until there are suitable monoclonal antibodies available against the relevant rat cytokines, it will not be possible to accurately determine the presence or absence of these cytokines in response to the delivery of the potential vaccine formulations.

Although no cytokines could be identified at the detection limits imposed by the Western blotting it is important to conclude that significant differences could be seen between the different formulations both *in vivo* and *in vitro* by SDS PAGE and 2D electrophoresis. Currently, the proteins seen by these techniques are under further investigation, and it is hoped that by transferring them to PVDF and subsequent micro-sequencing that the proteins can be identified from their sequence, or their novelty confirmed. Similarly, both the *in vivo* and *in vitro* systems have a group of proteins of a

similar MWt and pI, the similarity between these proteins is also an important point for investigation, which should be resolved by their sequence, or part thereof being determined.

From the data presented here, we can conclude that although significant further work is required for the identification of the proteins seen, the chamber has shown significant promise as a tool for the *in vitro* screening of vaccine formulations.

# Chapter 7

# GENERAL SUMMARY

Pharmaceutical scientists have seen nasal administration as an advantageous drug delivery route for some time. Several strategies have been successfully employed in overcoming the barriers inherent in nasal delivery, especially for unstable biological macromolecules such as proteins and peptides (chapter 1). The lack of a suitable *in vitro* model together with the current interest in nasal delivery not just for local and systemic drugs delivery, but together with the potential for antigen delivery to the mucosal immune system leaves an opportunity to develop a system for the evaluation of drugs and antigens for potential nasal delivery.

The stability of a drug at the site of delivery is undeniably of great significance. A NMR spectroscopic method was developed (chapter 2) for investigation of the stability of a number of small peptides. Small peptides, such as the tetrapeptides used here, are difficult to quantify using traditional techniques such as HPLC (due to poor fluorescence, or UV absorption) or gel electrophoresis (due to their size). The investigation of the peptide stability by NMR has two significant advantages, the structure of any degradation products can be easily determined, and only a small mass of sample (typically 10 mg per experiment) is required. Both degradation by active enzyme solutions, and, by nasal wash proteins was easily observable for positive control peptides. The actual peptide drug analogues considered in this study proved to be exceptionally proteolytically stable. Similarly, after recording the initial spectrum, storing the samples at elevated temperatures and then re-recording the NMR spectrum proved to be an effective method of analysing the thermal stability of the peptides. In the case of the tetrapeptide containing aspartic acid, the rearrangement and formation of the cyclic imide was clearly visible. The NMR technique proved to be capable of investigating the effect of pH, temperature, and proteolytic susceptibility, working on a very small sample mass, and providing quantitative, structural data on the decomposition products.

*In vitro* techniques for investigating oral delivery such as cell culture and the Ussing chamber have been available for some considerable time, interest in techniques suitable for investigating nasal delivery has until recently been limited. The work that has been performed to date has been limited to the Ussing chamber. A new system that overcomes some of the disadvantages of the Ussing chamber was developed (chapter 3). The key

difference between the newly developed chamber and the well established Ussing chamber is not only the horizontal tissue, but the ability to have a minimal aqueous volume on the upper tissue surface. *In vivo* the nasal epithelial surface is exposed to the air, and the mucosal aqueous phase was removed to mimic the conditions experienced *in vivo*. Investigation of the viability of epithelial tissues from a variety of sources and species proved the concept of the chamber, although the epithelial voltages generated by both the porcine and rabbit nasal tissue were somewhat lower than those obtained in control experiments where the tissue was monitored in the Ussing chamber. Investigation of rat ileal tissue showed that when the mucosal surface of the tissue was covered with a glass coverslip there was no difference in the voltage recorded by either the control (Ussing chamber) tissue or that exposed in the lower chamber. In parallel with the electrophysiological investigations a paracellular marker was used to monitor any physical damage to the tissue surface. In none of the cases were there any statistically significant paracellular marker permeation difference between the tissue in the new chamber and the Ussing chamber.

With the inclusion in the chamber design of the minimal mucosal volume the traditional approach of $P_{eff}$ and $P_{app}$ had to be modified making certain assumptions as highlighted in chapter 3. Using rat ileal tissue these assumptions were tested for two paracellular markers, and both in both cases the assumptions proved to be valid.

The voltage generated by the ileal tissue was increased by covering the tissue surface with a glass coverslip, for the nasal tissue a different approach was used to increase the viability of the tissue samples. In place of a glass coverslip, an environmental chamber was built over the entirety of the tissue viability chamber (chapter 4). To improve the viability of the tissues inside, the chamber was supplied with pre-warmed, pre-humidified air. The chamber system proved capable of increasing the epithelial voltage for the nasal tissues to a level comparable with reported literature values.

In addition to providing increased viability for the nasal epithelial tissues, the upper chamber provided a means for investigating nasal delivery devices *in vitro*. Existing techniques do not provide any means of investigating the effect of airflow, air temperature,

or humidity of the final applied dose. Frame-by-frame videography of deliveries to the new chamber revealed that for simple liquid delivery there were no discernable differences in deposition, however, when more complicated and realistic devices such as the nasal pump spray, were considered the environmental chamber was able to discern differences between different flow rates and humidities. Differences that could be seen by video analysis were then confirmed by the adaption of the chamber to be used inside a Malvern Instruments Mastersizer. This adaption allowed for the accurate sizing of the droplets in the resultant aerosol, proving that differences due to the conditions experienced inside the environmental chamber could be seen and measured.

The form that the formulation is in whilst inside the nasal cavity is one aspect that was investigated. However, what happens to the delivered dose when it hits the tissue surface is possibly more important (chapter 5). To investigate this, the tissue viability chamber by itself was adapted to fit under a confocal microscope. Confocal microscopy is a powerful imaging technique capable of producing clear three dimensional images of tissue and cell samples, however, in this case, individual images were used, and the optical density of the images was used to quantify the penetration of fluorescent labelled microspheres into excised nasal tissue with depth. From the studies here it was shown that it was possible to extract kinetic information as to the rate of penetration of microspheres into nasal tissue with time. For both the carboxylated, and plain latex 50 nm particles the depth-time profile is linear suggesting a passive mechanism for the particle uptake. Larger particles (100 and 200 nm) had a linear rate of penetration for the first 45 minutes, with the rate of penetration reduced after this, suggesting a different mechanism is involved, and the possibility of a size cut-off existing.

As well as providing data about the fate of the formulation and the kinetics of particle uptake, the serosal fluid contains the biological response of the tissue to an applied formulation (chapter 6). Administration of a vaccine formulation that is known to cause a significant protective immune response showed a changed pattern of protein secretions. Similarly, when *in vivo* experiments were performed, proteins of similar characteristics were seen in the plasma. These proteins were investigated by Western blotting, however, to date they have not been identified.

The aims of this thesis were to produce a chamber system for the investigation of nasal delivery. The key aims and objectives set out in section 1.6 were all met. The chamber system itself can now be considered to be optimised. Development of the system to fit into the Mastersizer, and under the confocal microscope show that the system is versatile, and that future developments of the chamber are possible. The initial vaccine screening work holds the most potential. The chamber provides for the viability of the epithelial tissue; if the proteins that are seen to be secreted prove to be of no significant interest, there is the potential to include other cell types in the chamber system, such as including isolated peritoneal macrophage, or cultured T cells in the serosal fluid. The aim of such experiments would be to see if there was any measurable effect on these components of the immune system due to the presence of active formulations on the epithelial tissues.

# Bibliography

Afzelius, B.A. (1997), Ciliary disfunction. In: Crystal, R.G. (ed.), The lung: Scientific foundations. Lippincott-Raven, Philadelphia, 2573-2578

Allen, J. D. (1992), A Mucus Secreting Cell Co-Culture Model for Drug Absorption Studies. PhD Thesis. Brighton Polytechnic, Brighton, UK

Almeida, A. J. (1994), . PhD Thesis, Aston University, Birmingham, UK

Almeida, A. J., Alpar, H. O. (1996) Nasal delivery of vaccines. *J. Drug Targeting*, **3**: 427-442

Alpar, H.O., Eyles, J.E., Williamson, E.D. (1998), Oral and nasal immunization with microencapsulated clinically relevant proteins. *STP Pharma Sci.*, **8**, 1, 31-39

Alpar, H.O., Ozsoy, Y., Bowen, J., Eyles, J.E., Conway, B.R., Williamson E.D. (1997), Potential of particulate carriers for the mucosal delivery of DNA vaccines, *Biochem. Soc. Trans.*, **25**, 2, S337

Alpar, H. O., Almeida, A. J., Brown, M. R. W. (1994), Microsphere absorption by the nasal mucosa of the rat. *J. Drug Targeting,* **2**: 147-149

Andersen, I., Camner, P., Jensen, P.L., Philipson, K., Proctor, D.F. (1974), Nasal clearance in monozygotic twins. *Am. Rev. Resp. Dis.*, **110,** 301-305

Andersen, I., Proctor, D.F. (1983), Measurement of mucociliary clearance. *Eur. J. Respir. Dis.*, **64**, 37-40

Artursson, P. (1990), Epithelial transport of drugs in cell culture. I: A model for studying the passive diffusion of drugs over intestinal absorptive (Caco-2) cells. *J. Pharm. Sci.*, **79**, 476-482

Artursson, P., Magnusson, C. (1989), Epithelial transport of drugs in cell culture. *J. Parm. Sci.*, **79**, 595-600

Artursson, P., Palm, K., Luthman, K. (1996), Caco-2 monolayers in experimental and theoretical predictions of drug transport. *Adv. Drug Del. Rev.*, **22**, 67-84

Audus, K.L., Bartel, R.L., Hidalgo, I.J., Borchardt, R.T. (1990), The use of cultured epitelial and endothelial cells for drug transport and metabolism studies. *Pharm. Res.*, **7**, 435-451

Bailey, C.A., Bryla, P., Malick, A.W. (1996), The use of the intestinal epithelial cell culture model, Caco-2, in pharmaceutical developement. *Adv. Drug Del. Rev.* **22**, 85-103

Baldwin, P.A., Klingbeil, C.K., Grimm, C.J., Longeneker, J.P. (1990), The effect of sodium tauro-24,25-dihydrofusidate of the nasal absorption of human growth hormone (hGH) in three animal models. *Pharm. Res.*, **7**, 547-552

Banerjee, P.K., Amidon, G.L. (1985), Design of pro-drogs based on enzyme substrate specificity. In: Bundgaard H. (ed.) Design of pro-drugs. Elsevier Science.

Bechgaard, E., Bindseil, E., Bagger., M., Nielsen, H.W. (1997), Reversibility and clinical relevance of morphological changes after nasal application of ephedrine nasal drops 1%. *Int. J. Pharm.*, **125**, 1, 67-73

Bechgaard, E., Gizurarson, S., Hjortkjaer, J.K., Sorensen, A.R. (1996), Intra nasal administration of insulin to rabbits using glycofurol as an absorption promoter. *Int. J. Pharm.*, **128**, 287-289

Bechgaard, E., Gizurarson, S., Jorgensen, L., Larsen, R. (1992) The viability of isolated rabbit nasal mucosa in the Ussing chamber, and the permeability of insulin across the mebrane. *Int. J. Pharm.*, **37**, 125-132

Becker, G.W., Tackitt, P.M., Bromer, W.W., Lefeber, D.S., Riggin, R.M. (1988), Isolation and characterisation of a sulfoxide and a desamido derivative of biosynthetic human growth hormone. *Biotechnol. Appl. Biochem.*, **10,** 326

Björk E., Isaksson U., Edman P., Arturson P. (1995), Starch microspheres induce pulsatile delivery of drugs and peptides across epithelial barriers by reversible separation of the tight junctions *J. Drug Targeting.* **2**, 501-507

Björk E., and. Edman P. (1988), Degradable starch microspheres as a nasal delivery system for insulin, *Int J. Pharm.*, **47,** 232-238

Björk E., and. Edman P. (1990), Characterisation of degradable starch microspheres as a delivery system for drugs, *Int J. Pharm.*, **62**, 187-192

Björk E. (1993), Starch microspheres as a nasal delivery system for drugs. PhD Thesis, Uppsala University, Sweden.

Brogden, R.N., Heel, R.C. (1987) Human insulin: A review of its biological activity, pharmacokinetics and therapeutic use. *Drugs,* **34**, 350-371

Bundgaard, H. (1992) The utility of the prodrug approach to improve peptide absorption. *J. Contr. Rel.,* **21**, 63-72

Camner, P. (1988) Minireview: How important is mucociliary clearance? *Exp. Lung Res.*, **14**, 423-429

Chien Y.W. (1985), Transnasal systemic medications, Elsevier, Amsterdam / Oxford / New York / Tokyo

Chien, Y. W., Su, K. S. E., Chang, S.-F. (1989) Nasal Systemic Drug Delivery. Marcel Dekker,, New York,

Christolini C. (1991), Intranasal DDAVP: biological and clinical evaluation in mild factor VIII deficiency. *Haemostasis* **21**, 273-277

Clarke M.A., Jepson M.A.,. Simmons N.L, Hirst B.H. (1995), Selective binding and transcytosis of *Ulex europaeus* I lectin by mouse Peyer's patch M cells in-vivo, *Cell Tissue Res.* **282**, 455-461

Cotton, C.U., Knowles, M.J., Gatzy, J.T., Boucher, R.C. (1987), Abnormal apical cell membrane in cystic fibrosis respiratory epithelium. An in-vitro electrophysiological analysis. *J. Clin. Invest.*, **79**, 80-85

Cremaschi, D., Rossetti, C., Draghetti, M.T., Manzoni, C., Aliverti, V. (1990), Active transport of polypeptides in rabbit respiratory nasal mucosa. *J Contr. Rel.*, **13** (Supplement), 319-329

Cremaschi, D., Rossetti, C., Draghetti, M. T., Manzoni, C., Aliverti, V. (1991), Ative transport of polypeptides in rabbit nasal mucosa: possible role in the sampling of potential antigens. *Pflugers Archiv-European J. Physiology,* **419**, 425-432

Crespi, C. L., Penman, B. W., Hu, M. (1996), Development of Caco-2 cells expressing high levels of cDNA -derived Cytochrome P450 3A4. *Pharm. Res.*, **13**, 1635-1641

Cruse, J.M., Lewis, R.E. (1999), Atlas of Immunology, CRC Press, Boca Raton, Florida, USA.

Cuana, N. (1982), Blood and nerve supply to the nasal lining. In: Proctor D.F. (ed.) The Nose: Upper Airway Physiology and the Atmosphere Environment. Elsevier, Amsterdam, 45-66

Cuana, N., Hinderer, K.H. (1969), Fine structure of the blood vessels of the human nasal respiratory mucosa. *Ann. Otol. Rhinol. Laryngol.*, **78**, 865

Dahl, A.R. (1988), The effect of cytochrome P450 dependent metabolism and other enzyme activities on olfaction. In: Margolis F.L. (ed.) Molecular neurobiology of the olfactory system. Plenum Press, New York., 51-70

Dawes, J.D.K., Pritchard, M.M.L. (1953), Studies of the vascular arrangement of the nose. *J. Anat.*, **87**, 311

Duchene, D., Ponchel, G. (1993), Nasal Administration: A Tool for Tomorrows Systemic Administration,. *Drug Dev. and Ind. Pharm.*, **19** (1&2): 101-122

Edman, P., Bjork, E., Isaksson, U., Artursson, P. (1991) Starch microspheres enance insulin absorption across epithelial cells by affecting the integrity of tight junctions. *Proc. Dispos. Deliv. Pept. Drugs.* Leiden, 15

Eldrich, J.H., Hammond C.J., Muelbroek J.A., Staas J.K., Gilley R.M., Tice T.R., (1990), Controlled vaccine release in the gut associated lymphoid tissue. I. Orally administered biodegradable microspheres target the Peyers patches. *J. Contr. Rel.*, **11**, 205-214

Ermak T.H., and Giannasca P.J. (1998), Microparticulate targeting to M cells, *Adv Drug Del. Rev.*, **34**, 261-283

Eyles J.E., Williamson E.D., Spiers I.D., Stagg A.J., Jones S.M., Alpar H.O. (2000), Generation of protective immune responces to plague by mucosal administration of microsphere coencapsulated recombinant subunits. *J. Contr. Rel.*, **63**, 191-200

Eyles J.E., Spiers I.D., Williamson E.D., Alpar H.O., (1998a) Analysis of local and systemic immunological responses after intra-tracheal, intra-nasal and intra-muscular administration of microsphere co-encapsulated Yersinia pestis sub-unit vaccines. *Vaccine*,**16**, 20,.2000-2009

Eyles J.E., Sharp G.J.E., Williamson E.D., Spiers I.D., Alpar H.O., (1998b) Intra nasal administration of poly-lactic acid microsphere co-encapsulated Yersinia pestis subunits confers protection from pneumonic plague in the mouse *Vaccine*, **16**, 7, 698-707

Eyles J.E., Alpar H.O., Conway B.R., Keswick M., (1997) Oral delivery and fate of poly(lactic acid) microsphere-encapsulated interferon in rats. *J. Pharm. Pharmacol.*, **49**, 7, 669-674

Geurkink, N. (1983), Nasal anatomy, physiology, and function. *J. Allergy Clin. Immun.* **72**, 123

Giannasca, P.J., Boden, J.A., Monath, T.P. (1997), Targeted delivery of antigen to hamster nasal lymphoid tissue with M-cell directed lectins. *Infection and Immunity.* **65**, 4288 - 4298

Gizurarson, S., Bechgaard, E. (1991), Study of nasal enzyme activity towards insulin *in vitro*. *Chem. Pharm. Bull.*, **39**, 2155-57

Gizurarson, S., Marriot, C., Martin, G.P., Bechgaard, E. (1990), The influence of insulin and some excipients used in nasal insulin preparations on mucociliary clearance. *Int. J. Pharm.*, **65**: 243-247

Gizurarson, S., Tamura, S., Kurata, T., Hasiguchi, K., Ogawa, H. (1991), The effect of cholera toxin and cholera toxin B subunit on the nasal mucosal membrane. *Vaccine* **9**, 825-832

Gulisano, M., Bryk, S.G., Gheri, G., Sgambati, E., Curreli, A., Masala, W., Pacini, P. (1994), Histochemical study of human nasopharyngeal epithelium by horseradish peroxidase conjugated lectins. *Epith. Cell Biol.*, **3**, 1-6

Hardy J.G., Lee S.W., Wilson C.G. (1995), Intranasal drug delivery by spray and drops, *J. Pharm. Pharmacol*, **37**, 294

Harris A.S., Nilsson I.M., Wagner Z.G., Alkner U. (1986), Intranasal administration of peptides - nasal deposition, biological response, and absorption of desmopressin. *J. Pharm. Sci.*, **75**, 11, 1085-1088

Hauri, H.-P., Sterchi, E. E., Bienz, D., Fransen, J. A. M., Marxer, A. (1985), Expression and intracellular transport of microvillus membrane hydrolases in human intestinal epithelial cells. *J. Cell Biol.*, **101**, 838-851

Hemlin, M., Jodal M., Lundgren O., Sjovall, H., Stage, L., (1988), The importance of the subepithelial resistance for the electrical properties of the rat jejunum *in vitro*. *Acta Physiol. Scand.*, **134**, 79-88.

Hilgers, A.R., Conradi, R.A., Burton, P.S. (1990), Caco-2 monolayers as a model for drug transport across the intestinal mucosa. *Pharm. Res.*, **7**, 902-910

Hirai, S., Yashiki, T., Hiroyuki, M. (1981a), Mechanisms for the enhancement of the nasal absorption of insulin by surfactants. *Int. J. Pharm.*, **9**, 173-184

Hirai, S., Yashiki, T., Matsuzawa, T., Mima, H. (1981b), Absorption of drugs from the nasal cavity of rats. *Int. J. Pharm.*, **7**, 317-325

Ho, N.F.H. (1993), Biophysical Kinetic Modelling of Buccal Adsorption. *Adv. Drug Deliv. Rev.* **12**, 61 - 97

Holbrook, P. (1991), PhD Thesis, Aston University, Birmingham, UK

Howell, S., Kenny, A.J., Turner, A.J. (1992), A survey of membrane peptidases in two human colonic cell lines, Caco-2 and HT-29. *Biochem. J.*, **284**, 595-601

Huang, C.H., Kimura, R., Bawarshi-Nassar, R., Hussain, A. (1985a), Mechanism of nasal absorption of drugs II: Absorption of L-tyrosine and the effect of strucural modification on its absorption. *J. Pharm. Sci.*, **74**, 1298-1301

Huang, C.H., Kimura, R., Bawarshi-Nassar, R., Hussain, A. (1985b), Mechanisn of nasal absorption of drugs I: Physicochemical parameters influencing the rate of in situ nasal absorption. *J. Pharm. Sci.*, **74**, 608-611

Humphrey, M.J. (1986), Oral bioavailability of peptides and related drugs. Delivery systems for peptide drugs. Plenum Press, New York and London, 139-151

Hussain N., Jani P.U., Florence A.T. (1997), Enhanced oral uptake of tomato lectin-conjugated nanoparticles in the rat. *Pharm. Res.*, **14**, 5, 613-618

Illum, L. (1996), Nasal delivery, the use of animal models. *J Drug Targeting* **3**, 427-442

Illum, L., Jorgensen, H., Bisgaard, H., Krogsgaard, O., Rossing, N. (1987), Bioadhesive microspheres as potential nasal drug delivery systems. *Int. J. Pharm.*, **39**, 189-199

Innanen, V.T., Korogyi, N., Jobb, E., Mcgarrity, J. (1988), An additional protein in 2d-page of plasma from the spontaneously hypertensive rat. Clinical Chemistry, **34**, 2, 432-433

Jester J.V., Maurer J.K., Petroll W.M., Wilkie D.A., Parker R.D., Cavanagh H.D. (1996), Application of in vivo confocal microscopy to the understanding of surfactant-induced ocular irritation. *Toxicol. Pathol.*, **24**, 4, 412-428

Kabok Z., Ermak T.H., Pappo J. (1994), Microhetrogeneity of folicle epithelium and M cells in rabbit gut-associated lymphoid tissues defined by monoclonal antibodies, *FASEB J.*, A1008

Kato T. (1990), A study of secretory Immunoglobulin A on membranous epithelial cells (M cells) and adjacent adsorptive cells of rabbit Peyer's patches *Gastroenterol. Jpn.*, **25** 15-23

Kublik H., Vidgren M.T. (1998), Nasal delivery systems and their effect on deposition and absorption, *Adv. Drug Del. Rev.*, **29**, 157-177

Laurenzi, G.A. (1973), The Mucociliary stream, *J. Occup. Med.*, **15** ,174-182

Lee, V.H.L. (1988a), Enzymatic barriers to peptide and protein absorption. *Crit. Rev. Therap. Drug Carrier Sys.* **5**, 69-97

Lee, V.H.L. (1988b), Peptide and protein drug delivery: opportunities and challenges. *Pharmacy International.* **7**, 208-212

Lee, V.H.L., Yamamoto, A. (1990), Penetration and enzymatic barriers to peptide and protein absorption. *Adv. Drug Del. Reviews.*, **4**, 171-207

Li H.F., Petroll W.M., MollerPedersen T., Maurer J.K., Cavanagh H.D., Jester J.V. (1997), Epithelial and corneal thickness measurements by in vivo confocal microscopy through focusing (CMTF), *Curr. Eye Res.*, **16**, 3, 214-221

Longenecker, J. P., Moses, A. C., Flier, J. S., Silver, R. D., Carey, M. C., Dubovi, E. J. (1987), Effects of taurodihydrofusidate on nasal absorption of insulin in sheep. *J. Pharm. Sci.*, **76**, 351-355

Mariassy, A.T., Plopper, C.G., George, J.A.S., Wilson, D.W. (1988), Lectin binding pattern of neuro-epithelial and respiratory epithelial cells in the mouse nasal cavity. *Anat. Rec.* **222**, 49-59

Maron, Z., Shelhamer, J., Kaliner, M. (1984), Nasal mucus secretions. *Ear Nose Throat J.* **63**, 36

Martiin, E., Schipper, N.G.M., Verhoef, J.C., Merkus, F.W.H.M. (1998), Nasal mucociliary clearance as a factor in nasal drug delivery. *Adv. Drug Deliv. Rev.* **29**, 13-38

Mathews, C.K., van Holder, K.E. (1990), Biochemistry. Benjamin Cummins

Mathias, N. R., Yamashita, F., Lee, V.H.L. (1996) Respiratory epithelial cell culture models for evaluation of ion and drug transport. *Adv. drug Del. Rev.* **22**, 215-249

Maurer, J.K., Jester, J.V. (1999), Use of in vivo confocal microscopy to understand the pathology of accidental ocular irritation *Toxicol. Pathol.*, **27**, 1, 44-47

Maurer, J.K., Li H.F., Petroll, W.M., Parker, R.D., Cavanagh, H.D., Jester_JV (1997), Confocal microscopic characterization of initial corneal changes of surfactant-induced eye irritation in the rabbit *Toxicol App. Pharmacol.*, **143**, 2, 291-300

Mayor, S., Illum, L. (1994) An investigation of the effect of anaesthetics on the nasal absorption of insulin in rats. *Proceed. Int. Symp. Contr. Rel. Bioact. Mater.*, 21: 334-335

McCrossin, L. (1999), Formulation Scientist, PowderJect Ltd, Oxford, UK, Personal Communication.

Merkus, F.W.H.M., Schipper, N.G.M., Hermens, W.A.J.J., Romeijn,S.G., Verhoef, J.C. (1993), Absorption enhancers in nasal delivery. *J. Control. Rel.*, **24**, 201-208

Merkus, F.W.H.M., Verhoef, J.C., Romeijn, S.G., Schipper, N.G.M. (1991), Interspecies differences in the nasal absorption of insulin. *Pharm. Res.* 8, 1343

Mygind, N. (1978), Nasal allergy. Blackwell Scientific Publications., Oxford

Newhouse, T. (1983), Primary ciliary diskinesia. What has it taught us about pulmonary disease? *Eur. J. Respir. Dis. Suppl.*, **127**, 151-157

Newton, C.L., Henderson, W.R., Sporn, M.B. (1980), *Cancer Res.* **40**, 3413-3425

Oechslein, C. R., Fricker, G., Kissel, T. (1996), Nasal delivery of octreotide: Absorption enhancement by particulate carrier systems. *Int. J. Pharm.* **139**, 25-32

Ogawa, H., Kami, K., Susuki, T., Mitsui, T. (1979) An immunohistochemical study of lysosyme in human nasal mucosa. *Keito J. Med* **28**, 73

Ohashi, Y., Nakai, Y., Ikeoka, H., Furuya, H. (1991) Regeneration of nasal mucosa following mechanical injury. *Acta Otolaryngol. Suppl.*, **486**, 193-201

Östh, K., Björk, E. (1997a) Characterisation of pig nasal tissue in a new horizontal Ussing chamber. *Int. Symp. Contr. Rel. Bioact. Mater.*, **24**, 417-418

Östh, K., Björk, E. (1997b) Characterisation of pig nasal tissue in a new horizontal Ussing chamber. (Uppsala). *Proceedings of the second symposium within the Nordic Network of Pharmaceutical Technology and Biopharmaceutics (NORFA).* Uppsala, 38

Patrick, G., Sterling, C. (1977), Measurement of mucociliary clearance in conscious and anaesthetised rats. *J. Applied Physiol.*, **42**, 451-455

Pappo J., Ermack T.H., Steiger H.J. (1991), Monoclonal antibody-directed targeting of fluorescent polystyrene microspheres to Peyer's patch M cells, *Immunology* **73**, 277-280

Pereswetoff-Morath L., and Edman P. (1995), Dextran microspheres as a potential nasal drug delivery system for insulin – in-vitro and in-vivo properties *Int J. Pharm.* **124**, 37-44

Petroll W.M., Jester J.V., Cavanagh H.D. (1996a), Quantitative three-dimensional confocal imaging of the cornea in situ and in vivo: System design and calibration, *Scanning*, **18**, 1, 45-49

Petroll W.M., Jester J.V., Cavanagh H.D. (1996b), In vivo confocal imaging, *Int. Rev. Exp. Path.*, **36**, 93-129

Phallen, R.F. (1984), Inhalation studies: Foundations and Techniques. CRC Press Inc.,, Boca Raton.

Pikal, M.J., Dellerman, K.M., Roy, M.L., Riggin, R.M. (1991), The effects of formulation variables on the stability of freeze dried hGH. *Pharm. Res.*, 8, 427

Pinto, M., Robine-Leon, S., Appay, M.D., Kedinger, M., Triadou, N., Dussaulx, E., Lacroix, B., Simon-Assmann, P., Haffen, K., Foght, J. (1983), Enterocytl like differentiation and polarisation of the human colon carcinoma cell line Caco-2 in culture. *Biology of the Cell.* **47**, 323-330

Popp, J.A., Monteiro-Riviere, N.A. (1985), Macroscopic, microscopic and ultrastructural anatony of the nasal cavity, Rat. In: Jones T.C., M. U., Hunts R.D., (ed.) Monographs on pathology of laboratory animals. Springer Verlag, pp 3-10

Proctor, D.F. (1977), The upper airways I. Nasal Physiology and defence of the lungs, *Am. Rev. Respir. Dis.*, **115**, 97

Proctor, D.F., and Anderson, I. (1982), The nose, upper airway physiology and the atmospheric environment, Elsevier, Amsterdam

Raehs, S.C., Sandow, J., Wirth, K., Merkle, H.P. (1988), The adjuvant effect of bactiracin on nasal absorption of gonadorelin and buserelin in rats. *Pharm. Res.*, **5**, 689-693

Rossen, R.D., Alford, R.H., Butler, W.T., Vannier, W.E. (1966a), The separation and characterisation of proteins intrinsic to nasal secretions. *Eur. J. Immunol.*, **97**, 369

Rossen, R.D., Schade, A.L., Butler, W.T., Kasel, J.A. (1966b), The proteins in nasal secretion: A longitudinal study of the A-globulin, G-globulin, albumin, siderophilin and total protein concentration in nasal washings from adult male volunteers. *J. Clin. Invest.*, **45**, 768

Roussel, P., Lamblin, G., Lhermitte, M., Houdret, N., Lafitte, J.J., Perini, J.M., Klein, A., Scharfman, A. (1988), The complexity of mucins. *Biochimie*, **70**, 1471-1482

Roy M.J., Varvayanis M, (1987) Development of dome epithelium in gut-associated lymphoid tissues: Association of IgA with M cells, *Cell Tissue Res.* **248,** 645-651

Rutiainen, M., Nuutinen, J., Kiukaannienii, H., Collan, Y. (1992), Ultractructural changes in human nasal cilia caused by the common cold, and recovery of ciliated epithelium. *Ann. Otol. Rhinol. Laryngol.* **101**, 982-987

Sambrook, J., Fritsch, E.F., Maniatis, T. (1989) Molecular cloning, a loboratory manual. 2nd Edition, Cold Harbour Springs Laboratory Press, Plainview, New York, USA

Sanderson, M.J., Sleigh, M.A. (1981), Ciliary activity of cultured rabbit tracheal epithelium: beat and metachrony. *J. Cell. Sci.* **47**, 331-347

Sarkar M. A. (1992), Drug metabolism in the nasal mucosa. *Pharm. Res.*, **9**: 1-9

Schipper N. G. M., Verhoef J. C., Merkus F. W. H. M. (1991), The nasal mucociliary clearance: Relevence to nasal drug delivery. *Pharm. Res.*, **8**, 807-814

Schipper N.G.M., Romeijn J.C., Verhoef J.C., Merkus F.W.H.M. (1993), Nasal insulin delivery with di-methyl-beta-cyclodextrinas an absorption enhancer in rabbits – powder more effective thanliquid formlations. *Pharm. Res.*, **5**, 682-686

Schmidt, M.C., Peter, H., Lang, S.R., Dintzinger, G., Merkle, H.P. (1998), In Vitro Cell models to study nasal mucosal permeability and metabolism. *Adv. Drug Deliv. Rev.*, **29**, 51 - 79

Schorn, K., Hochstrasser, K. (1979), Biochemical investigation of nasal secretions. *Acta Otorhinolaryngol. Bel.*, **33**, 603

Simpkin, G. (1996) Stability of RPR drug candidate (personal communication)

Smitz, J., Devroey, P., Camus, M., Deschacht, J., Waesberghe, L., Wisanto, A., Steirteghem, A.C. (1988), Inhibition of gonadotropic and ovarian function by intranasal administration of D-Ser(TBU)$^{6}$ EA$^{10}$-LHRH in normo-ovulatory women and patients with polycystic ovary disease. *J. Endocrinol. Invest.*, **11**, 647-652

Stratford, R.E., Lee V.H.L. (1986), Aminopeptidase activity in homogenates of various absorptive mucosae in the albino rabbit: Implications in peptide delivery. *Int. J. Pharm.*, **30**, 73

Taylor, M. (1974), The origin and function of nasal mucus. *Laryngoscope,* **84**, 612

Teh, L.C., Murphy, L.J., Huq, N.L., Surus, A.S., Freisen, H.G., Lazarus, L. (1987), Methionine oxidation in hGH and human chorionic somatomammotropin. Effects on receptor binding and biological activities. *J. Biol. Chem.* **262**, 6472

Turner, J.D., Alpar H.O., Randall, L., Simpkin, G., Irwin, W.J. (1999), Development of a novel nasal chamber designed to mimic Conditions found in the human nasal cavity. *Int. Symp. Contr. Rel. Bioact. Mater.*, **26**, 5108

Verdugo, P. (1990), Goblet cell secretions and mutagenesis. *Annu. Rev. Physiol.* **52**, 157-176

Vogel, A.I. (1989), Vogel's textbook of practical organic chemistry. Longman, Harlow

Wearley, L.L. (1991), Recent progress in protein and peptide delivery by non invasive routes. *Critical Rev. in Therap. Drug Carrier Syst.* **8**, 331-394

Werner, U., Kissel, T. (1995), Developement of a Human Nasal Epithelial Cell Culture model and its suitability for transport and metabolism studies under in vitro conditions. *Pharm. Res.*, **12**, 565-571

Werner, U., Kissel, T. (1996), In-Vitro cell culture models of the nasal epithelium: A comparative histochemical investigation of their suitability for drug transport studies. *Pharm. Res.*, **13**, 978-988

Wheatley, M.A., Dent, J., Wheeldon, E.B., Smith, P.L. (1988), Nasal drug delivery: an in vitro characterisation of transepithelial electrical properties and fluxes in the presence and absence of enhancers. *J. Control. Rel.*, **8**, 167 - 77

Widdicombe, J.H. (1984), Fluid transport across airway epithelia. *Ciba Found. Symposium,* **109**, 109-120

Widdicombe, J. H., Basbaum, C. B., Highland, E. (1981), *Am. J. Physiol.*, **241**, C184-C192

Williamson, E.D., Sharp, G.J.E., Eley, S.M., Vesey, P.M., Pepper,T.C., Titball, R.W., Alpar, H.O. (1996), Local and systemic immune response to a

microencapsulated sub-unit vaccine for plague, *Vaccine,* **14**, 17-18, 1613-1619

Wilson, C.G., Washington, N. (1990), Biological barriers to drug absorption Physiological pharmaceutics. Ellis Horwood Ltd., Chichester,

Wright, H.T. (1991), Sequence and structure determinants of the non-enzymic deamination of asparagine and glutamine residues in proteins. *Protein Eng.*, **4**, 283

Wulf, E., Deboben, A., Bautz, F.A., Faulstich, H., Wieland, T.H. (1976) Fluorescent phallotoxin, a tool for the visualisation of cellular actin. *Proc. Nat. Acad. Sci. USA* **76**, 4498-4502

Wuthrich, P., Buri, P. (1989), *Pharm. Acta Helv.*, **64**, 322-331

Zhou, M., Donovan, M. (1996), Recovery of the nasal mucosa following laureth 9 induced damage. *Int. J. Pharm.*, **130**, 93-102

Yu, B., Dong, C., Blankenstein, D., So, P.T.C., Mitragoni, S., Langer, R. (1999), Visualisation and quantification of transdermal chemical enhancement using two photon microscopy. *Int. Symp. Contr. Rel. Bioact. Mater.*, **26**, 312

Zweibaum, A., Hauri, H.P., Sterchi, E., Chantret, I., Haffen, K., Bamat, J., Sordat, B. (1984), Immunohistological evidence obtained with monoclonal antibodies, of small intestinal brush border hydrolases in human colon cancers and foetal colons. *Int. J. Cancer.* **34**, 591-598

# Appendix 1

# Appendix 1

## Macro for data analysis using Scion Image.

This macro is designed with several functions; firstly, assembling confocal images into the correct format (the "File assemble" command"); secondly the analysis of the mean OD of a selected area either for a single image or a series of images within the same file (the "Small area analysis" command); and finally, the analysis of the same area taken from a series of files containing Z sections (using the "Time Experiment Batch Analysis" command)

Initial BioRad confocal "name.pic" Z series files were converted to single images using the Confocal assistant software. These individual images were then re-constructed as a multi-image TIF file using the file assemble command in this macro. To analyse a time course experiment each time point Z series has to be individually converted to a multi-image TIF file, and then using the "Time Experiment Batch Analysis" command the multi-image TIF files are then analysed.

Caution should be exercised if this macro is ever used again together with the Scion Image (Beta 3b release) version used here, since this proved to be non optimal, and regularly caused the program to crash or hang. Scion Corporation, the makers of Scion Image, acknowledge to instability in their software (www.scioncorp.com), so it is not know if this is a problem due to the macro or the program itself.

```
{Note this uses line analysis rather than box analysis}
{it is a solid box if you make the line thick enough!}

macro 'Small area analysis [M]';
var
 nS,sS,x1,y1,x2,y2,px,py,thick:integer

begin
nS:=nSlices;
if nSlices=0 then begin
    PutMessage('This Macro requires a stack.');
```

```
    exit;
  end;

SelectSlice(1);

 GetLine(x1,y1,x2,y2,thick);
 MakeLineRoi(x1,y1,x2,y2);
 Reslice;
 Measure;
 ShowMessage(rMean[rCount]);

 MakeNewWindow('Z Section Results');
 SetNewSize(200,200);
 MoveTo(5,10);
 Write('section mean= ',rMean[rCount]);
 end;



 {macro for selecting line, and then getting mean density.}


 macro 'Z mean (horiz) [H]';

 var
  px,py,x,y,nS:integer


 begin
 nS:=nSlices;
 if nSlices=0 then begin
      PutMessage('This Macro requires a stack.');
      exit
    end;

  SelectSlice(1);

  repeat
    GetMouse(x,y);
```

```
  Until button;

GetPicSize(px,py);

 MakeLineRoi(0,y,px,y);
 Reslice;
 Measure;

MakeNewWindow('Z Section Results');
 SetNewSize(200,200);
 MoveTo(5,10);
Write('section mean= ',rMean[rCount]);
 end;
 end;



 macro 'Z mean (Vertical) [V]';

 var
  px,py,x,y,nS:integer


 begin

 nS:=nSl...
 if nSlices=0 then begin
      PutMessage('This Macro requires a stack.');
      exit
    end;

  SelectSlice(1);

  repeat
    GetMouse(x,y);
    Until button;

  GetPicSize(px,py);
```

```
MakeLineRoi(x,0,x,py);
Reslice;
measure;

MakeNewWindow('Z Section Results (v)');
 SetNewSize(200,200);
 MoveTo(5,10);
Write('section mean= ',rMean[rCount]);
end;
end;
```

```
Macro 'File assemble [A]';
{Unlike the menu command of the same name, the windows do
not}
{all need to be the same size.}
var
  s,x,y,fn,i,width,height,MinWidth,MinHeight,n,stack:integer;
  isStack:boolean;
begin
  if nPics>0 then begin
    PutMessage('No images should be open.');
    exit;
   end;

  isStack:=false;

   fn:=GetNumber('enter number of files:',0);
   Open('');
   GetPicSize(x,y);

   MakeNewStack('Stack');
   stack:=fn;
   SetNewSize(x,y);

   Selectpic(1);
   SelectAll;
```

```
Copy;
Dispose;
SelectWindow('Stack');
SelectAll;
Paste;

 for i:=2 to fn do begin
  Open('');
   if isStack then begin
    PutMessage('This macro does not work with stacks.');
    exit;
   end;
  SelectAll;
  copy;
  Dispose;
  SelectWindow('stack');
     AddSlice;
     SelectAll;
     Paste;
    end;
  { filter('smooth');
   filter('smooth more');}
  end;
 end;


Macro 'Time Experiment Batch Analysis[B]';


 var
  i,nx,nB,nS,sS,x1,yl,x2,y2,px,py,thick:integer


 begin

  PutMessage('This macro opens individual time point batch
  files','\',
             'and does a sectioning at fixed position on all
  batches.');
```

```
nB:=GetNumber('enter number of files to be processed:',0);

MakeNewWindow('Z Section Results');
nx:=10;
SetNewSize(200,200);

SelectPic(1);
 nS:=nSlices;
  if nSlices=0 then begin
   PutMessage('This Macro requires a stack.');
   exit;
  end;

  SelectSlice(1);

  GetLine(x1,y1,x2,y2,thick);
  MakeLineRoi(x1,y1,x2,y2);
  Reslice;
  Measure;
  SaveAs('');
  Dispose;
  SelectWindow('Z Section Results');
  MoveTo(5,nx);
  Write('section ',i,' mean= ',rMean[rCount]);
  nx:=nx+10;

 for i:=2 to nB do begin
  Open('');
  nS:=nSlices;
    if nSlices=0 then begin
     PutMessage('This Macro requires a stack.');
     exit;
    end;

    SelectSlice(1);

    GetLine(x1,y1,x2,y2,thick);
    MakeLineRoi(x1,y1,x2,y2);
    Reslice;
```

```
 Measure;
 SaveAs('');
 Dispose;
 SelectWindow('Z Section Results');
 MoveTo(5,nx);
 Write('section ',i,' mean= ',rMean[rCount]);
 nx:=nx+10;
 end;
end;
```

```
macro 'Smooth [1]'; begin filter('smooth') end;
macro 'Smooth More [2]'; begin filter('smooth more') end;
```

*To IBE*

*For showing me what might be in the future*